Geomorphology and tectonics at the intersection of Silurian and Death Valleys, southern California

2005 Guidebook
Pacific Cell Friends of the Pleistocene

Edited by David M. Miller and Zenon C. Valin

Open-File Report 2007–1424

U.S. Department of the Interior
U.S. Geological Survey

Trip leaders:
David M. Miller, Christopher M. Menges, and Matthew R. McMackin

With trip contributions from:
Kirk Anderson, Jordon Bright, Richard Hereford, Heather Green, Shannon Mahan, Jennifer Mendonça, Joanna Redwine, Kevin Schmidt, Roger Smith, and Jonathan Stock

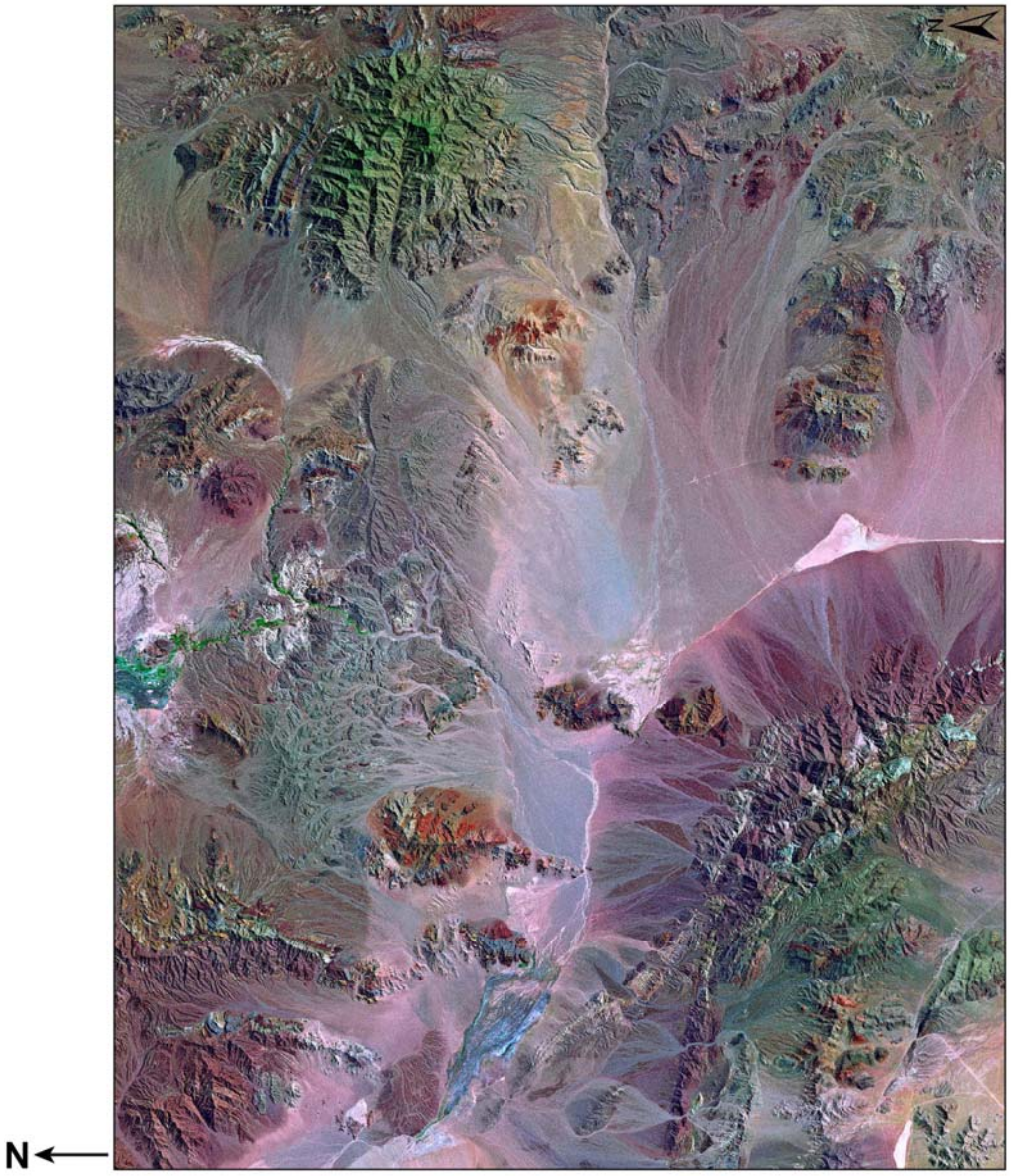

Landsat 7 image of the southern Death Valley and northern Silurian Valley area that is the subject of the field trip. Processing of the image by John Dohrenwend.

Front cover photograph: View to the south of the Amargosa River gorge where it cuts through the "Tecopa Hump." Salt Springs Hills in the middle distance lie in the bottom of the Silurian Valley trough, and the upthrust Avawatz Mountains frame the skyline. Photo courtesy of M. McMackin.

U.S. Department of the Interior
DIRK KEMPTHORNE, Secretary

U.S. Geological Survey
Mark D. Myers, Director

U.S. Geological Survey, Reston, Virginia 2007

For product and ordering information:
World Wide Web: http://www.usgs.gov/pubprod
Telephone: 1-888-ASK-USGS

For more information on the USGS—the Federal source for science about the Earth, its natural and living resources, natural hazards, and the environment:
World Wide Web: http://www.usgs.gov
Telephone: 1-888-ASK-USGS

Suggested citation:
Miller, D.M., and Valin, Z.C., eds., 2007, Geomorphology and tectonics at the intersection of Silurian and Death Valleys, southern California—2005 Guidebook, Pacific Cell Friends of the Pleistocene: U.S. Geological Survey Open-File Report 2007–1424, 171 p.

Contents

Introduction

By Christopher M. Menges[1] and David M. Miller[2]

Trip Overview

We will present contributions from new regional and detailed surficial geologic mapping, combined with geomorphologic, geochronologic, and tectonic studies, to a long-standing problem: the tectonic and geomorphic evolution of the intersection between three regional tectonic provinces: the eastern California Shear Zone, the Basin and Range region of southern Nevada and adjacent California, and the eastern Mojave Desert region. This intersection is centered on southeastern Death Valley and northern Silurian Valley and the bordering highlands to the southwest (Avawatz Mountains) and northeast (Sperry-Alexander Hills, Kingston Range and Shadow Mountains) (Fig. 1). During the course of this trip we will examine a variety of structures, deposits, and landforms that reflect neotectonic deformation in this region, many of which bear on the tectonic origin of the southern Death Valley and northern Silurian Valley "trough". In addition we will present new observations on processes of piedmont and fan development, the role of depositional processes on soil hydrology and pedogenesis, the evolution of axial-valley drainage systems, and new chronologic data on local and regional surficial stratigraphy.

The material presented in this trip is derived from a large body of work, much of which is previously unpublished, attested by the number of workers represented in the long list of contributors to this guidebook. The fundamental data sources for much of the work presented during the course of this trip are regional mapping of surficial deposits and neotectonic structures, which is in the process of being published through the U.S. Geological Survey as regional maps at 1:100,000 scale, including the Qwlshead Mountain sheet containing the actual area of the trip (Menges), and the adjoining Mesquite Lake sheet (Schmidt and McMackin, 2006) and Soda Mountains sheet (Miller and D.J. Lidke). This mapping involved basic photo-interpretive mapping and compilation supported by field study and data collection. McMackin has also completed geologic and structural mapping in bedrock highlands throughout the area. Many of the neotectonic interpretations also benefited greatly from the excellent geologic mapping in the northeastern Avawatz Mountains by Bennie Troxel and Roland Brady III (Brady, 1984). Detailed surficial mapping by Dave Miller and Jim Yount in the Valjean area provided not only the basic framework for the regional surficial mapping, but specific data for parts of this field trip. The results of a variety of more detailed or local mapping and (or) topical research programs are presented, as evidenced by summaries at specific stops in the road log, or included papers in this guidebook.

This trip and guidebook represent the first Friends of the Pleistocene (FOP) field excursion conducted in this specific area. The field area lies to the southeast of the location of the 1986 FOP

[1]U.S. Geological Survey, 520 N. Park Ave., Tucson, AZ 85719
[2]U.S. Geological Survey, 345 Middlefield Road, MS 973, Menlo Park, CA 94025

trip led by Roland Brady III, Paul R. Butler, and Bennie Troxel, which was centered on southern Death Valley between the Avawatz Mountains and the Confidence Hills (see Troxel and Brady, 1986). The FOP field trip led by Michael Machette, Ralph Klinger, and Jeff Knott in 2001 was located even farther north in central and northern Death Valley (see Machette and others, 2001).

Summary of Field Trip

The trip is designed for 2.5 days, and described in three daily road logs found in Chapter A of this guidebook. This road log is followed by Chapters B through I that either (a) provide regional neotectonic summaries for deformational features presented in the field trip, or (b) summarize research that supplements specific topics discussed at field trip stops.

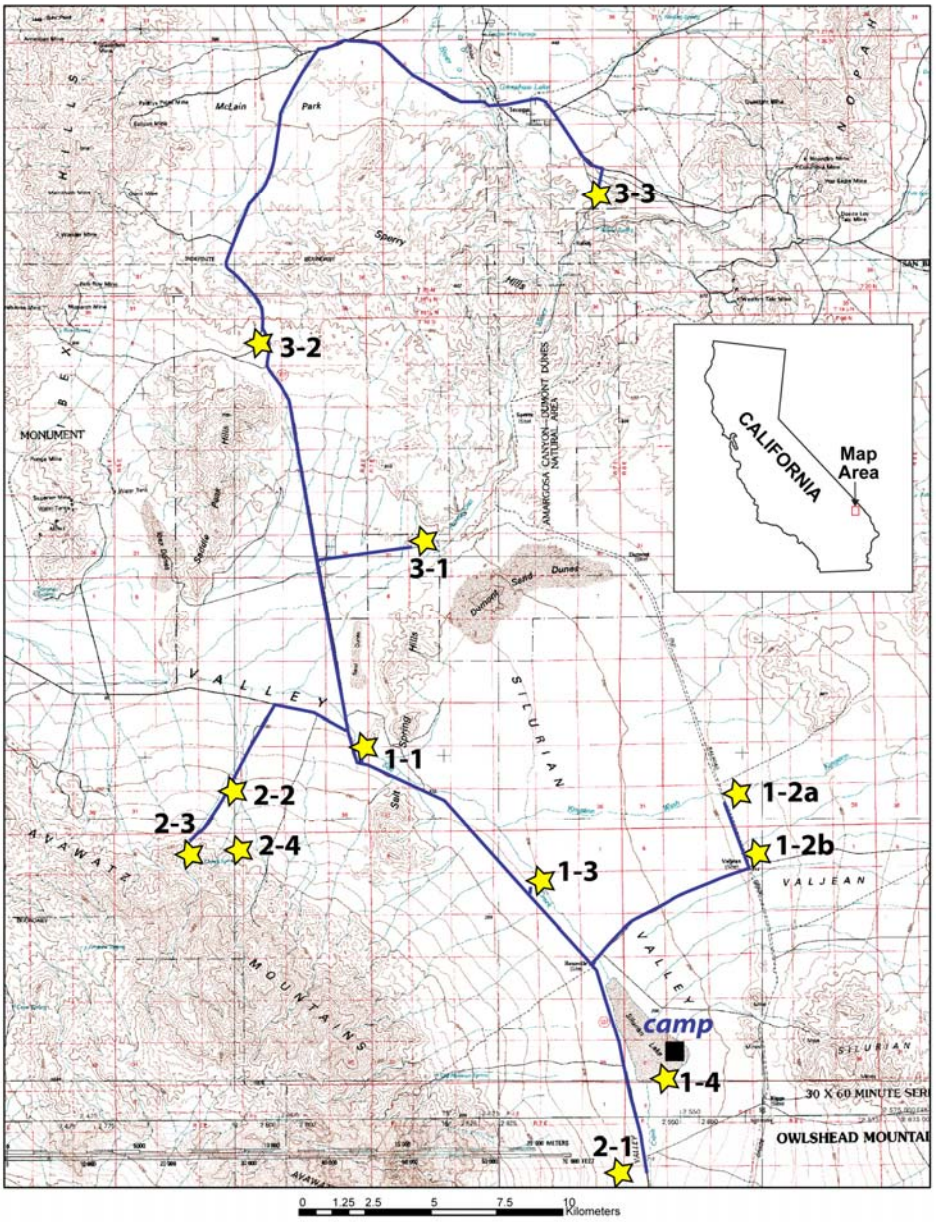

Figure 1. Map of trip stops, roads, and topography of the area. First number refers to day, second to stop sequence during the day.

On the first day we present an overview of the southern Death Valley and northern Silurian Valley area at a site in the southern Salt Spring Hills. At this stop we summarize major themes of the field trip, including the tectonic origin of the main valley system. We also describe fine-grained sediment on the east side of the hills and discuss evidence for lacustrine vs. ground-water origins for these deposits, as well as a pronounced marginal topographic bench. We also will discuss the significance of anomalous late Quaternary axial valley incision into bedrock along this reach of Salt Creek. From there we move to the Valjean piedmont and look at: (a) evidence for historic sediment yield and climatic variations from local deposits; (b) tectonic framework; (c) depositional history of the large Kingston Wash tributary drainage, including evidence for a large Holocene hyperconcentrated flow deposit; and (d) study of debris flow chronology in the Kingston Range. We continue with the study of the hyperconcentrated flow at Salt Creek, where we discuss possible tectonic controls on Salt Creek and Silurian Lake.

On the second day we examine evidence for neotectonic contractional deformation along and adjacent to the northern and eastern range fronts of the Avawatz Mountains that form the southern and western margin of the Death and Silurian valleys, respectively. We begin by traversing the lower piedmont below the eastern Avawatz Mountains front, looking at deposits, soils and evidence for warping and local faulting of Pleistocene fans. Then we move to the medial part of the southern Death Valley piedmont and discuss transportation mechanisms for alluvial fan deposits and their influence on deposit characteristics, intra-fan incision, and soil development. We continue to the base of the adjacent northern Avawatz Mountain front and look at exposures of late Quaternary thrust faults in bedrock and alluvium, tilted Quaternary fan deposits interpreted as fault-propagation folds above buried (blind) thrusts, and concomitant uplift and incision of Pleistocene fan heads. Finally we discuss implications of these deformational features to the Quaternary tectonic evolution of the range front.

On the third day, we examine evidence for a neotectonic uplift origin for the bedrock highlands ("Tecopa Hump") on the northern margin of southern Death Valley and northern Silurian Valley, which has implications for the history of the Tecopa basin and Amargosa River drainage. We begin near the mouth of the Amargosa Canyon on the southern flank of the highland and discuss the significance of fluvial terraces and river incision history for the formation of the Tecopa Hump from neotectonic warping or tilting. Also we summarize studies of eolian landforms and processes at the nearby Dumont Dunes. From there we move northwestward and discuss non-tectonic vs. tectonic origins for a sequence of inset strath (bedrock-floored) terraces and fans midway on the southern flank of the Tecopa Hump. Then we complete the trip at an overview of upper Amargosa Canyon and the northern flank of the Tecopa Hump near Tecopa with a discussion of the implications of active uplift across the hump for canyon formation and basin dissection. The trip concludes with a synthesis of major regional and local evidence for active tectonics in the area.

Trip Logistics

The trip will be run from a central group campsite on open public land on the northeastern margin of Silurian (dry) Lake. This site can be accessed by turning east from California State Highway 127 onto a small dirt road. The turn-off from CA 127 is located either: (a) from the south approximately 19 miles north of Baker CA (and Interstate 15), or (b) from the north approximately 36 miles south of Shoshone, CA, (which can be accessed via several highways from Death Valley proper, from US Highway 95 via the Amargosa Valley turnoff, or Pahrump, NV).

The nearest towns to this campsite are Baker to the south and Shoshone to the north. Both of these towns have some motel accommodations, expensive gas, and limited convenience-store-style markets (including block ice and bottled water). More complete provisions are available at distances of 60 to 90 miles in Pahrump and Las Vegas to the northeast in Nevada or Barstow to the southwest in California. We will not be formally entering any towns during the course of the trip, so plan accordingly for sufficient food, water, ice, and gas for the trip. Some field trip sites are accessible only by high clearance vehicles.

Nomenclature

We will try to avoid unnecessary use of area-specific and project-specific nomenclature, but a minimum common understanding of the alluvial units is key to communicating the soils-geomorphic concepts of alluvial fan architecture. Table 1 provides a short guide to this nomenclature for alluvial fan deposits, after Yount and others (1994): *Young deposits (Qya)* have weak soils and are typically part of an aggradational environment, in which surface flattening and weak pavement and varnish characteristics develop over time. *Intermediate deposits (Qia)* generally have strongly developed soils and are being eroded by inset channels and degradation of surface horizons. *Old deposits (Qoa)* have been strongly stripped by erosion, forming balenas and possessing ancient calcic soils.

Brief guide to soils-geomorphic features for Mojave Desert alluvial-fan deposits

Table 1. Summary of principal alluvial fan deposit characteristics and nomenclature used on this trip. Features in bold type are most diagnostic. Deposits are poorly dated, but as a general guideline, young deposits are younger than about 15 ka, intermediate are about 30-250 ka, and old are generally 500-800 ka

Map unit	surface topo	pavement	varnish	Av	B	K	plants
Qya1	**active wash or fan**	none	none	**none**	none	none	few; cheesebush
Qya2	**Bar & Swale strong**	none	none to v. weak	**generally none**	none	none	cheesebush, creosote, Ambrosia
Qya3	remnant B & S, somewhat flat	incipient	Weak	**weak –** sandy silt	weak (Bw) reddish	Stage I- (rind under pebbles)	creosote, Ambrosia
Qya4	**weak remnant B & S, fairly flat**	**weak** – some leveling of pebbles	**weak to mod**	**weak** – sandy silt, loose	Bw	Stage I	creosote, Ambrosia
Qia1	**flat, faint B & S**	weak to mod	mod	**structured silt, 2-6 cm**	**strong red**, weak clay	Stage II (complete pebble rinds)	sparse plants
Qia2	**flat, even pebble size, pebble tops level**	**mod to strong**	**mod to strong**	**structured silt, 4-8 cm**	**Bt** usually – mod clay	**Stage II to III**	**sparse; Mojave Yucca**
Qia3	**crowned**	strong to degraded; exposed Av	**strong – purplish casts**	structured silt, 4-15 cm	**Bt – strong clay**	**Stage III to IV** (pores filled)	sparse
Qoa	**whaleback**	**calcic chips in pavement**	secondary or none	secondary or none	secondary or none	**Stage IV** – layered and massive	common plants, many species

The soils-geomorphic framework (Bull, 1991; Birkeland, 1999) provides a means to discern and map the distribution of deposits of varying ages. The map patterns inform about the spatial variations of depositional process from place to place, and the variation of specific

characteristics among deposits provides data for interpreting tectonic- and climate-driven processes. This approach is the backbone for the surficial geology maps that were prepared for this area, and led to many of the focused studies we will present.

A key concept is that the age- and soils-specific groups of deposits are climate driven, both as depositional pulses and as specific climate-influenced soils. As a result, deposits have been shown to be nearly synchronous across broad regions (Menges and others, 2001; Green and others, this volume). Local departures from the regional climate-driven patterns become identifiable and can be evaluated for tectonic influences. We will highlight several unusual depositional and erosional environments on this trip and examine them for their tectonic implications.

Paleohydrology and paleoclimate

Climate events and the presence of lakes, springs, and streams strongly affect animal and plant life in the desert, and climate, biota, and surface water affect geomorphic systems ranging from weathering and sediment production to transport and deposition. For these reasons, the following review of literature on the paleohydrology and paleoclimate of the greater Silurian Valley and southern Death Valley area is provided for reference. All dates are in calendric years.

Paleohydrology of the area has been studied by many, and most recently evaluated in detail and synthesized by Wells and others (2003) and D.E. Anderson and Wells (2003). During the late Pleistocene the Amargosa River and Mojave River flowed to Death Valley, where they supported shallow brackish lakes from about 30 to 12.5 ka, with fresher intervals at ~30, ~21, and ~17 ka (Lowenstein and others, 1999; D.E. Anderson and Wells, 2003). Details for flow rates for the Amargosa River are not known, but it is known that the Mojave River only episodically overflowed the threshold of Lake Mojave at the north margin of present Silver Lake playa, from about 22 to 13.5 ka. The earlier presence of a moderately fresh lake in Death Valley supports the inference that the Amargosa River had sustained and high-volume flow starting approximately at 30 ka. The overflow channel at Silver Lake is the only part of the Mojave River system between Silver Lake and Death Valley that is preserved. Its cross-sectional area is 110 m^2, indicating a relatively small river at best. Fluvial contribution from Mojave River to the Salt Creek axial valley wash system probably created a more perennial, larger discharge system than was present after about 13.5 ka. Holocene flow probably has been highly ephemeral on both Amargosa River and Salt Creek (D.E. Anderson, 2005; K.C. Anderson and Wells, 2003), and inferences for temperatures and precipitation from other sources provide the best guide for inferring discharge during the Holocene.

Packrat (*Neotoma*) middens constitute a low temporal resolution record for vegetation and pollen, from which paleoclimate records may be inferred. Koehler and others (2005) presented several new records for Silurian Valley and adjacent uplands and summarized other findings to arrive at the following conclusions. In general, late Pleistocene vegetation zones were at least 400 m lower than present, with woodlands extending down onto the piedmonts, and all landscape was more densely covered by shrubs and possibly grass. The main climatic intervals defined by vegetation assemblages include: (1) Pleistocene vegetation such as pinyon pine, juniper, and Joshua Tree persisted until about 13.5 ka, after which (2) pinyon receded and sage brush entered during a continued cool and wet assemblage. (3) About 8.7 ka, a plant assemblage including white bursage, creosote bush, Mojave sage, and Mormon tea took over most lowlands, indicating much drier and warmer conditions. (4) This assemblage was modified at about 5.2 ka to an assemblage similar to today's, which includes cool-adapted species such as black brush at higher elevations. These climate periods are mirrored in many parts of the southwest and even globally,

lending strength to suppositions that geomorphic events may have differed among the climate periods.

Acknowledgments

We are grateful to Shannon Mahan for careful review of this contribution.

References cited

Anderson, D.E., 2005, Holocene fluvial geomorphology of the Amargosa River through Amargosa Canyon, California, *in*, Calzia, J.P., ed., Fifty years of Death Valley Research: A volume in honor of Lauren A. Wright and Bennie Troxel: Earth-Science Reviews, v. 73, p. 291-307.

Anderson, D.E., and Wells, S.G., 2003, Late Pleistocene lake highstands in Death Valley, California, *in* Enzel, Y., Wells, S.G., and Lancaster, N., eds., Paleoenvironments and paleohydrology of the Mojave and southern Great Basin Deserts: Geological Society of America Special Paper 368, p. 115-128.

Anderson, K.C., and Wells, S.G., 2003, Latest Quaternary paleohydrology of Silurian lake and Salt Spring basin, Silurian Valley, California, *in* Enzel, Y., Wells, S.G., and Lancaster, N., eds., Paleoenvironments and paleohydrology of the Mojave and southern Great Basin deserts: Geological Society of America Special Paper 368, p.129-141.

Birkeland, P.W., 1999, Soils and Geomorphology: Oxford University Press, New York, 430 p.

Brady, R.H., III, 1984, Neogene stratigraphy of the Avawatz Mountains between the Garlock and Death Valley fault zones, southern Death Valley, California: Implications as to late Cenozoic tectonism: Sedimentary Geology, v. 38, p. 127-157.

Bull, W.B., 1991, Geomorphic Responses to Climatic Change: Oxford University Press, New York, 326 p.

Koehler, P.A., Anderson, R.S., and Spaulding, W.G., 2005, Development of vegetation in the central Mojave Desert of California during the late Quaternary: Palaeogeography, Palaeoclimatology, Palaeoecology, v. 215, p. 297-311.

Lowenstein, T.K., Li, J., Brown, C., Roberts, S.M., Ku, T.-L., Luo, S., and Yang, W., 1999, 200 k.y. paleoclimate record from Death Valley salt core: Geology, v. 27, p. 3-6.

Machette, M.N., Johnson, M.L., and Slate, J.L., 2001, Quaternary and late Pliocene geology of the Death Valley region: Recent observations on tectonics, stratigraphy, and lake cycle—Pacific Cell-Friends of the Pleistocene Field-trip Guidebook: U.S. Geological Survey Open-File Report 01-51, 246 p.

Menges, C.M., Taylor, E.M., Workman, J.B., and Jayko, A.S., 2001, Regional surficial-deposit mapping in the Death Valley area of California and Nevada in support of ground-water modeling, *in* Machette, M.N., Johnson, M.L., and Slate, J.L., eds, Quaternary and late Pliocene geology of the Death Valley region: Recent observations on tectonics, stratigraphy, and lake cycle—Pacific Cell-Friends of the Pleistocene Field-trip Guidebook: U.S. Geological Survey Open-File Report 01-51, p. H151-H166.

Schmidt, K.M., and McMackin, M., 2006, Preliminary Surficial Geologic Map of the Mesquite Lake 30' X 60' Quadrangle, California and Nevada: U.S. Geological Survey, Open-File Report 2006-1035, scale 1:100,000, 89 p.

Troxel, B.W., and Brady, R.H., eds., 1986, Quaternary tectonics of southern Death Valley, California: Field Trip Guide: Pacific Cell-Friends of the Pleistocene Field-trip Guidebook, 44 p.

Wells, S.G., Brown, W.J., Enzel, Y., Anderson, R.Y., and McFadden, L.D., 2003, Late Quaternary geology and paleohydrology of pluvial Lake Mojave, southern California, *in* Enzel, Y., Wells, S.G., and Lancaster, N., eds., Paleoenvironments and paleohydrology of the Mojave and southern Great Basin Deserts: Geological Society of America Special Paper 368, p. 79-114.

Yount, J.C., Schermer, E.R., Felger, T.J., Miller, D.M., and Stephens, K.A., 1994, Preliminary Geologic Map of Fort Irwin Basin, north-central Mojave Desert, California: U.S. Geological Survey, Open-File Report 94-173, 25 p.

Chapter A

Geomorphology and tectonics at the intersection of Silurian and Death Valleys: Field trip road log

By David M. Miller, Christopher M. Menges, and Matthew R. McMackin[1]

Field trip road log details: All stops, comments, and notes are referenced by mileage sequentially by day, in the order traversed during the trip. Most of the trip follows California State Highway 127 and an adjacent network of secondary paved and variable quality dirt and gravel roads. Consequently, two types of field trip mileages are listed in the road log. Mileages along CA Highway 127, (Hwy Mile) are referenced to small black & white mileage signposts located at half-mile spacing in staggered fashion on both sides of the highway, with full-mile increments (every Mile X) on the east side and half-mile increments (every mile X + 0.5) on the west side of the highway. The highway mileage increases northward, starting at 0 miles at Baker CA. However, the mileage resets to 0 and again accumulates to the north where the highway crosses the San Bernardino-Inyo County line at Ibex Pass (marked by highway signs). The pass is located on the divide between Death Valley and Tecopa basin. Travel on secondary roads is given in cumulative mileage from the turnoff from Hwy 127. Locations for field trip stops are given in UTM zone 11, NAD 83 x,y pairs in brackets: [564946 3942949].

DAY 1

Trip starts at Silurian Lake northbound on Hwy 127.

Hwy Mile 21.5 Note a short paved road leading to the northeast. This road leads to Valjean townsite, and we will return to it later today. It is difficult to spot when traveling south on the highway, however. There is a good view to northwest and west of the eastern range front of the Avawatz Mountains. Note the prominent topographic scarps disrupting the Pleistocene alluvial fans below the main bedrock mountain front. This is the approximate area described by Mendonca (Chapter G, this volume). We will be examining similar features on a section of the northern range front of the Avawatz Mountains on Day 2.

Hwy Mile 27.5 We are driving through fine-grained sediments interpreted as lake and playa sediment by K.C. Anderson and Wells (2003) and re-interpreted as mostly wetland deposit by Bright and Anderson (Chapter B, this volume). Note the topographic bench to the southwest where the fine sediments abut the quartzite bedrock. Some workers interpret this bench as a wave

[1]San José State University, San José, CA 95192

cut platform (Hooke, 1999; K.C. Anderson and Wells, 2003) while others argue that the bench formed by corrosion of the quartzite by salty ground water from overlapping wetland deposits (Bright and Anderson, Chapter B, this volume).

Hwy Mile 28.6 Turn right on the road leading to the interpretive site for Salt Springs and park at parking lot. Follow the trail toward Salt Springs and cross Salt Creek on a bridge. Along the route, note the stream terraces cut into the dissected pediment carved onto the Mesozoic granite bedrock. From here the Salt Creek drains through the gap in the bedrock of the Salt Spring Hills into southeastern Death Valley. Continue along the trail across the burned area on alluvial fill in the valley bottom until it crosses the small channel on the north side of the valley. The brush here was largely tamarisk, burned in an aggressive effort to exterminate it in this riparian zone. Nonnative tamarisk once dominated the spring. Just across the northern channel, leave the trail and follow an incised bedrock channel northeast. Note the efflorescence of salt on some fractures and shaded faces. Exit up a side channel to the left (it will be marked for the trip) and climb to the pediment cut into the granitic rock, up bedrock slopes to the saddle and a small knob where we will congregate for Stop 1-1.

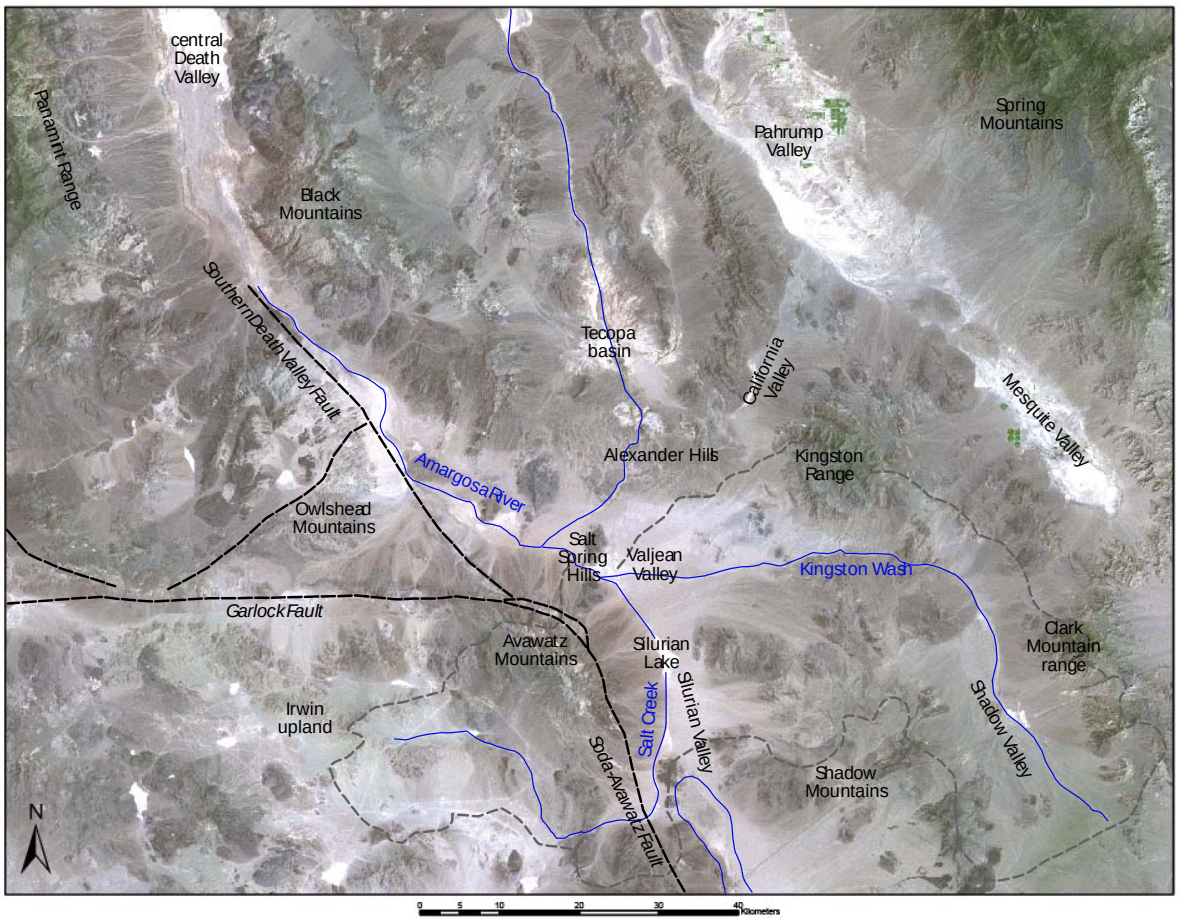

Figure 1. Regional map with place names, selected Quaternary faults, and selected major washes. Note the captured drainage basins of Shadow Valley and part of the Irwin upland (outlined by dashed gray line) that contribute to Salt Creek

STOP 1-1. Salt Spring Hills overview: [564946 3942949] Overview of southern Death Valley and northern Silurian Valley. At this stop, we can see southern Death Valley to the west and northwest and northern Silurian Valley to the south and east. The Kingston Range looms large to the east and the Avawatz Mountains rise in the southwest. From this ridge many of the geomorphic, geologic, and tectonic patterns of the region are visible. The rocks, structures, and processes inferred from them represent the underlying themes of this field trip and will be presented for discussion and examination at this first overview stop.

Both southern Death and Silurian valleys are broad elongate basins bordered by high, partly fault-bounded mountains, and both are occupied by low-gradient axial washes that drain northward and northwestward into the regional closed-basin sump of central Death Valley. Both valleys are flanked by high, low-gradient valleys (such as Shadow Valley) that are underlain by abundant Pleistocene deposits. Both valleys also are traversed by linear sets of hills, the eroded remnants of north to northeast trending mountain ranges that appear to descend into the valleys and lie athwart the main valley orientation. The Salt Spring Hills are an excellent example, descending from north to south from the highlands of the Sperry-Alexander Hills, reaching a minimum elevation near this stop in the axial trough of the basin, before ascending up the piedmont almost to the base of the Avawatz Mountains. Two more examples can be seen to the northwest where the range crests of two north-trending ranges appear to plunge southward into the basin interior down the northern flank of Death Valley, and more examples exist in Silurian Valley farther south and out of sight.

A variety of geomorphic and geologic data suggest that each major valley formed by integration of several valley segments. Silurian Valley itself remains to be fully integrated with the Mojave River to the south. Northern Silurian Valley is separated from the Mojave River drainage during dry periods but was connected during the late Pleistocene via overflow of Lake Mojave (Wells and others, 2003) at the northern end of Silver Lake. The hydrologic history in this area therefore informs on both geomorphic development and climate history. An example of drainage integration lies at our feet to the south, where Salt Creek flows through an incised bedrock channel in a gap across the Salt Spring Hills to hydrologically link Silurian Valley with the Amargosa River drainage in southeastern Death Valley.

Why do bedrock hills exist in the center of broad valleys otherwise similar in size to Basin and Range valleys? Several characteristics suggest that these valleys differ significantly from typical valleys of the extensional Basin and Range Province. These characteristics include the lack of large gravity lows indicative of thick accumulations of basin sediments, the distribution, pattern and incision patterns of drainage systems in both the axis and flanks of the valleys, and the location and type of active deformation within and along the margin of basins. We will present evidence during this trip that the valleys are not simple down-faulted grabens or half-grabens, but instead represent active downwarps or synclines that have down-folded antecedent ridges into the valley floors.

Salt Spring Basin Deposits: evidence for wetland origin. *[See Bright and Anderson, Chapter B, this volume, for more information]* New ostracode faunal analyses on core and outcrop samples in the Salt Spring basin suggest that basin sediments previously interpreted as lacustrine by K.C. Anderson and Wells (2003) are instead wetland deposits. Four wet intervals (intermittent between approximately 29 and 23 ka, and again at approximately 18 ka) are preserved in core. The ostracode faunas found in these intervals are unable to tolerate Mojave River chemistry, and suggest that the wetland deposits were fed by local water sources. Numerous outcrop samples, including one sample from a potential Salt Spring basin shoreline feature, contain the same

ostracode species as the core, suggesting they are also wetland rather than lacustrine deposits. The new data point to paleo-wetland origin for most of the deposits, which simplifies interpretations that invoked Mojave River flow in the basin before the river was known to overflow Lake Mojave upstream.

Basin Margin Features. The prominent bench or scarp at the base of the large bedrock hill of the Salt Spring Hills across the road to the southeast has been the subject of considerable discussion. Until recently, this feature has been interpreted as a wave-cut shoreline bench related to a local paleolake impounded behind this bedrock ridge in the Dumont basin to the east (K.C. Anderson and Wells, 2003). This lake was the site for deposition of the presumably lacustrine light colored fine-grained deposits so abundant in the lowlands to the east. More controversially, Hooke **(**1999) suggested the bench is a shoreline of the high stand of Lake Manly during the Blackwelder Stage in central Death Valley, now generally correlated with marine oxygen isotope Stage 6 at approximately 140,000 to 160,000 ka (Machette and others, 2001). Hooke proposed approximate 2 mm/yr subsidence in order to explain the discrepancy among elevations of features interpreted as correlated shoreline elevations along the 200-km extent of the proposed lake in Death Valley and Soda Lake.

However, there is a problem with interpreting this feature as a wave-cut bench. More recent, faunal data summarized in Bright and Anderson (Chapter B, this volume) indicate that the sediments are related to wetlands. Further, it is difficult to impound a lake behind this ridge, in that the elevation of the prerequisite sill in the gap occupied by Salt Creek to the south of this site is 12 m lower than the elevation of the proposed shoreline feature. Other points in the Salt Springs Hills also lie below the bench. The bench is cut into a colluvial slope composed of coarse-grained sandstone of the Late Proterozoic Wood Canyon Formation. The granular sandstone is subject to salt corrosion and the bench is located along the margin of the wetland deposits, a possible site of local spring or groundwater seepage. The absence of other shoreline-like features argues against the interpretation of a wave-cut terrace. Subsoil salt-corrosion and groundwater sapping offers at least one alternative mechanism for forming the bench, and are observed adjacent to some active springs (e.g., Mesquite Springs south of Soda Lake). These processes would likely be enhanced in the corrosive paleohydrologic wetland environment (Bright and Anderson, Chapter B, this volume). The effectiveness of salt corrosion as a weathering process in the Salt Springs basin is also clearly illustrated in the tafoni-like cavernous weathering and local slope undercutting on the stripped granitic pediment below us to the east.

Bedrock Geology. The granitic rocks of the Salt Spring Hills intrude Late Proterozoic sedimentary rocks that form ridges to the north and south of the spring. Garcia and others (2002) reported that the plutonic rock had a complex history, evolving from a biotite hornblende granodiorite phase to a muscovite biotite phase. The Ar/Ar age for biotite indicates crystallization before 149.65 ± 0.78 Ma. The granitic rock here is moderately to highly fractured which has note-worthy consequences for weathering, because salt corrosion is generally strongest where the fracture density is highest.

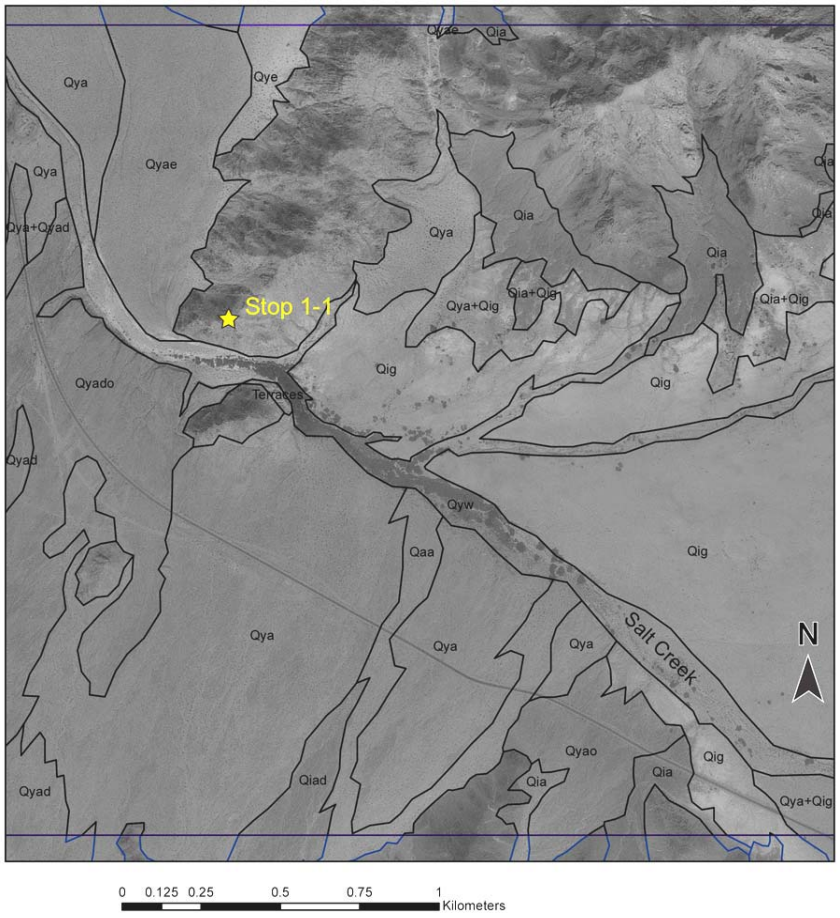

Figure 2. Geologic map of surficial deposits in the Salt Creek area near Stop 1-1, located on a small knoll of the bedrock ridge north of the bedrock gap where Salt Creek crosses the Salt Spring Hills. Major units shown include Qyw (Holocene channel deposits), Qya (Holocene alluvial deposits), Holocene and earliest Holocene debris flow deposits (Qyad and Qyado, respectively), Qyae (Holocene eolian influenced alluvial deposits, Qye (Holocene eolian deposits), Qia (late Pleistocene alluvial fan deposits) and Qig (late Pleistocene ground-water discharge deposits of Salt Springs basin).

Local Late Quaternary incision along Salt Creek As is evident from this vantage point, the axial drainage of Salt Creek is characterized by incision throughout a 7 km long reach centered on the point where it transects the Salt Springs bedrock ridge. This incision is anomalous in both extent and depth relative to other reaches of both Salt Creek and adjacent sections of the Amargosa River, which are otherwise either aggrading or not significantly incised (< 1-2 m). This incision extends continuously throughout this reach of Salt Creek, as well as most large tributary drainages, into all substrate material, including bedrock within the gap in the Salt Spring Hills, the fine-grained wetland deposits of Salt Spring basin, and all distal piedmont alluvium.

The most prominent record of the incision is several levels of terraces, truncated fan margins, and bluffs in fine-grained ground-water discharge deposits. The highest level of incision is marked by the uppermost level of wetland deposits, capped by a thin veneer of dissected Qia2-equivalent alluvial fans, on flanks of the bedrock hills along the northwest margin of Salt Spring basin. This upper surface projects down-gradient onto a stripped remnant bench, cut on wetland deposits, that reaches a maximum height of 12.5 to 13 m above the north edge of the valley floor of Salt Creek east of the bedrock gap. Generally correlative Qia2 surfaces in this region have been dated by various means at between 30 ka and <140 ka, and mostly <80 ka (see Mahan and others, Chapter C, this volume). This upper level of dissected basin deposits is approximately equivalent in height to the lower extent of the dissected and largely stripped erosional surfaces cut into the granitic slopes we traversed across while climbing to this overlook point (Fig. 3).

Figure 3. View to southwest, from dissected and stripped bedrock pediment and erosion surface, into the gap in bedrock ridge of Salt Spring Hills (left middle area) where Salt Creek enters into southern Death Valley from northernmost Silurian Valley. Note the locally dense riparian vegetation near active springs and seepage zone and strath terrace benches within and adjacent to the Salt Creek valley floor in the gap.

Below this high bench level is an intermediate set of terraces and truncated fan margins especially prominent along the southern edge of the valley lowland of Salt Creek in the Salt Spring Hills area. The highest intermediate height feature is a truncated margin of a prominent fan, derived from the northeastern Avawatz Mountains to the south, that stands approximately 7.5 to 8 m above Salt Creek, several hundred meters west of the bedrock gap. The soils and surface characteristics of this fan deposit suggest a correlation with Qya4 units dated elsewhere in this region as early Holocene to latest Pleistocene (i.e., approximately 9 to 15 ka; Mahan and others, Chapter C, this volume: McDonald and others, 2003). Below this is an inset terrace correlative with the series of strath terraces in the bedrock gap itself. Terrace gravels with the mixed lithologic assemblage of Salt Creek overlie a strath terrace, at heights of 3.5 to 4.5 m, cut on the granitic bedrock exposed in the gap. These terrace deposits have very weakly developed soils, minimal clast weathering, and weak varnish development on suitable lithologies, characteristics that collectively suggest a correlation with young Qya3 deposits in the region with dates commonly between 2-3 and 6 ka (Mahan and others, Chapter C, this volume). This age estimate indicates that a significant amount of the incision occurred into alluvium and locally into bedrock along this reach of Salt Creek in late to middle Holocene time.

In summary, a series of terraces and truncated fans at varying heights record long-term dissection over at least a late Pleistocene to late Holocene interval along this reach of Salt Creek. Salt Creek is anomalous for drainages along major valley axes in the area. The maximum heights of all terraces (12 to 5 m) is close to the bedrock gap, and rapidly decrease and disappear within 2 to 4 km in either direction along the channel.

The stream incision patterns suggest several possible controlling factors. The spatial coincidence of the incision with the western downstream section of the ground-water discharge deposits of Salt Spring basin suggest a possible causal linkage between these two features. Enhanced ground-water discharge with low initial sediment load may have entered the system during pluvial intervals in the essentially unconfined western section of the valley discharge area. This increased stream discharge could have triggered stream incision and the concomitant reduction in stream gradient that would have propagated in both upstream and downstream directions until the gradient was adjusted to the increasing entrained sediment load. Enhanced development of relatively incised large channels has been observed in otherwise un-incised drainage systems where they transect large tracts of paleogroundwater discharge deposits in other valleys to the north (e.g., Ash Meadows and Chicago Valley).

Some of the incision may be related to tectonism in the southern Salt Spring Hills that is presumably related to active thrust-fault deformation along the Avawatz Mountain front to the south but no fault scarps have been identified. We will be examining structural and geomorphic

features related to active deformation along the Avawatz Mountain front on the second day and will return to this topic at that time.

Return to Hwy 127 and turn left, proceeding south.

Hwy Mile 27.5 Pass the Dumont wetland deposits again.

Hwy Mile 21.5 Valjean turnoff. Take sharp left turn and proceed east on dirt road.

Mile 0.2 Cross Salt Creek, the axial valley drainage for Silurian Valley. Note the multiple stream threads, each just a few meters wide, and the shallow incision compared to the stream at Salt Springs, and the low gradient (<1%).

Mile 4.4. Turn left after crossing the old rail bed for Tonopah and Tidewater Railroad.

Mile 6.3. Stop in stream bed and park in such a way that many others can park as well.

STOP 1-2. Valjean Valley piedmont This stop is split into two segments to facilitate vehicle parking. At one site, we will discuss debris flow timing and the nature of deposits on the piedmont, and at the other, recent sedimentary deposits that provide evidence for the frequency and magnitude of overland flow on this piedmont and the regional tectonics.

STOP 1-2a. [578376 3941187] Geology of Valjean Valley piedmont and large-volume Holocene boulder deposit, and debris-flows of the Kingston Range. Proceed to the wash crossing and hike up the wash to the northeast to a prominent north wall of the wash at coordinate [579220 3941285].

Valjean Valley lies between the Silurian Hills to the south and the Valjean Hills, draped with sand ramps, to the north (Fig. 4). It forms a subtly undulating, nearly planar piedmont consisting of several drainage systems. The Kingston Wash system lies to the north. Farther south, three distinct fluvial systems can be distinguished by channel sources and clast types. Downslope, each drainage meets Salt Creek and Silurian Lake with a complex of Pleistocene and Holocene deposits mapped by Miller and Yount (unpublished mapping suggesting long-term base-level stability and efficient removal of detritus transported to Salt Creek (see Fig. 2, Mahan and others, Chapter C, this volume). However, Salt Creek is a very low-gradient wash (0.9%) and Silurian Lake is essentially flat, raising questions about their ability to carry alluvial fan debris. Upstream, the three southern drainage systems pass through hourglass canyons, and two of these drainages originate on the same mountain. The upper reach of each stream has Qoa deposits of middle Pleistocene age associated with it. These features suggest rather unusual origins and have tectonic implications for Valjean Valley but we know little more about their evolution. Despite the long-term base-level stability and nearly planar piedmont, the upper reaches of each drainage apparently has evolved relatively recently by some combination of tectonic uplift, forming antecedent stream valleys, or stream capture through aggressive headward erosion. In either case, tectonic uplift of the Shadow Mountains just east of the Valjean Valley piedmont is a likely driver for the hourglass drainage basins. Differential erosion of resistant materials in the hills as opposed to Miocene gravels under Valjean Valley probably also plays a role in the topographic evolution of these streams.

Large-volume boulder deposit of Kingston Wash. Kingston Wash drains Shadow Valley, a high-altitude, gently sloping valley that drains several of the highest mountains in the area such as the Clark Mountain Range (Fig. 1). The wash forms a prominent hook shape where it leaves Shadow Valley and takes a steeper, straighter course west to Silurian Valley (Fig. 1), suggesting capture of the Shadow Valley drainage system. We are in the lower, depositional realm of the drainage, along one of several threads of Kingston Wash. This wash carries a clast assemblage similar to that of washes farther south in Valjean piedmont but the proportion of clasts composed of the Kingston Peak granite is somewhat higher, reflecting the prominent granitic sources in the Kingston range on the north side of the proximal Kingston Wash.

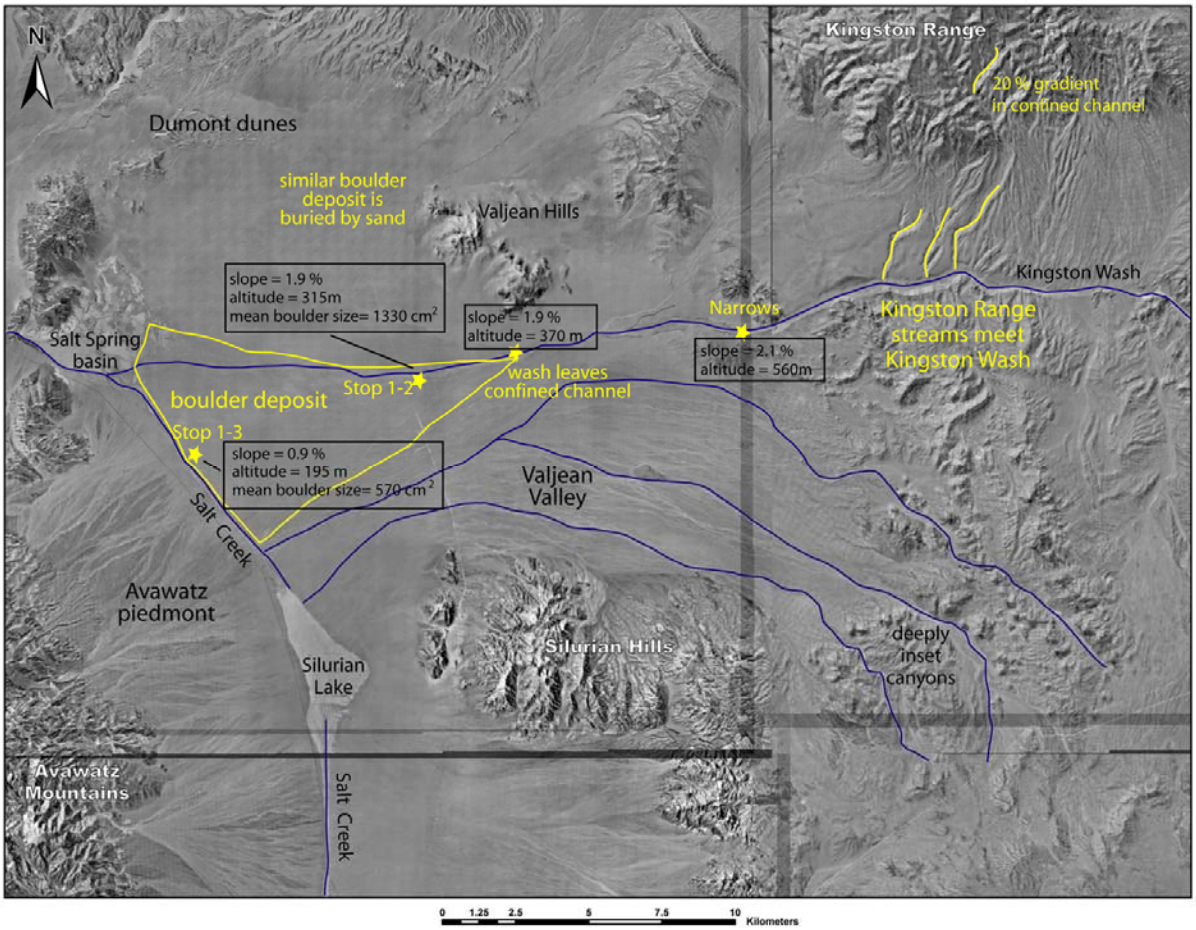

Figure 4. Map of Valjean Valley area, showing topographic elements that bear on the interpretation of the Kingston Wash boulder deposit. Slopes for washes are calculated from 1:24,000 scale topographic maps. Boulder size is averaged from measurements made on four plots at each of medial and distal positions, each plot being 100 m^2.

At this position near the Tonopah and Tidewater railroad bed, the bouldery deposits with pronounced levees, bars, and channels stand in great contrast to the deposits elsewhere on the piedmont. Most boulders are composed of Kingston Peak granite, with a small fraction of limestone and gneiss, most of which are much smaller in diameter than granite boulders. This location in Kingston Wash displays a rare vertical profile through the boulder deposit, showing it to be less than one meter thick here, and lying concordantly on much finer grained wash deposits. In other places nearby, thickness to 1.5 m can be demonstrated. The deposit possesses a sandy

matrix, which appears to support the boulders. In some outcrops, vague imbrication is suggested but in general imbrication is not apparent except adjacent to modern channels, which probably indicates local reworking of boulders. The boulder deposit underlies an area of about 43.5 x 10^6 m^2, and is the only deposit of its kind in the Holocene and latest Pleistocene record of Kingston Wash. It has a weak soil consisting of a thin sandy Av horizon, weak cambic horizon, and stage I calcic morphology. Weak varnish on boulders, pronounced ventifact fluting of boulders, weak pavements and vivid surface bar and swale topography all attest to a deposit age of mid to early Holocene. Underlying gravel and sand in this exposure is well bedded, imbricated, and moderately well size sorted, and granitic boulders are present in small numbers.

Slopes and volumes, shown on Fig. 4, summarize the main attributes of this deposit. The large size of boulders, fine gravel and sand of the matrix, and lack of imbrication and bedding all point to a mass wasting origin for the deposit, possibly debris flow or hyperconcentrated flow. Sufficient relief to drive debris flows is present in the Kingston Range. For instance, a total of nearly 2000 m of relief exists between Kingston Peak and our current position, and steep confined channels on the south side of Kingston Peak that lead to Kingston Wash, and might have carried a deposit such as this one, have slopes in the 20% range. The possibility of a debris flow sourced in the Kingston Range is therefore reasonable. However, the pebble and finer gravel fraction of the deposit is not granitic, and therefore sourced from someplace other than the Kingston Range, and the deposit where it leaves the confinement of Pleistocene shoulders of Kingston Wash (Fig. 4) is at a gradient of 1.9%, a low stream gradient for debris flows. Boulder size decreases down fan (Fig. 4), as does the finest gravel fraction, but pebble and cobble fractions stay roughly constant. These data suggest that fluvial admixtures to a debris flow, perhaps as it entered Kingston Wash, are likely, and that the deposit in Kingston Wash was transitional between hyperconcentrated flow and fluvial.

Deposition of this boulder deposit was rapid and possibly catastrophic. At the Narrows (Fig. 4) a boulder-bed trim line on flanking hills of Miocene rock exists about 5 m above the wash bed. If the wash geometry was like today's, it is possible to estimate the time needed to pass the sediment found in the boulder deposits through the Narrows. The volume of sediment, ignoring eroded parts and sediment flushed by Salt Creek, is conservatively estimated as 21.7 x 10^6 m^3. At bank-full levels in the Narrows, this sediment would pass in 50 minutes at 5 m/sec. With greater sediment volume plus water, the time for emplacement is still just a few hours at most at this velocity. We consider this an extremely rapid depositional event.

We will examine the toe of this deposit at Salt Creek in Stop 1-3 to evaluate the age of the deposit, its role in shaping Salt Creek, and implications for the origin of Silurian Valley.

Kingston Range debris flows through the ages. *[See Chapter D, Schmidt and Menges, this volume for more information]* Alluvial fans proximal to the steep, granitic hillslopes of the Kingston Range reveal abundant debris-flow deposits spanning the Quaternary. The number of primary debris-flow depositional stages characterized by large boulders with a matrix support are commensurate in age with nearby fluvial or traction transported alluvial fan deposits. This chronostratigraphic differentiation is based upon time-dependent characteristics such as relative boulder strength, degree of surface desert varnish, pedogenesis, and vertical separation. Rock strength is highest for Holocene-aged boulders and decreases for Pleistocene-aged boulders weathering to grus. Volumes of age-stratified debris-flow deposits, constrained by deposit thickness above bedrock, GPS surveys, and geologic mapping, are greatest for Pleistocene deposits. Shallow landslide susceptibility, derived from a topographically based GIS model, in

conjunction with deposit volumes produces watershed-scale erosion rates up to tens of mm ka^{-1}, with time-averaged Holocene rates exceeding Pleistocene rates.

STOP 1-2b. [579351 3938378] Return along the railroad bed to the turnoff with the Valjean Valley road.

Ponded deposits of the last century, Valjean Valley and elsewhere in the Mojave Desert. The purpose of this stop is to examine 20th century alluvial deposits that have accumulated in an artificial pond on the upstream side of the abandoned rail bed of the Tonopah and Tidewater Railroad, which was constructed in 1906. This is one of several sites along abandoned rail beds in the Mojave Desert that were studied by the U.S. Geological Survey to determine the frequency of surface runoffand long-term sediment yield. Sediment yield and particularly runoff frequency are poorly understood in arid environments. The rate of occurrence of surface runoff is important, as runoff is one of the principal means of landscape change. We will discuss the sedimentology of the deposits and how the number of times sediment and water entered the pond is recorded.

Figure 5. Photographs of Tonopah & Tidewater rail bed and excavated alluvium.

Tectonic setting of Valjean Valley. Geologic mapping of pre-Quaternary deposits (McMackin, unpublished mapping) in mountains bordering Valjean Valley reveals several fault systems that appear to be directly related to the Quaternary landscape and those faults are represented on Figure 6. Some of the faults shown cut Quaternary deposits but in most cases they are buried by Quaternary deposits and, in some cases, latest Tertiary surficial deposits. All of the faults shown on this map (real or otherwise) are younger than the 12.3 Ma age of the Kingston granite by virtue of cutting the granite or late Tertiary conglomerates derived from the granite.

The cross-cutting relations among the faults and the beds that overlie them indicate a general pattern of intersecting faults that may lead to locking of the faults with development of thrust faults where fault motion is translated into localized uplift and subsidence. The pattern is seen in the Valjean Hills and eastward to the Kingston Range. In the northern part of the Shadow Mountains, late Tertiary conglomerates are folded in a broad anticline about an east-west-trending axis (Shadow Hump).

East of the Dumont Dunes, northwest-striking faults, largely right-lateral, of the Shadow Mountain shear zone intersect northeast-striking, left-lateral faults of the Crystal Springs fault zone. Where the fault zones intersect, several fault segments that trend roughly east-west and top-to-the-south reverse slip occur. The reverse faults adjacent to the Valjean Hills place Late

Proterozoic Kingston Peak Formation over Cambrian and late Tertiary sedimentary rocks, but extensive Holocene sand blankets obscure the detail on these faults. The reverse fault near the west end of Kingston Wash cuts late Tertiary conglomerate and eolian deposits that may be early Quaternary.

The Kingston Range, a prominent topographic and tectonic feature of the southern Death Valley area, is underlain by granite in most of the area shown in Fig. 6. Kingston Granite shows intrusive contacts on the north and east sides but on the west the granite is bounded by northwest-striking faults with evidence of right-oblique slip (McMackin, 1992). The granite can be divided into a quartz and feldspar porphyry facies and an aplite facies; both contain mafic inclusions.

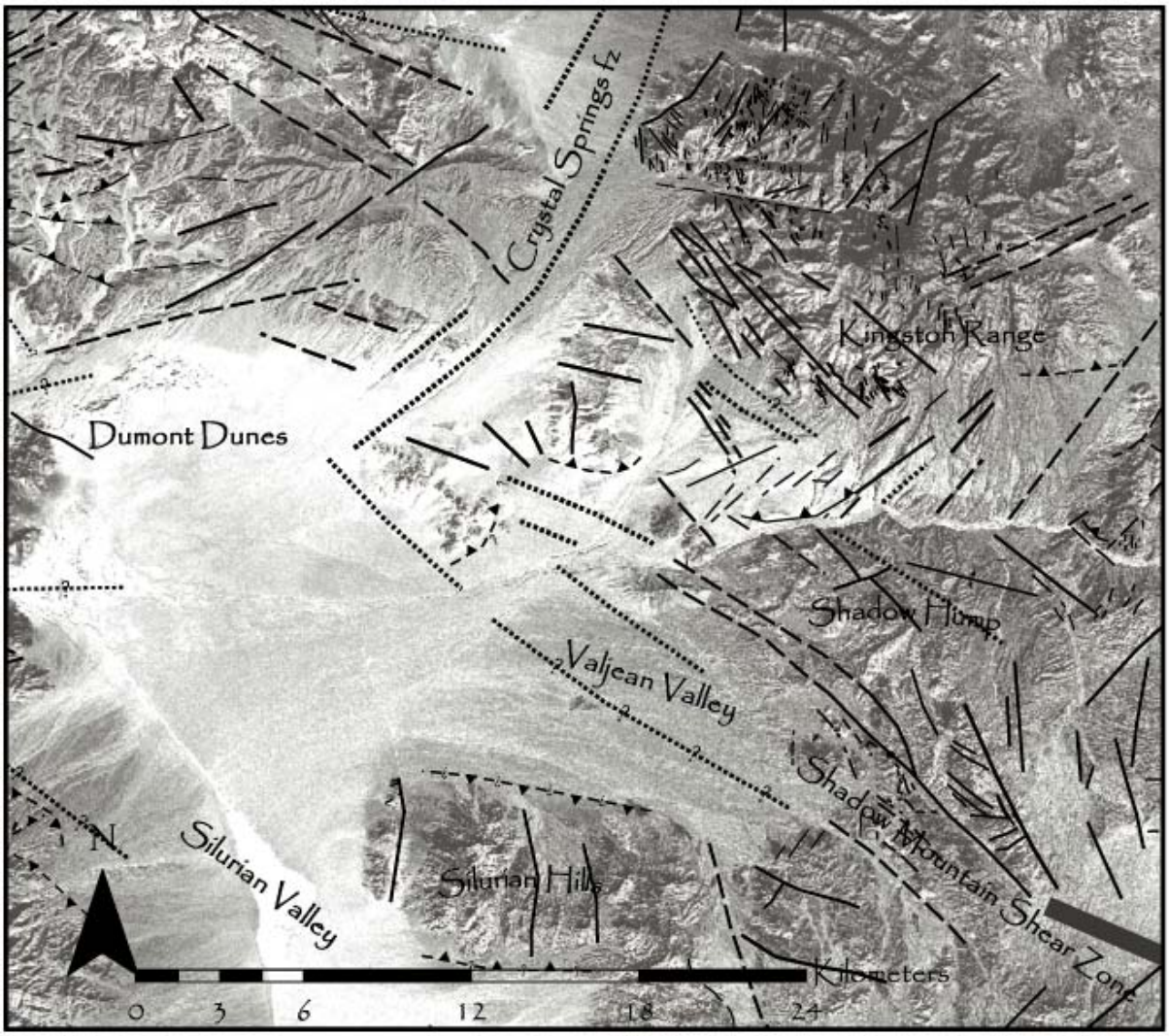

Figure 6. Generalized map of faults related to Quaternary landscape, showing major branches of the Shadow Mountain shear zone where its faults intersect northeast-striking faults in the southwestern Kingston Range. Based on unpublished mapping by McMackin. Solid line, well-located fault; dashed line, uncertain location; dotted, concealed. Sawteeth on hanging wall of thrust fault.

Calzia and Ramos (2000) reported K-Ar ages of 12.1 to 12.4 Ma for biotite and hornblende in the feldspar porphyry facies. Zircon from the northwestern part of the Kingston Granite yielded a fission-track age of 12.3 ± 0.4 Ma, while apatite from the same area yielded a fission track age of

9.1 ± 0.7 Ma (Topping, 1993). Topping suggested that the apatite age marks uplift of the granite and cooling to moderate temperatures.

The quartz and feldspar porphyry facies of the Kingston Granite is widespread in the northern and eastern parts of the range. In the southwestern part of the range, the granite contains more mafic inclusions, some tens of meters across, and the feldspar porphyry is interlayered with sills of biotite–rich granodiorite with feldspar porphyroclasts (unpublished mapping, McMackin). The granite and granodiorite facies forms a stack of sills with comagmatic textures suggesting that magma-mixing was ongoing. Lister and Baldwin (1993) predicted the formation of stacked sills in syntectonic intrusions formed during crustal extension. Their interpretation was that thinning of the overlying crust reaches a point where the confining pressing exerted by overlying rocks decreases to approximately the fluid pressure of the intruding magma, resulting in uplift and intrusion of layers of magma parallel to Earth's surface.

In the northern and eastern Kingston Range, detachment faults thinned upper plate strata at approximately the same time the granite was emplaced. The granite cuts the detachment fault in several places suggesting the emplacement of the granite stopped movement on the detachment fault in the Kingston Range while low-angle faults continued activity in the Mesquite Mountains and Alexander Hills. Much of the post-12 Ma faulting is associated with strike-slip faults, vertical displacements on high angle faults, and distributed shear (McMackin, 1992).

The range-bounding fault on the southwest side of the Kingston Range exhibits oblique right slip, with down to the west displacement. Normal dip-slip seems to occur on secondary faults oriented approximately north-south (McMackin, 1992). The larger northwest-striking faults are shear zones with multiple sub-parallel fault planes and pervasive brecciation, defining zones tens to hundreds of meters wide. Some of the northwest-striking faults caused foliated granite, suggesting the faults may have initiated in the granite shortly after crystallization and while temperatures where high enough to permit ductile flow of the granite. Faults within the granite generally appear to be inactive since late Tertiary but parallel faults west of the range cut older Quaternary deposits and may be associated with the western bounding fault.

The northwest-striking shear zone between the Kingston Range and Valjean Hills has matched piercing points in Late Proterozoic rocks that indicate a minimum of 12 km dextral offset. There are no constraints on the amount of early Quaternary slip along faults in the Valjean Hills but some eroded scarps in older alluvial deposits have 2 to 3 meters of relief.

Extensional fault models invoke isostatic rebound as a mechanism to explain the uplift of the Kingston Range. As an alternative, McMackin argues that the uplift could be produced by local contraction along the southern margin. This might be similar to the thrust faults flanking the Avawatz Mountains (stop 2-3). The result was rapid uplift of the granite consistent with Topping (1993), Freidman (1999), and McMackin (1992).

Return to Hwy 127, and turn north.

Hwy Mile 24.2 [**570660 3938125] Turn right** onto a short paved section, drive to the end of pavement and park near a pile of white talc. Walk east to Salt Creek where a few acacia trees grow next to a prominent cut bank (Fig. 7) [**571215 3938240]**.

STOP 1-3. Toe of boulder deposit at Salt Creek: At this position, we can examine stratigraphy and deposit characteristics for the distal part of the Kingston Wash boulder deposit. Here, the deposit lies along an abrupt, scoured contact on a thin-bedded sequence of gravelly sand that represents wash and distal fan deposits. Boulder size is less than at the previous stop (Fig. 4), but

cobble to pebble fractions are similar in size, suggesting that the transportation mechanism for boulders differed from the matrix. Diminished height of flow in the broad distal fan is a likely cause for decreased boulder size. Note that thin-bedded sand, silt and fine gravel under the boulder bed is of two provenances, as indicated by clast composition and cross-bed orientation. Beds bearing Kingston Granite and marble clasts have west-dipping cross-beds and represent distal fan deposits. Mixed-provenance beds bearing a fraction of dark plutonic rocks from the Avawatz Mountains have north-dipping cross-beds and represent Salt Creek wash deposits. These relations are well exposed in a tributary to Salt Creek about 80 m south of here.

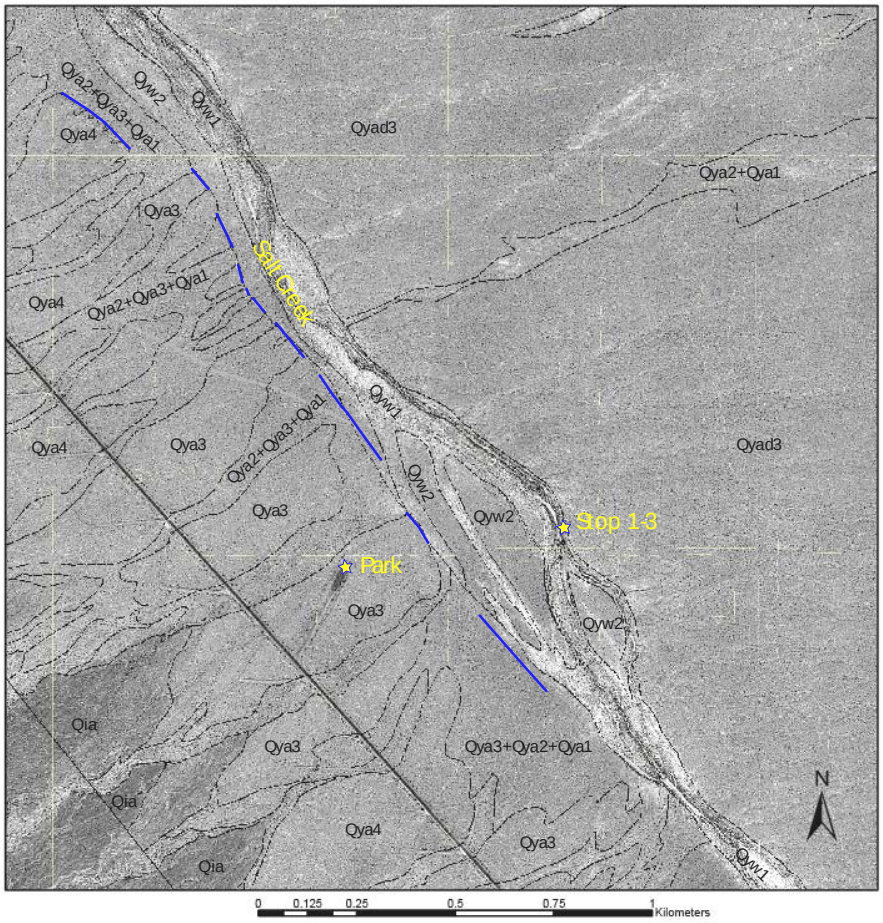

Figure 7. Map of wash geometry, deposits associated with alluvial fans, and cutbanks of Salt Creek at Stop 1-3. Stop location is the site of OSL samples (see text). Heavy lines represent cutbanks against Qya4 (15-9 ka) and Qya3 (~6-3 ka) fan deposits along west side of Salt Creek. Deposit types denoted by third letter in symbol: Qya = alluvial; Qyw = wash; Qyad = alluvial debris flow. Complex areas of multiple units are denoted with plus (+) symbols, with most abundant first.

The short, steep-banked side channels to Salt Creek here attest to the youthful age for incision, as do inset terraces of probably latest Holocene age. We collected samples in wash sediment below the boulder bed at this location to determine optically stimulated luminescence (OSL) ages (Mahan et.al., Chapter C, this volume). Because the boulder deposit may have been transported under cloudy or turbid flow conditions, there is a distinct probability of inadequate grain bleaching during the depositional event. In order to mitigate this possibility, we sampled

underlying fine-grained beds. We collected two samples in stratigraphic order, from 15 to 25 cm below (and the second bed below) the boulder deposit and from 105 cm lower, and 9 depositional units below the upper sample bed. The upper sample yielded 4,912 ± 328 years and the lower yielded 5,283 ± 243 years (K-feldspar from IRSL); the lower sample was checked with blue-light OSL and yielded 4,982 ± 161 years. We interpret the ages as indicating a time span between the two samples of about 100 to 1100 years, or a rate of deposition of about 10 to 100 years per bed. This allows us to suggest that the debris flow is about 20 to 200 years younger than the upper dated bed, or 4.4 to 5.2 ka.

Do climate records offer insight for this fluvial event? Paleoclimate clues for this ~5 ka timeframe are provided by Koehler and others (2005), based on analysis of plant and pollen remains in packrat middens in Silurian and Shadow Valleys. The transition from the mid Holocene thermal maximum to the late Holocene wetter and cooler period roughly coincided with the timing for the boulder deposit, suggesting that either a climate transition with a possible change in vegetation cover or the beginning of a wetter climate episode with more rain storms triggered the large volume deposit. However, Koehler and others (2005) also established that Shadow Valley experienced an unusual period of intensified summer monsoon storm activity during the end of the thermal maximum (approximately 5.6 to 5.2 ka calibrated ^{14}C) based on the presence of agave in middens. This period of monsoon activity roughly coincides with the Salt Creek wash and distal fan deposit record at this location, raising the additional possibility that summer monsoon events triggered the large-volume boulder deposit.

We were intrigued with the possibility that Silurian Lake might have formed in part owing to damming from the boulder deposit emplacement, and sought to test that hypothesis by dating playa beds immediately below a subtle lacustrine bar at the north end of the playa. The age of ~6.5 ka (Mahan et.al., Chapter C, this volume) seems too old to account for bar development associated with fan events.

There is an intriguing juxtaposition of a seemingly small axial wash and apparently massive and catastrophic boulder deposit emplacement here at Salt Creek. Did the axial valley wash shift in position, aggrade, or otherwise change to accommodate the emplacement of this huge deposit? We think not. The map relations (Fig. 7) demonstrate that cutbanks along the wash are preserved not far downstream on the Avawatz side, providing a limit on lateral wash migration, and no boulder deposit remnants exist on the Avawatz side, suggesting little or no aggradation. The beds that underlie the boulder deposit here are partly wash origin, as attested by mixed clasts and imbrication, so the long-term position of the wash is essentially its current location. It appears that the wash moved neither laterally nor vertically in response to the emplacement of the boulder deposit, which implies great base-level stability in this reach of Salt Creek. As a result, the geomorphic drivers for fan aggradation in this case are clearly hillslope delivery systems. The ability of a small wash system like Salt Creek to accommodate major depositional and flood events with little geomorphic record of disturbed stream profile, damming, bulging westward, or any other effect suggests that some, and maybe most, desert geomorphic systems are highly resilient.

Return to Highway 127 and drive south to Silurian Lake.

***Potential* STOP 1-4. [576200 3930410] Silurian Lake spits dating to 850 years:** Drive to southeast end of the lake, park next to the low spit with shrubs.

This bar at the south end of Silurian Lake is a long, broad feature that shows little sign of erosion; a few small channels cut through it and carry flow from Salt Creek to the playa, but

cutbanks are sharp and little rounding of the surface is apparent. The bar is composed of thin bedded to laminated fine gravel and sand in moderately- to well-sorted parallel beds. Little evidence for illuvial silt or sand is present, so we dated a silty sand bed 38 cm deep, and recovered an IRSL age of 952 ± 229 years, surprisingly young (see Mahan and others, this volume, for more information). To test whether we inadvertently sampled a burrow or other disturbed sediment we re-sampled 5 m distant in a gravelly sand bed beneath the bed previously sampled, at a depth of 45 cm. The second sample yielded similarly young ages of 733 ± 119 and 953 ± 206 years on duplicated dates. If IRSL methods are reliable, as the excellent replication suggests, the southern bar is about 800-850 yrs old (Mahan and others, Chapter C, this volume). Timing of the lake stand is similar to that of a flood event bracketed by extreme droughts in the record of Walker River (Stine, 1994) and Carson Sink (Adams, 2003) in northwest Nevada, among several examples, and offers support for widespread flooding in arid environments at this time.

The nearly-straight lower Salt Creek aligns with the northeast margin of Silurian Lake to form an intriguing lineament in Silurian Valley. Its origin may be tectonic, based on the fact that the playa sediment is greater than 30 m thick (Anderson and Wells, 2003) and Pleistocene fans grade smoothly from Valjean Valley to the playa margin. Because the flat playa is incapable of transporting alluvial fan bedload, and the Holocene fan is not aggrading, it would appear that Silurian Lake must be down-dropping relative to the fan. The linear boundary argues for a fault or steep kink-like flexure. However, no structure has been identified during geologic mapping. Lateral migration of the playa due to eastward progradation of the Avawatz fans is unlikely to cause this relation, as the Valjean fans have not aggraded as would be necessary with lateral playa migration and aggradation. Holocene fan materials do not bury the Pleistocene fans on the Valjean side of the playa.

DAY 2

Depart camp, drive to Highway 127 and turn south.

Hwy Mile 16.1 Pull off on the right (west) side of the highway, being sure not to block traffic. Be careful, as large trucks drive this highway constantly! [575610 3926205]

STOP 2-1. Warped and faulted Pleistocene surfaces and deposits, and soil characteristics, on south Avawatz piedmont: implications for tectonics. *[See Chapter E, Green and others, Chapter E, this volume, for more information]*

Walk up the desert pavement surface about 460 m to the west to a shallow pit, where we will discuss soils and tectonics. A pit in the desert pavement Qia deposit is at [575157 3926121].

Pits in early Holocene Qya4 deposits are located about 500 m farther up the pavement, and then 325 m north across incised Qia deposits with inset terraces: [574547 3926348].

Soils. Several soil pits were constructed in the alluvial fan to examine the relation of soil development to surficial characteristics of three ages of alluvial deposits. There is the expected progression of soil development and profile development indices from the oldest to the youngest deposits, as established by inset geometries and surficial characteristics. The oldest of these fans has unusually weak soil development for its associated surficial characteristics when compared to

other deposits in this part of the Mojave Desert. This may reflect a young age for the deposit, a slowed rate of soil development and carbonate accumulation at this site, or natural variations in soil development within a single deposit.

Tectonics. The tectonic study examined a northwest-aligned zone of deeply incised deposits several kilometers up the fan. These deposits are early to late Pleistocene and exhibit anomalous dips, numerous fractures, and a few faults and scarps. The orientations of the scarps, most fractures, and three thrust faults are subparallel to the alignment of incised deposits. Most structures here can be explained by a blind thrust fault. Regionally, the Avawatz fan is located in an area where the primary structural interactions are poorly known. This area is a transition zone from the Mormon Spring thrust fault to the Soda-Avawatz dextral-slip fault. If complex oblique slip in the north is partitioned in the south, a blind thrust fault on the Avawatz fan could represent the thrust component and the Soda-Avawatz fault the dextral component.

Middle to late Pleistocene deposits are fractured, faulted, and folded. Although we found no faults cutting latest Pleistocene alluvium (Qya4), this unit is deposited in entrenched channels within the uplifted Pleistocene deposits, where it forms flights of 2 to 3 terraces with much greater vertical separation than is observed on other parts of the piedmont. These data suggests that rapid incision of the channels was occurring, and/or that deformation was continuing, in latest Pleistocene time (15-9 ka) time.

A new analysis of Quaternary faults in the northern Mojave Desert (Chapter H, Miller and others, this volume) suggests that the Soda-Avawatz fault zone, leading from Soda Lake to the mountain front you see to your west, is one of just three active zones of faulting. However, little evidence for Holocene fault activity exists north of Soda Lake. The potential for latest Pleistocene deformation on intra-fan blind thrusts and folds suggests that some or all of the strain may be accommodated in folding and faulting within Silurian Valley, not along the Pleistocene fault trace. Distributed small structures may be much harder to identify.

Return to the cars, and turn carefully on Hwy 127, driving north. Drive past the turnoffs to Stop 1-2 (Valjean piedmont) and Stop 1-1 (Salt Spring Hills overlook) of Day 1. Continue past the bend in road toward north-northwest and begin a descent into southeastern Death Valley along the distal piedmont of the Avawatz Mountains. The broad low-relief floor of the valley traversed by the highway consists of a Holocene to Recent channel fan, with several distributary channels, that is part of the Amargosa River axial drainage.

Hwy Mile 29.8 Turn left on Harry Wade Exit road [564250 3943480] . This graded gravel road heads west generally down the southern margin of the valley floor, coincident with the southeastern border of Death Valley National Park. The road suitable for high-clearance vehicles (both 2W and 4W), continues for 25 miles down southern Death Valley, where it intersects with California State Highway 178 near Ashford Mills.

1.8 miles. Turn left [561508 3944518] on the road heading up Sheep Creek fan, apart of the northern piedmont of the Avawatz Mountains, the steep rugged range front in the middle distance. To the right (north) of the turnoff is the southern margin of a channel fan within this un-incised reach of the Amargosa River axial drainage. The Sheep Creek fan road traverses a complex mixture of gravelly active channels and Holocene fans for the first 1.2 miles. This section of the road is locally very bouldery and rough, and, while not requiring 4W drive, can be very difficult to negotiate in low clearance sedans or vans. It would be best for participants in sedans, and those

vans with low clearance or long wheel bases, to park to the right just past the turnoff and car pool in a more suitable high clearance vehicle for the remainder of the day. The prominent white spot just below the mountain front at the head of the dark colored Pleistocene fan is a mine-working located very near Stop 2-3.

3.6 miles. Stop near prominent rock cairn [560041 3942066] to the left (east) of the road, along a crest of Pleistocene fan exhibiting a fairly flat surface with pronounced desert pavement and dark-toned well developed varnish on most clasts. Park along both sides of the road without completely obstructing the road, if possible. Do not turn around, as after this stop we will be continuing up this road to the head of the fan.

Walk approximately 70 m east and congregate for the Stop 2-2 discussion along the nearest (west) margin of the prominent deep gully incised into this fan (just below (north of) the gully confluence).

STOP 2-2. Sheep Creek fan [560110 3941990]: We will examine the topography, surficial deposits, and soils associated with a mid-Pleistocene fan on the Avawatz Mountain piedmont, and discuss the significance of these characteristics for unusual patterns of incision within the fan relative to the adjacent piedmont.

We have just walked across the surface of a fan correlated with the mid-Pleistocene Qia3 unit of the regional stratigraphy summarized in *Introduction, Table 1*. This correlation is based on the well developed pavement, strong varnish on suitable clast lithologies, degree of clast weathering on susceptible rock types, and relative position of this unit within the local suite of adjacent surfaces on the piedmont.

However, there are a few aspects of this unit that are uncharacteristic or even anomalous for most Qia3 deposits in the area. For example, the soils in this deposit are less well developed than those typically associated with Qia3 deposits in this area, including less soil depth, and weaker development of argillic and carbonate soil horizons. The soil characteristics observed here more closely resemble those associated with younger Qia2 deposits. Also, although most Qia3 units in the region exhibit some degree of internal dissection, the amount of incision producing the very deep, wide and steep walled gully at our feet is very unusual for this type of unit. This degree of fan dissection is especially unusual on fans with such a relatively low degree of surface degradation on wide almost-flat interfluves. For example, this gully has incised 7.0 m below this surface in a 20-m-wide canyon with extremely steep, commonly subvertical gully walls. This extreme level of dissection is strictly limited to the internal area of this and a few other fans on this piedmont. For example, notice the relative similarity in heights (within 1.5 m) between the margin of this fan and adjacent unincised active channels and Holocene surfaces. Also, the depth of incision in these intrafan drainages rapidly decreases to a similar low value of less than 1 to 2 m where they exit from this Qia3 unit.

The explanation for the unusual internal dissection and retarded soil characteristics may lie in the character of the deposits exposed in the canyon walls. A close inspection of these deposits reveals a large percentage of fine-grained sand, silt, and clay in the common matrix-rich beds. Many beds are tabular bodies with little or no internal stratification indicative of fluvial transport and deposition. Overall, these characteristics suggest deposition by debris flows and hyperconcentrated flow mechanisms. The fine textured matrix in this fan is typically very dense and hard, and thus acts similar to low permeability cement that significantly reduces the

infiltration of precipitation falling directly on the fan surface. Instead, these sediment characteristics tend to enhance and promote surface runoff. This increased discharge in the absence of increased sediment loads or gradient changes tends to increase erosion and dissection along intrafan drainages. The reduced surface infiltration would also inhibit downward transport and translocation processes required for soil development. This proposed mechanism does not require invoking some unusual combination of external factors not observed on correlative units in the region. Rather, it is based on atypical material properties that produce significant process changes via a series of internal feedback mechanisms.

Return to vehicles and continue on the road toward the Avawatz Mountains to the head of the Sheep Creek fan.

5.4 miles. [558520 3939655] Stop at the head of the fan in the graded area near the talc waste rock, so noticeable earlier from the base of the road. Carefully turn around and park in the graded area, and if necessary, on the adjacent fan surface, taking care to minimize disruption of the surface away from the mine site. This is the parking area for lunch and the remaining two stops of the day. Walk upstream to Stop 2-3, located approximately 200 m to the southwest, at the broad mouth of the smaller canyon immediately above the parking area (**not** the main canyon mouth of the Sheep Creek drainage further west along the continuation of this road).

Overview, Stops 2-3 and 2-4 on the Northern Avawatz Mountain Front. The final two stops of the day will examine evidence for active contractional deformation as the primary structural mechanism for uplift of the Avawatz Mountains along the steep northern and eastern topographic escarpments of the range. Specifically we will look at a suite of excellent exposures in the walls of gullies incised into uplifted alluvial fans at two localities along a 1.5-km section of the range front at and east of the Sheep Creek fan and drainage. In these exposures, Quaternary surficial deposits are tilted, fractured, and locally faulted in patterns interpreted as reflecting deformation in fault-propagation folds above a series of shallow-depth blind thrust faults. At several places emergent thrust faults displace bedrock over Quaternary alluvium. At the end we will summarize temporal and spatial patterns of deformation and discuss their implications for the structural evolution of the Sheep Creek section of the frontal thrust fault system and resultant range-front morphology in this tectonic setting.

Tectonic Framework. The Sheep Creek thrust complex at this locality is part of a system of thrust faults that form the structural boundary between the northern and eastern range fronts of the Avawatz Mountains and the southeastern and northwestern margins of Death Valley and Silurian Valley, respectively (Fig. 8). These thrust faults were first identified as the primary range-bounding structures in geologic mapping of the Avawatz Mountains by R. Jahns and L.A. Wright (as shown by Jennings and others, 1962.**)** Brady (1984) studied late Tertiary to early Quaternary deformation related to the intersection of the Garlock and southern Death Valley fault zones. His map compilation included significant mapping from B.W. Troxel, who also made his unpublished mapping available to us. A map of the intersection zone incorporating the work of Troxel and Butler, reported at FOP 1986, is in preparation for publication by USGS.

These workers recognized that the Avawatz thrust faults were clearly active in the Quaternary, based on exposures of basement rocks thrust over Quaternary deposits along a major strand of the range-bounding fault zone they named the Mule Spring fault. This geologic mapping forms the basic data source for significant parts of the neotectonic compilations we

summarize here. The magnitude and recent age of uplift and exhumation of the Avawatz Mountain block bounded by the thrust- system was confirmed by a recent study by Reinhart and others (2003). They used apatite (U-Th/He) age-distribution data from the range block to infer rapid block uplift commencing no earlier than 7.1 Ma at exhumation rates of 0.27 mm/yr.

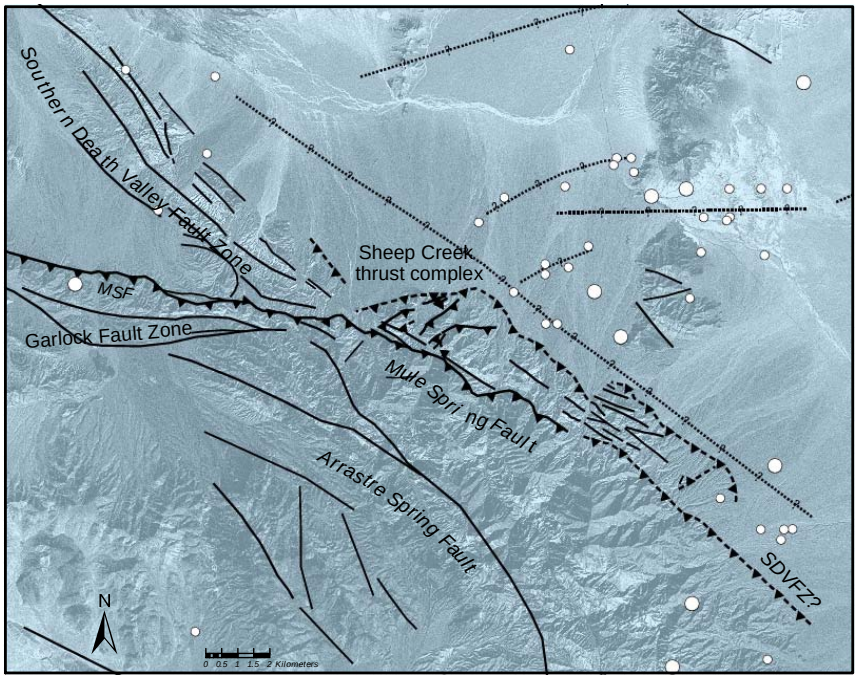

Figure 8. Generalized fault map of the northwest Avawatz Mountain front showing major faults. White dots represent historical seismicity. Based largely on mapping by Brady (1984) and Troxel (unpublished mapping.) Stops 2-3 and 2-4 are located below the word "complex."

The arcuate trace of the Avawatz Mountains thrust fault is situated just east of the intersection between two major regional strike-slip fault zones, the northwest-striking right-lateral southern Death Valley fault zone (SDVF) and the east-striking left-lateral eastern Garlock fault zone (EGFZ). This intersection, as well as the adjacent Avawatz Mountain thrust and any continuation of right lateral faulting to the southeast, is generally considered the approximate eastern boundary of the eastern California shear zone in this area (Dokka and Travis, 1990; Miller and Yount, 2002). The nature of this intersection and possible resultant terminations of these fault systems has been a subject of debate that has relevance for interpretations of the Avawatz thrust system. Early compilations indicated that the SDVF terminated against the EGFZ (Jennings and others, 1962), but subsequent studies have proposed that the reverse is true (Brady, 1984). In particular, Brady (1984) noted that the Mule Spring fault strand of the EGFZ merges directly into the SDFZ, which appears to continue to the east as an interior strand of the Avawatz Mountain thrust system (Fig 8).

Brady (1984) emphasized the importance of transpressional uplift to the termination of the EGFZ against the SDVF in producing uplift of the Avawatz Mountains and generating a southwest-to-northeast directed contractional strain across the boundary. For the Mule Spring fault, he collected slickenline data that showed left-oblique slip on the steeply-dipping western strand of the Mule Spring were it merges with the EGFZ and dip-slip where the EGFZ terminates into the Avawatz thrust complex. This suggests a fundamental transition in structural geometries, style, and mechanics of the fault in this transition and it also suggests that at least some slip is

transferred between the intersecting faults. The Arrastre Spring fault in the interior of the range block has no evidence of significant Quaternary activity (Spencer, 1981) and is clearly truncated by the Garlock fault. Apparently there is no slip transfer in that case, and the Arrastre Springs fault is kinematically isolated and presumably an inactive fault, even though it is parallel to faults on the eastern range front.

Bedrock Geology. This part of the Avawatz Mountains is composed largely of Mesozoic intrusive rocks, chiefly a quartz monzodiorite complex of variable composition including diorite, quartz monzodiorite, granodiorite, granite, and quartz monzonite (Spencer, 1981). K-Ar dating by Spencer (1981) yielded variable, somewhat equivocal results suggesting a minimum age of 176 Ma. Analyses of Rb-Sr from monzodiorite near Sheep Creek yielded an age of 195 $\pm$ 35 Ma, indicating that much of the quartz monzodiorite was homogenized with respect to strontium at that time. The quartz monzodiorite comprises the bulk of the hanging wall of the Mule Spring Thrust within the Avawatz Mountains. It is also constitutes a significant lithologic component of detritus in the alluvial fans in the piedmont below the thrust front, as noted earlier at Stop 2-2.

Rocks within roof pendants include gneiss (1.38 Ga) and Proterozoic to Paleozoic sedimentary rocks. Of particular interest are rocks of the Late Proterozoic Crystal Spring Formation, which includes arkosic sandstone, diabase sills, and talc. Triassic metavolcanic rocks are also observed on the west side of the range, and may be included in the float among the very abundant diorite clasts from the east slope of the Avawatz Mountains.

The older sedimentary rocks near here are in the footwall of the lowest bedrock thrust fault exposed in this complex. Locally the footwall of this thrust also contains fault-bounded blocks of late Tertiary fine- to coarse-grained clastic sedimentary rocks with locally interbedded evaporite beds generally correlated with the middle to late Miocene Military Canyon Formation as defined by Brady (1984). Commonly these rocks are highly brecciated and (or) internally deformed. See Mendonça (Chapter F, this volume) for more information on these units and their structural relations.

Structure and Topography of the Sheep Creek Section of the Avawatz Mountain Front. Bedrock and surficial geologic mapping in this area reveal that the structural boundary along this section of the northern Avawatz Mountain front consists of numerous individual thrust faults that interact with Quaternary alluvial fan and terrace deposits (Fig. 9). The surface traces of these faults commonly define elongate to lozenge-shaped fault blocks that collectively form a convex outward frontal fault system. As a result, the range front is a complex landform of recesses and salients in the bedrock range front. In cross-section, most of these faults dip steeply to moderately to the south toward the Mule Spring thrust, which is the innermost strand of this imbricate fault system in the range block interior.

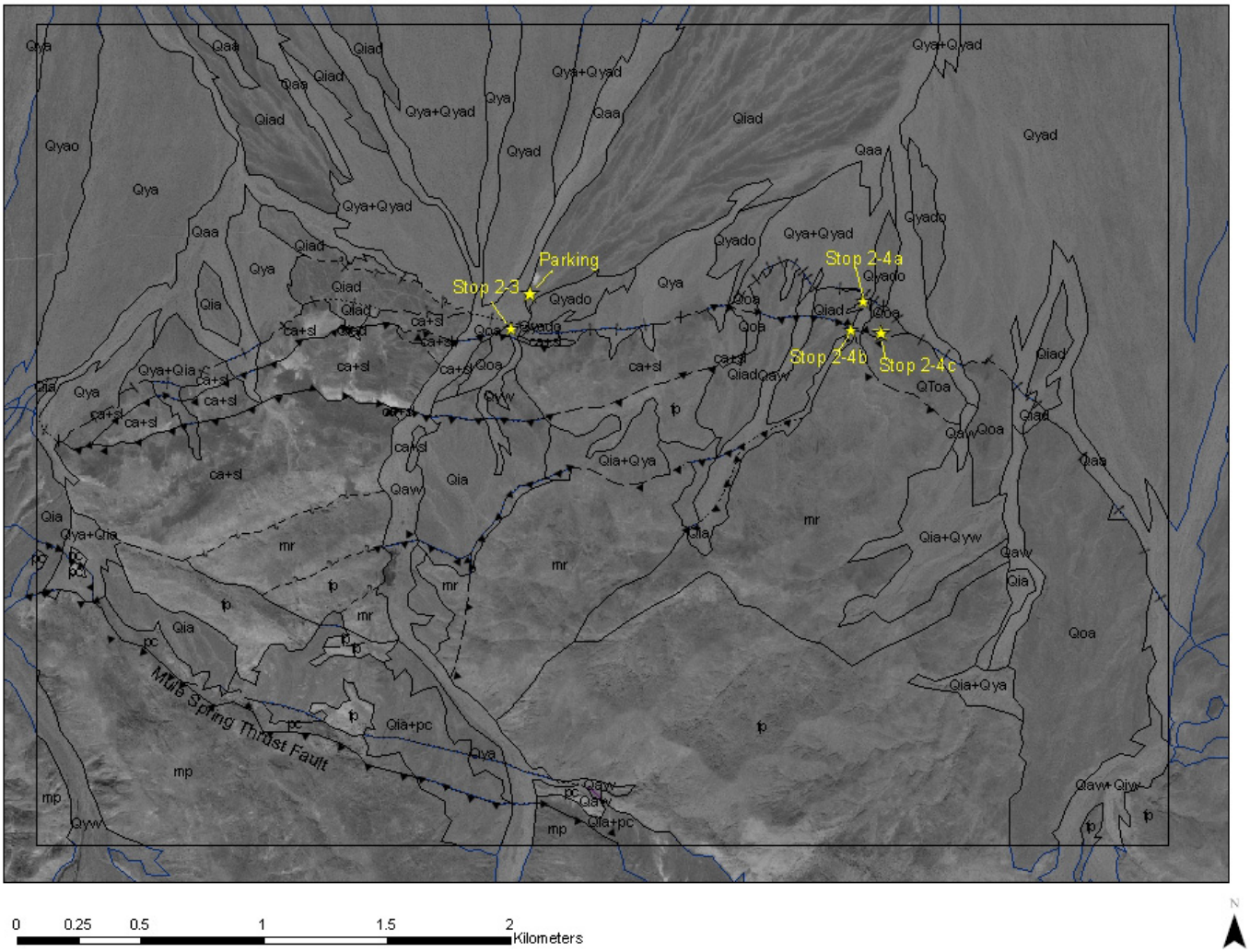

Figure 9. Geologic map of the northern mountain front of the Avawatz Mountains, in the vicinity of Sheep Creek drainage and fan and Stops 2-3 and 2-4 of fieldtrip. The map shows simplified surficial units, structural features, and bedrock geology generalized in generic rock types. The locations of specific stops and locations referenced in the roadlog are shown in yellow. Specific surficial units include: Qaa (active depositional systems on fans), Qaw (active washes), Qya and Qyad (Holocene alluvium and alluvial debris flows, respectively), Qyw (Holocene wash deposits), Qyao and Qyado (mid to early Holocene alluvium and alluvial debris flows, respectively),Qia and Qiad (Pleistocene alluvium and alluvial debris flows, respectively), and Qiw (Pleistocene alluvial terraces in washes). Complex areas of multiple units are denoted with plus (+) symbols, with most abundant first. Generalized bedrock units are: fp (felsic plutonic rocks or granitic gneisses), mp (intermediate to mafic plutonic rocks), mr (foliated metamorphic rocks), ca+sl (mixed carbonate and siliciclastic sedimentary rocks), and pc (partially consolidated sedimentary rocks). Individual structures are shown in solid (certain), dashed (approximate), dashed with question marks (approximate and queried), and dotted (concealed), with following symbology on linework: sawteeth (thrust and reverse faults, teeth on hanging wall), arrows (fault propagation folds above inferred blind thrust faults, arrow in direction of forelimb dip direction); solid lines, no symbols (high-angle fault, sense of slip undetermined).

There is close correspondence between the surface traces of individual thrust faults and the overall stepped topography associated with the range front. Many of these relations occur elsewhere along the Avawatz Mountains (e.g., Mendonça, Chapter F, this volume). That is, successive fault zones within the bedrock range front commonly occur at the base of steeply sloping topographic steps or escarpments varying in height from 20 to 400 m; the largest and

highest of these interior bedrock escarpment rises on the hanging wall above the Mule Spring thrust. The fault blocks between successive fault strands and associated escarpments generally underlie subhorizontal to gently sloping benches that vary from 0.1 to 3 km in width. The upper surfaces of most of these benches are associated with a beveled bedrock surface that is dissected by deep canyons oriented transverse to both internal fault zones and the range-front escarpment.

In many places, the outer basal margin of the range front is overlain by a variable thickness of alluvium that appears to be uplifted and dissected remnants of alluvial fans and channels (Fig. 9). The soils and surface characteristics of most of this capping alluvium on the structural benches suggest correlations with Qia3, Qoa, and, in places, Qia2 units in the basin. In many places, the alluvial mantle, or correlative colluvial debris fans at the base of the interior escarpments, overlie without disruption the subjacent surface traces of intra-bedrock faults of the Avawatz thrust complex. These relations indicate the absence of activity on these interior faults within the range front since deposition of the capping surficial deposits.

The character and form of the outermost (relative to mountain block) basal step or scarp of the range front varies spatially, including the Sheep Creek section. End members include: (a) alluvial tectonic scarps of varying heights developed at the margins of uplifted alluvial fans or terraces that are commonly associated with basinward-convex salients or bulges in the bedrock range front; and (b) large steep fault-bounded bedrock escarpments that are generally linear, located in range front re-entrants, and have either no, or few, narrow internal structural benches. We will see many variants of these basal escarpments between the two stops visited in this afternoons hike.

STOP 2-3. [558447 3939512] At this stop we will look at range-front deformation of bedrock and Quaternary gravels at the mouth of a tributary canyon, just east of the canyon mouth of the Sheep Creek drainage. We will first summarize the general stratigraphy and structures within the outcrop, as illustrated in Fig. 10, and interpret their relevance to the style and progression of surface deformation at the outer bedrock range front. Then we will briefly describe the general setting of this exposure within the range front and discuss relevance of structures to the style and history of surface deformation along this part of the range front.

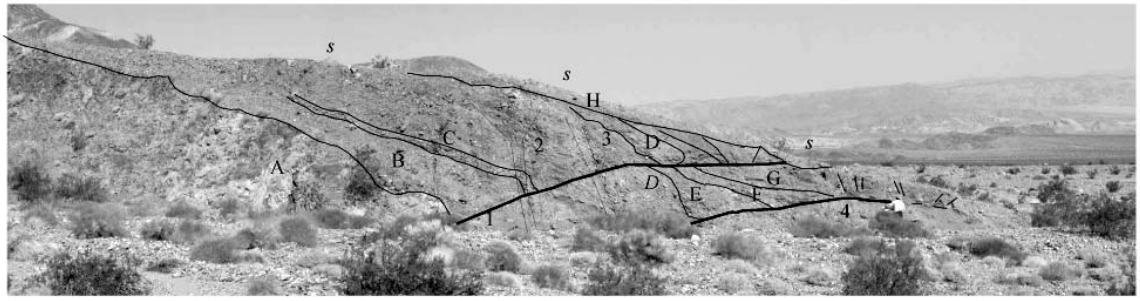

Figure 10. Annotated profile showing the main features of the cut bank section exposed just east of the mouth of Sheep Creek Canyon. See text for description of features.

Stratigraphy. The stratigraphic units exposed in the primary outcrop are subdivided into three main groups. From left to right, these include bedrock overlain by two major packages of surficial deposits consisting of a primarily alluvial sequence overlapped by several draped, wedge-shaped accumulations of colluvium (Fig. 10). Both the bedded alluvial deposits and the underlying basal contact on bedrock have a pronounced basinward (north) dip, consistent with the general direction of wedge thickening and taper in the overlying colluvium.

Bedrock. The bedrock is composed largely of the old sedimentary rocks that occur only in the footwall of the outermost bedrock thrust, which is exposed approximately 100 meters up the canyon as a fault zone approximately 50 m thick. The overall form of the upper bedrock contact at this stop, although irregular in detail, defines a distinctly sloping surface generally concordant with bedding of the overlying alluvium.

Unit A: Alluvium. The sediment deposited on bedrock exhibits characteristics associated with alluvium. These include moderately to well-defined bedding, poor to locally moderate sorting, subrounded to subangular gravels, and a diorite-rich assemblage of clasts commonly exposed in nearby hills. Thus, the present bedding dips of 25° to 35° require post-depositional tectonic rotation of the bedrock and alluvium package. Correlation of unit A with the regional stratigraphy (Introduction, Table 1) is difficult, but most of the unit resembles Qoa paleochannel deposits exposed in the canyon to the south (see below). This unit is subdivided into several variably distinct subunits based on secondary variations in some of the characteristics described above. Unit A1 includes a few lensoidal gravelly channel-like bodies inset into bedrock that grade upward into a prominently bedded sequence with the most diagnostic alluvial characteristics. To the right (north) are several groups of less well bedded matrix-rich sediments disrupted by thrust faults with characteristics more typical of alluvium, but with some affinities to the superjacent colluvium of unit B.

Unit B: Colluvium. Reddish-brown deposits that overlie Unit A in the upper and northern sections of the outcrop can be distinguished not only by color, but also by less well defined bedding, a greater percentage of fine-textured matrix, and a more compositionally diverse clast assemblage derived from remnant fan deposits capping the higher ridge to the south. Most subunits also display pronounced wedge to sigmoidal geometries typical of deposition as colluvial wedges on developing scarp faces. Many of the units are deposited adjacent to and appear subsequently deformed by thrust faults. These colluvial deposits are provisionally correlated with Qia3 alluvium in the region based on similarities in color, degree of induration, stratigraphic relations, and amount of deformation.

Deformation. All of the units in this exposure are deformed by several structures related to the range-front uplift.

Basinward rotation. Basinward rotation of bedded alluvium of Unit A and its underlying bedrock is a prominent deformational feature in the outcrop. The degree of rotation of Unit B colluvium is more difficult to establish due to uncertainty in the primary depositional dip of these hillslope deposits.

Thrust faults. Two partially overlapping thrust faults are interpreted from variably distinct ledges, creases, and planar disturbed zones that transect stratigraphic units across most of the outcrop. These faults ramp upward and outward (northward) from the left base of exposure at 20° angles that decrease < 5° where they terminate or feather out before rupturing the bounding scarp slope. Bedrock appears to override alluvial deposits at the exposed base of the upper thrust. Displacement amounts and slip orientation have not been determined due to lack of marker units and absence of slickenline data.

High-angle fractures and fissures. At least three large and several smaller fractures and (or) fissures cut the deposits and thrust faults at high to moderate angles in several zones distributed across the outcrop. Two particularly well developed steeply north-dipping fissures with upward flaring walls and local fissure fill cut across tilted beds of Unit A and the upper thrust without detectable displacement in the center of the exposure. To the right are several moderately south dipping fractures that appear to ramp from and crosscut the tip of the lower thrust below the

lower scarp face. These features are interpreted to reflect bending moment adjustments in the hanging wall as it translates above a curving fault surface beneath the outcrop level. These features cut all exposed thrust faults, which requires movement on a younger subjacent buried thrust fault.

Structural interpretations. The relations between tilting and thrust faulting are interpreted as fault propagation folds developed above shallowly buried blind thrust faults. The steeply dipping strata and bedrock formed in the forelimb of this fold. The general geometry, spatial distribution and cross-cutting relations of the two exposed and the proposed subjacent blind thrust faults suggest the progressive development of faults in an active thrust stack, prograding basinward, even at this outcrop scale along the base of the range front. The fracture zones rising from the lower thrust in this exposure cut the overlying thrust suggesting that a thrust or set of thrusts at given structural and elevation level either decrease in activity or deactivate as a new blind thrust develops in the subsurface and propagates outward toward the basin. This process in effect extends the base of the scarp basinward as formerly buried alluvium and toe-slope colluvium is uplifted and (or) folded in advance of the outward propagating tip of the buried thrust fault. At the same time, in a situation like this, where the successively developing thrust faults are closely spaced together, formerly buried early developing thrust faults are uplifted and exposed, and possibly back-rotated towards the range front, on the hanging wall of the currently active blind thrust. Slip on this subsurface fault also produces the high-angle fracturing and fissuring through the upper plate; the presence of these features in this outcrop suggests significant curvature on this fault that is consistent with the proximity of this outcrop to a major zone of thrust faults at the base of the large bedrock escarpment to the east.

Relations to the mountain front. This outcrop is located on the dissected remnant of the lowermost outer fault scarp, defining the steeply basinward sloping boundary on the right (north) side of the exposure, developed along the base of the range front escarpment at this locality (Fig. 10). The scarp rises at an angle of 18° to 19° to a height of 13 m above the channel and at the active part of the fan at its base. Correlative units to those in the outcrop are not exposed below the scarp. This scarp forms the outer margin of a gently sloping to subhorizontal bench, mantled by a thin gravel cap, cut discordantly across both steeply dipping alluvium and highly fractured bedrock. Above this bench is another steeply sloping ridgeline that probably represents another highly eroded scarp above a steeply south-dipping reverse fault locally exposed in shattered bedrock in the canyon wall. To the south, above this upper scarp and fault zone, is another narrow bench, capped by fan deposits, that merges southward into a highly dissected set of alluvial fan deposits. These fan deposits are generally thin and overlie an uplifted structural bench consisting of bedrock and an older suite of Quaternary alluvium that is well exposed as an uplifted paleochannel in the walls of the canyon to the south of this outcrop. These fans and their associated surfaces continue southward without disruption across several older reverse faults exposed in a subjacent bedrock bench, before merging with unfaulted debris fans at the base of another escarpment within the mountain front generated by pre-fan reverse faulting at its base. Thus these fans represent the remnants of an earlier piedmont uplifted and stranded by the faulting at and adjacent to these outcrops on the present range front. The soils and surface characteristics of these fans suggest correlations mostly with Qia3 units, except for a local cap of Qoa deposits on the high ridge above this exposure. The age of the underlying alluvium in the canyon is uncertain, but is likely at least Qoa age or older. Collectively these relations suggest that sometime after deposition of Qoa units, probably during the Qia3 depositional interval, thrust

faulting responsible for range front development migrated northward from the base of interior escarpment to its present position near this outcrop. This fault migration uplifted the former basin-margin depositional system above the intervening structural bench, initiating drainage incision and introduction of quartz monzodiorite clasts marking the establishment of drainage from the quartz monzodiorite core of the range.

Return to vehicles and prepare for a 1.4 km walk to the next stop. The best route involves angling gradually down to the nose of the fan salient. At the salient nose, note the moderately dipping alluvial deposits exposed on the east side of the scarp. Climb up and across another fan until reaching the mouth of the final canyon at the east side of the uplifted alluvial fan.

STOP 2-4a. [559840 3939627] We will examine the main active zone of deformation and uplift at the current outer margin of the range front. In particular we will discuss the morphology and origin of the alluvial fault scarp, stratigraphic evidence for fault propagation folding, and stratigraphic constraints on surface deformation at this site.

Outer alluvial fault scarp. We are standing at the approximate projection of the main fault scarp across this drainage. This is the northeastern edge of this scarp where it forms the outer (northern) margin of the uplifted alluvial fan on this small salient in the base of the bedrock range front (Fig. 9). The total height of the scarp is 24 m to the upper surface of the fan where it was measured approximately 50 m to the west of this spot. The maximum scarp slope is 26°, but this value probably is anomalously high because of undercutting by a fan-margin stream.

The morphology of this fault scarp is compound, containing a pronounced bench on the upper part of the scarp, at a height of 14 m. This scarp bench appears to merge to the southeast into a distinct strath terrace high on the west margin of this canyon (we will see this terrace at the next substop, 2-4b). This bench and terrace probably records an earlier stage of development of the scarp and associated uplift and resulting incision of the fan prior to northward migration of deformation and establishment of the scarp at its present position. This pattern is consistent with the model of outward stepping fault and scarp propagation developed at the previous stop.

This scarp is clearly tectonic, as we discuss here and at later stations at this stop. However, it is difficult to use the morphology of this scarp to estimate many paleoseismic parameters such as displacement amounts or surface-rupture ages in the manner commonly applied to scarps on mostly normal faults in the Basin and Range province (e.g., McCalpin, 1996). For example, the height of the scarp is only a minimum value because nowhere along its base is a lower original surface exposed correlative with the upper original surface of the fan due to deposition of younger alluvial fans along the entire length of the feature. In fact, the location of the measured height in an interfan low area was selected as the *largest possible* scarp height in this area, but even this value is a minimum. Secondly, the topographic profile across this scarp, including the maximum slope angle, cannot be used for morphologic analyses of scarp degradation for estimation of age of fault displacement ages, including diffusion or linear regression analyses developed and applied to many normal fault scarps in the Basin and Range province (e.g,, Bucknam and Anderson, 1979; Nash, 1980; Andrews and Bucknam, 1987). The problem lies in a fundamental assumption of steeply dipping surface rupture as an initial condition for scarp degradation. As evidenced in the previous stop and in the next series of substops, the causative thrust faults are very shallowly dipping and commonly blind, which implies a commonplace absence of discrete surface rupture anywhere on the scarp face itself. Even worse, these topographic features are really not fault scarps, *sensu strictu*, but more properly considered

fold scarps, in that their morphology and evolution is directly related to the progressive development of the forelimb of fault propagation folds that underlie the scarp slope, and only indirectly to rupture on the subjacent blind thrust-fault systems.

Fault propagation folding of surficial deposits. There are good exposures of tilted surficial deposits in the gully walls behind the canyon mouth. On the west side, approximately 30 m south of the outer scarp, is an exposure of light-colored deposits with variable but distinct bedding that dips 20° northward in the same direction and orientation as the outer scarp (Fig. 11). Close inspection of these deposits indicates a generally similar clast composition comprising mainly intermediate plutonic rocks of the Avawatz Mountains monzodiorite with a significant component of felsic granitic gneiss. The fine textured matrix varies among units from sparse to abundant (e.g. Units B and C vs. units D and E, respectively; Fig. 11), suggesting mixed depositional modes for the sequence ranging from debris flows to alluvial fan and channel environments. This is also supported by the irregular shape of individual units ranging from tabular to lenticular, with significant thinning and wedging suggesting local channelization and scour, perhaps similar to the channel or distributary fan environments. These environments require tectonic rotation of deposits with original shallow dips to the present moderate dips. We infer this rotation to reflect their position on the forelimb of a large fault propagation fold above a blind thrust fault responsible for producing the nearby outer fault scarp. However, unlike the previous stop (2-3) this section lacks the continuous high-angle fractures and fissures.

From here, walk approximately 20 m to the southeast and note the steeply dipping dark green well-bedded alluvium exposed at several locations along the channel wall beneath remnants of inset Holocene terraces and fans. These deposits are very distinctive in several ways compared to other surficial deposits. The clast component is predominantly composed of dark green, chloritized Avawatz Mountains monzodiorite assemblage with a general absence of the granitic gneiss clasts observed in the previous outcrop. As at Stop 2-3, this contrast of clast compositions is presumed to mark the headward erosion of evolving drainages across the Mule Spring fault. Notable are the persistent steep northeast dips (40° to 55°) of strata rotated in a forelimb of the same fault propagation fold and blind thrust described earlier.

Figure 11. Annotated profile for Stop 4a. Units and features are described in the text.

Age constraints on range front deformation. This site provides some stratigraphic constraints on age of deformation. The range-front deformation at this and the previous stop clearly involves all Pleistocene and older units. The steeply rotated dark green deposits are the oldest and most strongly deformed unit with Quaternary affinities. The unusual clast assemblages, relative position, and degree of deformation suggest a correlation with Qoa deposits, and they may be even older. The age of the light-colored deposits in the first outcrop we examined is difficult to estimate, but the degree of induration and position relative to the capping alluvial Qia3 deposits, associated with the uplifted fan above the scarp, suggest these units are Qoa, although they could be older elements of Qia3 as well. The Qia3 deposits here, as well as elsewhere along the front, are typically deformed and uplifted along scarps related to the outer fold-thrust system.

Minimum constraints on range-front deformation in this area are provided by the inset Holocene terraces and fans on the east side of the main channel, above the outcrops of tilted dark green deposits. These include several low terrace levels near the channel correlated with Qya3 units. Further east adjacent to the east wall of the canyon is a prominent higher terrace with soils and surface characteristics similar to the Qya4 unit. All of these terraces and fans continue without disruption across the projected trace of the range-front deformation. Elsewhere along the front there is equivocal evidence for small scarps on Qya4 type deposits. Thus, the most recent surface deformation on the frontal fold-thrust system is estimated to precede or possibly occur within the latest Pleistocene time range of the Qya4 unit.

Walk approximately 125 m to the south up this channel along exposures of moderately indurated alluvium generally similar to the sediments exposed near the front in the previous stops. Note the change in dips southward from the front into the range block: from steep north, to subhorizontal, to south dips. This folding represents at least 10° of net tectonic rotation toward the range-block interior, relative to the present 3° to 4° northward slope of the present channel. This fold is interpreted as representing an active fault propagation fold on the present range front discussed at the previous substop (2-4a). Also note the numerous high-angle fractures developed in these rotated strata, with the highest density at or slightly south of the crest of the fold. The fractures are interpreted as bending moment fractures related to post-depositional fold development.

Continue up the canyon until reaching the location of the pronounced channel bifurcation. This is the location of substop 2-4b.

STOP 2-4b. [559830 3939500] We will examine thrust faults, well-exposed in the canyon wall, (Fig. 12) to consider their geometric and temporal relations to the deformation at the range front. Below are summaries of the major alluvial stratigraphic units displaced by the thrust faults in the western canyon wall, followed by descriptions of key structural features.

Stratigraphy. The stratigraphic units exposed in the west wall of the canyon to either side of the thrust faults are divided into four major groups. These include bedrock restricted to the hanging wall and three sedimentary sequences displaced by the thrust fault and lying beneath the alluvial deposits of the uplifted Qia3 fan.

Bedrock. Highly fractured granitic gneiss is exposed in a small area between the top of large colluvial talus cone and the base of alluvium on the hanging wall of the thrust faults at the south end of the canyon wall. Similar bedrock is not exposed anywhere within the canyon on the footwall side of the faults. However, outcrops of fractured gneiss are nearly continuous beneath the alluvial fan deposits in the canyon walls to the south of the colluvial debris near the fault.

Threrefore, the thrust faults form the northern structure bounding the bedrock bench underlying Quaternary deposits of the uplifted alluvial fan.

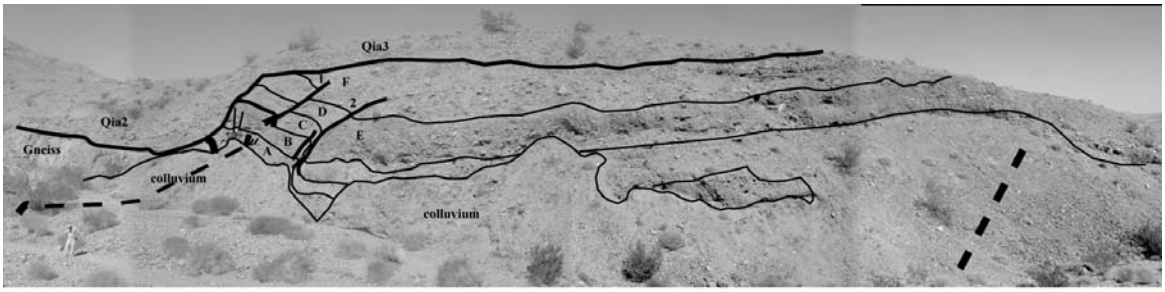

Figure 12 (above). Annotated profile for Stop 4b. Units and features are described in the text.
Figure 13 (below). Unannotated photographs of left part of Figure 12. Note faster-than-light human for scale.

Units A to D. A sequence of sediments subdivided into four variably distinct subunits, labeled A to D up section, are well exposed on the hanging wall above the top of the colluvial debris slope at the base of the wall. Gravel clasts in this poorly bedded sequence contain a mixed assemblage of Avawatz Mountains intermediate plutonic rocks and granitic gneiss. Variable amounts of fine-grained matrix relative to gravel suggests a mixture of alluvial and debris flow deposits. Generally similar deposits with similar textures and proportions of clast lithologies occur near the base of the exposure and are provisionally correlated with the upper three units (units B-D) in the hanging wall of the thrust faults.

Unit E. This unit consists of a poorly- to moderately-bedded alluvial sequence with clasts of predominantly granitic gneiss and an unusually small percentage of monzodiorite rocks of the Avawatz Mountain assemblage. This unit only occurs on the footwall beneath the northern lower thrust fault. A variety of textures from gravel rich to gravel poor are distributed throughout the unit, with more gravelly alluvial units concentrated near the thrust fault bounding the unit on the south. Several lenticular gravel layers truncated against the thrust fault pinch out to the north in a pattern suggesting faulted half-channels.

Unit F. This deposit is the uppermost unit in the sequence exposed in the canyon wall beneath the alluvial gravels associated with the Qia3 fan and terrace. The unit is a poorly bedded sequence of sand and gravel, and is present on both sides of the fault.

Deformation. The most prominent structures exposed in the wall are two subparallel thrust faults that dip southward at angles of 45° to 55° (Figs. 12, 13). The faults displace units A through E in

the middle and lower part of the wall, but disappear in the middle of the highest unit F at the top the wall. The vertical separation is much larger on the lower thrust fault, which is the master structure of the pair of faults. Stratal dips appear to decrease upsection and the half-channel bodies in unit E only occur on the footwall, relations that strongly suggest shallow growth faulting. In outcrop, the lower fault is associated with a well-defined narrow zone of gouge and brecciation.

Units displaced by the faults are sharply deflected into the fault by tight drag folds in the footwall and broader bending on the hanging wall. Units A through D in the hanging wall dip progressively more steeply to the north approaching the fault; this geometry is consistent with drag folding, but given the observations presented elsewhere in the area, more likely is related to forelimb development on a fault propagation fold. Footwall strata generally dip south, and are interpreted as back-tilted on the backlimb of the fault propagation fold formed by slip on the inferred blind thrust system to the north at the present boundary of the range front (described in Stop 2-4a).

Timing constraints on deformation. An undeformed gravel cap associated with a Qia3 terrace bench overlies all of the stratigraphic units and structures exposed in the western canyon wall. The thrust faults cannot themselves be traced directly upward to the terrace gravels, and the gravels disconformably truncate the rotated and folded underlying strata deformed by the thrust faults. This terrace is related to the initial incision of the main Qia3 fan as it was uplifted on the frontal scarp and associated blind thrusts. These relations clearly indicate a cessation on this inner set of thrust faults during or prior to the initiation of deformation on the active range front to the north, and require a basinward migration of thrust faulting on a scale of hundreds of meters.

A small bedrock outcrop at the confluence of the two streams contains an excellent exposure of a south-dipping thrust fault that places highly-sheared and fractured bedrock in the hanging wall against alluvial deposits in the footwall (Fig. 14). The thrust fault in this outcrop projects directly to the northwest into the thrust fault on the western canyon wall and thus is correlated with this structure. On the hanging wall of this thrust, another distinct subvertical fault bisects the outcrop and appears to project into the thrust in the shallow subsurface. The two structures bound an intensely brecciated wedge of amphibolite that contrasts with highly-fractured granitic gneiss to the south of the steeply dipping fault.

Walk back down the canyon toward stop 2-4a, then climb up on the eastern Holocene terraces and walk to the base of a large alluvial scarp at the base of the mountain front on the east side of the canyon mouth. Climb up this scarp slope onto a gently south-sloping narrow alluvial bench, interpreted as a possible fault-bounded and back-rotated structural block. Note the large percentage of greenish diorite gravel littering the surface.

STOP 2-4c. [559950 3939495] We will view the uplifted fans along the range front salient and summarize key observations and our model for structural and topographic evolution of this part of the range front of the Avawatz Mountains.

Congregate on the western margin of the bench for an excellent overview looking west across the uplifted fan along the range front salient (Fig. 15). The canyon of the previous substops lies immediately below us, with the thrust fault exposures in the steep vertical face (stop 2-4b) on the left (south) and the dipping beds behind the outer alluvial fault scarp (stop 2-4a) on the right (north). Beyond the canyon is the dissected surface of the uplifted Qia3 fan. Note the benches and

Figure 14. Don't trip over this outcrop. Small outcrop exposing bedrock thrust over Quaternary alluvium in the stream divide at Stop 2-4b. View to southeast.

surfaces that reflect early stage dissection of the fan as it was tectonically uplifted at the range front. Beyond the main fan surface are several south-dipping higher ridges below the bedrock knobs in the distance. Note the progressive change in slope from the active channel to these highest ridges on the uplifted salient. That is, the northward slope of the progressively higher and older relict fans, terraces, and ridges decreases relative to the modern channel until the highest ridges in the distance have a reversal of dip to the south into the range block. This is interpreted as a visual record of progressive cumulative back rotation of the uplifted fan complex with time on the backlimbs of spatially overlapping fault propagation folds.

Key observations and model interpretations for the tectonic and topographic evolution of this part of the range front of the Avawatz Mountains include: (a) the contractional nature of deformation along the range front; (b) numerous structural blocks, locally capped by uplifted alluvium, commonly arranged in salients and reentrants; (c) the prevalence of thrust faults in uplifted bedrock blocks within the front; (d) basin-ward dipping beds on scarps at the modern margin reflecting fault propagation folding above blind thrust faults; stratigraphic evidence for lateral migration of the loci of active folding and faulting at a variety of scales, from outcrop to range front, that produces progressive encroachment of the range front into the basin.

Carefully climb back down the scarp and retrace the route west to the parking area at Stop 2-3. From there return to the campsite.

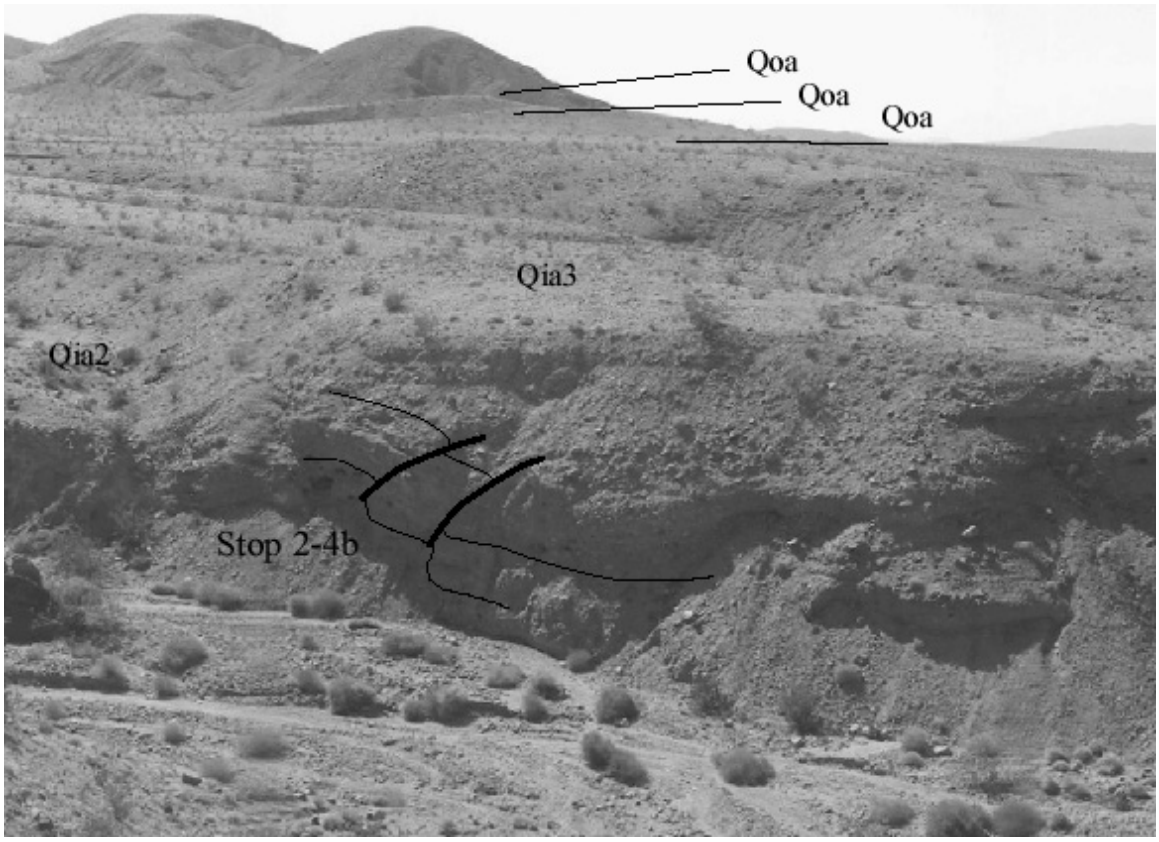

Fig. 15 Overview from Stop 2-4c**.** Note progressive rotation of fan surfaces associated with back-rotation on fault propagation folds.

DAY 3

Today we will visit the Tecopa Hump and look at geomorphic features and characteristics interpreted as relating to Late Tertiary to middle Quaternary tectonics associated with the Tecopa Hump. This feature is a northwest-trending elongate highland located between the Kingston Range on the east and Ibex Hills on the west (Fig. 1). The Hump forms the topographic divide between Tecopa basin on the north and the southeastern Death Valley–Silurian Valley lowland area on the south. The feature is breached by the Amargosa River where it flows through the Amargosa Canyon south of Tecopa. The crest of the highland area is complex in detail; it comprises a number of individual bedrock ridges, including the Alexander, Dumont and Sperry Hills interspersed between several highly dissected remnants of Tertiary basins (e.g., China Ranch basin). Topographic profiles across the Hump define a basic cross-sectional form characterized by a strongly asymmetric ridge with much greater relief (700 m) and steeper slopes on the southern and southwestern Death Valley side.

The bedrock geology of the Hump is remarkable by its very high degree of pervasive fracturing, which may promote distributed shear and quasi-ductile deformation as a mechanism of deformation. We will argue that deformation may be active, albeit at slow rates, and that the deformation has had a profound influence in the development of the southern side of the ridge. This day we will visit (a) the mouth of the Amargosa Canyon, where the river exits from the south flank of the Tecopa Hump, and with an overview of the Dumont Dunes, (b) a midslope stop on the southern flank of the Hump; and (c) a final overview stop of the field trip astride the Tecopa Hump near the northern entrance to the Amargosa Canyon.

Depart camp. Drive north on Highway 127 to the Dumont Dunes road. We will pass some of the turnoffs to the stops of previous days as we drive north past the western side of the Salt Spring Hills.

Hwy Mile 29. North of the broad turn into southern Death Valley, note the small sand dunes and sheets on the east side of the road, which comprise the southwest end of the Dumont Dunes. The main part of the dunes field lies to the northeast partly hidden by the northern end of the Salt Spring Hills.

Hwy Mile 30. Cross Salt Creek Wash, here incised to 3-4 m depths into the distal Avawatz Mountain piedmont on the south and a Holocene channel fan of Salt Creek on the north.

Hwy Mile 31.9. Cross one of the more active distributary channels of the Amargosa River, here on the southeastern margin of a broad late Holocene alluvial fan issuing from the mouth of the Amargosa River Canyon.

Hwy Mile 33.9. Turn right on the Dumont Dunes road and drive east to an area where the road takes a gentle bend around the edge of a high terrace, to the west of the canyon mouth where the river channel exits from the south flank of the Tecopa Hump. The road follows the broad tread of a Qia2 terrace of the Amargosa River, which near the parking site is inset into higher remnants of truncated Qia3 surfaces. Park on both sides of the road and walk up the sandy slope north of the road to the top of the dissected remnant of a Qia3 fan that formerly graded to a high Amargosa River terrace. This spot provides a vantage point to view the geology of the Avawatz Mountains where we ended our trip yesterday and to present the Tecopa Hump that will be the focus of today's stops. We'll also consider the geomorphology and fluvial stratigraphy of the Amargosa River in the context of the Hump and discuss the main Dumont Dunes across the river to the south.

STOP 3-1. Overview of the Tecopa Hump [565641 3950678]

Looking southeast, the Dumont Dunes flank the northern end of the Salt Spring Hills, beyond which is the Avawatz Mountain front, where Sheep Creek can be identified by the white talc waste stock pile at the mouth of the canyon. As we discussed yesterday, the Avawatz Mountain block is being thrust northeast over Quaternary fan deposits along the mountain-piedmont junction. In contrast, the Tecopa Hump to the north and east forms a smoothly sloping piedmont and pediment that continues practically to the Hump crest with no prominent mountain-front faults or steep fault-controlled range-front escarpment.

The Tecopa Hump is an informal name for a distinctive geologic structure that lies between the Ibex Hills, the prominent bedrock ridge on the skyline to the west, and the Kingston Range, the high range to the west. McMackin (1997) defined the Tecopa Hump as a contractional structure that forms a set of hills (including the Alexander and Dumont Hills on the southeast and the Sperry Hills to the northwest) with a complexly-faulted internal structure that is sheathed by a set of surficial deposits.

From the vantage point of this stop, the broad, nearly planar southern flank of the Hump is displayed. Later, we will drive over the Hump, where we can observe the crest of the Hump and a shorter north flank that is locally covered by intact Pliocene and Quaternary deposits of Lake Tecopa (Hillhouse, 1987; Morrison, 1999). The asymmetry of the Hump and lack of deformation

on the north flank are constraints for arguments one can make from observations on the south flank alone, and should be borne in mind at the next stop.

The Tecopa Hump is a late Tertiary feature, because much sediment exposed in canyons along the flanks of the Hump, including basin deposits and alluvial conglomerate, post-dates an 8.4 Ma volcanic ash bed. This sediment is modestly deformed by normal and strike-slip faults and associated block rotation. Quaternary alluvial fans correlated with Qia3 units are the oldest widely distributed surficial deposits across the Hump, but older deposits exist locally, including a Qoa fan that contains the Bishop ash (Table 1, Introduction, Menges and Miller, this volume). Many of the Pleistocene and early Holocene deposits form stair-stepped flights of terraces and (or) thin alluvial fans that overlie stream-cut strath surfaces beveled across the fractured bedrock. Much of the bedrock exposed by this progressive incision is related to a partially exhumed pediment flanking bedrock highlands in the core of the Hump. As described later, these suites of strath terraces and fans are associated with long-term Pleistocene and probably Holocene incision into rock that can be interpreted as a fluvial response to uplift or tectonic steepening of the slope.

The stream incision associated with the strath development is commonplace in most drainages developed on the crest and flanks of the Hump. It is most prominent on the steeper south flank and crest of the Hump, but can be traced a short distance (2 to 3 km) down the northern flank as well. Just east of this stop, however, incision along the Amargosa River has carved a deep canyon that crosses the axis of the Hump. This sub regional-scale interbasin river system is the only drainage that has breached the divide along the crest of the Hump. It has been suggested that a large paleolake filled the Tecopa basin and eventually overtopped at about 200 ka at the lowest point in a paleodivide that generally coincided with the crest of the Hump. The resulting outflow from Lake Tecopa at the breach point is considered responsible for carving the Amargosa Canyon (Morrison, 1999). One problem with the paleoflood overflow hypothesis is the absence of any discernable flood-generated deposit at this location near the canyon mouth cut by the proposed overflow discharge. Also, inset terraces of late Pleistocene Qia2 age and younger record progressive incision of the drainage through that time interval with no sudden spike in terrace or fan heights indicative of a major discrete dissection event. Interpretations of the incision history in the Amargosa Canyon based on ongoing mapping are that initial breaching and canyon cutting was more likely initiated sometime between Qia3 and Qia2 time by a less dramatic combination of groundwater-discharge sapping and uplift-driven headward erosion of streams across the paleodivide.

The basic sequence of surficial deposits is correlative with the regional climate-controlled stratigraphic framework of Table 1 in Menges and Miller (Introduction, this volume). Many of the deposits reflect deposition and incision related to climatically-driven perturbations in fluvial systems. Suites of deposits of varying ages occur at approximately similar elevation in the southwest corner of the Tecopa basin, where they are isolated from local base level changes related to the Hump or dissection along the axial drainage of the Amargosa River in central Tecopa basin. This contrasts with patterns on the Hump characterized by persistent vertical separation between stair-stepped sequences of these same units developed by incision through the surficial deposits into underlying bedrock, as will be demonstrated at Stop 3-2. These relations suggest that terrace formation is fundamentally controlled by regional climate change that is superimposed on a more continuous background incision into the substrate beneath terrace gravels, which is potentially related to deformation of the Hump. As will be discussed in more detail at Stop 3-2, the morphology, height variations, and distribution of terraces and incised fan surfaces display a distinctive pattern relative to the Tecopa Hump that is not consistent with

discrete surface faulting at its margin, but rather suggests uplift or warping at or near the apex region.

Dumont Dunes. *[See Smith, Chapter G]* The Dumont Dunes are a field of mixed dune types that formed on a mid-Pleistocene Qia3 alluvial fan surface. The Dumont Dunes are divided into two main dune fields. The main part of the dunes is a complex of star dunes located at the north end of the Salt Spring Hills. The southwest part of the Dumont dunes has a small field of transverse dunes. The sand supply is limited in southern Death Valley so that the accumulation of sand is particularly sensitive to orographic and climatic influences. Dunes change form and position seasonally, as demonstrated by repeat photography.

Interesting Bedrock: A snowball's chance in Death Valley. The bedrock ridge just north of this stop, known locally as Fatzinger Ridge, is composed of Neoproterozoic rocks of the Pahrump Group, including the dark red rocks of the Kingston Peak Formation overlain by buff-colored Noonday Dolomite. The dark beds at the top of the ridge are paleochannels filled with sandstones of the Johnnie Formation that marks the beginning of the transition into the siliciclastic units at the base of the Cordilleran miogeosyncline (unpublished mapping of B.W. Troxel.)

The uppermost Kingston Peak Formation and the Noonday Dolomite are part of the Neoproterozoic section thought to represent one cycle of the Snow Ball Earth. The Kingston Peak Formation is composed largely of debris flow deposits but locally it is capped by a discontinuous unit of diamictite, with cobbles and pebbles supported in a dark red matrix. Beveled and polystriated clasts in the diamictite make a good case for a glacial origin of these capping beds. They are overlain sharply by the Noonday, which is considered a cap carbonate. Here it is composed largely of algal laminated dolomite that forms large mounds. This section is interpreted as the rapid conclusion of a glacial event followed by a period of high atmospheric carbon dioxide leading to rapid development of the carbonate mounds. It is remarkable to consider that these rocks record extreme climate changes that perturbed the Earth System to the extent that the biosphere made the evolutionary leap from bacteria to metazoans, and the world's oceans experienced dramatic shifts in their isotopic composition.

Amargosa River Terraces. To the south is a prominent set of paired terraces and incised alluvial fans on either side of the Amargosa River. We are standing on a sand-mantled truncated remnant of a Qia3 alluvial fan derived from bedrock on the Tecopa Hump. This surface now stands 25 m above the Amargosa River, but was once graded to a high-level former channel of this river. This surface is approximately equivalent to the large incised coalescent fan surface underlying the Dumont Dunes across the valley. The vehicles are parked on an inset Qia2 terrace 4.5 m above the channel, and an equivalent inset Qia2 terrace is visible on the other side of the valley. Note the progressive change in height of the terraces and incised fan surfaces along the channel of the Amargosa River. The heights of both Qia2 and Qia3 surfaces decrease, or converge, toward the active channel, in the downstream direction away from the canyon mouth. In fact, the heights of both Qia surfaces eventually merge at the approximate level of the active channel downstream where the river crosses Highway 127. Note that the upstream divergence, or increase in height, of these terraces and fan remnants past the canyon mouth and into the southern bedrock flank of the Tecopa Hump. Although not visible, the zone of divergence increases to maximum approximately where the drainage crosses the paleodivide on the crest of the Tecopa Hump.

Stream down-cutting along a given reach can occur in response to a variety of external or internal fluvial factors. When observed within a suite of strath-floored surfaces, it commonly, but not uniquely, indicates that base level change localized in or near that reach (either fall or rise) is inducing persistent channel down cutting. However, the source of this base-level change must be carefully analyzed. The downstream convergence of terraces and straths indicates the absence of base-level fall in that direction, such as observed at the Avawatz Mountain front yesterday related to range-front faulting. Upstream terrace divergence of itself is not diagnostic of tectonic deformation, and is commonly observed between the piedmont and source areas of cut and fill terraces associated with climatically induced cycles of deposition and downcutting (Bull, 1991). However, bedrock incision and (or) divergence of flights of strath terraces is commonly related to vertical uplift in the system (e.g., Hamblin and others, 1981), although the individual fill terraces above the straths are likely climate controlled. The observed pattern of upstream terrace and strath divergence into and across the core of the Hump, including commonplace notching and gullying into substrate in the headwater divide areas, is best explained by uplift-induced base level rise in that region. Further note that the terrace divergence increases with increasing height both above the channel, which in a persistently down cutting environment can be a proxy for increasing age, as well as relative to each other. This fanning upward pattern is best interpreted as progressive steepening of older and successively higher fan surfaces and underlying straths related to tilting, warping, or folding centered in the direction of divergence within the core of the Hump. These topics will be further explored in the next stop along small drainage systems incised into the flank of the Tecopa Hump to the west.

Return to Highway 127. Turn right onto Highway 127 and travel up hill to the south.

Hwy Mile 39.6. [560973 3958891] **Turn left** across Highway 127 onto the graded dirt road that leads to the repeating station and park in the wide area below.

Mile 0.3. Park in the broad area around the microwave tower.

Stop 3-2. [560694 3958393] We will traverse north around this hill of highly fractured Tertiary granite into an embayment in the bedrock flank of the highlands to the north where streams are downcutting through a suite of surfaces into bedrock. The objective at this stop is to discuss the significance of stream incision for identifying and interpreting tectonic events, and consider the significance of rock fabric to the deformation processes.

Sperry Hills Granite, the makings of the matrix. The bedrock at this stop is known as the Sperry Hills granite. Topping (1993) calculated the age of this granite at 12.3 ± 0.4 Ma from fission-track studies of zircon. Calzia and Ramos (2000) reported a K-Ar age of 12.6 ± 0.6 Ma and also note that the granite is "modally, chemically, and isotopically equivalent" to the granite of the Kingston Range. However, a quick inspection of the granite exposed at this stop reveals the Sperry Hills granite is mechanically quite different from the granite of the Kingston Range.

As discussed at Stop 1-2, the presence of granite and basaltic volcanic rocks mixed with feldspar porphyry is characteristic of the granite in the southwest Kingston Range. The same rocks exist here, although highly fractured. In contrast, the peak to the northwest contains granite and Pahrump rocks more typical of those at Ibex Pass, where late Tertiary granite lacks the biotite-rich facies and is composed almost entirely of leucocratic granite. These two facies are interpreted to be in fault contact here. The fault is disarticulated, probably representing a strike-

slip fault that was deformed in a cross-cutting fault zone. A breccia fabric is pervasive in granite exposed to the east and northeast of this area, where brecciated granite is overlain by small, fault-bounded masses of highly brecciated Tertiary volcanic rocks, Early Proterozoic gneiss, arkosic quartzite, and diabase of the lower Crystal Spring Formation.

To the west, rocks are cut by late Tertiary reverse faults and a northeast-striking fault zone**.** The Saddle Peak Hills are composed mostly of the Kingston Peak Formation, here composed largely of iron-rich debris flow deposits that range from boulder conglomerate to shale. These are overlain by the buff colored Noonday Dolomite that caps the ridge and forms the prominent saddle that gives this range its name. The range block contains many listric normal faults, evidence of late Tertiary extension (B.W. Troxel, unpublished geologic map) and the faults are in turn intruded by dikes that yield a K-Ar age of 12.7 Ma (Calzia and Ramos, 2000). At the north end of the ridge, Proterozoic rocks overlie late Tertiary volcanic rocks on a south-dipping, high-angle reverse fault that bounds the north edge of the range block (McMackin, unpublished map). Biotite from a rhyodacite unit in the middle of the volcanic assemblage yields a K-Ar age of 12.3 ± 0.31 Ma (Calzia and Ramos, 2000.) West of Ibex Pass, a west-dipping reverse fault places Sperry Hills granite over the same volcanic rock. These antithetic reverse faults are dramatic evidence of late Tertiary contractional strains in the basement.

Topping (1993) interpreted this crushed granite as a rock avalanche deposit of exceptional size that was shed from the Kingston Range and then moved to this location by strike-slip faults. However, Prave and McMackin (1999) noted that the granite-bearing conglomerate in the Sperry Hills area is interbedded with late Tertiary basin deposits exposed in the Amargosa River Canyon and that sequence predates an 8.4 Ma tuff, so that the Sperry Hills granite was in place before 8.4 Ma. Also, alluvial fan deposits from the Kingston Range, containing the same 8.4 Ma tuff, can still be distinguished in the Alexander Hills at the eastern end of the Sperry Hills. An alternate interpretation is that the granite was translated to this position by strike-slip faults (McMackin, 1997) that pervasively fractured the mass.

Traversing northward around the hill we will cross several channels incised into a pre-Qia3 pediment. The pediment was cut into fractured bedrock exposed in the floors of the incised channels.

A speculative cause for uplift at this site is that trapped strain from a cut-off fault within the Sperry Mountain domain caused pervasive fracturing and folding. Widespread fracture flow in a transpressional setting between rigid range blocks may produce broadly distributed uplift in the Tecopa Hump. We have not been able to document any common form of deformation, such as faults or folds, so if uplift is occurring a distributive strain possibly is at play. We acknowledge that this model is not mechanically viable by conventional fracture and flow theory but offer it for discussion.

Relevance of bedrock incision to deformation. Steam incision and terrace development is relevant to interpretations of uplift or tilting on the flank of the Tecopa Hump. First, note that the depth of incision and height of incised fans has increased from zero at the intersection of the Dumont Dune road with the highway to a modest but significant depth of several meters in this area. Depths of incision continue to increase up the drainages almost to the drainage divide at Ibex Pass on the crest of the Tecopa Hump to the north. In contrast, on the more gently sloping north slope of the Tecopa Hump small drainages show depth of incision decreases and convergence to a null point of un-incised alluvium approximately 3 km north of the crest. Thus the pattern of terrace divergence again is maximized near the crest of the Hump, a pattern similar to that observed in the previous stop for the large terraces of the Amargosa River drainage.

Simple up-gradient terrace divergence is not always diagnostic of tectonic uplift or tilt. Many climatic terraces converge in the basin and diverge through nontectonic, or inactive, mountain fronts into headwater basins in the source area. Several other characteristics are required to establish a tectonic origin. One important criterion is whether streams are downcutting through terrace or fan alluvium into the underlying substrate and laterally planing to form a stream-cut surface, or strath, beneath the terrace or fan deposits. The presence of bedrock straths below terrace gravel deposits implies a transient establishment of an equilibrium stream profile interrupted or terminated by a disequilibrium condition that induces stream down-cutting below the strath into underlying bedrock. This bedrock downcutting is fundamentally related to various intrinsic fluvial adjustments to variations in sediment load and discharge that may or may not be associated with changes in external forcing parameters such as climate or tectonics (Bull, 1991; Whipple and Tucker, 1999; Whipple, 2004).

Another important terrace characteristic in this area is the presence of multiple strath levels and associated deposits that increase in height with progressive increase in age. This stepped sequence indicates persistent bedrock incision between strath-cutting intervals that is reestablished between successive individual climate-controlled cycles of alluviation and downcutting. Uplift is one mechanism that can produce long term bedrock incisions between straths. Downstream terrace convergence and cessation of incision eliminates downstream base level fall, such as fault-bounded or fold-generated valley-axis subsidence or linkage to actively downcutting axial streams such as the Amargosa River, which is aggrading in this part of the valley, as potential causes for the incision in this area. Any other nontectonic explanations require external and (or) internal disequilibrium conditions in the fluvial system conducive to bedrock incision that persist across a number of regional climate-driven cut and fill cycles over time intervals of hundreds of thousands of years, a time frame commonly associated with intermediate-scale fluvial responses to deformation (Burbank and Anderson, 2001).

Another characteristic suggestive of active uplift in the core of the Hump is the presence in the Ibex Pass divide area of beheaded surfaces isolated from source terranes by deeply incised transversely oriented valleys. These patterns are commonly associated with stream piracy or capture indicating dynamic adjustments of downcutting low-order tributaries in this part of stream network. This rearrangement requires some form of base-level change in the immediate divide area that, in the absence of linkage to externally downcutting higher-order parts of the network, is likely related to uplift across the Hump.

We note several other geomorphic and stratigraphic features in the region that place constraints or limits on any tectonic interpretations. For example, old undeformed deposits of Tecopa basin lie on the north flank of the Hump, enforcing a strong south-directed asymmetry not only to the topography but also to the tectonic manifestations that drive the bedrock incision. Although warping might produce this geometry, it is difficult to effect without disturbing the Tecopa basin. Likewise, southward tilting of the Tecopa Hump by block faulting should be marked by a fault north of the Hump, which is not the case. Another possibility is that deformation of Silurian and Death Valleys has acted to steepen the gradient on the south flank of the Hump. The exact tectonic mechanism in this case remains obscure. However, as noted previously, the divergence-convergence patterns of terrace incision requires that this flexure-related steepening be localized very near the divide region at the crest of the Hump. Lastly, it should be noted that the south flank of the Hump is a pediment, and pediments may undergo stream incision as a result of climate change reducing the rate of weathering into the underlying bedrock and increasing the rate of fluvial downcutting. Many pediments in the Mojave Desert exhibit bedrock incision by streams throughout the Holocene, and that effect may be contributing

to the geomorphology of the southern Tecopa Hump. However, the ubiquitous presence of flights of Holocene to Pleistocene terraces requires the repeated establishment of this climate-related stripping and incision mechanism across the feature throughout this time interval.

In sum, we propose that the overall stream incision patterns observed on the Hump, including stepped surfaces associated with bedrock straths, the divergence-convergence patterns, the local presence of fanning upward multiple surfaces, and local stream capture adjustments on or near the divide, are best explained overall by active uplift centered on the axis and southern flank of the Tecopa Hump or southward tilt and accompanying steepening of gradient. We recognize the non-uniqueness of this tectonic interpretation for any one or subset of these features, and indeed other nontectonic intrinsic fluvial or nontectonic external factors have undoubtedly influenced these patterns. The basic sequence of Quaternary terrace and fan veneer deposits is easily correlated with the regional climate-controlled stratigraphy of Table 1 (Menges and Miller, this volume) and summarized in Menges and others (2001) and Green and others (Chapter E, this volume); thus most of these units are likely fundamentally controlled by similar regional climate factors. Also, large-scale incision along the main-stem Amargosa River has induced enhanced dissection along all of its tributaries where the river crosses the Tecopa Hump and adjacent parts of the southernmost Tecopa basin. Nevertheless, tectonic uplift best explains the characteristics and distribution of bedrock incision and strath terrace development across the Hump. Additional work, including longitudinal profile analyses of terraces and channel networks and comparative studies with highland drainages in nontectonic areas to the northeast, are required to more confidently substantiate this interpretation.

Walk from the parking area up a channel at the mouth of a small embayment between bedrock knobs and hills on the south flank of the Tecopa Hump. This embayment at first appears to be mantled by several levels of alluvium. However, closer inspection reveals the presence of bedrock exposed at varying heights in the gully system. This area is actually a formerly buried bedrock pediment that is being stripped and cut by progressively down-cutting streams. Much of the bedrock exposure is related to incision beneath several levels of strath surfaces associated with different age surficial deposits. At this site we will traverse a stepped inset sequence of alluvial deposits, beginning with Qya3 deposits in washes and progressing up interfluves through Qya4, Qia2, and eventually Qia3 terrace and fan deposits. Basal stream-cut surfaces, or straths, beveled across bedrock are observed beneath all but the youngest Holocene terraces. Surface and strath heights increase in a generally similar fashion from 0.5 to 5 m within the embayment. We will also examine soil and surface characteristics (varnish and pavement development) that allow local differentiation and regional correlation of these units that support the inference of increasing age of surface with increasing height (i.e., incision depth) relative to active channels.

Return to highway 127. Turn left onto Highway 127 and drive north toward the crest of the Tecopa Hump.

Hwy Mile 41.5 Cross Ibex Pass, located on the crest and coincident with topographic drainage divide of the western Tecopa Hump. As you drive up the hill toward Ibex Pass, note the discontinuous exposures of highly fractured granite in the Sperry Hills to the right. Also note the pervasive incision into Tertiary granite and sediments beneath several stepped levels of alluvial units at and north of the divide. The low north-sloping surface to the right (east) of the highway immediately north of the pass is the beheaded remnant of a thin capping Qia2 gravel deposit, overlying Tertiary sediments, with the most likely source somewhere near the hills south of the pass and across the adjacent east-flowing incised drainage. A series of Qia3 surfaces and alluvial

deposits also isolated from any nearby source highlands cap the higher section of the divide to either side of the gap where the highway crosses the pass. The Ibex Hills are a north-trending bedrock ridge located across the intervening alluvial divide west of the pass.

Note: Highway mileage is reset to zero at the San Bernardino-Inyo County line at Ibex Pass. Mileage begins accumulating from zero entering into Inyo County.

Hwy Mile 3.2 This is undissected piedmont beyond the northern flank of the Tecopa Hump. Here Qia and Qya deposits are within 0.5 m of one another and the active channels.

Hwy Mile 4.2. This is the beginning of dissection through Qya and Qia alluvial surficial deposits into subjacent light colored, fine-grained sediments of the Tecopa basin. The depth of this dissection increases to the northeast in response to nontectonic base-level fall related to down cutting along the axial drainage of the Amargosa River in the center of the Tecopa basin.

Hwy Mile 6.5 Turn right from Highway 127 onto the Old Spanish Trail paved road. Follow signs to Tecopa Hot Springs.

Mile 3.4 The road traverses along the north edge of a gravelly facies of Tecopa basin fill at the southwest margin of the alluvial valley floor of the Amargosa River.

Mile 3.6 The road crosses the main channel of the Amargosa River just north of the entrance into the Amargosa Canyon.

Mile 3.8 Continue past the triangle T-junction in the center of "downtown" Tecopa. The road to the left (north) crosses the nearby Tecopa Hills to Tecopa Hot Springs, and continues northwest to eventually cross the Amargosa River again and intersect Highway 127, 5 miles south of Shoshone.

Mile 5.3 Turn right onto Furnace Creek Road toward China Ranch Date Farm. Note: The Old Spanish Trail highway continues east past this turnoff through upper California Valley into Pahrump Valley and eventually intersects Nevada highway 160. This route leads directly eastward over the Spring Mountains to Interstate 15 and Las Vegas.

Mile 7.1. **Turn right** (south) on the road to China Ranch Date Farm.

Mile 7.8 Park in the dirt lots to either side of the road just before it begins a steep drop into Willow Wash where the China Ranch Date Farm is located. Collect at the southwest edge of the pullout.

Stop 3-3. Tecopa Hump Overlook. This last stop is on the crest of the Tecopa Hump. From this vantage point, looking west, you can see the Quaternary surfaces flanking the Hump. In the valley below you can see some of the highly faulted bedrock that constitutes the core of the Hump. To the southeast are the Salt Spring Hills and the Avawatz Mountains, visited early during the trip. This is a good place to end our trip and sum up what we've seen and what it means. Most importantly, we hope you enjoyed your trip and that you learned something new about the geology of Silurian Valley and southern Death Valley.

We are standing on the surface of a late Tertiary to Quaternary fan complex shed from the Alexander Hills, which lie to the southeast, and this same surface continues south across Willow Wash. This fan contains unique clasts that can only be derived from the Alexander Hills on the other side of the Willow Wash canyon, so the age of the fan places an upper constraint on the initiation of canyon cutting on this major tributary of Amargosa River in the Amargosa Canyon area. The surface characteristics of the fan suggest that it is mid Pleistocene, Qia3, and from this point, looking west, you can see a similar fan extending eastward from the Sperry Hills. These fans merged in the low divide to our west during Qia3 time. The gradient appears to have been relatively low. You can see where these fans meet but note that the canyon of the Amargosa River is entrenched across the toe of the Sperry Hills fan. By all appearances, that was the drainage divide between the Alexander and Sperry Hills until the formation of the Amargosa River canyon.

The oldest common terrace deposits inset within the incised canyons are Qia2, although scraps of Qia3 strath terraces indicate that the progressive incision of the Amargosa began roughly at the end of Qia3 time. Numerous springs emerge in the valley below and it is also likely that incision was initiated by sapping and driven in part by spring-fed streams.

Several questions remain about the interpretation of Tecopa Hump. Among them are: 1) Do Quaternary sediments record a response to former deformation or ongoing deformation? 2) What is the geometry of deformation: asymmetric fold, tilt, or the sag of Silurian Valley? 3) Why is Tecopa Basin relatively high and old compared to Silurian and Death Valleys? We have made some of the observations that are key to resolving the origin of the Hump, but more work remains.

Synthesis

This trip sought to deliver to attendees the accessible high points of our studies directed toward understanding the neotectonic evolution of southern Death Valley and Silurian Valley. We have applied tools of geomorphology and Quaternary mapping to address the development of this anomalous low trough nested between adjacent highlands, its prominent bend at the Avawatz Mountains, and the characteristics of the faults.

The essential features of the trough are: a) Quaternary drainage captures of major catchments occurred; b) adjacent ground (such as Shadow Valley and Tecopa Basin) is high and generally contains old geomorphic elements, c) the trough is broad and lined by middle Pleistocene and younger piedmont deposits, d) narrow mountain belts transected by the trough descend to low elevations in the trough as if folded down, e) gravity data suggests thin or absent sediment accumulations in the trough during the late Cenozoic, f) the trough jogs at the point where the Garlock fault intersects it, g) drainage basin integration within the trough is still incomplete, and h) the trough parallels the easternmost faults of the Eastern California Shear Zone. These features strongly suggest youthful tectonic origin for the trough, but few folds and faults have been identified in or marginal to the trough. Adjacent to the trough are numerous complex Neogene faults that attest to a long tectonic activity of the area.

We demonstrated the following during this trip:

1. Drainages such as Kingston Wash in the Valjean Valley exhibit long-term stability, with major changes in sediment delivery having remarkably small impact on distal fan and axial valley (Salt Creek) systems.
2. Sediment delivery from small catchments was very low during the last century, as evidenced by ponded deposits behind the Tonopah and Tidewater rail bed.
3. Distal piedmonts adjacent to Silurian Lake are not stably aggrading, implying that Silurian Lake is down-dropping by a tectonic mechanism and that it is storing the piedmont bedload.

4. Avawatz piedmonts are deformed by blind thrusts as young as latest Pleistocene, raising the possibility that distributed, subtle tectonic features are present elsewhere in Silurian Valley.
5. The boundary thrust faults along the Avawatz Mountain front display valley-ward growth via arcuate sets of blind thrusts that step basinward beneath scarp-forming propagation fold sequences, all in middle Pleistocene sediment.
6. Along the south flank of the Tecopa Hump, drainages exhibit up-piedmont diverging terraces, many cut into bedrock, indicating a steepening of gradient in Quaternary time, possibly by uplift of the Hump.

We believe that these collective observations point to middle and late Quaternary tectonic activity of several styles in various places within the southern Death Valley-Silurian Valley trough. These observations greatly strengthen inferences from regional features such as the Eastern California Shear Zone for youthful tectonics, but they do not yet point conclusively to those tectonic mechanisms that produced the trough.

Possible tectonic mechanisms for the origin of the trough include (1) simple folding of upper crust, 2) thrust-fault loading and isostatic depression, 3) transpressional strain localized along the east margin of the Eastern California Shear Zone, and combinations of these. Because tectonism is localized within the trough and to the southwest, but not to the northeast, simple folding is inadequate. Because thrust faulting is only known near the Avawatz Mountains, thrust loading cannot be a general mechanism for forming the trough. We favor at this time that the Quaternary tectonism of the trough is related to downfolding and complex minor folding and faulting in a zone adjacent to the east boundary of the Eastern California Shear Zone. Particularly compelling evidnece is that the trough lies adjacent to the easternmost fault of the ECSZ, even following the jog in that fault where it encounters the Garlock fault zone. More detailed studies are needed to unravel the complete set of tectonic features, their histories, and their origins.

Unofficial Field Activities. We highly recommend a short trip to the end of this road to the China Ranch Date Farm, owned and operated by Brian and Bonnie Brown. They make spectacular milkshakes, date bread, and chocolate chip cookies, among many other products.

Acknowledgments

We are grateful to Shannon Mahan and Allison Duvall for careful reviews of this contribution.

References cited

Adams, K.D., 2003, Age and paleoclimatic significance of late Holocene lakes in the Carson Sink, NV, USA: Quaternary Research, v. 60, p. 294-306.

Anderson, K.C., and Wells, S.G., 2003, Latest Quaternary paleohydrology of Silurian lake and Salt Spring basin, Silurian Valley, California, *in* Enzel, Y., Wells, S.G., and Lancaster, N., eds., Paleoenvironments and paleohydrology of the Mojave and southern Great Basin deserts: Geological Society of America Special Paper 368, p.129-141.

Andrews, D.J., and Bucknam, R.C., 1987, Fitting degradation of shoreline scarps by a model with nonlinear diffusion: Journal of Geophysical Research, v. 90, no. 10, p. 12,857-12,867.

Brady, R.H., III, 1984, Neogene stratigraphy of the Avawatz Mountains between the Garlock and Death Valley fault zones, southern Death Valley, California: Implications as to late Cenozoic tectonism: Sedimentary Geology, v. 38, p. 127-157.

Bucknam., R.C., and Anderson, R.E., 1979, Estimation of fault scarp ages from a scarp-height-slope-angle relationship: Geology, v. 7, p 11-14.

Burbank, D.W. and Anderson, R.S., 2001, Tectonic Geomorphology: Blackwell Science, Massachusetts, 274 pp.

Bull, W.B., 1991, Geomorphic Responses to Climatic Change: Oxford University Press, New York, 326 p.

Calzia, J.P., and Ramos, O.T., 2000, Late Cenozoic crustal extension and magmatism, southern Death Valley region, California: *in* Lageson, D.R., Peters, S.G. and Lahren, M.M., eds., Great Basin and Sierra Nevada: Geological Society of America Field Guide 2, p. 135-164.

Dokka, R.K., and Travis C.J., 1990, Late Cenozoic strike-slip faulting in the Mojave Desert, California: Tectonics, v. 9, no. 2, p. 311-340.

Freidmann, S.J., 1999, Sedimentology and stratigraphy of the Shadow Valley basin, eastern Mojave Desert, California, *in*, Wright, L.A, and Troxel, B.W., eds., Cenozoic basins of the Death Valley Region, Geological Society of America Special Paper 333, p. 213-243.

Garcia, C., Erickson, R.C., Spell, T., 2002, Petrology of the Salt Creek pluton, northern Salt Spring Hills, California: Abstracts with Programs, Cordilleran Section, Geological Society of America v. 34, p. 29

Hamblin, W.K., Damon, P.E., and Bull, W.B., 1981, Estimates of vertical crustal strain rates along the western margins of the Colorado Plateau: Geology, v.9, p. 293-298.

Hillhouse, J., 1987, Late Tertiary and Quaternary geology of the Tecopa Basin, southeastern California: U.S. Geological Survey, Miscellaneous Investigation Series, Map I-1728.

Hooke, R. LeB., 1999, Lake Manly Shorelines in the Eastern Mojave Desert, California: Quaternary Research, v. 52, p. 328-336.

Jennings, C.W., Burnett, J.L., and Troxel, B.W., 1962, Geologic map of California; Trona sheet: California Division of Mines and Geology, scale 1:250,000.

Koehler, P.A., Anderson, R.S., and Spaulding, W.G., 2005, Development of vegetation in the central Mojave Desert of California during the late Quaternary: Palaeogeography, Palaeoclimatology, Palaeoecology, v. 215, p. 297-311.

Lister and Baldwin, 1993, Plutonism and the origin of metamorphic core complexes: Geology, v. 21, p. 607-610.

Machette, M.N., Johnson, M.L., and Slate, J.L., 2001, Quaternary and late Pliocene geology of the Death Valley region: Recent Observations on tectonics, stratigraphy, and lake cycle—Pacific Cell-Friends of the Pleistocene Field-trip Guidebook: U.S. Geological Survey Open-File Report 01-51, 246 p.

McCalpin, J.P., 1996, Paleoseismology: Academic Press: New York, 588 p.

McDonald, E. V., L. D. McFadden, and S. G. Wells. 1995. Regional response of alluvial fans to the Pleistocene-Holocene climatic transition, Mojave Desert, California, *in* Enzel, Y., Wells, S.G., and Lancaster, N., eds., Paleoenvironments and paleohydrology of the Mojave and southern Great Basin Deserts: Geological Society of America Special Paper 368, p. 189-209..

McMackin, M.R., 1987, Extension tectonics in the southeastern Kingston range and northern Mesquite Mountains reinterpretation of the Winters Pass "thrust" fault: Unpublished Master's Thesis, University of California Davis, 96 p.

McMackin, M.R., 1992, Tectonic evolution of the Kingston Range, Death Valley, California: Pennsylvania, Pennsylvania State University, Ph.D. Dissertation, 158 p.

McMackin, M.R., 1997, Late Tertiary evolution of the southern Death Valley Fault system: The origin of the Tecopa Hump, a tectonic dam on the Amargosa River, *in* Reynolds, R.E. (ed), Death Valley: The Amargosa Route: San Bernardino County Museum Quarterly, v. 44 (2), p**.** 37-42.

Menges, C.M., Taylor, E.M., Workman, J.B., and Jayko, A.S., 2001, Regional surficial-deposit mapping in the Death Valley area of California and Nevada in support of ground-water modeling, *in* Machette, M.N., Johnson, M.L., and Slate, J.L., eds, Quaternary and late Pliocene geology of the Death Valley region: Recent observations on tectonics, stratigraphy, and lake cycle—Pacific Cell-Friends of the Pleistocene Field-trip Guidebook: U.S. Geological Survey Open-File Report 01-51, p. H151-H166.

Miller, D.M., and Yount, J.L., 2002, Late Cenozoic tectonic evolution of the north-central Mojave Desert inferred from fault history and physiographic evolution of the Fort Irwin area, California: Geological Society of America Memoir, 195, p. 173-197.

Morrison, R.B., 1999, Lake Tecopa: Quaternary geology of Tecopa Valley, California, a multimillion-year record and its relevance to the proposed nuclear-waste repository at Yucca Mountain, Nevada, *in*, Wright, L.A,, and Troxel, B.W., eds., Cenozoic basins of the Death Valley Region, Geological Society of America Special Paper 333, p. 301-344.

Nash, D.B., 1980, Morphological dating of degraded normal fault scarps: Journal of Geology, v. 88, p. 353-360.

Prave, A.R., and McMackin, M.R., 1999, Depositional framework of mid- to late-Miocene strata, Dumont Hills and southern Kingston Range: Implications for the tectonostratigraphic evolution of the southern Death Valley, *in*, Wright, L.A, and Troxel, B.W., eds., Cenozoic basins of the Death Valley Region, Geological Society of America Special Paper 333, p. 259-275.

Spencer, J.E., 1981, Geology and geochronology of the Avawatz Mountains, San Bernardino County, California: Massachusetts, Massachusetts Institute of Technology, Ph.D Dissertation, 183 p.

Stine, S., 1994 Extreme and persistent drought in California and Patagonia during Medieval time: Nature, v. 369, p. 546-549.

Topping, D.W., 1993, Paleogeographic reconstruction of the Death Valley extended region: Evidence from Miocene large rock-avalanche deposits in the Amargosa Chaos Basin, California: Geological Society of America Bulletin, v. 105, p. 1190-1213.

Wells, S.G., Brown, W.J., Enzel, Y., Anderson, R.Y., and McFadden, L.D., 2003, Late Quaternary geology and paleohydrology of pluvial Lake Mojave, southern California, *in* Enzel, Y., Wells, S.G., and Lancaster, N., eds., Paleoenvironments and paleohydrology of the Mojave and southern Great Basin Deserts: Geological Society of America Special Paper 368, p. 79-114.

Whipple, K.X., 2004, Bedrock rivers and the geomorphology of active orogens: Annual Review of Earth and Planetary Sciences**,** v. 32, p.151-185.

Whipple, K.X., and Tucker, G.E.., 1999, Dynamics of the stream-power river incision model: Implications for height limits of mountain ranges, landscape response timescales, and research needs: Journal of Geophysical Research, Volume 104, p. 17661-17674.

Yount, J.C., Schermer, E.R., Felger, T.J., Miller, D.M., and Stephens, K.A., 1994, Preliminary Geologic Map of Fort Irwin Basin, north-central Mojave Desert, California, U.S. Geological Survey, Open-File Report 94-173, scale 1:24,000, 25 p.

Chapter B

Re-interpretation of Pleistocene Lake Dumont, Salt Spring basin, California, based on ostracode faunal analyses

By Jordon Bright[1] and Kirk C. Anderson[2]

Abstract

New ostracode faunal analyses on core and numerous outcrop samples in the Salt Spring basin suggest that basin sediments previously interpreted as lacustrine are instead wetland deposits. Four wet intervals (intermittent between about 29 and 23 ka, and again at about 18 ka) are preserved in core DU-2. The ostracode faunas found in these intervals are unable to tolerate Mojave River chemistry, and suggest that the wetland deposits were fed by local water sources. Numerous outcrop samples, including one sample from a potential Salt Spring basin shoreline feature, contain the same ostracode species as core DU-2 suggesting that the outcrops also represent wetland rather than lacustrine deposits. One sample from sediments near the center of the basin contains very limited numbers of *Limnocythere ceriotuberosa* and *Limnocythere sappaensis*, ostracodes indicative of Mojave River water chemistry. These sediments are fluvial in nature, and the *Limnocythere* species co-occur with incompatible ostracode species, implying they are reworked.

Introduction

The Salt Spring basin is a small basin situated on the divide between the Mojave and Death Valley watersheds. It is the last in a series of basins along the course of the Mojave River that were periodically inundated during the late Pleistocene (Fig 1). Upstream basins (e.g., Soda and Silver basins) contained large lakes (Lake Mojave) during the late Pleistocene. After the incision of Afton Canyon (<22 ka; Wells et al., 2003), the additional discharge from the Mojave River forced Lake Mojave to overflow northward, with the overflow eventually reaching the Salt Spring basin. Reduced clays in a core recovered from the Salt Spring basin have been interpreted as lacustrine sediments deposited when the overflow from Lake Mojave was impounded and formed Lake Dumont roughly 18,000 years ago. A prominent horizontal feature along portions of the western and southern margins of the Salt Spring basin has been interpreted as the probable highstand shoreline of Lake Dumont (Anderson and Wells, 2003; Anderson and Wells, 1997).

The current paleohydrologic interpretation of the Salt Spring basin was based primarily on numerous outcrop lithologic descriptions, and on three ostracode samples from two cores (DU-1

[1]Dept. of Geology, Northern Arizona University, Flagstaff, AZ 86011
[2]Bilby Research Center, Northern Arizona University, Flagstaff, AZ 86011

and DU-2) taken from the western margin of the basin (Fig. 2). The two ostracode faunal samples from core DU-1 contained "*Limnocythere staplini*, *Candona rawsonoid*, and *Heterocyprix* sp.". The ages of these samples were based on correlations to similar clay in core DU-2 that yielded an uncalibrated ^{14}C age of ~ 27,500 BP based on bulk-sediment ^{14}C. A third ostracode sample from core DU-2, which was dated to 18,150 BP (uncalibrated), contained "*Candona caudata* and *Candona rawsonoid*" (Anderson and Wells, 2003). [Note: The ostracode name "*Candona rawsonoid"* is not an accurate taxonomic designation, but instead refers to an unidentified species of *Candona* with visual affinities to the ostracode *Candona rawsoni*.]

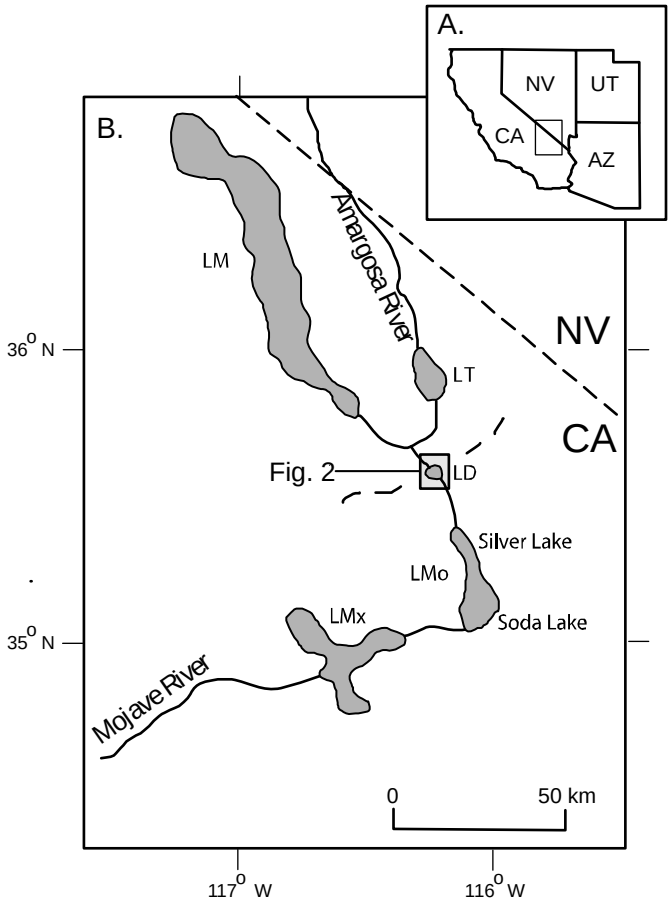

Figure 1. Lake Dumont study area relative to (A.) the western United States; and (B.) to other pluvial lakes along the Amargosa and Mojave Rivers. Wavy dashed line is approximate divide between the Mojave and Amargosa River watersheds. LM – Lake Manly; LT – Lake Tecopa; LD – Lake Dumont; LMo – Lake Mojave; LMx – Lake Manix. Figure modified from Morrison (1991).

Additionally, the genus name "*Heterocyprix*" and "*Heterocypric*" from Anderson and Wells (2003) are both spelling errors and should read *Heterocypris*. Anderson and Wells (2003) concluded that the ostracode faunas in core DU-1 (~ 30-25 ka) represented a shallow lake or wetland supported by local groundwater and runoff, whereas the younger ostracode fauna from DU-2 (~ 18 ka,) represented a second lake cycle supported by Mojave River flow rather than local spring discharge. New ostracode analyses and field observations presented here allow for refinement and reinterpretation of the younger ostracode-bearing sediment.

Methods

Core DU-2 was re-sampled for ostracode analyses in 2004. The core is archived in its original liners in cold storage at Northern Arizona University. All of the core segments were severely desiccated. Carbonate-rich (potentially ostracode bearing) intervals were located by testing with dilute (0.1 M) HCl. Reactive sections were sampled at ~ 10 cm intervals for a total of 78 samples.

Sediments along the south and southeastern flanks of the northern Salt Spring Hills (Fig. 2) were mapped as "Pleistocene basin fill" by Anderson and Wells (2003, 1997). Numerous (n = 22; Fig. 2) outcrops (arroyo cut-banks and hills) in these deposits were sampled for ostracodes in June 2005. Test pits were dug through the overlying salty crust down to moist, cohesive sediments. As with the core, only acid-reactive sediments were collected.

All samples were disaggregated by soaking several days in a weak sodium hexametaphosphate solution (~ 2 g/L), and then washed over 150 μm sieves. The residues were air dried in their sieves. Ostracodes were identified to genus and species level under a binocular microscope. Ostracode valves were not counted, but are reported as a visual estimate of abundance.

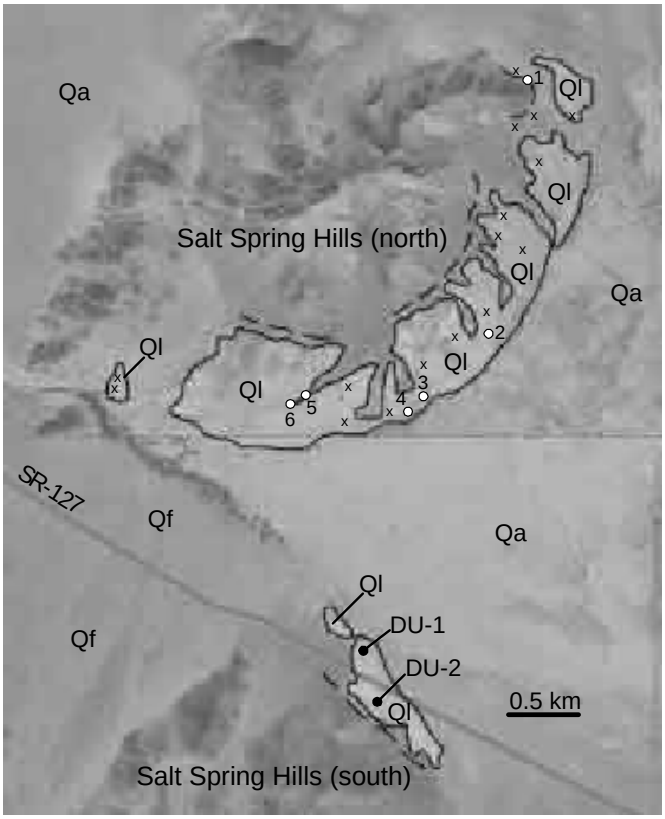

Figure 2. Salt Spring basin, showing surficial units, locations of cores DU-1 and DU-2 and ostracode-bearing outcrop sites 1 through 6. Non-ostracode bearing sites delineated by X. Qf = Quaternary fan deposits; Qa = Quaternary alluvium, spring, playa and eolian deposits; Ql = Pleistocene basin-fill deposits. Dashed lines are approximate locations where Salt Spring Hills "shoreline" features are preserved. Figure based on Anderson and Wells (2003).

Results

Core DU-2

Of the 78 samples taken from core DU-2, 41 contained ostracodes. A total of six ostracode species were recovered from four zones in the core (Fig. 3). The most common ostracodes were *Limnocythere staplini*, *Candona patzucaro*, and *Cyprideis beaconensis*. The less common species were *Limnocythere paraornata*, *Heterocypris incongruins*, and juvenile valves of a *Potamocypris* species.

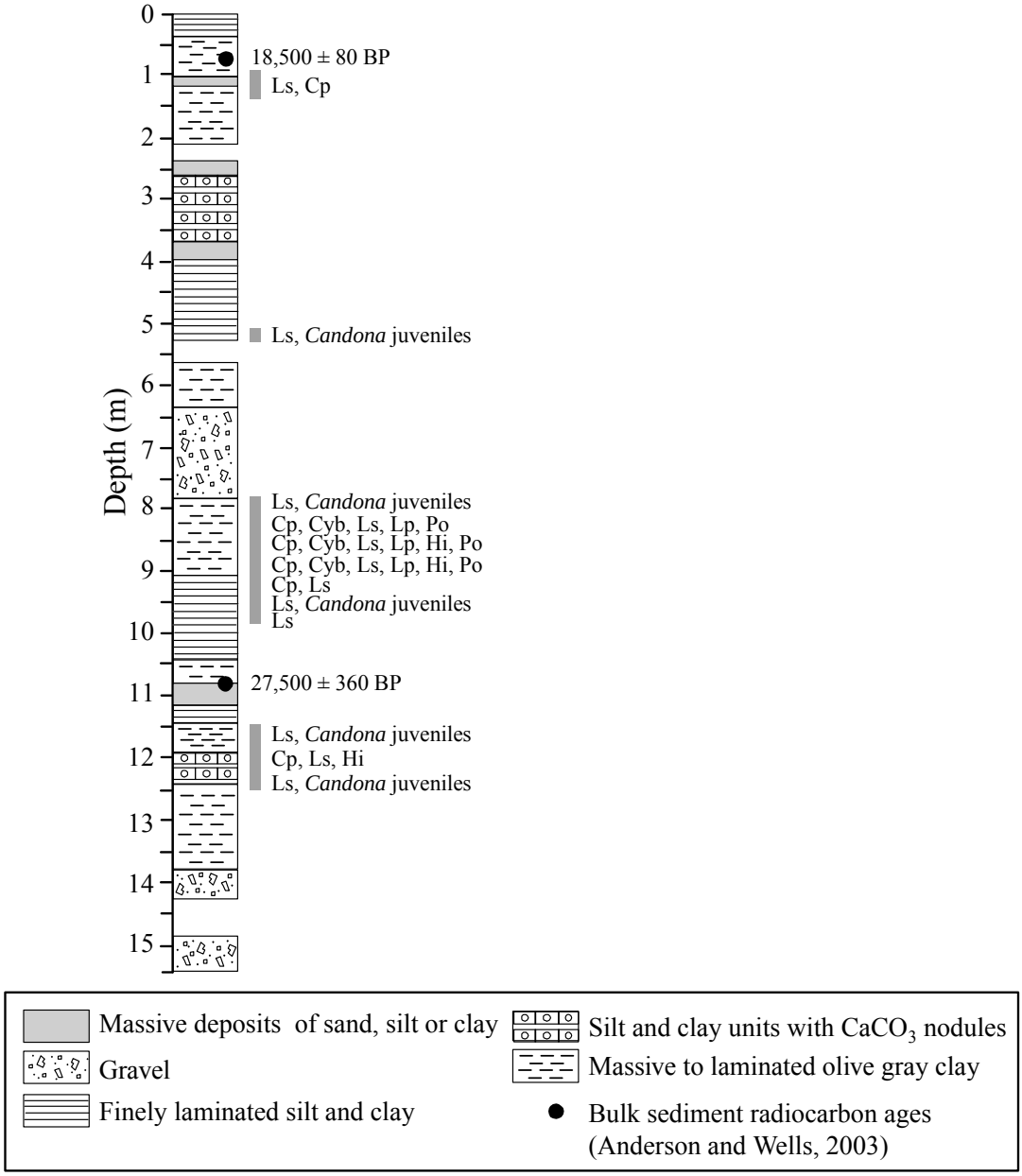

Figure 3. Generalized stratigraphy and chronology (based on Anderson and Wells, 2003) and ostracode zones in core DU-2 (this study). Ls = *Limnocythere staplini*; Cb = *Cyprideis beaconensis*; Cp = *Candona patzucaro*; Hi = *Heterocypris incongruins*; Lp = *Limnocythere paraornata*; Po = *Potamocypris* sp.

Salt Spring Hills Outcrops

Of the 22 outcrops sampled, only six contained ostracodes. Sample 7 from Site 1, at the northern end of the Salt Spring Hills (Fig. 2, Table 1), contained whole and fragmented valves of *Cyprideis beaconensis*. The other five ostracode-bearing sites (Sites 2-6; Fig. 2, Table 1) contained the same fauna as in core DU-2, dominated by *Cyprideis beaconensis*, *Candona patzucaro* and *Limnocythere staplini*. As with the core sediments, *Cypridopsis vidua*, *Heterocypris incongruins* and *Potamocypris* sp. were locally present in the outcrop samples. In addition to these species, Site 3 (Fig. 2), a large hill truncated on its western and eastern flanks by fluvial erosion, exposes sediments with a distinctive ostracode fauna. A total of 13 samples were collected from this site (Fig. 4 and 5; Table 1). The sandy, bedded, basal part of the uppermost unit (sample 20A; Fig. 4, Table 1) was dominated by the typical *Cyprideis beaconensis* - *Limnocythere staplini* fauna. But the sediment also contained rare valves of *Limnocythere ceriotuberosa*, *Limnocythere sappaensis* and *Ilyocypris bradyi* (estimated < 5% of the fauna). Additional samples from the uppermost unit (sample 20F, 20G, 28C and 29C; Fig 4 and 5, Table 1) gave similar results in that *Limnocythere ceriotuberosa* were again rare (only found in samples 20G and 28C; Fig. 4 and 5), but no *Limnocythere sappaensis* or *Ilyocypris bradyi* were recovered. All of the remaining ostracode-bearing samples at Site 3 contained the typical Salt Spring basin fauna (Table 1).

Table 1. Site locations, sample designations and ostracode faunas fromcarbonate-bearing outcrops in Salt Spring basin

Site	Lat.	Long.	Sample	Ostracode fauna (in relative order of abundance)
1	35º 38.390’	116º 15.360’	JEB05CA-07	*Cyprideis beaconensis*
2	35º 37.865’	116º 15.497’	JEB05CA-16	*Cyprideis beaconensis, Candona patzucaro, Limnocythere staplini, Cypridopsis vidua*
3	35º 37.597’	116º 15.728’	JEB05CA-20A	*Cyprideis beaconensis, Limnocythere staplini, Candona patzucaro, Cypridopsis vidua, Limnocythere ceriotuberosa, Limnocythere sappaensis, Ilyocypris bradyi*
			JEB05CA-20B	*Candona patzucaro, Cypridopsis vidua, Limnocythere staplini, Potamocypris* sp., *Heterocypris incongruins*
			JEB05CA-20C	None
			JEB05CA-20D	None
			JEB05CA-20E	None
			JEB05CA-20F	*Cyprideis beaconensis, Candona patzucaro, Potamocypris* sp.
			JEB05CA-20G	*Candona patzucaro, Cyprideis beaconensis, Limnocythere staplini, Limnocythere ceriotuberosa*
			JEB05CA-28A	*Limnocythere staplini*
			JEB05CA-28B	*Limnocythere staplini, Candona* juveniles
			JEB05CA-28C	*Limnocythere staplini, Candona patzucaro, Cyprideis beaconensis, Heterocypris incongruins, Potamocypris* sp., *Limnocythere paraornata, Limnocythere ceriotuberosa*
			JEB05CA-29A	*Limnocythere staplini, Candona* juveniles
			JEB05CA-29B	*Candona patzucaro, Limnocythere staplini*
			JEB05CA-29C	*Limnocythere staplini, Candona* juveniles, *Cyprideis* juveniles
4	35º 37.547’	116 15.815’	JEB05CA-21A	*Candona patzucaro, Cyprideis beaconensis, Limnocythere staplini, Heterocypris incongruins, Potamocypris* sp.
			JEB05CA-21B	*Candona patzucaro*
5	35º 37.553’	116º 16.313’	JEB05CA-25A	*Candona* juveniles
			JEB05CA-25B	*Candona patzucaro, Limnocythere staplini, Heterocypris incongruins*
6	35º 37.513’	116º 16.357’	JEB05CA-26	*Candona patzucaro, Limnocythere staplini*

Discussion

The ostracode perspective on local versus Mojave River water sources in Salt Spring basin

Ostracodes are millimetre-sized aquatic crustaceans. The environmental and hydrologic constraints on their distributions have been studied for over 30 years (Delorme 1969; Forester, 1986; Smith, 1993; Curry, 1999). The environmental parameters of many common ostracodes are relatively well known, and they have been frequently used in paleohydrologic reconstructions (Forester et al., 2003; Quade et al., 2003; Quade et al., 1998). The most important controls on ostracode distribution are water temperature and chemistry (Forester, 1986). Water chemistry and solute evolution have been described in some detail by Eugster and Jones (1979) and Eugster and Hardie (1978). In general there are three common types of water. For the purpose of this paper, Type A waters are dilute waters where calcium (Ca) ions and alkalinity (alk; primarily HCO_3 at intermediate pH's) are in roughly equal concentrations (equivalencies or milliequivalencies). Type B waters are those where the Ca concentration exceeds alkalinity (high Ca/alk ratio) and Type C waters are those where alkalinity exceeds the Ca concentration (low Ca/alk ratio). Ostracodes have evolved to take advantage of all these water types. The present understanding (based on modern collections etc.) is that ostracodes adapted to living in high Ca/alk waters cannot survive in low Ca/alk water, and the opposite is true as well.

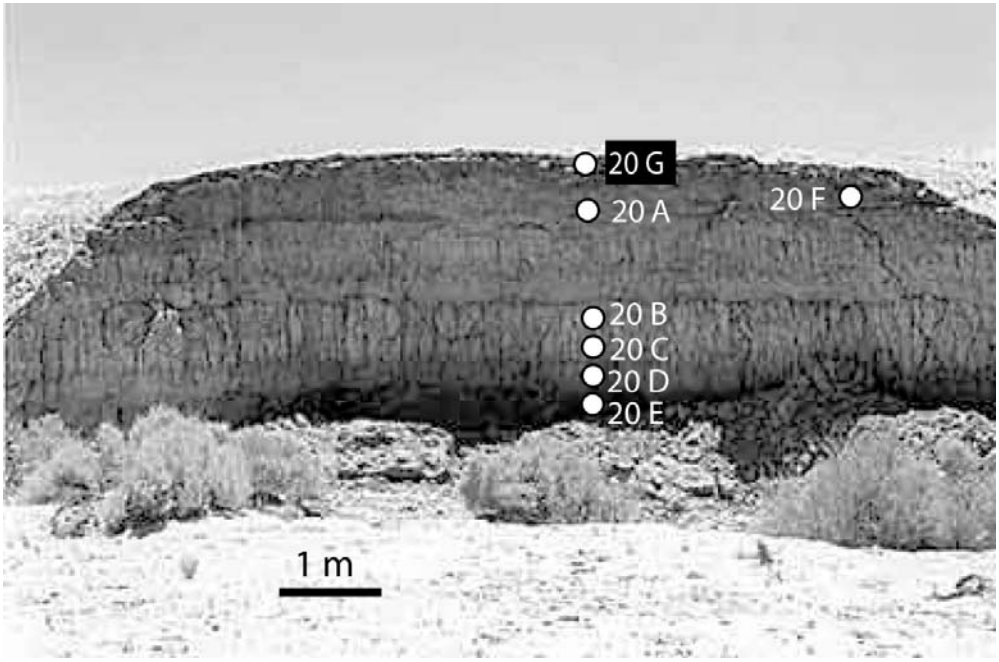

Figure 4. Photograph of Site 3 (Fig. 2) on the western flank of hill showing location of ostracode samples JEB05CA-20A to G (Table 1). Sampling gap between 20A and 20B represents sediments that did not react with dilute HCl, indicating a lack of carbonate (ostracode valves or otherwise).

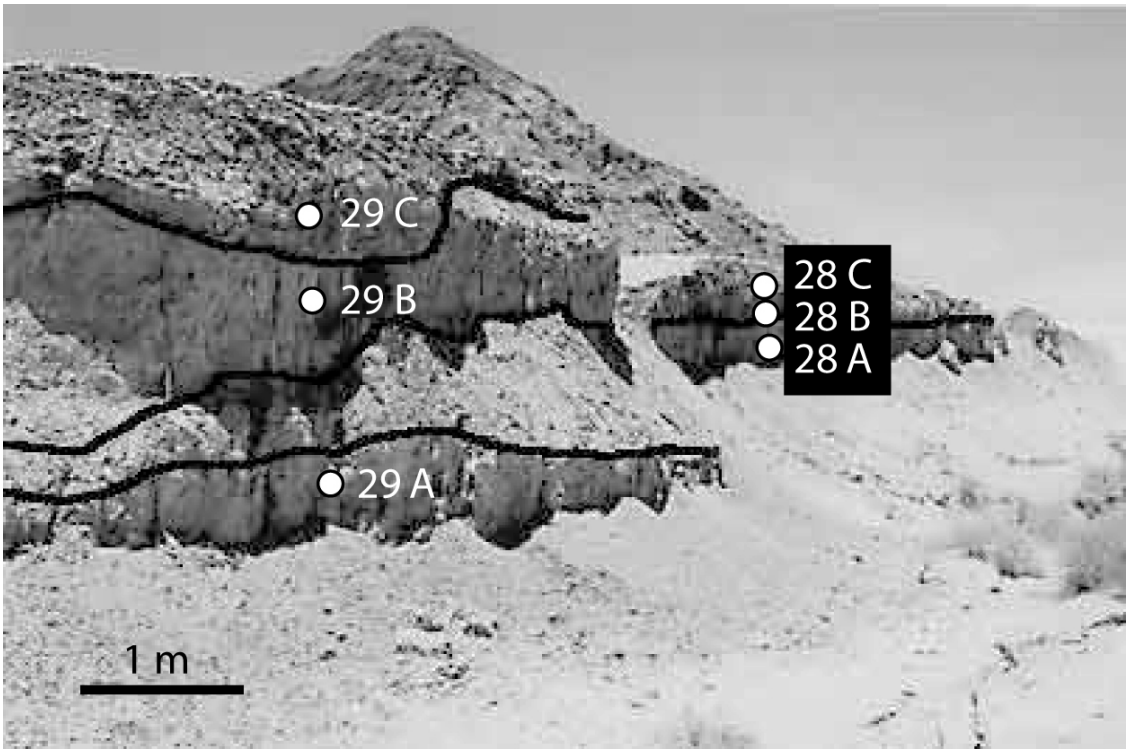

Figure 5. Photograph of Site 3 (Fig. 2) on the eastern flank of hill showing location of ostracode samples JEB05CA-28A to 28C, and 29A to 29C (Table 1).

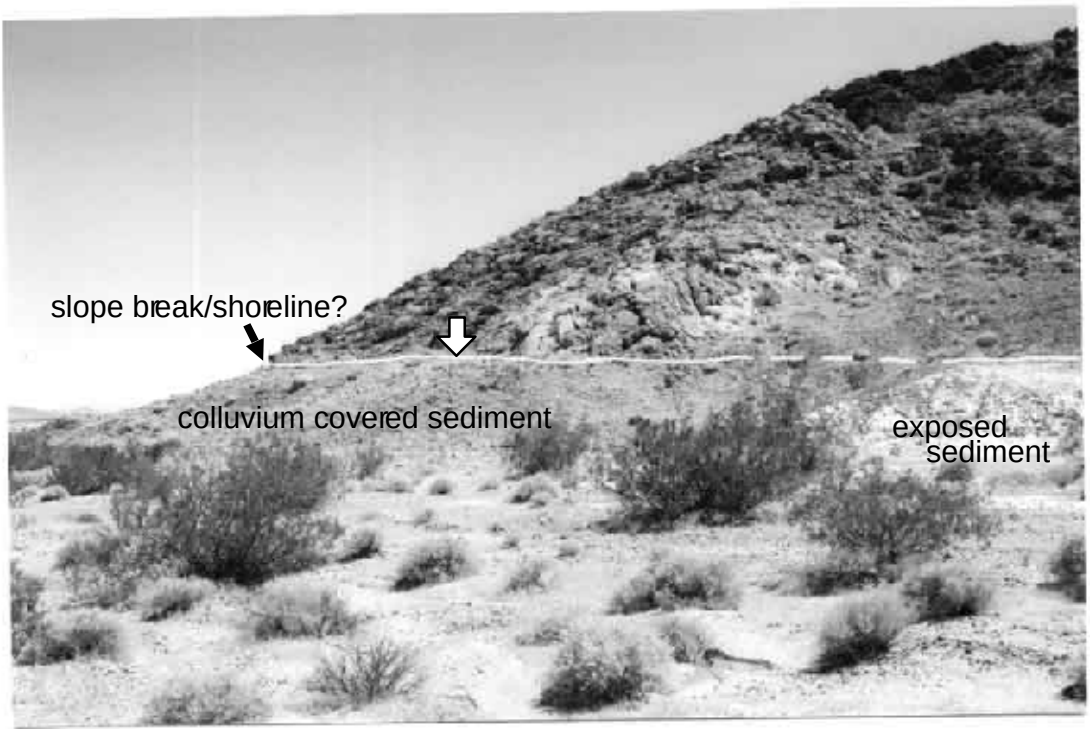

Figure 6. Photograph of Site 1 (Fig. 2) at the northern end of the Salt Spring Hills, view is to the south. White arrow is approximate location of ostracode sample JEB05CA-07 (Table 1). Black arrow highlights contact between fine-grained bench sediment and bedrock. Largest bush (right of center) is approximately 2 m tall. Sediment samples taken from the exposed sediments on the right margin of the figure did not contain ostracodes.

Two of the primary ostracode species (*Limnocythere staplini* and *Cyprideis beaconensis*) recovered from the Salt Spring basin are commonly viewed as indicator species for Type B waters, with *Cyprideis beaconensis* having an even lower tolerance for alkalinity than *Limnocythere staplini* (R. Forester, USGS, pers. comm., 2005). Its presence probably reflects waters derived from either marine salt dissolution or hydrothermal sources (R. Forester, USGS, pers. comm., 2005). *Cyprideis beaconensis* cannot tolerate Type C (low Ca/alk) water and would find it lethal. This distinction is important to understanding the paleohydrology of the Salt Spring basin because the Mojave River is a Type C water. Paleolake deposits from Lake Manix (Jefferson, 2003), Soda Lake and Silver Lake (Wells et al., 2003), which were fed by the Mojave River, contain a different ostracode fauna, as does sediment deposited during the pluvial lake cycles in Death Valley (Lowenstein et al., 1999). These lake deposits typically contain abundant *Limnocythere ceriotuberosa* or *L. bradburyi* valves, or sometimes both. The modern distributions of both of these species are confined to Type C waters (Forester, 1985, 1986) and they would find most (specifically *Cyprideis*-supporting) Type B waters lethal. The presence of *Cyprideis beaconensis* and *Limnocythere staplini* in the sediments of Salt Spring basin suggests that the local water chemistry was significantly different from the waters that filled Lake Manix, or the other Mojave River-supported paleolakes along the path of the Mojave River. Aside from the rare *Limnocythere ceriotuberosa* and *L. sappaensis* valves at Site 3 (Fig. 1), none of the aquatic settings reported here could be derived from Mojave River water.

Salt Spring Basin Paleohydrologic Interpretations

Core DU-2

The ostracode faunas found in the Salt Spring basin sediment represent shallow, high Ca/alk groundwater-supported wetlands. Three of the four ostracode-bearing horizons (12.5 to 11.5, 5.4 to 5.3, and 1.3 to 0.9 m; Fig. 3) in core DU-2 probably record ephemeral or short-lived environments. These horizons typically only contain *Candona patzucaro* and *Limnocythere staplini*, although the horizon at ~ 12 m also contains *Heterocypris incongruins*. As mentioned previously, *Limnocythere staplini* inhabits high Ca/alk settings ranging from springs to wetlands and lakes, and can tolerate ephemeral conditions. *Candona patzucaro* typically inhabits shallow lakes and wetlands that have strong seasonal variability in TDS. Its shell morphology is similar to *Candona rawsoni* (see Delorme, 1970) and may be the *"Candona rawsonoid*" referred to by Anderson and Wells (2003). *Candona patzucaro* has a more southerly distribution than *Candona rawsoni* (Stout, 1975) and may require slightly warmer water. *Heterocypris incongruins* inhabits the edges of springs, shallow wetlands, and littoral zones of some lakes, and has a strong association with slow-moving or stagnant water.

The ostracode horizon from 9.9 to 7.8 m (Fig. 3) displays a gradational progression from the *C. patzucaro/L. staplini* ephemeral wetlands, through a more substantial ostracode fauna consisting of six species, before returning to the *C. patzucaro/L. staplini* setting. This is the only zone in the core that contains *Cyprideis beaconensis.* The remaining fauna consists of low numbers of *Heterocypris incongruins*, *Limnocythere paraornata* and juvenile moults of *Potamocypris* sp. The presence of *Cyprideis beaconensis* not only indicates high Ca/alk water, but it also suggests a more permanent environment. The continued presence of *Candona patzucaro* and *Heterocypris incongruins* suggests a shallow, slow moving or stagnant, seasonally variable environment. The addition of *Limnocythere paraornata* may suggest intervals or areas within the

wetland complex where flowing water existed. *Potamocypris* sp. is common in groundwater discharge settings.

On the basis of the sedimentation rate from Anderson and Wells (2003; ~ 1000 yr m^{-1}), the more permanent wetland setting persisted from ~ 27 to ~ 25 ka, whereas the more ephemeral wetlands occurred at ~ 29, 23, and 18 ka. No ostracodes indicative of high spring discharge (e.g., *Strandesisa meadensis*) or stream conditions (e.g., *Candona caudata*, *Ilyocypris bradyi*) were found. The *Candona caudata* reported in Anderson and Wells (2003) was not found in this analysis.

Salt Spring basin outcrops

With the exception of Site 3 (Fig. 2), all of the ostracode faunas found in the sediments outcropping along the southern flank of the Salt Spring Hills are identical to those recovered in core DU-2, and suggest the outcrop sediments also represent ephemeral to perennial, high Ca/alk wetlands. The few *Limnocythere ceriotuberosa* and *L. sappaensis* at Site 3 (Fig. 2) are presently the only ostracode species tolerant of low Ca/alk (indicative of Mojave River-type waters) yet found in the Salt Spring basin. The sediment at Site 3 is most likely fluvial (note U-shaped surface cut into underlying unit in Fig. 5). The sparse *Limnocythere ceriotuberosa* and *L.sappaensis* valves (estimate ~ 5% of the fauna) mixed with incompatible species, the presence of *Ilyocypris bradyi*, the sandy, bedded sediment, and the channel scour all suggest a fluvial setting, with the *Limnocythere* species reworked from somewhere upstream. This site has not yet been dated, and may be correlative with the Holocene alluvium (> 9.3 to ~ 2.5 ka) described in Anderson and Wells (2003).

Also of interest is the ostracode fauna recovered from Site 1 (Fig. 2). The site is a bedrock point that is ringed by a thick (~ 3 m) package of sediment that in places creates a conspicuous horizontal bench as much as 2 m wide extending out from the local bedrock (Fig. 5). The sample was taken from a shallow pit dug ~ 25 cm into the horizontal surface of these sediments. These sediments have not been dated and are several kilometres north of the prominent slope-break feature near the site of core DU-2 (Fig. 1) that has been interpreted as a shoreline (Anderson and Wells, 2003). The spatial and chronologic relationships between the bench feature at Site 1 and the proposed shoreline feature near core DU-2 are not understood. The Site 1 bench feature is at an elevation of ~ 176 m, which is similar to the shoreline elevation cited in Anderson and Wells (2003). It is possible that they are related but further investigations are required.

Several authors have attributed the Salt Spring basin shoreline feature to either a late Pleistocene, Mojave River-fed highstand of Lake Dumont (e.g., Anderson and Wells, 2003), or to an older highstand of Lake Manly which filled Death Valley (Hooke, 1999). The late Pleistocene Lake Mojave beach deposits from the northern end of Silver Lake (Tidewater Basin and Silver Lake Quarry) and Soda Lake (Baker Highway quarry and Baker Dump quarry) include fine-grained sediment containing *Limnocythere ceriotuberosa* or *L. bradburyi* (Wells et al., 2003; Bright, unpublished data), which are indicative of a low Ca/alk water (Mojave River supported) lake. Deep-lake sediment from Death Valley (Lake Manly) also contain *L. ceriotuberosa* (Lowenstein et al., 1999). In contrast, the bench deposits from Site 1 contain the high Ca/alk water indicator *Cyprideis beaconensis*, rendering it unlikely that these sediments were associated with a Mojave River-fed lacustrine setting. If the sediments at Site 1 are in fact contemporaneous with the "Pleistocene basin fill" sediments cored at the DU-2 site, then taken together it becomes increasingly improbable that a Mojave River-fed lake inundated the Salt Spring basin.

Based on the ostracode faunas, no indication of any Mojave River-supported lakes are preserved in core DU-2 or in outcrop. Anderson and Wells (2003) state that the oldest and most

persistent wet period lasted from ~ 30 to ~ 25 ka, which correlates well with the deepest ostracode zones in core DU-2 (Fig 3). They interpret the highstand of Lake Dumont to have occurred at ~ 19-18 ka and attribute it to the overflow of Lake Mojave, which brought Mojave River water into Lake Dumont, creating the shoreline feature found near the core site (and possibly at Site 1). Based on the results of this study, the ostracode fauna from the ~18 ka sediments in core DU-2 and those undated from Site 1 are not indicative of impounded Mojave River water. Possible explanations for the discrepancy include: (1) Mojave River was not impounded at ~ 18 ka and the "shoreline" was not created by a late Pleistocene highstand of Lake Dumont. It is conceivable that wetland deposits aggraded in Salt Spring basin to the level of the "shoreline" prior to the arrival of the Mojave River. Overflow from Lake Mojave may have flowed essentially unimpeded through the basin. The bench features at the DU-2 core site and Site 1 may be erosional in nature, related to more recent deflation and erosion within the basin. (2) Lake Dumont highstand sediment has been eroded from the basin and is not preserved in the core or outcrops. Without any age control, it is permissible that the sediment at Site 1 (Fig. 2), and all of the outcrops visited in this study, are relatively young (Holocene) and are not "Pleistocene basin fill" related to Lake Dumont (e.g., the majority of the deposits identified as Ql in Anderson and Wells (2003, 1997) are not Pleistocene in age). However, the 18 ka age within a meter of the surface at the DU-2 core site suggests that at least those sediments are late Pleistocene in age, yet they do not contain Mojave River-tolerant ostracodes.

Conclusions

The lack of evidence for a Mojave River-supported lake in the Salt Springs basin is unexpected. All presently available information suggests that the basin was not inundated by a late Pleistocene lake (Lake Dumont). The majority of the sediment previously interpreted as "lacustrine" in Salt Spring basin and the ostracode-bearing sediment in core DU-2 are here reinterpreted as representing local groundwater-supported, high Ca/alk wetlands. The presence of the Mojave River in the basin is not contested, as it logically must have flowed through the basin when the sill at Silver Lake (Lake Mojave) was breached. The hilltop sediments at Site 3 contain extremely few of the requisite Mojave-tolerant ostracodes, but these sediments are probably fluvial, and reworked and may be relatively young. New ostracode-based information from a potential Salt Spring basin "shoreline," when compared with shoreline deposits from Silver Lake and Soda Lake, suggest that it was not formed by a Mojave River-supported lake.

References cited

Anderson, K. C., and Wells, S. G., 2003. Latest Quaternary paleohydrology of Silurian Lake and Salt Spring basin, Silurian Valley, California. *In* Enzel, Y., Wells, S. G., and Lancaster, N., (Eds.), Paleoenvironments and paleohydrology of the Mojave and southern Great Basin Deserts. Geological Society of America Special Paper 368, Boulder, CO., pp. 129-141.

Anderson, K. C., and Wells, S. G., 1997. Late Pleistocene and Holocene valley-fill deposits of Lake Dumont. San Bernardino County Museum Association Quarterly 44(2), 29-32.

Curry, B. B., 1999. An environmental tolerance index for ostracodes as indicators of physical and chemical factors in aquatic habitats. Palaeogeography, Palaeoclimatology, Palaeoecology 148, 51-63.

Delorme, L. D., 1969. Ostracodes as Quaternary paleoecological indicators. Canadian Journal of Earth Sciences 6, 1471-1746.

Delorme, L. D., 1970. Freshwater ostracodes of Canada. Part III. Family Candonidae. Canadian Journal of Zoology 48, 1099-1129.

Eugster, H. P., and Hardie, L. A., 1978. Saline lakes. *In* Lerman, A. (Ed.), Lakes - Chemistry, Geology, Physics. Springer Verlag, Berlin, pp.237-293.

Eugster H. P., and Jones, B. F., 1979. Behaviour of major solutes during closed-basin brine evolution. American Journal of Science 279, 609-631.

Forester, R. M., Miller, D. M., Pedone, V. A., 2003. Ground water and ground-water discharge carbonate deposits in warm deserts. *In* Reynolds, R. E., (Ed.), Land of Lost Lakes: 2003 Desert Symposium, California State University, Fullerton, CA., p. 27-36.

Forester, R. M., 1985. *Limnocythere bradburyi* n. sp.: A modern ostracode from central Mexico and a possible Quaternary paleoclimatic indicator. Journal of Paleontology 59, 8-20.

Forester, R. M., 1986. Determination of the dissolved anion composition of ancient lakes from fossil ostracodes. Geology 14, 796-798.

Hooke, R. L., 1999. Lake Manly (?) shorelines in the eastern Mojave Desert, California. Quaternary Research 52, 328-336.

Jefferson, G. T., 2003. Stratigraphy and paleontology of the middle to late Pleistocene Manix Formation, and paleoenvironments of the central Mojave River, southern California. *In* Enzel, Y., Wells, S. G., and Lancaster, N., (Eds.), Paleoenvironments and paleohydrology of the Mojave and southern Great Basin Deserts. Geological Society of America Special Paper 368, Boulder, CO., pp. 43-60.

Lowenstein, T. K., Li, J., Brown, C., Roberts, S. M., Ku, T.-L., Luo, S., Yang, W., 1999. 200 k.y. paleoclimate record from Death Valley salt core. Geology 27, 3-6.

Morrison, R. B., 1991. Quaternary stratigraphic, hydrologic, and climatic history of the Great Basin, with emphasis on Lakes Lahontan, Bonneville, and Tecopa, *in* Morrison, R. Ed., Quaternary nonglacial geology: Conterminous U.S., The Geology of North America, v. K-2, Geological Society of America, Boulder, CO., p. 283-320.

Quade, J., Forester, R. M., Whelan, J. F., 2003. Late Quaternary paleohydrologic and paleotemperature change in southern Nevada. *In* Enzel, Y., Wells, S. G., and Lancaster, N., (Eds.), Paleoenvironments and paleohydrology of the Mojave and southern Great Basin Deserts. Geological Society of America Special Paper 368, Boulder, CO., pp. 165-188.

Quade, J., Forester, R. M., Pratt, W. L., Carter, C., 1998. Black mats, spring-fed streams, and Late-Glacial-age recharge in the southern Great Basin. Quaternary Research 49, 129-148.

Smith, A. J., 1993. Lacustrine ostracodes as hydrochemical indicators in lakes of the north-central United States. Journal of Paleolimnology 8, 121-134.

Stout, L. N., 1975. Polytypic species and hybridization in Quaternary fresh-water ostracodes of North America. Palaeogeography, Palaeoclimatology, Palaeoecology 17, 257-266.

Wells, S. G., Brown, W. J., Enzel, Y., Anderson R. Y., McFadden, L. D., 2003. Late Quaternary geology and paleohydrology of pluvial Lake Mojave, southern California. *In* Enzel, Y., Wells, S. G., and Lancaster, N., (Eds.), Paleoenvironments and paleohydrology of the Mojave and southern Great Basin Deserts. Geological Society of America Special Paper 368, Boulder, CO., pp. 79-114.

Chapter C

Late Quaternary stratigraphy and luminescence geochronology of the northeastern Mojave Desert, with emphasis on the Valjean Valley area

By Shannon A. Mahan[1], David M. Miller, Christopher M. Menges, and James C. Yount[2]

Abstract

The chronology of the late Pleistocene and Holocene deposits of the greater Silurian Valley area, south and east of Death Valley, California, has been refined by luminescence dating of sediments at Valjean Valley, Silurian Lake, California Valley, Red Pass and the Silver Lake overflow. The ages determined by several luminescence techniques are concordant (or consistent) with geomorphic and stratigraphic relations as well as other widely-dated climatic events. Correlations are made herein with regional alluvial fan chronology, Salt Creek and Silurian Lake paleohydrology, Amargosa River drainage history, and groundwater-discharge deposit (GWD) events. Newly established ages for some events are determined by feldspar and quartz luminescence dating. Of particular interest are two clearly identified groundwater-discharge events bracketed at 90 to 140 ka and 20 to 50 ka. The age of latest Pleistocene and early Holocene fan deposits dated elsewhere at 9 to 15 ka are confirmed by optically stimulated luminescence (OSL) ages of 12 ka in Red Pass deposits. Formation of spits in south Silurian Lake dated with OSL at 720 to 1,150 years also correlates well to a regional Southwestern US flood event 800-850 years ago.

Introduction

Because a geochronologic framework is critical for geologic mapping and hazards assessments in the Mojave Desert, we have undertaken investigations using luminescence dating. Quaternary deposits in semi-arid and desert environments present challenges for standard radiocarbon geochronology because the incumbent alkaline environment destroys organic material rapidly, providing rare opportunities for any survival. A substantial body of work detailing absolute age chronologies already existed for such areas as the lower Colorado River, Silver Lake north of Baker, Kelso Valley, Pahrump Valley, Las Vegas Valley and central Death Valley (Bull, 1991; Reheis and others, 1989; Wells and others, 1990; McDonald and McFadden, 1994; Menges and others, 2001; Lundstrom and others, 2003; Machette and others, 2003; Page and others, 2005). Intervening areas, however, provided good opportunities for correlations between these solidly dated deposits and those that remain poorly or not dated.

The Mojave Desert contains a large number of Quaternary eolian sand fields, some of which include large sand streams (Lancaster, 1999; Lancaster and Tchakerian, 2003) (Fig. 1).

[1] U.S. Geological Survey, Box 25046, Denver Federal Center, MS 974, Denver, CO 80225
[2] U.S. Geological Survey, Box 25046, Denver Federal Center, MS 980, Denver, CO 80225

One of these areas, the Kelso dune field, has been studied extensively. In particular, several sand ramps comprised of colluvium and eolian sand have been dated using infrared stimulated luminescence (IRSL) methods (Edwards, 1993; Rendell and others, 1994; Wintle and others, 1994; Clarke, 1994). Elsewhere in the Mojave, eolian deposits have been widely sampled and correlated using luminescence dating (Rendell and Sheffer, 1996; Clarke and others, 1996; Clarke and Rendell, 1998). Other workers have dated multiple short duration periods of eolian deposition from Cronese Basin, Devil's Playground and Kelso Dunes that correlated with the level of Lake Mojave (Busacca and others, 2004).

Luminescence methods utilizing the feldspar minerals have been widely applied to eolian sand deposits (Roberts and others, 2003; Bray and Stokes, 2003; Berger and others, 2003; Clarke and Rendell, 2003), but only recently has OSL using quartz been applied to eolian and fluvial deposits with success. In recent years, advances in feldspar and quartz OSL techniques have allowed dating of eolian and fluvially transported sediments in a wide variety of environments, particularly where materials for radiocarbon dating cannot be found (Eriksson and others, 2000; Wallinga, 2002; Rittenour and others, 2003, Sohn and others, 2007).

In this paper we report luminescence dates for eolian sand obtained using feldspar and quartz OSL, as well as new quartz OSL ages for lacustrine, alluvial, and groundwater-discharge deposits (GWD). We collected about 70 luminescence samples desert-wide during the years 1999 to 2005 from deposits that span an enormous range of depositional and climatic conditions; of these, about 21 were sampled in the Silurian Valley area south and east of Death Valley (Fig. 1, Table 1 and Table 2). Within this area, lacustrine sediments from Silurian Lake playa, stream deposits from Salt Creek, and alluvial fans of Valjean Valley and Red Pass were found suitable for both kinds of OSL dating techniques. The California Valley deposits were used to test several parameters involved in the OSL dating of groundwater-discharge deposits: some deposits proved to be beyond the range of OSL dating (Table 1). Eolian sands from the Silver Lake spillway were also analyzed, again with generally favorable results. Fine-grained stream sediment, alluvial sediment that incorporates eolian sand, and GWD all proved useful for OSL dating using adaptations to existing techniques.

One of the goals of our luminescence dating is to provide a chronologic framework for regionally mappable deposits in the Mojave Desert, particularly for GWD deposits (Quade, 1986; Quade and others, 1995, 1998, 2003; Forester and others, 2003, Lundstrom and others, 2003; Page and others, 2005, Owen and others, 2007). Another goal is to establish new chronologic and stratigraphic relationships in the eastern Mojave Desert with an emphasis on the Valjean Valley area, in order to establish timing for late Quaternary depositional events. A third goal is to fill gaps in the geochronology of desert deposits, which can provide data relevant to understanding the responses of several depositional systems to regional changes in climate.

Regional geologic setting

Silurian Valley is in the northeastern Mojave Desert, which extends from Baker and the Soda Mountains at the south to Death Valley at the north (Fig. 1). The valley floor ranges from about 100 m to 300 m in altitude, whereas fringing piedmonts, mountains, and upland valleys reach up to 2600 m in altitude. Salt Creek and the Amargosa River, the two main drainages in the area, meet near the junction of Death Valley and Silurian Valley.

In late Pleistocene time the south end of Silurian Valley was occupied by pluvial Lake Mojave between about 20 and 10 ka (Wells and others, 2003); overflow from this lake traversed northern Silurian Valley to join the Amargosa River, which emptied into Lake Manley in Death Valley (Anderson and Wells, 2003a).

Table 1. Feldspar IRSL and quartz OSL ages from the Mojave Desert study area

Lab ID Sample information ID, area and genesis	Field Moisture (%)	Dose Rate (Gy/ka) (±1 σ %)	Equivalent Dose (Gy) (±1 σ %)	Age (yr) IRSL[a]	Dose Rate (Gy/ka) (±1 σ%)	Equivalent Dose (Gy) (±1 σ %)	N	Age (yr) quartz OSL[b]
Valjean Valley alluvial fan								
M99VJ-990	0.8	4.53 ± 0.11	20.7 ± 0.53	4,583 ± 288				
Alluvial fan unit			20.6 ± 0.52	4,583 ± 291				
M99VJ-991	0.1	4.73 ± 0.18	16.8 ± 0.59	3,584 ± 197				
Alluvial fan unit			13.8 ± 0.62	2,918 ± 243				
Kingston Wash								
M99VJ-992	0.4	5.35 ± 0.19	>112 ± 2.91	>20,872 ± 1,334				
Eolian sand in Qia2 alluvium			>83.4 ± 4.71	>15,522 ± 1,036				
M99VJ-993	15[c]	4.90 ± 0.11	277 ± 6.91	51,686 ± 3,957				
Cemented sand in Qoa alluvium			282 ± 9.59	52,819 ± 3,308				
M99VJ-994	0.3	4.90 ± 0.11	183 ± 21.9	37,362 ± 2,447				
Eolian sand in Qia2 alluvium			187 ± 23.3	38,254 ± 2,453				
Salt Creek Wash								
M99VJ-989	2.4	6.47 ± 0.20	31.8 ± 0.38	4,912 ± 328				
Sand just under debris flow								
M01OM-1843	0.3	6.27 ± 0.09	33.1 ± 0.54	5,283 ± 234	3.78 ± 0.06	18.8 ± 0.42	42 (52)	4,982 ± 161
Below M99VJ-989, sand								
SMVJ-modern	1.1	6.07 ± 0.22	1.86 ± 0.06 (top)	306 ± 24	6.07 ± 0.22	3.18 ± 0.41 (top)	13 (24)	524 ± 138
Mud-cracked block from active channel			2.46 ± 0.06 (mid)	406 ± 26		3.71 ± 0.41 (mid)	12 (24)	610 ± 143
			2.27 ± 0.05 (mid)	666 ± 82		4.58 ± 0.29 (mid)	21 (24)	755 ± 99
			2.55 ± 0.06 (bot)	1,157 ± 78		4.79 ± 0.32 (bot)	22 (24)	790 ± 107

Table 1. Feldspar IRSL and quartz OSL ages from the Mojave Desert study area—Continued

Lab ID Sample information ID, area and genesis	Field Moisture (%)	Dose Rate (Gy/ka) (±1s%)	Equivalent Dose (Gy) (±1s%)	Age (yr) IRSL[a]	Dose Rate (Gy/ka) (±1s%)	Equivalent Dose (Gy) (±1s%)	N	Age (yr) quartz OSL[b]
Silurian Lake Playa								
M99VJ-987 northern bar	1.3	6.18 ± 0.19	41.2 ± 1.32 39.3 ± 0.98	6,664 ± 478 6,347 ± 451				
M99VJ-988 southern bar	1.2	6.19 ± 0.19	5.89 ± 0.68	925 ± 229				
M01OM-1844 southern bar (duplicate)	0.1	6.31 ± 0.10	4.63 ± 0.37 6.02 ± 0.66	733 ± 119 953 ± 206	4.26 ± 0.06	1.52 ± 0.26	32 (47)	356 ± 121
California Valley								
LCW-1a Qia deposit (upper)	20[c]	6.13 ± 0.25	>804 ± 60.3 >823 ± 74.1	>131,080 ± 28,574 >134,219 ± 13,468		Not suitable		
LCW-1b Qia deposit (lower)	15[c]	4.97 ± 0.17	>722 ± 46.6 >663 ± 46.4	>145,233 ± 14,152 >133,467 ± 12,171		Not suitable		
LCW-3a Upper GWD calcareous sand	20[c]	5.16 ± 0.12	114 ± 1.30	22,167 ± 1,178	3.68 ± 0.08	72.4 ± 2.43	31(36)	19,682 ± 1,580
LCW-3b Yellow sand	15[c]	4.92 ± 0.07	saturated		3.36 ± 0.05	saturated		
LCW-3c Lower GWD calcareous sand	15[c]	6.01 ± 0.08	309 ± 9.03	51,515 ± 3,338	4.08 ± 0.06	239 ± 11.3	44 (48)	58,652 ± 4,049
M01OM-1842a top GWD gravelly silt	15[c]	4.48 ± 0.07	>440 ± 24.8 >607 ± 43.5	>98,231 ± 11,509 >153,368 ± 22,524				

Table 1. Feldspar IRSL and quartz OSL ages from the Mojave Desert study area—Continued

Lab ID Sample information ID, area and genesis	Field Moisture (%)	Dose Rate (Gy/ka) (±1s%)	Equivalent Dose (Gy) (±1s%)	Age (yr) IRSL[a]	Dose Rate (Gy/ka) (±1s%)	Equivalent Dose (Gy) (±1s%)	N	Age (yr) quartz OSL[b]
M01OM-1842b Lower sand	15[c]	10.9 ± 0.38	disequilibrium in dose		6.36 ± 0.22			
Red Pass								
M01OM-1849a Upper sand, Qya4	1.2	5.31 ± 0.08	64.3 ± 1.22 67.9 ± 0.93	12,112 ± 588 12,788 ± 524	3.88 ± 0.06	44.8 ± 0.67	46 (48)	11,537 ± 234
M01OM-1849b Lower sand, Qia2?	1.4	4.85 ± 0.07	150 ± 1.70 104 ± 1.87	30,894 ± 1,108 21,419 ± 986	3.85 ± 0.06	142 ± 2.55	31(40)	36,881 ± 1,290
Silver Lake overflow channel								
M01SM-1852a Top GWD indurated carbonate	15[c]	2.15 ± 0.05	56.8 ± 1.00	26,400 ± 1,465	1.42 ± 0.03	45.5 ± 2.32	13 (40)	32,027 ± 3,496
M01SM-1852b Bottom GWD indurated carbonate	15[c]	3.50 ± 0.09	214 ± 3.08	61,065 ± 3,737	2.50 ± 0.06	124.5 ± 2.58	18 (30)	49,827 ± 5,551
M01SM-1853 Eolian sand ramp	0.8	4.49 ± 0.06	45.7 ± 0.88	10,172 ± 483	3.30 ± 0.05	35.6 ± 0.71	25 (30)	10,740 ± 268

[a]Data from Daybreak Reader, fine-grained silt (4-11 micron). See Table 3 for specific parameters.

bData from Riso Reader, fine-grained sand (90-105, 105-125, 125-150, 150-180 fractions). See Table 4 for specific parameters. N = Number of replicated equivalent dose (De) estimates used to calculate the mean. Figures in parentheses indicate total number of measurements made including failed runs with unusable data.

[c]Average water content had to be assumed as the sample was indurated, collected as a solid block and required HCL treatment for disaggregation.

Table 2. Sample location data

Sample No.	UTM E	UTM N	date	deposit	feature sampled
M99VJ-990	579355	3938206	10/17/99	Qya3	eolian sand lens
M99VJ-991	580056	3929066	10/17/99	Qya3	sand-rich alluvium
M99VJ-992	586066	3942713	10/17/99	Qia2	eolian sand lens
M99VJ-993	585942	3942763	10/17/99	Qoa	eolian sand lens
M99VJ-994	586756	3942774	10/17/99	Qia2?	eolian sand lens
M99VJ-989	571220	3938243	10/17/99	wash	sand bed
M01OM-1843	571213	3938241	12/04/01	wash	sand bed
mud block	571220	3938243	10/17/99	active channel	mud-cracked block
M99VJ-987	574130	3933553	10/17/99	lake bar	playa bed
M99VJ-988	576194	3930412	10/17/99	lake bar	sand bed
M01OM-1844	576202	3930409	12/04/01	lake bar	sand bed
LCW-1a	586095	3963330	12/03/01	>Qia2; $\leq$ Qia3	ground-water enhanced sand-silt bed
LCW-1b	586116	3963318	12/03/01	>Qia2; $\leq$ Qia3	ground-water enhanced sand-silt bed
LCW-3a	585881	3963746	12/03/01	GWD	sandy mud
LCW-3b	585881	3963746	12/03/01	GWD	sand bed
LCW-3c	585881	3963746	12/03/01	GWD	sandy mud
M01OM-1842a	590542	3978404	12/04/01	Tertiary?	muddy sand
M01OM-1842b	590542	3978404	12/04/01	Tertiary?	muddy sand
M01SM-1849a	564267	3909254	12/05/01	Qia2	sand bed
M01SM-1849b	564267	3909254	12/05/01	Qia2	sand bed
M01SM-1852a	578518	3917293	12/05/01	Qia2	groundwater carbonate
M01SM-1852b	578518	3917293	12/05/01	Qia2	groundwater carbonate
M01SM-1853	578413	3917354	12/05/01	sand ramp	colluvial wedge facies

Note: All UTM coordinates are from Zone 11 using NAD83 projection

A smaller lake, Lake Dumont, existed where Valjean Valley meets Silurian Valley, and Kingston Wash enters the Silurian Valley system at Salt Spring Hills. Lake Dumont existed before Lake Mojave and started to fill before 26,000 calibrated yrs BP (Anderson and Wells, 2003). Recent studies have suggested that some or all of the Lake Dumont deposits are wetland deposits (Reynolds and others, 2003; Bright and Anderson, this volume), rather than widely spread lacustrine deposits.

The Pleistocene to Holocene transition in the Silurian Valley area is marked by hydrologic responses of several kinds. The histories of the desert rivers (Amargosa and Mojave) and the pluvial lakes (Mojave, Dumont and Manley) were closely linked and driven by changes in climate (Wells and others, 2003) and in drainage patterns. Regional aquifer hydrology drives changes in springs and wetlands in Tecopa Basin and California Valley (Quade and others, 1995; 1998; 2003). In contrast, local aquifers probably controlled the timing of wetland discharge in and near Silurian Valley. Piedmont systems underwent widespread deposition during the Pleistocene-Holocene transition (McDonald and others, 2003) with later Holocene depositional events being more restricted in both volume and area. Eolian sand and dust deposition in the greater Silurian Valley area is widespread, with prolific sources in the many lakes and playas as well as distal alluvial fan systems (Fig. 1).

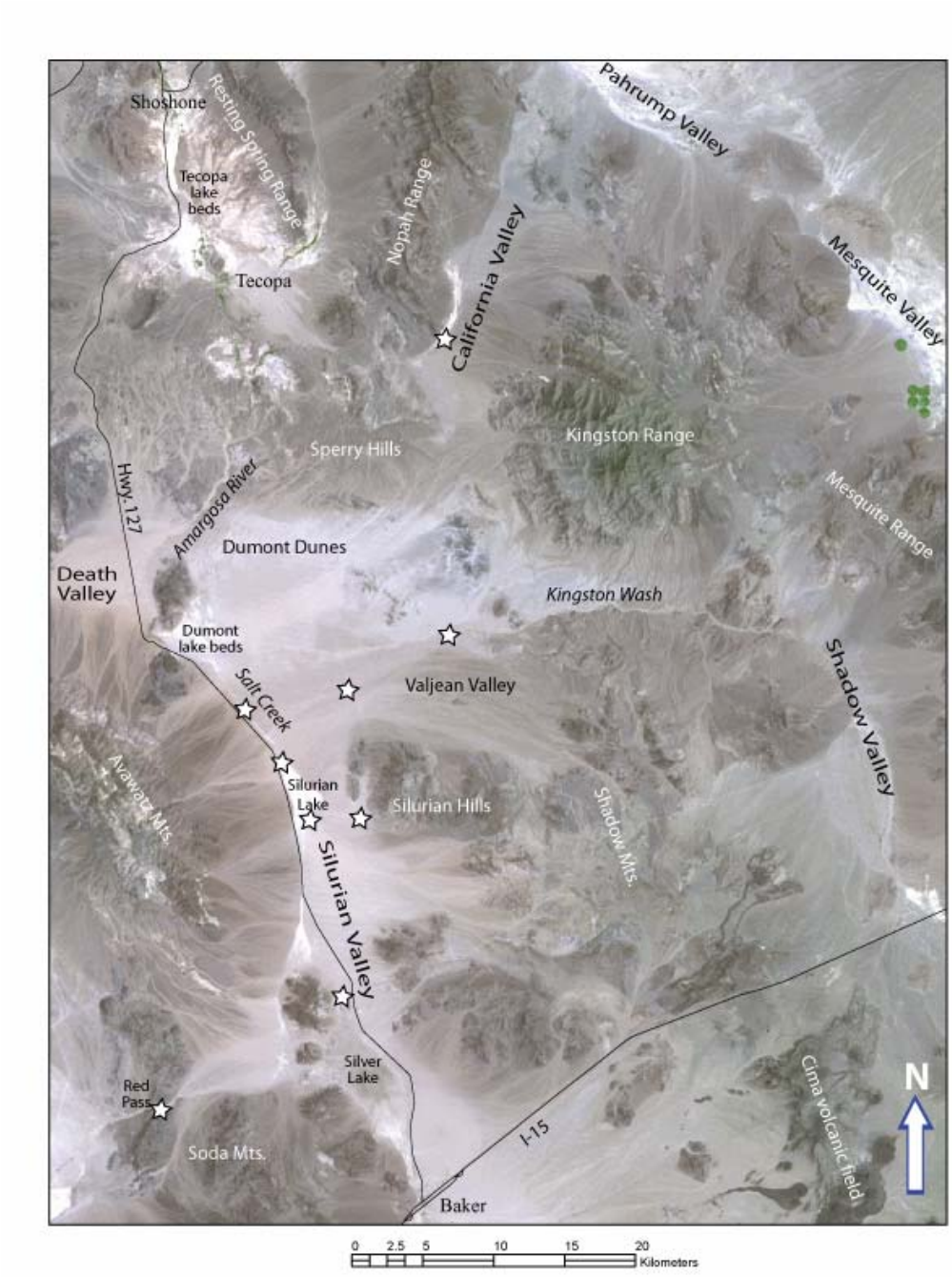

Figure 1. Landsat 6 image of the northeast Mojave Desert showing locations of the OSL sampling sites (stars) discussed in this paper and principal geographic features. Pluvial Lake Mojave occupied the area of Silver Lake and regions farther south.

Previous chronologic studies in the northeastern Mojave Desert include magneto-stratigraphic studies and tephrochronology of the upper Pliocene to middle Quaternary Tecopa beds (Sarna-Wojcicki and others, 1987: Hillhouse, 1987; Morrison, 1999; Cox and Hillhouse, 2003), dating of Lake Mojave deposits and associated piedmont alluvial units (Wells and others, 2003; Reheis and others, 1989), Silver Lake Playa (Owen and others, 2007) and studies of eolian sand sheets and dunes (Wintle and others, 1994).

Much of the stratigraphic and geologic control for our study is from recent refinements in geologic mapping. The surficial geology of the greater Silurian Valley area was mapped at a scale of 1:100,000 (Menges and Miller, unpublished data; Schmidt and McMackin, 2006) and locally in more detail (Miller and Yount, unpubl. mapping) by standard field methods that included description of landforms, deposit characteristics, and pedogenesis. Stereoscopic study of aerial photographs was used to extrapolate observations and, in places such as Valjean Valley where aerial photographs did not provide adequate resolution, extensive field traverses provided additional map information. During these field studies, locations of potentially datable deposits were noted and those that showed the most promise and the most relevance for dating regionally extensive units or aspects of particular local problems were selected for OSL or added cross-dating. At these locations, stratigraphic sections were measured and described and sediments were sampled. Related sub-sample splits for particle size analysis, paleontology, or other purposes were taken from field samples as needed.

Luminescence methods

Sampling and Dosimetry

Samples were collected by auguring into a freshly cleaned face (natural exposure or man-made pit), driving a polyvinyl chloride (PVC) tube into the sediment, and capping the ends of the tube under shielding that protected the face from sunlight. Samples were also collected for water content and dose rate measurements, except for a few samples collected in 1999, for which a portable gamma-ray spectrometer was used in the field to obtain the dose measurements. Dosimetry measurements of potassium (K), uranium (U), and thorium (Th) were taken *in situ* using a portable Exploranium® gamma ray spectrometer, which counts elemental concentrations with an internal sodium-iodide (NaI) crystal detector. The gamma-ray spectrometer provides the isotopic discrimination of gamma rays; correspondingly, beta and alpha dose rates may also be estimated. At each OSL sample location there least two 1,000-second counts were recorded (about 16.5 minutes) from the gamma-spectrometer.

For lab dosimetry, bulk samples were dried in the lab, homogenized by lightgrinding, weighed, sealed in plastic planchets having a diameter of 15.2 by 3.8 cm (some modification from Murray and others, 1987), then immediately placed in a gamma-ray spectrometer for about 8.5 hours. Samples were stored for a minimum of 21 days to allow radon to achieve radioactive equilibrium, and then the measurement was repeated. The fraction of radon emanation was estimated from the difference of these two spectrometer measurements. The gamma-ray spectrometers were calibrated on measurements of laboratory standards with known concentrations of K, U, and Th. Standards were measured at intervals throughout the period of time during which the samples were measured. The observed errors for the standards indicate that the absolute accuracies for measuring sample concentrations are approximately 0.1 % K, 0.4 ppm U, and 0.3 ppm Th, for this gamma-spectrometer configuration (Snyder and Duval, 2003). Alpha and beta contributions to the dose rate were corrected for grain-size attenuation (Aitken, 1985). Cosmic-ray dose rate was estimated for each sample as a function of depth, elevation above sea level and geomagnetic latitude (Prescott and Hutton, 1988). Saturation moisture was estimated by packing dry soil into plastic tubes with known volumes, thoroughly wetting the sediment and re-measuring the volume. This packing is done to simulate an overburden that was experienced by the OSL sample site.

For comparative purposes, we also determined the concentrations of K, U and Th using instrumental neutron activation analysis (INAA) following the procedures described in Budahn

and Wandless (2002). Measured elemental concentrations, associated dose rates, and cosmic ray contributions for both gamma-ray spectrometry and INAA are presented in Table 3. The agreement between *in-situ* and laboratory gamma-ray measurement as well as INAA results suggests negligible or no disequilibrium in the uranium and thorium dose-rate components, with the exception of some GWD deposits. For the GWD deposits we followed dosimetric approximations over time using formulas developed in Rich and others (2003).

Sample preparation and determination of the equivalent dose

Using subdued orange-light in our laboratory, possible light-exposed end material from each tube (~ 3 cm) was discarded and samples prepared for dating using standard procedures with appropriate modifications (Aitken, 1998; Millard and Maat, 1994; Roberts and Wintle, 2001; Singhvi and others, 2001). Generally, the largest usable sand-size was determined to be 125-90 μm, although sometimes the 150-125 μm and the 250-180 μm sizes were also utilized for OSL.

Two types of luminescence dating were performed on different grain sizes and mineral fractions. Blue-light OSL (that OSL which uses a blue wavelength to stimulate the quartz) was done on fine sand-size quartz separates. IRSL (the OSL which uses infra-red wave length stimulation on K-feldspars) was done on a polymineralic (no mineral separation) fine silt fraction (4-11 μm). The samples were pretreated with 4N hydrochloric acid (HCl) and 35-50% hydrogen peroxide (H_2O_2), and then wet sieved to isolate the sand-size grains. The silt-size grains passing through the 170 mesh were saved and the 4-11 μm grains were separated using a Stoke's Law settling procedure. To remove feldspars and isolate pure quartz from the selected sand fraction, we centrifuged the sand sequentially in Lithium Sodium Tungstate (LST), a heavy liquid solution with varied densities of 2.58 and 2.67 g ml^{-1}. The float from 2.67 was subjected to a 50% solution of Hydrofluoric (HF) acid for forty minutes while in an ultrasonic bath. After decanting the HF, we rinsed the sample in 4N Hydrochloric (HCl) for ten minutes and re-sieved to winnow broken grains. For blue-light OSL, we affixed sand-size grains to the center of a 1-cm diameter steel disc with a light cover of Silkospray®. For IRSL, polymineral silt was evaporated from a methanol slurry, covering the entire 1-cm diameter aluminum disc.

All sand-size quartz samples were analyzed by single-aliquot regeneration (SAR) procedures (Murray and Wintle, 2000; Banerjee and others, 2001) with blue-light excitation. Dose recovery and preheat plateau tests were performed to ensure that the sediments were responsive to optical techniques and that the proper preheat temperatures were used in producing the equivalent dose (D_e) values. Run parameters for the blue-light OSL data are given in Table 4 and run parameters for IRSL are given in Table 5.

The fine-grain (4-11 μm) polymineral extracts from all samples were dated using the total-bleach multiple-aliquot additive-dose (MAAD) method (Singhvi and others, 1982; Lang, 1994; Richardson and others, 1997; Forman and Pierson, 2002). At least two attempts were made per IRSL sample to provide MAAD ages. Anomalous fading tests on the stability of the luminescence signal indicated little to no signal instability (recording ratios of 0.91 to 1.07). These values are a ratio of luminescence emission after storage of >30-60 days divided by the immediate measurement; a ratio of 1.0 indicates stable luminescence. IRSL ages agree well with available quartz blue-light OSL age control (Table 1) and, to a lesser extent, with any known radiocarbon dates of similar stratigraphy, and seem to obviate the need for an extensive correction factor (Huntley and Lamothe, 2001).

® (Use of trade names is for descriptive purposes only and does not imply endorsement by the U.S. Geological Survey).

Table 3. Concentration of potassium, uranium, thorium and their contributions to the dose rate. Also listed are rubidium contribution and the cosmic dose rate. These contributions show alpha, beta and gamma components. Dose rates for blue-light OSL do not have an alpha component and only 90% of the beta component and are not shown

Sample ID	K (%)	U (ppm)	Th (ppm)	Elevation (m)	Depth (cm)	Dose rate[c] (Total Gy/ka)	K (Gy/ka)	U (Gy/ka)	Th (Gy/ka)	Rb (Gy/ka)	Cosmic ray (Gy/ka)
Valjean Valley alluvial fan											
M99VJ-990	2.03	2.24	6.00	309	25	4.53	2.146	1.189	0.911	0.040	0.242
M99VJ-991	2.01	2.53	6.04	298	20	4.73	2.148	1.359	0.928	0.040	0.252
Kingston Wash											
M99VJ-992[a]	2.14	2.20	10.70	462	125	5.35	2.284	1.180	1.642	0.043	0.196
M99VJ-993[b]	2.07	2.34	10.65	462	125	5.34	2.209	1.256	1.635	0.041	0.196
M99VJ-993	2.19	2.31	11.01	462	125	5.51	2.338	1.239	1.690	0.044	0.196
M99VJ-994[a]	2.46	3.16	8.00	485	125	4.90	2.224	1.413	1.026	0.041	0.197
Salt Creek Wash											
M99VJ-989[a]	2.70	3.01	10.31	188	25	6.23	2.820	1.577	1.546	0.053	0.236
M99VJ-989[b]	2.64	2.90	12.70	188	25	6.47	2.757	1.519	1.904	0.052	0.236
M99VJ-989	2.65	2.85	11.10	188	25	6.21	2.768	1.493	1.664	0.052	0.236
M01OM-1843	2.72	2.58	11.42	188	130	6.27	2.900	1.382	1.751	0.054	0.183
SMVJ-modern[b]	3.06	5.41	14.50	188	5	8.65	3.235	2.872	2.202	0.060	0.286
SMVJ-modern	2.88	4.99	15.13	188	5	8.33	3.044	2.649	2.298	0.057	0.286
Silurian Lake Playa											
M99VJ-987[a]	2.41	3.51	9.94	208	40	6.18	2.547	1.863	1.510	0.048	0.214
M99VJ-988[a]	2.66	3.35	8.60	197	25	6.19	2.812	1.778	1.306	0.053	0.236
M01OM-1844	3.18	2.03	10.06	197	40	6.31	3.398	1.091	1.546	0.064	0.213

Table 3. Concentration of potassium, uranium, thorium and their contributions to the dose rate. Also listed are rubidium contribution and the cosmic dose rate. These contributions show alpha, beta and gamma components. Dose rates for blue-light OSL do not have an alpha component and only 90% of the beta component and are not shown—Continued

Sample ID	K (%)	U (ppm)	Th (ppm)	Elevation	Depth (m)	Dose rate[c] (cm)	K (Total Gy/ka)	U (Gy/ka)	Th (Gy/ka)	Rb (Gy/ka)	Cosmic ray (Gy/ka)
California Valley											
LCW-1a	2.71	3.89	13.14	2334	350	6.13	2.450	1.740	1.686	0.046	0.205
LCW-1b	2.61	2.37	10.78	2334	770	4.97	2.359	1.060	1.383	0.044	0.125
LCW-3a	2.51	3.20	11.54	2340	350	5.16	2.157	1.355	1.403	0.040	0.205
LCW-3b	2.53	2.33	10.63	2340	435	4.92	2.287	1.042	1.364	0.043	0.184
LCW-3c	2.67	3.75	13.31	2340	520	6.01	2.413	1.677	1.708	0.045	0.166
M01ML-1842a	2.11	2.98	6.05	2323	5	4.48	1.907	1.333	0.776	0.036	0.424
M01ML-1842b	2.74	16.32	7.42	2323	610	10.92	2.477	7.299	0.952	0.046	0.149
Red Pass											
M01ML-1849a	2.84	2.32	10.65	2331	75	5.31	2.567	1.038	1.366	0.048	0.287
M01ML-1849b	2.61	2.22	9.84	2331	395	4.85	2.359	0.993	1.262	0.044	0.193
Silver Lake overflow channel											
M01SM-1852a	0.56	1.85	3.92	2327	50	2.15	0.506	0.827	0.503	0.009	0.302
M01SM-1852b	1.68	1.30	9.10	2327	350	3.50	1.519	0.581	1.168	0.028	0.205
M01SM-1853	2.43	1.79	9.35	2314	200	4.49	2.196	0.801	1.200	0.041	0.248

[a]counted in-situ with portable gamma spectrometer (see text for discussion).

[b]counted using instrumental neutron activation analyses (INAA) (see text for discussion).

[c]dose-rate figures have been rounded to three significant figures, but the total dose rates and contributions have been calculated using values prior to rounding. Dose rates were calculated assuming a field water content (expressed as % dry mass) between 1 to 10 ± 5% and 15-20 ± 5% (indurated block values), using a value of 0.040 ± 0.002 (Rees-Jones, 1995). Central values are given for dose rates, errors are incorporated into that given for the total dose rate.

Table 4. Single aliquot quartz OSL Measurement Parameters

Instrument: Riso TL/OSL-DA-15A/B **Stimulation source**: 6 clusters LED, emission centered 470 nm **Power delivered to aliquot:** 22 mW/cm^2 **Duration of Stimulation:** 40 seconds **PMT:** EMI 9236Q **Aliquot Temp:** 125°C **Detection filters:** 2 Hoya U-340 **Preheat:** 220°C to 260°C/10 sec with cut heat of 160°C/10 sec **Analytical Procedures:** IRSL 100 seconds "wash", Boetter-Jensen, et al., 2000; Duller, 2001 and Minitab 14

Table 5. Multiple aliquot feldspar IRSL Measurement Parameters

Instrument: 1100 Automated TL Systems **Stimulation source:** 30 IR diodes, emission centered on 880 nm **Power delivered to aliquot:** 19 mW/cm^2 **Duration of Stimulation:** 100 to 30 seconds **PMT:** Thorn-EMI 9635Q **Aliquot Temp:** 30°C **Detection filters:** Schott BG-39 & Kopp 7-59 **Preheat:** 124°C/64 hours or 140°C/6 hours **Analytical Procedures:** TLApplic 4.2 6 software & Minitab 14

Results and Discussion

Valjean Valley including site description

Valjean Valley meets Silurian Valley approximately where Kingston Wash joins Salt Creek Wash and is important because it contains an array of deposits that were luminescence dating targets (Fig. 2). Valjean Valley is a gently undulating broad plain of alluvial sediment derived from three trunk streams that drain the uplands of Squaw Mountain and nearby land, as well as from Kingston Wash. Kingston Wash drains Shadow Valley and consequently is a much larger wash than Salt Creek Wash. Eolian sand sheets distal to Dumont Dunes overlie and are interbedded with alluvium in much of the valley north of Kingston Wash. South of the wash, eolian sand deposits are present only near the east end of Silurian Lake playa, but eolian sand is an abundant constituent of the alluvium much farther up the fans (Fig. 2). The bed of Salt Creek Wash is composed of muddy sand for the most part, although gravel beds are present where it flows into and exits Silurian Lake playa.

For dating, we targeted eolian sand lenses in Pleistocene alluvium exposed in the cut bank of Kingston Wash and another sand lens in alluvium at Riggs Quarry (Fig. 2). These eolian sand beds are interbedded with alluvium that shows no apparent break in deposition, as evidenced by a soil or angular unconformity. At Kingston Wash, sample M99VJ-993 was taken from a gravelly sand lens that is probably fluvially reworked eolian sand. The bed is bouldery at its base (Fig. 3a), where it is possibly of debris-flow origin. The bed lies high in an old alluvial unit (Qoa) (Miller and Yount, unpublished data) that is characterized by a ballena landform and an extensive stage IV + morphology calcic horizon. The sample was taken 170 cm below the eroded crest of the

deposit as an intact block since the material was indurated and tube sampling was impossible. This block was tightly wrapped in aluminum foil and black plastic and transported to the lab for sub-sampling.

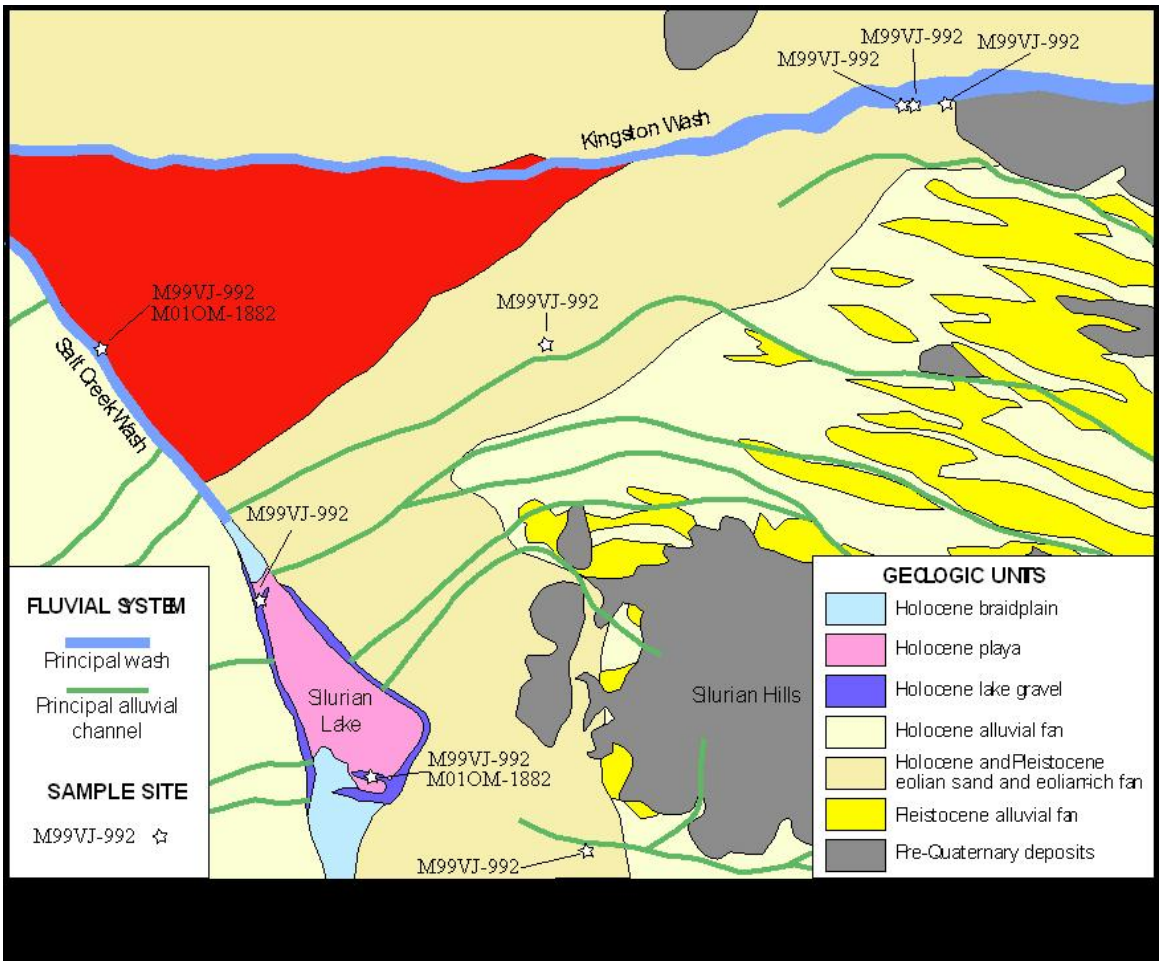

Figure 2. Map of sample sites and principal geologic features in Valjean Valley, Salt Creek and Silurian Lake. The massive, widespread debris flow of Kingston Wash is indicated by a red color. This map is adapted from detailed geologic mapping of Miller and Yount (unpub. data).

The base of the calcic horizon extends into the upper part of the sand bed, above the sampled interval. The resulting 52 ka IRSL age is much younger than we expected for this deposit, as other mapped Qoa units with this degree of soil development and landform characteristics contain the Bishop Ash and are 600 to 700 ka. We are uncertain how to interpret the results, although it is almost certain that the mid-Pleistocene age of the deposit is beyond IRSL and TL dating limits. The IRSL age may reflect infiltration of fines associated with soil development after stripping to form the ballena, or sampling problems that have created an artificially young age. An alternative hypothesis says that the assumption that Qoa deposits are middle Pleistocene is incorrect.

Also at Kingston Wash, samples M99VJ-992 and M99VJ-994 were taken from eolian sand lenses in intermediate age alluvial units (Qia2 of Miller and Yount, unpublished data) that are characterized by a nearly flat surface, moderate varnish on pavement clasts, and a pronounced stage II+ to III calcic horizon. At both sites the upper soil horizons above the calcic horizon were removed and are now overlain by a thin sheet of gravelly reworked eolian sand. Sample M99VJ-

992 was taken from 1.0 m below the calcic horizon for OSL dating (Fig. 3b). The muddy sand bed contains matrix-supported cobbles in the base, possibly representing a debris flow deposit, just like sample site M99VJ-993. The reported age is a minimum value >21 ka. The sample showed OSL saturation at high dose levels indicating the luminescence age is a minimum and for this reason could not be more precisely dated. It is also possible that the grains were poorly exposed to sunlight during deposition, although the histogram of equivalent dose data does not suggest this (Fig. 4). Adjacent to the deposit minimally dated by sample M99VJ-992 is an inset strath terrace cut into the fan. The deposit here has a slightly weathered stage II+ calcic horizon (Fig. 3c); we sampled 65 cm below this, into a fluvially reworked eolian sand bed. This sample (M99VJ-994) yielded IRSL ages of ~38 ka (Table 1). The two samples from older deposits therefore yielded results that only modestly constrain the true depositional ages at 52 ka and >21 ka, and the third sample indicated a depositional age of ~38 ka.

To the southwest of Silurian Hills, the deposit we next dated at Riggs Quarry is part of a widespread mid-Holocene unit (Qya3 of Menges and Miller, this volume) that is known to be younger than pluvial lake stands formed at about 10 ka (Reheis and others, 1989). The Qya3 deposit consists of thin- to medium-bedded sheetflow and channel deposits. An eolian sand lens lies about 60 cm below the surface. Sample M99VJ-991, (Fig. 2) taken from this sand lens, yielded IRSL ages of 2.92 ± 0.24 ka and 3.58 ± 0.20 ka. These deposits may correlate with a known short wet period around 3.6 ka (Wells and others, 2003).

Eolian sand is present throughout Valjean Valley, but not as discrete eolian depositional forms. Instead it forms sand-rich alluvial deposits, as evidenced by depositional structures such as channel cross-beds and poorly sorted grain size that includes gravel. We hypothesize that the eolian sand fraction is blown across the alluvial fan at times, and later worked into the alluvial fan deposit by fluvial processes. If so, these deposits might be good targets for OSL dating. To test this hypothesis, we sampled a sandy fan deposit near the townsite of Valjean, where unit Qya3 is characterized by a remnant bar and swale topography, a very weak pavement, weak reddening, and stage I calcic horizon development. We sampled ~ 30 cm deep in the Bk horizon to avoid illuvial fines (sample M99VJ-990, Table 1). Replicate IRSL ages on the same sample are 4.58 ± 0.30 and 4.54 ± 0.29 ka. This remarkable duplication indicates that the deposit was well bleached and the data show a normal dose distribution (Fig. 5).

Distal Kingston Wash forms a broad fan that is correlative to a unit Qya3 deposit based on soil development and surface characteristics (Fig. 2). This deposit contains abundant boulders and was evidently placed in a single catastrophic event as a debris flow or hyperconcentrated sediment flood deposit (Miller and others, Chapter A, this volume); herein we refer to it as “debris flow” for brevity. The debris flow extends 10.3 km along Kingston Wash and is 7 km wide along Salt Creek (Fig. 2). At most exposures, the deposit is currently less than 1 m thick; it is about 40 cm thick at the distal toe. Based on the current thickness, the volume of the deposit must be greater than 36×10^6 m^3. Boulders are commonly 1 m diameter, and up to 2 m diameter upstream from the Tonopah and Tidewater railroad grade.

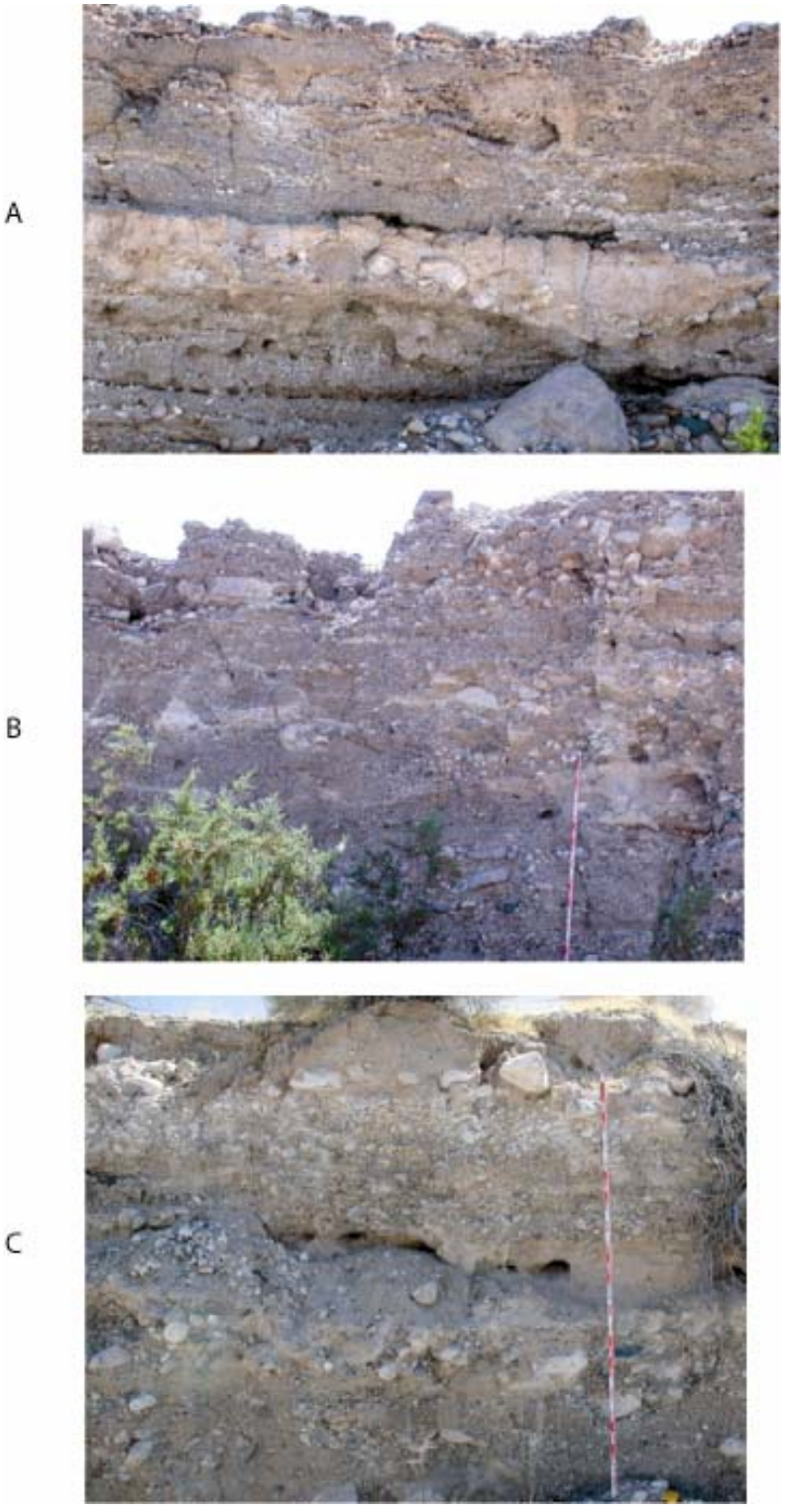

Figure 3. Photographs of the south bank of Kingston Wash, showing sampled sand beds and wash sediments. Tape is 2 m long in C. **A**. Qoa site for sample M99VJ-993. Sample taken just to right of photographed interval. Section approximately 3 m high. Note boulders in lower part of sand bed. **B.** Qia2 site for sample M99VJ-992. Block sampled from irregular shaped sand lens near top of tape. **C.** Qia2 site for sample M99VJ-994. Sampled bed is recessive weathering, near center of tape; hole to the left of tape is mammal-modified OSL sample site.

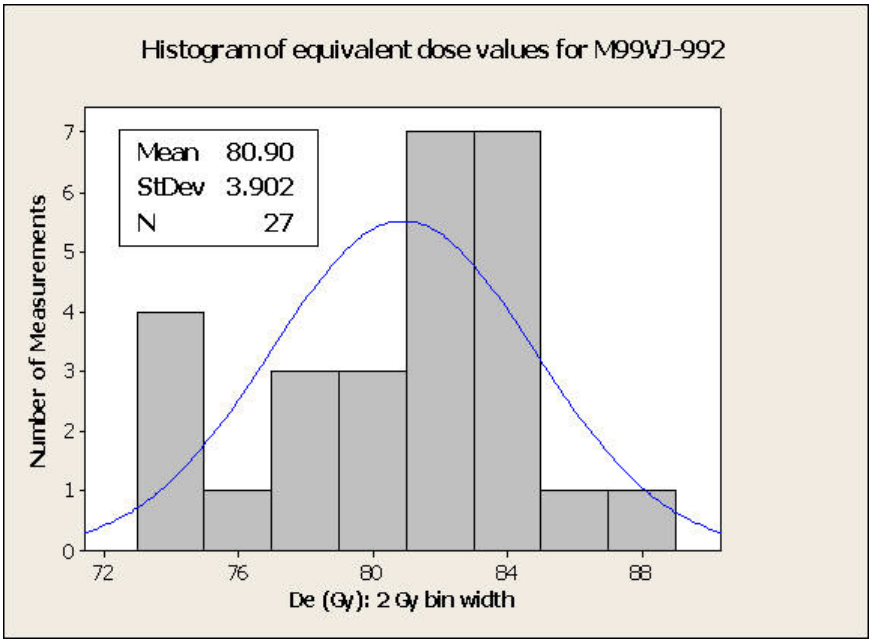

Figure 4. Histogram of MAAD-IRSL distributions in Equivalent Dose for M99VJ-992. Blue curve shows a normal distribution fit. Grays (Gy) are standard units of absorbed radiation, Equivalent Dose is D_e, N is total number of individual D_e measurements for one age and the standard deviation (StDev) is given to one sigma.

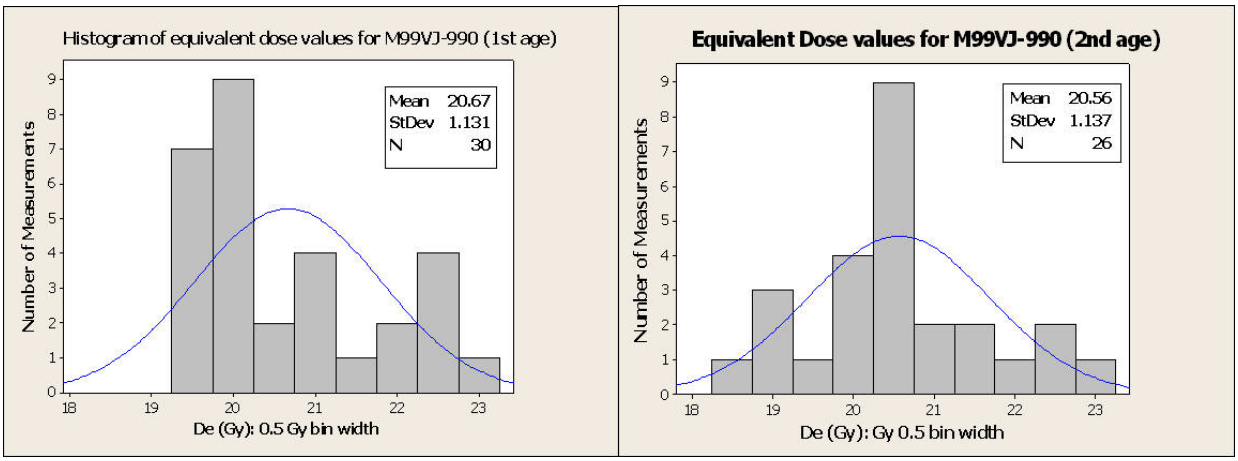

Figure 5. Histogram of MAAD-IRSL distributions in Equivalent Dose for M99VJ-990. Blue curve shows a normal distribution fit. Grays (Gy) are standard units of absorbed radiation, Equivalent Dose is D_e, N is total number of individual D_e measurements for one age and the standard deviation (StDev) is given to one sigma.

To date the debris flow bed, we had to sample in wash and distal fan deposits beneath it. The debris flow may have been deposited under cloudy or turbid flow conditions, resulting in inadequate grain bleaching during deposition. Instead, we sampled a fine-grained bed below the debris flow to approximate the age of the debris flow and another fine-grained bed farther below to test for stratigraphic consistency and rate of deposition.

At Salt Creek Wash, thin-bedded, well-sorted sand of the distal fan and Salt Creek Wash underlies the debris-flow deposit and is the most suitable for OSL dating based on the fine grain sizes and the likelihood of deposition by shallow flow from hours to days in streams. We collected two samples; 1) M99VJ-989, the second bed down and 15 to 25 cm below the debris-flow base and 2) M01OM-1843, the ninth bed down and 105 cm lower than M99VJ-989 (Fig. 6). The

samples were analyzed about two years apart and the later sample (M01OM-1843) was analyzed using both IRSL and blue-light OSL. The upper sample (M99VJ-989) yielded an age of 4.91 ± 0.33 ka and the lower yielded ages of 5.28 ± 0.24 ka (K-feldspar from IRSL) and 4.98 ± 0.16 ka (quartz from blue-light OSL). The ages for the lower bed are within overlapping error and indicate an age of ~ 5.1 ka. The ages are in stratigraphic order and consistent with deposition rates of ~ 2 mm/yr, and thus are internally consistent. This allows us to suggest that the debris flow is slightly younger than the upper dated bed, or less than 4.9 ka.

A modern mud-cracked sediment block was sampled from the floor of Salt Creek Wash to study the effect of muds in the deposit on luminescence properties. The mud block had recently dried out from a fluvial event sometime prior to October, 1999, but was still moist within its center. The mud block was divided in the lab into four equal samples (Table 1) and the silt of 4-11 microns was analyzed for each. The top layer was dated using IRSL to 306 ± 24 years and with blue-light OSL at 524 ± 138 years, which indicates some inherited component of silt grains that were not bleached during deposition since the ages are not closer to a truly "zeroed age." The ages progressively increase downward to the bottom where dates of 1,157 ± 78 years with IRSL and 790 ± 107 years with blue-light OSL were obtained. The downward increase in ages suggests that although the depositional conditions were too turbid to allow full bleaching of previous inherited luminescence signals (oral communications, Ken Lepper, North Dakota State University, 2005), there was enough partial bleaching to allow the upper water column grains to begin to respond. Otherwise we would expect to see ages with overlapping errors for the "mudcrack" sample and not the gradational changes we did see.

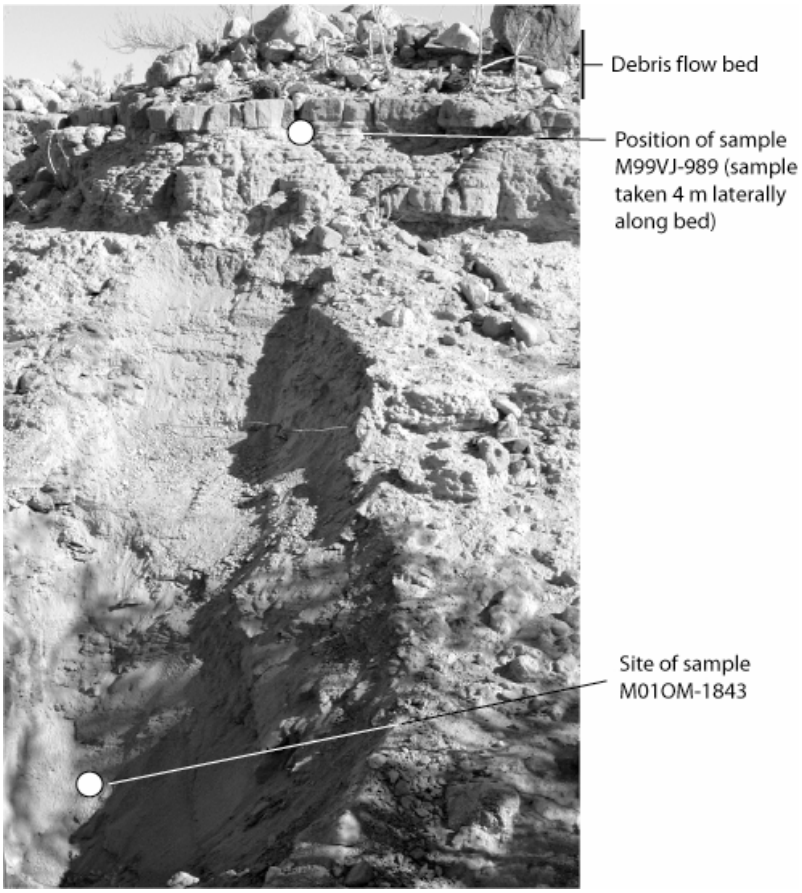

Figure 6. Photograph of sampled section at Salt Creek. M99VJ-989 was sampled from the indicated bed but out of the field of view. Note boulders and cobbles of granite in the overlying debris-flow bed, in contrast to sand and finer grain sizes of lower, thin beds of distal alluvial fan and wash origin. The total section thickness is about 1.35 m.

Silurian Lake

Silurian Lake is an unusual playa, one that we term a "through-flow playa," because Salt Creek Wash enters it on the south side at about elevation 205 m and exits on the north at about elevation 204 m. The playa is not a true depositional basin, but rather a stretch in the wash that is broad, nearly horizontal, and experiences both bed load and suspended load deposition. During deep flow events, much of the water and sediment goes downstream and beds are typically thin and sediment poorly sorted, ranging from sand to clay in size. If the playa was in its current through-flow configuration during the Holocene, as suggested by wash deposits above and below the playa that range widely in age, it might be a sensitive recorder of stream dynamics, including damming by the Kingston Wash debris flow. Subtle lacustrine bars are present on the north and south sides of the playa (Fig. 2, 7) and represent shallow lakes either from sustained high-volume stream flow or from temporary damming of Salt Creek. In order to explore the possibility that the debris flow from lower Kingston Wash dammed Salt Creek we conducted reconnaissance luminescence sampling of bars in Silurian Lake, reasoning that thinly bedded fine sand and silt beds were likely exposed to sunlight in the shallow waters.

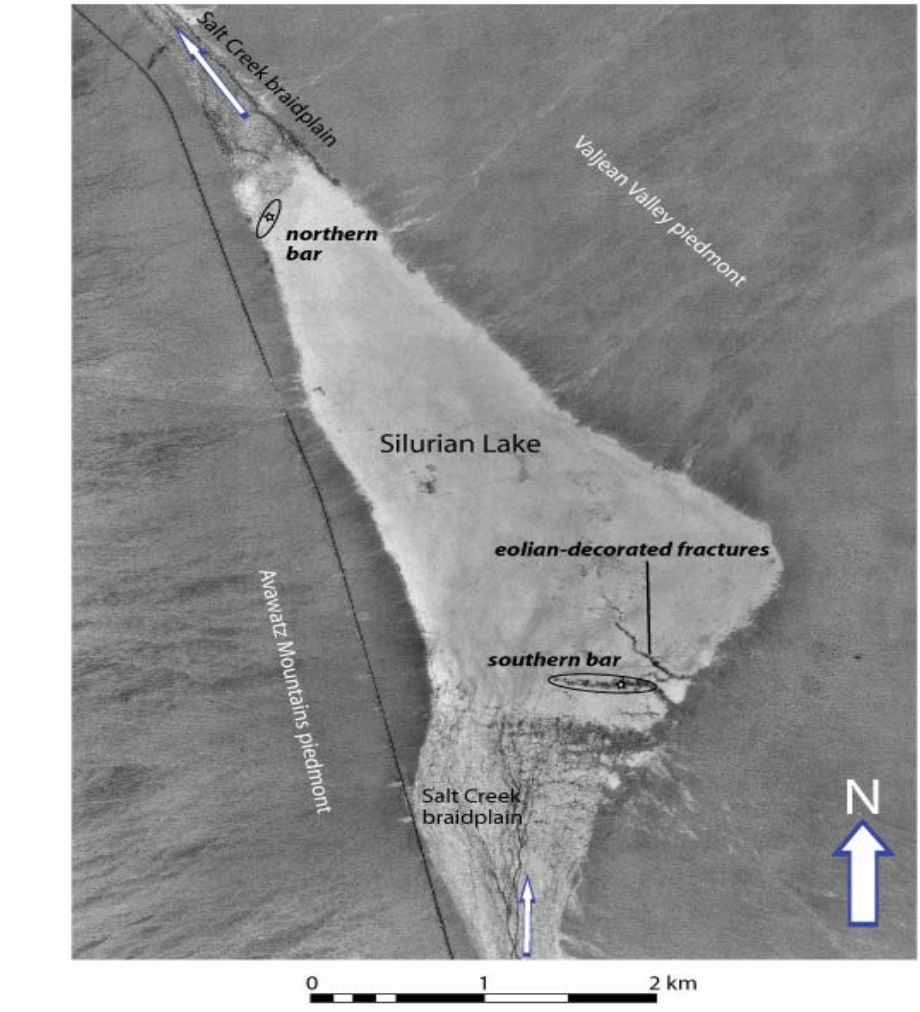

Figure 7. Aerial photograph of Silurian Lake showing sample sites and lacustrine bars. Smaller arrows indicate flow direction through Silurian Lake playa.

The bar at the north end of Silurian Lake is around 205 m in elevation and is about 20 cm higher than the playa floor. The bar is very rounded and capped by fine gravel that is moderately well sorted. We dug a pit through the bar, which consists of 12 cm of lacustrine sand and gravel on 7 cm of sandy playa mud. Underlying playa deposits, which are poorly sorted and less distinctly bedded than the overlying bar deposits, are about 10 cm thick. Under this interval is ripple-laminated sand. Because the lacustrine beds of the bar were so thin and contained abundant silt of probable illuvial origin, we sampled underlying playa beds that contained abundant sand and silt. The resulting age for M99VJ-987 at ~ 6.5 ka indicates that the bar formed sometime after 6.5 ka, and probably significantly before the debris flow emplacement around 4.6 to 5.2 ka.

The bar at the south end of Silurian Lake is a long, broad feature that shows little sign of erosion; a few small channels are cut through it and carry flow from Salt Creek to the playa, but the channel cutbanks are sharp and little rounding of the surface of the bar is apparent. It appears morphologically younger than the bar at the north end of the playa. This southern bar is composed of thin bedded to laminated fine gravel and sand in moderately- to well-sorted parallel beds. Little evidence for illuvial silt or sand is present, so we dated a silty sand bed that was 38 cm below the surface. Sample M99VJ-988 yielded an IRSL age of 952 ± 229 years, surprisingly young. To test the validity of the young date we re-sampled 5 m away in a gravelly sand bed beneath the bed previously sampled, at a depth of 40 cm. Sample M01OM-1844 yielded similarly young ages: IRSL ages of 733 ± 119 and 953 ± 206 years, and a blue-light OSL age on quartz of 356 ± 121 years (Fig. 8).

Figure 8. Photographs of sampled sections at a lacustrine bar near southern Silurian Lake. **A:** View of two sample sites looking eastward along the crest of the bar. Note the vegetation-choked channel cutting through the bar behind samplers Mahan and Menges. The photo was taken on 12/4/01. **B:** Sampling pit for M01OM-1844. Note the concentration of gravel at the surface, but the lack of an Av horizon, as most of the pit is composed of thin beds of moderately sorted sand and fine gravel. The sample was taken at the bottom of the pit, which was near tape measure 0.8, and was 40 cm deep.

The large discrepancy between the blue-light OSL and IRSL ages can be explained by the fact that the quartz grains used in blue-light OSL are more sensitive to resetting by sunlight, but also more sensitive to sampling irregularities. The uncertainty between IRSL and OSL methods is much greater than the analytical uncertainty, but the deposit seems reasonably dated between 500 to 1,100 years old and suggests that the bar is 800-850 years old. The mean age and weighted error from IRSL dates is 816 ± 119 years. This southern bar certainly is much younger than the bar at the northern end of Silurian Lake.

California Valley

At least two generations of groundwater-discharge (GWD) deposits are exposed along incised reaches of the axial channel and adjacent tributaries of the California Wash drainage in lower California Valley (Figs. 1 and 9). Since GWD are so important in the desert, attempts to date their depositional history via luminescence are well warranted. These GWD deposits record at least two significant, local intervals of paleodischarge of ground water at this site, a valley that currently has seepage only at the lower end. Also, the two GWD deposits are intricately intermixed alluvium associated with both the incised axial drainage and adjoining dissected piedmont fans. Thus these GWD deposits have the potential for constraining the ages of alluvial stratigraphy and geomorphic processes in this part of the valley.

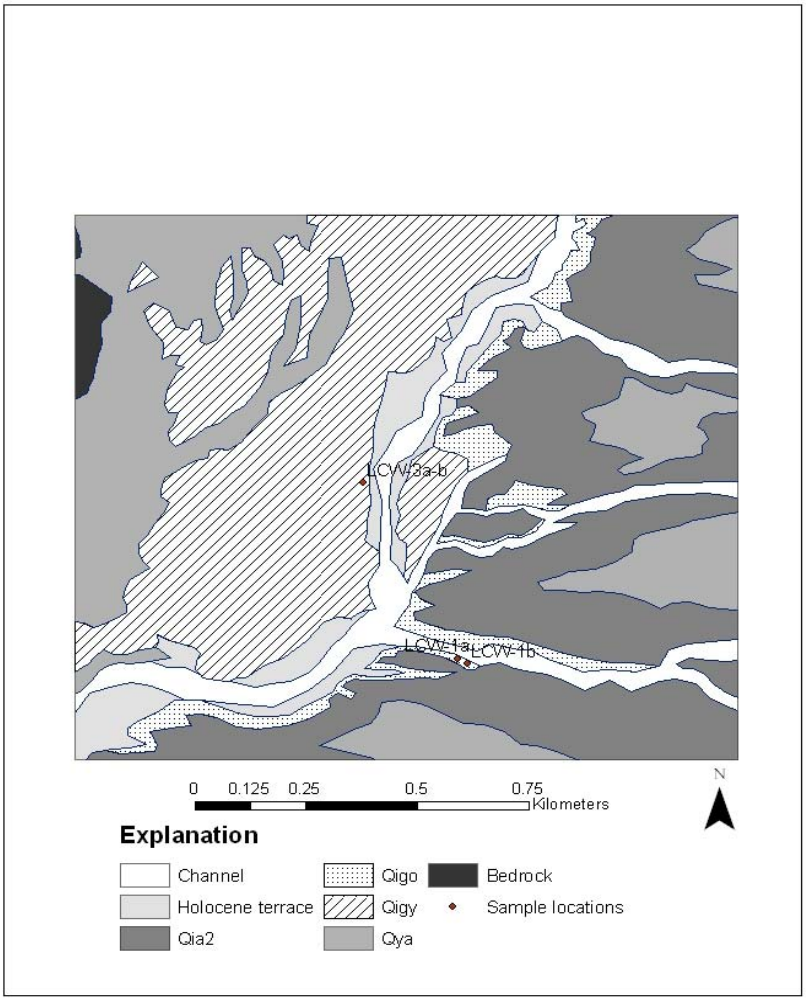

Figure 9. Geologic map of southern California Valley area, showing sample sites, axial drainage channels, and major surficial deposits discussed in text. These include the intermediate-age alluvial fan deposit (Qia2), the younger (Qigy) and older (Qigo) ground-water discharge deposits, and Holocene terrace and alluvial fan (Qya) deposits.

The entire sequence forms a series of bluffs that flank a complex landscape of anastomosing active channels and related Holocene fill terraces associated with young incision by the axial drainage of lower California Wash. The younger deposit (Qigy) consists of a poorly bedded, 5.5-m thick section of fine-grained sand, silt and clay (Fig. 10a). This fine-grained section is locally capped by a 1.5 m-thick cemented zone of secondary carbonate that commonly contains nodular and tubular textures suggestive of carbonate-replaced root networks. No organic material suitable for radiocarbon dating was found. Several characteristics, including the textures of both sediments and secondary carbonate, strongly suggest a deposition within a ground-water related wetland environment (Quade and others, 1995), an inference supported by the presence in the Qigy unit of ostracodes with ground-water fed wetland affinities (oral communication, Rick Forester, U.S. Geological Survey, Denver CO, USA).

The entire Qigy unit as well as subsequent axial channels and terrace deposits are inset, as former ground-water dominated valley fill, within older deposits of Qigo that are exposed along the walls of incised tributary washes to the east of the axial valley (Fig. 9). These older deposits make up a 7 m-thick section of poorly bedded to massive fine sand and silt with some clay, carbonate-replaced organic material (rhizoliths), and secondary matrix carbonate dispersed throughout the unit (Fig. 10b). The section also contains two prominent >1 m-thick zones, each consisting of a slightly reddened, weakly clay-enriched horizon above a more indurate layer of carbonate accumulation, that greatly resemble buried paleosols. However, there are no other sharp stratigraphic discontinuities indicative of long depositional hiatuses in this generally aggradational sequence. Characteristics of the deposits include fine-grained texture, absence of large gravel beds, locally abundant carbonate-replaced organic material, and a distribution and texture of secondary carbonate, suggesting distal piedmont or basin interior alluvial deposition with significant eolian and ground water influence. These deposits are truncated below dissected remnants of a thin (<40-50 cm) capping gravel deposit with surface and soil characteristics similar to intermediate-age Qia_2 alluvial fan deposits found in this and other valleys in the region.

U-series methods have been used to date many GWD deposits or travertine mounds (Grun and others, 1988). These deposits have been problematic to date by radiocarbon and U-series because of open-system behavior and contamination effects (Viles and Goudie, 1990; Ford and Pedley, 1996), though Paces and others (1996) work is a notable exception. Early attempts to date GWD mounds using luminescence on the secondary carbonates also were not successful (Grun and others, 1988; Wieser and others, 1993; Singhvi and others, 1996). However, attempts to date the detrital eolian sediment grains instead of the carbonate cement were more successful (Paces and others, 1996; Lundstrom and others, 2003; Rich and others, 2003). For our study of the GWD in California Valley we closely followed luminescence techniques in both Paces and Rich, since these papers include previous work in the Mojave and south Texas that showed good concordance with U-series and ^{14}C on the young GWD episodes. Another compelling argument for dating these deposits with luminescence dating is that modern marsh areas with emergent plants are efficient as eolian sediment traps, thus favoring luminescence ages on eolian detritus.

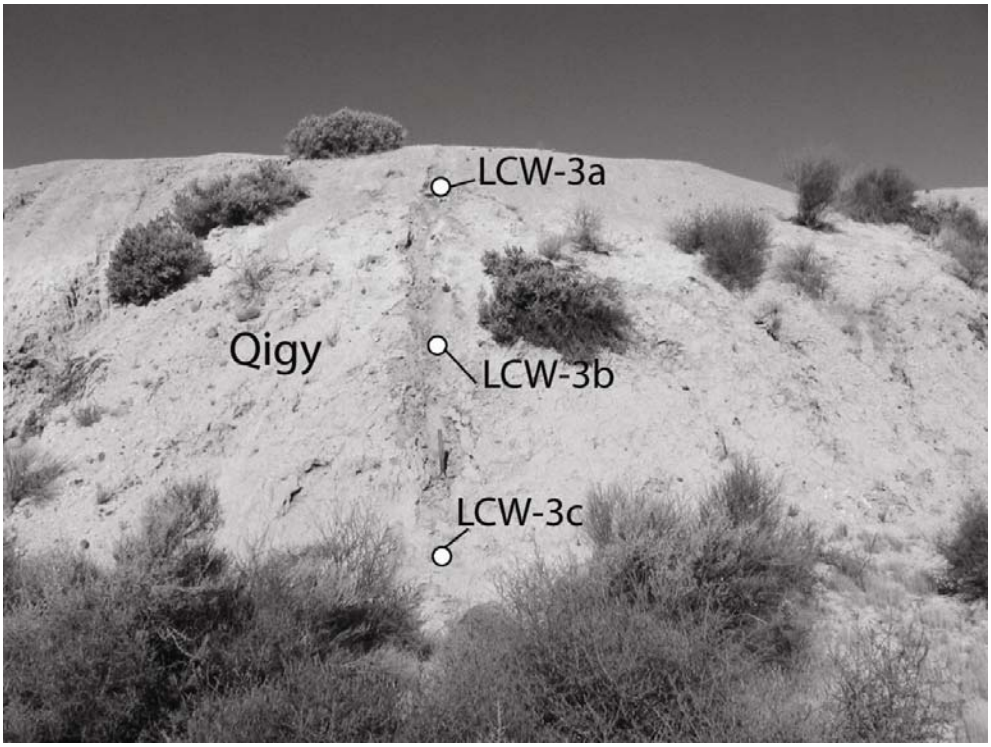

Figure 10a. Photograph of younger ground-water discharge deposits (Qigy) inset within paleovalley along axial drainage of southern California Valley. Sample locations are described in Table 1 and in text. The total exposed thickness of the section is 5.5 m. Note the general fine-grained texture, weak consolidation, gradational nature of subunits, and absence of well defined buried paleosols or other stratigraphic discontinuities in the section.

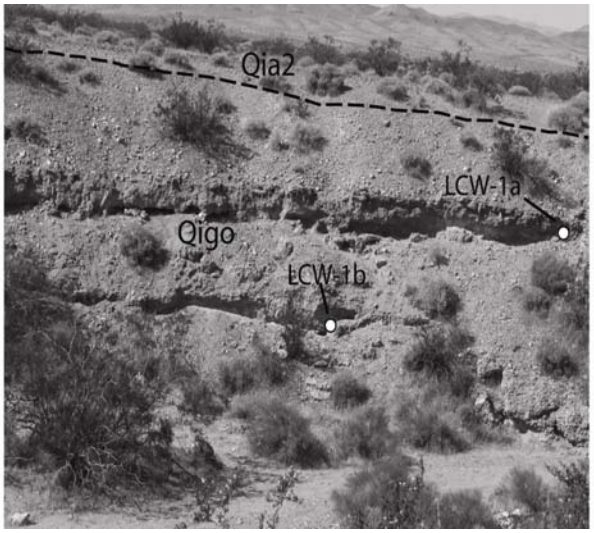

Figure 10b. Photograph of older ground-water discharge deposits (Qigo) exposed in wall of incised tributary canyon to east of axial valley of southern California Valley, showing sample locations described in Table 1 and in text. The section has a total exposed thickness of 7.8 m, with the top truncated below the base (dashed line) of a thin gravel cap of intermediate age alluvial fan gravel (Qia2). The entire Qigo section is fine grained and weakly to moderately indurated with dispersed to locally concentrated secondary carbonate. The two ledges near the sample intervals are related to more indurated zones with enhanced clay and carbonate accumulations interpreted as ground-water enhanced paleosols.

Luminescence ages of three samples from the younger Qigy set of GWD deposits described above (LCW-3a, -b, -c; Table 1) ranged from 22 ± 1.12 ka (IRSL) and 19.9 ± 1.58 ka (blue-light OSL) for the top (LCW-3a) to between 58.6 ± 4.05 ka (blue-light OSL) and 51.5 ± 3.34 ka (IRSL) years at the bottom (LCW-3c). A cross check using TL on two of these samples yielded ages of 23.3 ± 1.93 ka for LCW-3a and 52.2 ± 23.3 ka for LCW-3c. The TL was run as a check on the dynamics of the luminescence systematics and to validate any samples that were only suitable for TL analysis.

The upper and lower samples were collected 5.2 m and 0.2 m, respectively, above the base of the exposed section of Qigy deposits. Sample LCW-3b, collected from a yellow middle sand zone (3.5 m above section base), could not be dated. The yellow sand sample had a low OSL signal, poor dose recovery, and large changes in sensitivity. These characteristics could be due to the young sedimentary history of the sand and the general lack of evidence (e.g., stratigraphic discontinuities or paleosols) indicative of multiple cycles of erosion and deposition (Preusser and others, 2005).

The older GWD deposits (Qigo) described above as comprising a 7 m-thick section of poorly bedded to massive fine sand and silt with some clay, carbonate-replaced organic material (rhizoliths), and secondary matrix carbonate dispersed throughout the unit, were also sampled for luminescence dating (Table 1; Fig. 10b). Two large block samples were taken, one from the top (LCW-1a) and one from near the bottom (LCW-1b) of the exposed section in the gully wall (5.0 and 1.7 m from the base of the exposed section, respectively). These samples were assumed to be older than 100 ka due to the presence of two paleosols and the amount of moderately cemented secondary carbonate in the section (see above), although influxes of groundwater could introduce additional silt and carbonate. Because the ages may approach the quartz OSL dating limits, feldspar IRSL was attempted, due to feldspar's ability to retain a luminescence signal for longer periods of time (Aitken, 1985; Huntley and Lamothe, 2001). Not unexpectedly, the samples were saturated with respect to equivalent dose levels and only minimum ages of ~135 ka were obtained (Table 3). However, these samples were also run for TL, which does not saturate as quickly as OSL, and is commonly utilized for dating samples in excess of 200 ka (Berger, 1988). TL is not generally recommended for dating sandy water-laid deposits because a preheat plateau cannot be commonly obtained from these samples. However, if the TL is used on fine-grained portions of the water-laid sediments, relatively accurate ages may be recorded (Berger, 1994; Berger, 1985; Berger, 1987). TL ages obtained for LCW-1a and LCW-1b are within error at 158 ± 18.3 ka and 163 ± 22.6 ka. Thus, the section must have been accumulating and incorporating silt during part of the interval ~ 140 to 185 ka (the permissible range from the dates).

The dated GWD deposits, when combined with their stratigraphic context, provide several important time constraints on alluvial stratigraphy and geomorphic processes in lower California Valley. A thin Qia2 fan deposit overlying the older GWD deposits (Qigo) abuts at its distal margin against a terrace with otherwise generally similar Qia2 characteristics but a slightly lower elevation. Both Qia2 fan and terrace units are truncated by the eastern margin of the paleovalley containing both the younger GWD deposits (Qigy) and the terrace-channel system of the Holocene to modern axial drainage. These relationships bracket the age of the Qia2 units, which represent a major regional depositional interval, between the older and younger ages of Qigy and Qigo, respectively at approximately 55 ka and 160 ka.

Furthermore, these same geochronologic and stratigraphic relations constrain two major intervals of incision along the axial drainage of lower California Valley. The first incision episode, to a minimum depth of 9 m at the junction of the tributary wash and the Qigo site, occurred in the paleovalley that truncates the Qigo and its capping Qia2 deposits and encloses the inset GWD deposits of Qigy. This brackets this paleovalley incision between the same 65 ka and

160 ka time interval described above, which appears to be the earliest significant dissection along the axial drainage in this primarily aggradational part of a formerly undissected lower valley during Qigo time. A second, younger interval of incision along the present axial channel system at the Qigy sample sites is evident. This incision cuts down 8.2 m above the modern channel, the total height of the upper part of this section, and is dated at approximately 20-25 ka. At least two stages of this incision event are further indicated by the 5.5 m height of the Qigy section above the late Holocene fill terrace and the 2.5 m height of these terraces above the nearest active channel.

The third GWD mound we sampled for luminescence dating did not yield satisfying results. The mound consists of a sand and mud matrix between abundant angular fragments of Tertiary bedrock, and may represent discharge from disrupted bedrock or a mound built on colluvium. Sample M01ML-1842a was collected near the top of the mound, about 4 m below the ground surface. Sample M01ML-1842b was collected near the bottom of the mound, 1.75 m above the present day wash. IRSL dating of the top sample yielded only minimum ages because of saturation; the TL signal was saturated as well. The oldest minimum age is >174 ± 39.8 ka. The bottom sample was not dated due to the saturation and disequilibrium in the dose rate for the upper sample (Table 3).

Red Pass

Deposits at Red Pass record the capture of a large watershed that drains eastern Fort Irwin by the Salt Creek system. Red Pass is occupied by a wash that flows east in a narrow, deep gorge. The oldest deposits adjacent to the gorge mantle faulted Miocene strata of the Avawatz Formation; these strata have the characteristic soils and landform of Qoa deposits. The old alluvium (Qoa) dips west and has clasts derived from the Soda Mountains. Inset into the eroded Qoa deposits, and carrying a different clast composition derived from the north, are Qia2 deposits with associated desert pavements and typical soils. The base of these deposits is several meters above the modern wash in Red Pass, but the surface of the deposits and sediment structures indicate streams and sediment flowed east, parallel to the modern drainage. Within the gorge itself is a compound alluvial unit 6.6 m thick with a Qya4 (latest Pleistocene) deposit on top of two older deposits, each separated by weak paleosols.

The Qya4 alluvial deposit we dated contains two partly reworked eolian sand lenses, in an otherwise thin- to thick-bedded wash deposit characterized by thin to medium beds with lateral continuity and moderate grain-size sorting (Fig. 11). We sampled eolian sand lenses, the first 170 cm beneath the weak desert pavement surface of the Qya4 deposit and 130 cm beneath a stage I calcic horizon (sample M01SM-1849a). A lower sample, tentatively labeled Qia2, was 90 cm deeper (sample M01SM-1849b). The upper paleosol lies below the upper sand bed, which consists of fine sand and contains local "popcorn" texture GWD carbonate. The upper sample yielded an average age of 12.5 ± 0.55 ka on feldspar and 11.5 ± 0.23 ka on the quartz. These two ages overlap within their error limits.

The lower Qia2 sample (M01SM-1849b) from a sand bed between two paleosols had one IRSL age of 21.4 ± 0.99 ka that was much younger than the other two ages of 30.9 ± 1.11 ka (feldspar) and 36.9 ± 1.29 ka (quartz). The younger IRSL age is almost certainly a result of inadequate or incomplete disc coverage which was addressed more robustly in the second sample. There still exists a discrepancy between the ~ 31 ka feldspar age and the ~ 37 ka quartz, but these ages probably represent a mixture of partially bleached grains within the sample, such that the true age is somewhere between 30 ka to 38 ka when we use the error limits. This age corresponds with several well-known climatic events at approximately 32 to 35 ka, including deposition during interstadials 5-7 and associated stadial periods (a period of rapid Dansgaard/Oeschger cycling

during marine isotope stage 3) (Grootes and others, 1993; Stuiver and others, 1999). The upper sample represents deposition of the Qya4 unit at about 12 ka.

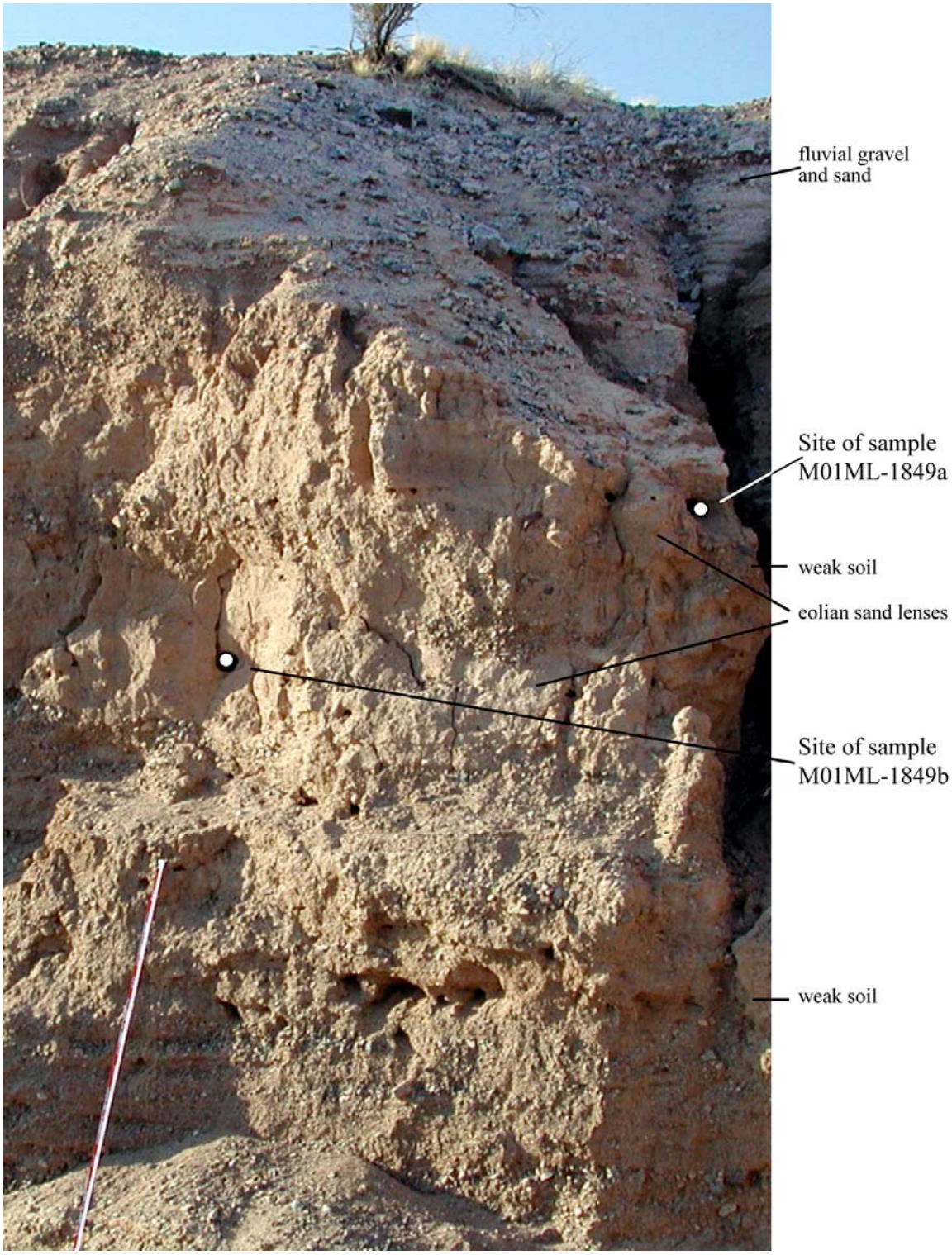

Figure 11. Photograph of fluvial and alluvial fan deposits at Red Pass. Metric tape is 2 m long; although only a portion is shown. The total section is 6.6 m thick. Two sand beds were sampled for OSL; top is M01-OM-1849a and bottom is M01-OM-1849b.

Silver Lake Overflow

The natural dam for Lake Mojave, which forms the present northern margin of Silver Lake playa (Fig. 1), has been occupied several times in the late Pleistocene. The shoreline's chronology has been determined by several workers and was summarized recently by Wells and others (2003). High stand occupations were intermittent but extended over the time period from about 22 to 9 ka, based on radiocarbon dating of shells in shoreline deposits and dates from organics in cores from the lake. The lake overflowed principally from 18.4 to 16.6 ka and 13.7 to 11.4 ka, and was within one meter of the spillway as recently as 9.4 radiocarbon ka (Wells and others, 2003). When the lake overflowed, the outflow created a fairly straight, deeply incised spillway channel in Pleistocene fan deposits on the north side of the bedrock hills that form the dam. We studied that fan and eolian sand ramps within the former spillway channel to gain knowledge of the timing of the overflow.

The fan adjacent to the overflow channel has a smooth surface with moderately developed pavement and varnish, features that are characteristic of Qia2 intermediate age deposit. Beneath the thick, sandy Av horizon is an irregularly developed red, clay-rich (argillic) Bt horizon that is partly engulfed in nodular-textured calcium carbonate ("popcorn"). Massive carbonate extends throughout the lower 3.5 m thick exposed section. The carbonate forms a porcelainous, white calcrete that lacks pebble rinds except in the upper part, and seems to have replaced the matrix of the alluvial fan deposit. We propose that this carbonate is the result of groundwater-discharge through the fan, leaking from Lake Mojave, which is above and to the south of the carbonate. With this model in mind, we sampled the carbonate in two places, hypothesizing that eolian dust captured by the wetland above would be carried into the underlying fan deposits and could be sampled to provide luminescence ages for the groundwater flow. It is also possible that groundwater flowed directly through the fan from the lake and a surface wetland did not exist prior to calcrete formation and blockage, in which case OSL dates should be consistent with lake chronology or represent the age of alluvial fan deposition.

We sampled this Bt horizon in large, intact blocks, about 50 cm below the surface, and about 1.5 m deeper in massive carbonate (Fig. 12a). Luminescence ages on the dust contained within the upper carbonate were 26.4 ± 1.5 ka (IRSL) and 32.0 ± 3.5 ka (blue-light OSL). This represents modest agreement between the techniques although the blue-light OSL carries a higher error because of the greater uncertainties in the equivalent dose. The age range of this deposit is 25 to 35 ka.

The dust in the lower carbonate sample yielded ages of 61.1 ± 3.74 ka (IRSL) and 49.8 ± 5.55 ka (blue-light OSL). The agreement between the two techniques is less robust, even when accounting for the large standard deviation for the blue-light OSL age. The age for the lower sample is therefore between 45 to 65 ka. It seems clear that lower dust incorporated in to the carbonate sample is indeed older than the dust in the upper sample, and both predate the Lake Mojave established chronology. If we consider the dates to reflect a mixture of original alluvial deposit, perhaps some illuvial fines, and possibly some additional fines delivered by groundwater flow then the alluvial fan deposit must be older than 45 to 65 ka. Alternative interpretations, such as long-lived groundwater flow from 60 to 25 ka, before the existence of Lake Mojave, seem less reasonable at this time.

The overflow channel is partly filled by eolian sand and shows little evidence for late Holocene fluvial flow. We sampled (M01SM-1853) near the base of an extensive sand ramp on the west side of the channel to establish the time of sand deposition and thereby limit the timing of

last spillway flow (Fig. 12b). We dug through about 95 cm of thin-bedded eolian sand that overlies a rocky sand ramp-avalanche facies. The OSL sample was 40 cm below the top of a ramp facies, which we estimated extended another 80 to 100 cm deeper to the channel floor. The sand ramp yielded similar IRSL and OSL ages of 10,172 ± 483 and 10,740 ± 268 years. These ages are roughly 500 to 1,000 years younger than the youngest dated lake feature of Lake Mojave (after calibrating radiocarbon dates) and strongly assert that Lake Mojave did not overflow after about 11 ka (Wells and others, 2003).

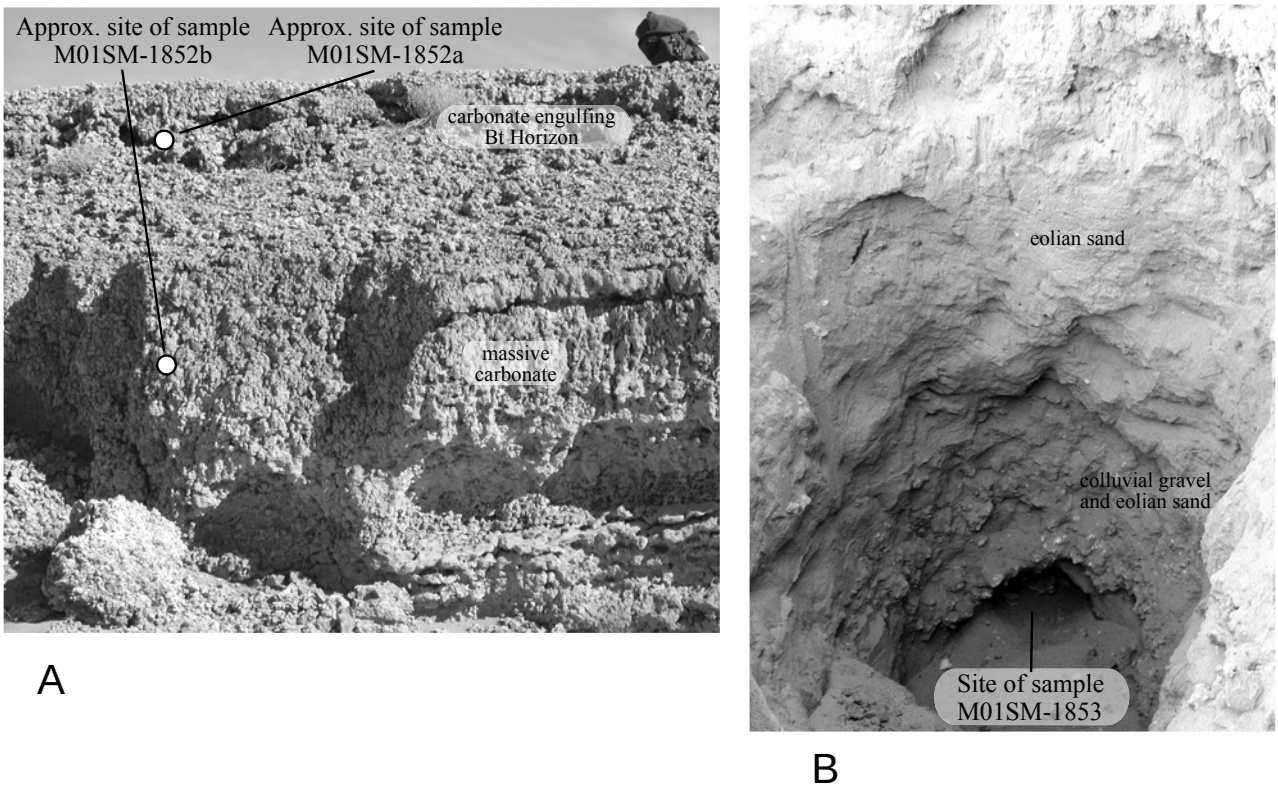

Figure 12. Photographs of features discussed and sampled in Silver Lake overflow channel. **A:** Calcium carbonate-enriched section in Pleistocene alluvial fan that we interpret as evolving with groundwater deposition in fan. The section is about 3.5 m high. **B:** A pit excavated into sand ramp along the west wall of the overflow spillway. Pit base is about 1.5 m below surface. Beds dip east and north, although this is not obvious in the photograph

Correlations with regional and alluvial fan chronology

The stratigraphic and luminescence data from a number of critical Quaternary sites in the Mojave Desert as presented above generally support the existing chronologic framework for alluvial fan activity in the Mojave Desert. The ages also compare moderately well with additional geochronologic data from the Yucca Mountain area of southern Nevada. The oldest widespread alluvial deposits (Qoa) are >52 ka as dated by luminescence, although the degree of original surface modification and strong relict soil development suggest that the deposits are middle Pleistocene and may be significantly older than this minimum age. Also, elsewhere in the area, Qoa deposits exposed below and west of Ibex Pass contain an interbedded air-fall ash correlated with the Bishop tuff dated at 730 ka near the base of the unit. The strength of the relict surface soil and degree of surface modification of Qoa is generally similar to the Qa1 deposit at Yucca Mountain, which also contains an interbedded ash (Bishop tuff?) near its base (Whitney and others, 2004).

Widespread intermediate-age alluvial deposits (Qia) yield fairly consistent ages ranging from >140 ka to ~33 ka. These deposits also have a wide range of soil development, raising the possibility that they represent two or more distinct alluvial fan depositional pulses within this broad age range that are difficult to distinguish from each other using surface characteristics alone. The suggested age range for Qia2 fan deposits appears to correlate with ages reported for the Qa4 and all but the oldest range of Qa3 deposits at Yucca Mountain (Whitney and others, 2004). There is a general similarity in the surface characteristics and soil properties between Qia2 and these surfaces at Yucca Mountain, although some Qa3 units have more eroded surfaces and stronger soils than typically are observed with Qia2 fan deposits in the area of this study. The age range of the Qia2 deposits in the study area generally correlates with reported ages of late Pleistocene units in adjacent areas to varying degrees (Menges and others, 2001). These include older Qf2 units at Silver Lake (Reheis and others, 1989; Wells and others, 1990), the Q2c unit in the lower Colorado River region (Bull, 1991), the Qf4 and perhaps the younger elements of Qf3 alluvium in Kelso Valley near the Providence Mountains (McDonald and McFadden, 1994; Wang and others, 1996), Qai alluvium in central Death Valley (Machette and others, 2003), and the Qai alluvium in Pahrump Valley (Lundstrom and others, 2003).

Latest Pleistocene to early Holocene fan deposits are widespread in the desert southwest (McDonald and others, 2003) and date from ~15 to ~9 ka across the region (e.g., Reheis and others, 1989; Page and others, 2005). Our OSL date of ~12 ka for the upper sand unit in Qya4 in Red Pass corresponds well with previous dating.

Holocene alluvial fan deposits dated here at 4.5-3.2 ka correlate on the basis of soils and surface morphology to mid-Holocene deposits at Silver Lake (Reheis and others, 1989). Wash deposits inter-fingering with these fans yielded ages of ~5 ka in Valjean Valley. Deposits of this age with similar surface characteristics and soils are widely recognized in many dated stratigraphic sequences cited above.

Salt Creek and Silurian Lake paleohydrology

Following overflow of Lake Mojave about 11.4 ka (calibrated ^{14}C yrs) (Wells and others, 2003) Salt Creek has been fed principally from a broad watershed west of the Avawatz Mountains and local alluvial fan channels within and east of Silurian Valley. The Holocene hydrologic system within Silurian Valley includes two low-gradient stretches north of Silver Lake, the through-flow playa of Silurian Lake, a junction with Kingston Wash near the Dumont wetland deposits of the Salt Springs area (Bright and Anderson, this volume), and then a junction with Amargosa River and flow to Death Valley. We have not dated all elements of this system, but offer several observations and dates of hydrologic events for some parts of the system. Shallow lakes built gravel bars at Silurian Lake about 6,500 and 800-850 years ago, indicating obstructed outflow from the playa and high-volume sustained fluvial conditions. Timing of the last lake stand is similar to that of a flood event bracketed by droughts in the record of Walker River (Stine, 1994) and Carson Sink (Adams, 2003) in northwest Nevada and offer support for widespread flooding at this time.

The primary purpose for dating the Kingston Wash debris-flow deposit and lake-stand deposits of Silurian Lake was to examine whether the debris-flow event influenced the development of Silurian Lake. This debris-flow marks a rare, possibly catastrophic event, one that deposited more than 36×10^6 m^3 of material onto a distal piedmont, including deposition at the axial valley wash of Salt Creek. Silurian Lake playa is an unusual through-flow playa midway along Salt Creek, and positioned 2.1 km south of, and only 1 to 2 m higher than, the toe of the debris flow where it meets Salt Creek. Could this debris-flow have caused a temporary damming of Salt Creek to form Silurian Lake playa?

Our dating indicates that the debris-flow is unlikely to have formed the Silurian Lake playa, and it probably played no role in temporarily damming the Holocene playa. Silurian Lake playa deposits extend greater than 30 m in the subsurface (Anderson and Wells, 2003b), suggesting that it is a long-lived feature. In addition, fluvial terraces flanking Salt Creek are similar in age and morphology above and below Silurian Lake, and incision of the wash reaches maximum depths well to the north of, rather than at, the potential damming site at the south edge of the flow. There is no evidence that the debris-flow ran out onto the Avawatz fan across Salt Creek or was much deeper than the current exposure of about 40 cm thick. This 40 cm elevation places it 1-2 m below the bar at the north end of Silurian Lake. Our OSL dating indicates that the debris flow was emplaced about 4,400 to 5,200 yr ago, whereas the small lacustrine bars at Silurian Lake are about 6,500 and 850 yr old. The debris-flow and the damming events for the Holocene playa apparently are not contemporary.

Salt Creek apparently was able to receive and transport downstream the water and sediment load from the debris flow event with only slight perturbations to stream course and size. This remarkable resilience of Salt Creek provides evidence for arid land fluvial systems being tuned to a wide range of runoff conditions.

Amargosa River Drainage History

The early paleovalley incision of lower California Valley inferred from the groundwater-discharge stratigraphy and our new geochronology has important implications to the drainage evolution of the Amargosa River and its tributaries in Amargosa Canyon, Tecopa basin, and adjacent valleys. The early-stage axial dissection in California Valley is probably related to regional incision along the Amargosa River, which is the master base-level stream in this area (Fig. 1). The axial valley drainage of California Valley is directly linked, via downstream confluence with Willow Wash, to the Amargosa River within central Amargosa Canyon. Dissection by the Amargosa River in this area is interpreted by most workers as related to breaching of a former paleodivide along the Amargosa River paleo-drainage south of Tecopa (Morrison, 1999; Anderson, 2005; Menges and Anderson, 2005) sometime between 144 ka and 190 ka. This breach, in turn, initiated canyon cutting and upstream dissection along both the master stream and its tributaries. The paleovalley incision at the Qigo sample sites perhaps records the arrival of this incision knickpoint in lower California Valley between about 65 ka and 140 ka.

The relation of the younger phase of post-Qigy incision to other downstream sections of the Amargosa River drainage is less clear. Certainly all of the dissected reaches of the system contain stepped terrace sequences indicating significant post Qia2 incision. At least some of this incision likely correlates with the younger as well as early-stage dissection intervals in lower California Wash, but none of the dissected reaches elsewhere in the regional drainage contain a ground-water dominated valley fill sequence similar to the Qigy unit in California Wash. Thus, it is difficult to partition the post-Qia2 incision in other sections of the Amargosa drainage without additional dating for terraces of this age. However, Anderson (2005) has documented, via radiocarbon dated terrace alluvium, several pulses of late Holocene (<2,400 years) to recent channel aggradation and downcutting in the Amargosa Canyon. One or more of these terraces likely correlate in part with the youngest set of fill terraces inset into Qigy valley fill along axial channels of California Wash.

Groundwater-discharge events

The sedimentology, stratigraphy, and geochronology of groundwater-discharge deposits within and adjacent to the axial drainage of lower California Valley (Table 1) clearly identify two

hitherto unrecognized intervals of enhanced groundwater-discharge in this area whereas currently there is only minor spring or seepage activity. The minimum age interval for each discharge event is established by luminescence dates from near the top and bottom of the exposed groundwater-discharge sections. An older event, broadly bracketed between 140 ka and 190 ka, is associated with slow accumulation of distal-piedmont to basin-interior, fine grained alluvial sediment in a probable ground water enhanced wetland environment. There is no indication of significant erosional or degradational events during this period, although several possible depositional hiatuses are suggested by the presence of two weak to moderate buried paleosols within the groundwater sections.

A younger discharge event or events with ages between about 20 ka and 52 ka is reflected in a fine-grained accumulation of mixed eolian and alluvial sediments within a wetland environment. This wetland deposition almost filled the complete extent of a formerly incised paleovalley, approximately coincident with the modern axial drainage and inset into the older discharge deposits to the east. The young wetland deposits in the outcrop are fairly homogeneous, having poorly defined gradational boundaries and containing no buried soils or obvious erosional discontinuities. Therefore, we could not recognize discrete discharge subunits despite the long time interval of the section. The top of the section is locally associated with a pronounced relict soil with abundant secondary carbonate and root-like rhizoliths. This soil implies a long period of stabilization of the upper surface of this valley fill within a ground water environment prior to initiation of subsequent dissection and excavation by the present axial drainage system.

This young (Qigy) groundwater-discharge event in California Valley appears to correlate with some recognized groundwater paleo-discharge events in other basins in southern Nevada and eastern California. This interpretation is based on varying degrees of overlap in the age ranges from groundwater-discharge deposits in California Valley and similar deposits identified and dated by radiocarbon, luminescence, and (or) U-series disequilibrium methods in this region. Specific correlative sites are present in Las Vegas Valley (Haynes, 1967; Quade, 1986; Bell and others, 1999; Page and others, 2005), Pahrump Valley (Quade and others, 1995; Lundstrom and others, 2003; Page and others, 2005), Tecopa basin and the northern Amargosa Desert (Paces and others, 1996, Lundstrom and others, 1998). The best age correlation among the basins is in the upper part of the Qigy range (i.e., 20-25 ka or unit D of Haynes and later workers; (Haynes, 1967; Quade and others, 1995, 1998; Lundstrom and others, 1998). However some basins contain more limited groundwater-discharge deposits with ages in the 50-60 ka range or unit C of Haynes and others (Haynes, 1967; Bell and others, 1999; Page and others, 2005). Of particular interest is a U-series age of 72 ± 2 ka for spring-mound carbonate in eastern Tecopa basin (Nelson and others, 2001). A paleodischarge event correlative to all or part of the Qigy event also may be represented by undated groundwater-discharge deposits in Chicago Valley and the Ash Meadows area of the Amargosa Desert.

However, there are discrepancies in dated groundwater-discharge sequences among these basins as well. For example, these ubiquitous deposits range as young as 16 ka to 8 ka in the Pahrump and Las Vegas Valleys (Quade and others, 1995; Quade and others, 2003), where they typically are capped by distinctive black organic mats. These black mats are not evident in the dated groundwater-discharge deposits in lower California Wash. Also, there are relatively few dates on groundwater-discharge deposits in other basins in the region that fall within the 140-190 ka age range of the older Qigo sequence in California Valley, although there are several U-series ages at ~ 160 ka for spring mound carbonates in eastern Tecopa basin (Nelson and others, 2001). Luminescence ages on Haynes' units Qsa and Qsb (LV-19 and LV-20 in Table 1) overlap with the age range of 140 to 190 ka (Page and others, 2005), as do some results from the Amargosa Valley described by Paces and others (1996).

The 140 ka to 190 ka interval also coincides with the last deep stand of Lake Manley in Death Valley during oxygen-isotope stage 6 (Lowenstein and others, 1999; Machette and others, 2001; Machette and others, 2003). Dates from the carbonates in basin fill of Brown Spring, the oldest set of groundwater-discharge deposits in Pahrump Valley, fall within a broadly defined age range of 200 ka to 400 ka (Lundstrom and others, 2003). Groundwater-discharge deposits or related deposits of this age are either absent or not exposed at the present levels of dissection in lower California Wash; however, they are present as the oldest dated spring mounds (265 ka to 300 ka: average about 283 ka) in Tecopa basin (Nelson and others, 2001).

Conclusions

Our results indicate that OSL is suitable for dating fine grains associated with three widespread deposits of the northeastern Mojave Desert: (1) eolian sediment captured in GWD deposits, (2) eolian sand reworked into alluvial fan sediments, and (3) lacustrine sand in beach bar deposits. Deposits of these types, when carefully selected and sampled, greatly expand targets for dating in deserts.

Two distinct episodes of groundwater-discharge deposition are evident from both stratigraphic relations and the luminescence geochronology in lower California Valley. Dates from near the top and bottom of exposed sections from each groundwater-discharge deposit indicate age ranges of about 20 ka to 52 ka and 140 ka to 185 ka for the two groundwater paleo-discharge events in the valley. Indicators of major depositional discontinuities such as such as erosional unconformities, channel cut and fill, or strong paleosols are absent from both sections, which suggests long lived continuity, or at most minor periodicity, in ground water discharge during each interval. The lower part of the younger Qigy interval and the groundwater-discharge carbonate at the Silver Lake overflow site have similar ages, but the dates at the latter site are interpreted as reflecting fan deposition.

A long-lived sand transport system in Dumont Dunes area is indicated by eolian sand inter-fingering with alluvial deposits from at least the middle Pleistocene to modern time. Ages from eolian sand ramps/sheets range from 3.2 ka to > 52 ka in various locations, but our sampling was not dense or systematic enough to date eolian sand activity.

The southern spit of Silurian Lake is about 800 to 850 years old, which coincides with a regional southwest USA flood event that is bracketed by two prolonged droughts. Uncertainties in ages preclude a definite correlation, but the temporal coincidence is intriguing.

OSL dating of modern muddy sediment in Salt Creek Wash demonstrates that OSL ages are in excess of modern, and depart progressively with depth from modern, yielding ages from 300 to 1,200 years. The older ages are probably induced by incomplete bleaching due to turbid flow conditions, unlike eolian processes and shallow fluvial deposits of well-sorted sand where bleaching is typically rapid and complete.

Luminescence methods yield well-behaved reliable dates for groundwater-discharge deposit fines, reworked eolian sand in alluvial fans, axial-valley wash deposits, and playa and lacustrine sands. These targets greatly expand the depositional environments in the deserts that are amenable to OSL dating.

Acknowledgements

We thank John Vogel and Dave Bedford for valuable field assistance and advice. Discussions with Rick Forester, Marith Reheis, Kirk Anderson, Steve Wells, and Dave Bedford clarified ideas presented in this paper, although interpretations and conclusions are strictly the responsibility of the authors. This manuscript was critically reviewed by Scott Lundstrom and

Mike Machette and their valuable comments and insights resulted in many improvements and clarifications.

References cited

Adams, K.D., 2003, Age and paleoclimatic significance of late Holocene lakes in the Carson Sink, NV, USA: Quaternary Research, v. 60, p. 294-306

Aitken, M.J., 1998, An Introduction to Optical Dating, Oxford, Oxford University Press, 267 p.

Aitken, M.J., 1985, Thermoluminescence Dating, London, Academic Press, 359 p.

Anderson, D.E., 2005, Holocene fluvial geomorphology of the Amargosa River through Amargosa Canyon, *in* Calzia, J.P., ed., Fifty years of Death Valley in research-A volume in honor of Lauren A. Wright and Bennie Troxel: Earth Sciences Review Special Issue, v. 73, p. 291-307.

Anderson, D.E., and Wells, S.G., 2003a, Late Pleistocene Lake Highstands in Death Valley, California, *in* Enzel, Y., Wells, S.G., and Lancaster, N., eds., Paleoenvironments and plaeohydrology of the Mojave and southern Great Basin deserts: Geological Society of America Special Paper 368, p. 115-128.

Anderson, K.C., and Wells, S.G., 2003b, Late Quaternary geology and paleohydrology of Silurian Lake and Salt Spring basin, Silurian Valley, California, *in* Enzel, Y., Wells, S.G., and Lancaster, N., eds., Paleoenvironments and plaeohydrology of the Mojave and Southern Great Basin Deserts: Geological Society of America Special Paper 368, p. 129-141.

Banerjee, D., Murray, A.S., Boetter-Jensen, L. and Lang, A., 2001, Equivalent dose estimation using a single aliquot of polymineral fine grains: Radiation Measurements, v. 33, no. 1, p. 73-94.

Bell, J.W., Ramelli, A.R., dePolo, C.M., Maldonado, F., and Schmidt, D.L., 1999, Geologic Map of the Corn Creek Springs Quadrangle, Clark County, Nevada: Nevada Bureau of Mines and Geology Map 121, 1:24,000 scale.

Berger, G.W., Murray, A.S., and Havholm, K.G., 2003, Photonic dating of Holocene back-barrier coastal dunes, northern North Carolina, USA: Quaternary Science Reviews, v. 22, no. 1, p. 1043-1050.

Berger, G.W., 1984, Dating Quaternary deposits by Luminescence; Recent Advances: Geoscience Canada v. 13, p. 15-21.

Berger, G.W., 1985, Thermoluminescence dating studies of rapidly deposited silts from south-central British Columbia: Canadian Journal of Earth Sciences v. 22, p. 704-710.

Berger, G.W., 1987, Thermoluminescence dating of the Pleistocene Old Crow tephra and adjacent loess, near Fairbanks, Alaska: Canadian Journal of Earth Sciences, v. 24, p. 1975-1984.

Berger, G.W., 1988, Dating Quaternary events by Luminescence, *in* Easterbrook, D. J., ed., Dating Quaternary Sediments*:* Geological Society of America Special Paper 227, p. 13-51.

Botter-Jensen, L., Bulur, E., Duller, G.A.T., and Murray, A.S., 2000, Advances in luminescence instrument systems: Radiation Measurements, v. 32, p. 523-528.

Bray, H.E., and Stokes, S., 2003, Chronologies for Late Quaternary barchan dune reactivation in the southeastern Arabian Peninsula: Quaternary Science Reviews, v. 22, p. 1027-1032.

Budahn, J.R., and Wandless, G.A., 2002. Instrumental neutron activation by abbreviated count, U.S. Geological Survey Open-File Report 02-223, Chapter X, on-line only at http://pubs.usgs.gov/of/2002/ofr-02-0223/.

Bull, W.B., 1991, Geomorphic Responses to Climate Change, New York, Oxford University Press, 326 p.

Busacca, A.J., Beget, J.E., Markewich, H.W., Muhs, D.R., Lancaster, N. and Sweeney, M.R., 2004, Eolian Sediments *in* Gillespie, A.R., Porter, S.C. and Atwater, B.F., eds., The Quaternary period in the United States, Developments in Quaternary Science, vol. 1 (Series Editor Jim Rose): Elsevier, p. 275-310.

Clarke, M.L., 1994, Infra-red Stimulated Luminescence ages from aeolian sand and alluvial fan deposits from the Eastern Mojave Desert, California: Quaternary Geochronology (Quaternary Science Reviews) v. 13, p. 533-538.

Clarke, M.L, Richardson, C.A. and Rendell, H.M., 1996, Luminescence dating of Mojave Desert sands: Quaternary Science Reviews, v. 14, p. 783-790.

Clarke, M.L., and Rendell, H.M., 1998, Climatic change impacts on sand supply and the formation of desert sand dunes in the south-west U.S.A.: Journal of Arid Environments v. 39, p. 517-532

Clarke, M.L., and Rendell, H.M., 2003, Late Holocene dune accretion and episodes of persistent drought in the Great Plains of Northeastern Colorado: Quaternary Science Reviews, v. 22, p. 1051-1058.

Cox, B.F., and Hillhouse, J.W., 2003, Pliocene and Pleistocene evolution of the Mojave River, and associated tectonic development of the Transverse Ranges and Mojave Desert, based on borehole stratigraphy studies and mapping of landforms and sediments near Victorville, California: Geological Society of America, Special Paper 368, p. 1-42.

Duller, G.A.T., 1991, Equivalent dose determination using single aliquots: Nuclear Tracks and Radiation Measurements, v. 18, p. 371-378.

Edwards, S.R., 1993, Luminescence dating of sand from the Kelso Dunes, California, *in* Pye, K., ed., The Dynamics and Environmental Context of Aeolian Sedimentary Systems*:* Geological Society of London Special Publication 72, p. 59-68.

Eriksson, M.G., Olley, J.M., and Payton, R.W., 2000, Soil erosion history in central Tanzania based on OSL dating of colluvial and alluvial hillslope deposits: Geomorphology, v. 36, p. 107-128.

Ford, T.D., and Pedley, H. M., 1996, Review of tufa and travertine deposits of the world: Earth Science Reviews, v. 41, p. 117-175.

Forester, R.M., Miller, D.M., and Pedone, V.A., 2002, Ground water and ground-water discharge carbonate deposits in warm deserts, *in* Reynolds, R.E., ed., Land of Lost Lakes: 2003 Desert Symposium, Fullerton, California State University, p. 27-36.

Forman, S.L., and Pierson, J., 2002, Late Pleistocene luminescence chronology of loess deposition in the Missouri and Mississippi river valleys, United States: Paleogeography, Paleoclimatology, Paleoecology, v. 186, no. 1 and 2, p. 25-46.

Grootes, P.M., Stuiver, M., White, J.W.C., Johnsen, S., and Jouzel, J., 1993, Comparison of oxygen-isotope records from the Gisp2 and Grip Greenland ice cores: Nature, v. 366, no. 6455, p. 552-554.

Grun, R., Schwartz, H.P., Ford, D.C., and Hentzsch, B., 1988, ESR dating of spring deposited travertines: Quaternary Science Reviews, v. 7, p. 429-432.Haas, H., Holliday, V.T., and Stuckenrath, R., 1986, Dating of Holocene stratigraphy with soluble and insoluble organic fractions at the Lubbock Lake archaeological site, Texas: An ideal case study: Radiocarbon, v. 28, p. 473-485.

Haynes, C.V., 1967, Quaternary geology of the Tule Springs area, Clark County, Nevada, *in* Wormington, H.M. and Ellis, D., eds. Pleistocene Studies in Southern Nevada: Nevada State Museum of Anthropology Paper No. 13, p. 1-104.

Hillhouse, J.W., 1987, Late Tertiary and Quaternary geology of the Tecopa basin, southeastern California: U.S. Geological Survey Miscellaneous Investigations Series Map I-1728 (with 16 p. accompanying text), scale 1:48,000.

Huntley, D. J., and Lamothe, M., 2001, Ubiquity of anomalous fading in K-feldspars and the measurement and correction for it in optical dating: Canadian Journal of Earth Sciences, v. 38, p. 1093-1106.

Lancaster, N., 1999, Studies of late Quaternary eolian deposits of the Mojave Desert, California, *in* Wells, S.G., Tinsley, J.C., McFadden, L.D., and Lancaster, N., Quaternary stratigraphy and dating methods -Understanding geologic processes and landscape evolution in southern California: Geological Society of America Cordilleran Section Meeting Field Trip 8 Guidebook, p. 172-175.

Lancaster, N., and Tchakerian, V.P., 2003, Late Quaternary eolian dynamics, Mojave Desert, California, *in* Enzel, Y., Wells, S.G., and Lancaster, N., eds., Paleoenvironments and paleohydrology of the Mojave and Southern Great Basin Deserts: Geological Society of America Special Paper 368, p. 231-249.

Lang, A., 1994, Infrared stimulated luminescence dating of Holocene reworked silty sediments: Quaternary Science Reviews, v. 13, no. 5-7, p. 525-528.

Lowenstein, T.K., Li, J., Brown, C., Roberts, S.M., Ku, T.L., Luo, S., and Yang, W., 1999, 200 k.y. paleoclimatic record from Death Valley salt core: Geology, v. 27, p. 3-6.

Lundstrom, S.C., Mahan, S.A., Blakely, R.J., Paces, J.B., Young, O.D., Workman, J.B., and Dixon, G.L., 2003, Geologic Map of the Mound Spring Quadrangle, Nye and Clark Counties, Nevada, and Inyo County, California.: U.S. Geological Survey Miscellaneous Field Studies Map MF-2339, scale 1:24,000.

Lundstrom, S.C., Paces, J.B., and Mahan, S.A., 1998, Late Quaternary history of Fortymile Wash in the area near H-road crossing, *in* Taylor, E.M., ed., Quaternary Geology of the Yucca Mountain Area, Southern Nevada; Pacific Cell-Friends of the Pleistocene Field Trip, October 9-11, 1998, p. 63-76.

Machette, M.N., Klinger, R.E., and Knott, J.R., 2001, Questions about Lake Manley's age, extent, and source, *in* Machette, M.N., Johnson, M.L., and Slate, J.L., eds., Quaternary and late Pliocene geology of the Death Valley region-Recent observations on tectonics, stratigraphy, and lake cycles: Pacific Cell Friends of the Pleistocene Field Trip, February 17-19, 2001: U.S. Geological Survey Open-File Report 01-51, p. G143-G149.

Machette, M.N., Phillips, F.M., and Slate, J.L., 2003, New cosmogenic ^{36}Cl ages for relict soils on alluvial fans in Death Valley, California (Abstract): Geological Society of America, Abstracts with Programs, v. 35, no. 6, p. 257-258.

McDonald, E.V., and McFadden, L.D., 1994, Quaternary stratigraphy of the Providence Mountains piedmont and preliminary age estimates and regional correlations of Quaternary deposits in the eastern Mojave Desert, *in* McGill, S.F. and Ross, T.M., eds., Geological investigations of an active margin: Geological Society of America Cordilleran Section Meeting Field Trip 8 Guidebook, p. 205-213.

McDonald, E.V., McFadden, L.D., and Wells, S.G., 2003, Regional response of fans to Pleistocene-Holocene transition, Mojave Desert, California, *in* Enzel, Y., Wells, S.G., and Lancaster, N., eds., Paleoenvironments and paleohydrology of the Mojave and Southern Great Basin Deserts: Geological Society of America Special Paper 368, p. 189-205.

Menges, C.M., and Anderson, D.E., 2005, Late Cenozoic drainage history of the Amargosa River, southwestern Nevada and eastern California, *in* Reheis, M., ed., Geologic and biotic perspectives on Late Cenozoic drainage history, Conference Abstracts, U.S. Geological Survey Open-File Report 05-1404 (on-line only), p. 8. http://pubs.usgs.gov/of/2005/1404/pdf/OFR-2005-1404.pdf

Menges, C.M., Taylor, E.M., Workman, J.B., and Jayko, A.S., 2001, Regional surficial-deposit mapping in the Death Valley area of California and Nevada in support of ground-water modeling, *in* Machette, M.N., Johnson, M.L., and Slate, J.L., eds., Quaternary and late Pliocene geology of the Death Valley region-Recent observations on tectonics, stratigraphy, and lake cycles, Pacific Cell Friends of the Pleistocene Field Trip, February 17-19, 2001: U.S. Geological Survey Open-File Report 01-51, p. H151-H166.

Millard, H.T., and Maat, P.B., 1994, Thermoluminescence dating procedures in use at the U.S. Geological Survey, Denver, Colorado: U.S. Geological Survey Open-File Report 94-249, 112 p.

Morrison, R.B., 1999, Lake Tecopa-Quaternary geology of Tecopa Valley, California, a multimillion-year record and its relevance to the proposed nuclear-waste repository at Yucca Mountain, Nevada, *in* Wright, L.A., and Troxel, B. eds., Geological Society of America Special Paper 333, p. 301-344.

Murray, A.S., and Wintle, A.G., 2000, Luminescence dating of quartz using an improved single-aliquot regenerative-dose protocol: Radiation Measurements, v. 32, no. 1, p. 57-73

Murray, A.S., Marten, R., Johnston, A., and Martin, P., 1987, Analysis for naturally occurring radionuclides at environmental concentrations by gamma spectrometry: Journal of Radioanalytical and Nuclear Chemistry, Article 115, p. 263-288.

Nelson, S.T., Karlsson, H.R., Paces, J.B., Tingey, D.G., Ward, S., and Peters, M.T., 2001, Paleohydrologic record of spring deposits in and around Pleistocene pluvial Lake Tecopa, southeastern California: Geological Society of America Bulletin, v. 113, no. 5, p. 659-670.

Owens, L.A., Bright, J.B., Finkel, R.C., Jaiswal, M.J., Kaufmann, D.S., Mahan, S, Radtke, U., Schneider, J.S., Sharp, w., Singhvi, A.S., Warren, C.N., 2007, Numerical dating of a late Quaternary spit-shoreline complex at the northern end of Silver Lake playa, Mojave Desert, California: A comparison of the applicability of radiocarbon, luminescence, terrestrial cosmogenic nuclide, electron spin resonance, U-series and amino acid racemization methods: Quaternary International, v. 166, p. 87-110.

Paces, J.B., Forester, R.M., Whelan, J.F., Mahan, S.A., Bradbury, J.P., Quade, J., Neymark, L.A., and Kwak, L.M., 1996, Synthesis of ground-water discharge deposits near Yucca Mountain, DOE Administrative Report 3GQH671M to DOE-YMPSCO, 21 p., 3 appendixes, 25 figures.

Page, W.R., Lundstrom, S.C., Harris, A.G., Langenheim, V.E., Workman, J.B., Mahan, S.A., Paces, J.B., Dixon, G.L., Rowley, P.D., Burchfiel, B.C., Bell, J.W., and Smith, E.I., 2005, Geologic and geophysical maps of the Las Vegas 30 x 60 minute quadrangle, Clark and Nye Counties, Nevada, and Inyo County, California: U.S. Geological Survey Scientific Investigations Map 2814, scale 1;100,000.

Prescott, J.R., and Hutton, J.T., 1988, Cosmic ray and gamma ray dosimetry for TL and ESR: Nuclear Tracks and Radiation Measurements v. 14, p. 223-230.

Preusser, F., Andersen, B.G., Denton, G.H., and Schulter, C., 2005, Luminescence chronology of Late Pleistocene glacial deposits in North Westland, New Zealand: Quaternary Science Reviews, v. 24, p. 2207-2227.

Quade, J., 1986, Late Quaternary environmental changes in the upper Las Vegas Valley, Nevada: Quaternary Research, v. 26, p. 340-357.

Quade, J., Mifflin, M.D., Pratt, W.L., McCoy, W., and Burckle, L, 1995, Fossil spring deposits in the southern Great Basin and their implications for changes in water-table levels near Yucca Mountain, Nevada, during Quaternary time: Geological Society of America Bulletin, v. 107, no. 2, p. 213-230.

Quade, J., Forester, R.M., Pratt, W. L., and Carter, C., 1998, Black mats, spring-fed streams, and late-glacial-age recharge in the southern Great Basin: Quaternary Research, v. 49, p. 129-128.

Quade, J., Forester, R.M., and Whelan, J.F., 2003, Late Quaternary paleohydrologic and paleotemperature change in southern Nevada, *in* Enzel, Y., Wells, S.G., and Lancaster, N., eds., Paleoenvironments and paleohydrology of the Mojave and Southern Great Basin Deserts: Geological Society of America Special Paper 368, p. 165-188.

Rees-Jones, J., 1995, Optical dating of young sediments using fine-grain quartz: Ancient TL, v. 13, p. 9-13.

Reheis, M.C., Harden, J.W., McFadden, L.D., and Shroba, R.R., 1989, Development rates of late Quaternary soils, Silver Lake playa, California: Soil Science Society of America Journal v. 53, p. 1127-1140.

Rendell, H.M., and Sheffer, N.L., 1996, Luminescence dating of sand ramps in the eastern Mojave Desert: Geomorphology v. 17, p. 187-198.

Rendell, H. M., Lancaster, N., and Tchakerian, V.P., 1994, Luminescence Dating of Late Quaternary aeolian deposits at Dale Lake and Cronese Mountains, Mojave Desert, California, Quaternary Geochronology (Quaternary Science Reviews) v. 13, p. 417-422.

Reynolds, R.E., Miller, D.M., and Bishop, K., 2003, Land of Lost Lakes-The 2003 Desert Symposium field trip, *in* Reynolds, R.E., ed., Land of Lost Lakes-2003 Desert Symposium: California State University, Fullerton, p. 3-26.

Rich, J., Stokes, S., Wood, W., and Bailey, R., 2003, Optical dating of tufa via in situ aeolian sand grains-A case example from the Southern High Plains, USA: Quaternary Science Reviews, v. 22, p. 1145-1152.

Richardson, C.A., McDonald, E.V. and Busacca, A.J., 1997, Luminescence dating of loess from the northwest United States: Quaternary Science Reviews, v. 16, no. 3-5, p. 403-415.

Rittenour, T.M., Goble, R.J. and Blum, M.D., 2003, An optical age chronology of Late Pleistocene fluvial deposits in the northern lower Mississippi Valley: Quaternary Science Reviews, v. 22, no. 10-13, p. 1105-1110.

Roberts, H.M., Muhs, D.R., Wintle, A.G., Duller, G.A.T., and Bettis, A.E., 2003, Unprecedented last-glacial mass accumulation rates determined by luminescence dating of loess from western Nebraska,: Quaternary Research, v. 59, 411-419.

Roberts, H.M., and Wintle, A.G., 2001, Equivalent dose determinations for polymineralic fine-grains using the SAR protocol-application to a Holocene sequence of the Chinese Loess Plateau: Quaternary Science Reviews, v. 20, no. 5-9, p. 859-863.

Sarna-Wojcicki, A. M., Morrison, S. D., Meyer, C. E., and Hillhouse, J. W., 1987, Correlation of upper Cenozoic tephra layers between sediments of the western United States and eastern Pacific Ocean and comparison with biostratigraphic and magnetostratigraphic age data: Geological Society of America Special Bulletin, v. 98, p. 207-223.

Schmidt, K.M., and McMackin, M., 2006, Preliminary surficial geologic map of the Mesquite Lake 30' X 60' Quadrangle, California and Nevada: U.S. Geological Survey Open-File Report 2006-1035, v. 1.0, scale 1:100,000, 89 p.

Singhvi, A.K., Bluszcz, A., Bateman, M.D ,and Rao, M.S., 2001, Luminescence dating of loess-palaeosol sequences and coversands: methodological aspects and palaeoclimatic implications: Earth-Science Reviews, v. 54, no. 1-3, p. 193-211.

Singhvi, A.K., Banerjee, D., Ramesh, R., Rajaguru, S. N., and Gogte, V., 1996, A luminescence method for dating 'dirty' pedogenic carbonates for paleoenvironmental reconstruction: Earth and Planetary Science Letters, v. 139, p. 321-332.

Singhvi, A.K., Sharma, Y.P., and Agrawal, D.P., 1982, Thermo-luminescence dating of sand dunes in Rajasthan, India: Nature, v. 295, no. 5847, p. 313-315.

Snyder, S.L., and Duval, J.S., 2003, Design and construction of a Gamma-ray Spectrometer system for determining natural radioactive concentrations in geological samples at the U.S. Geological Survey in Reston, Virginia,: U.S. Geological Survey Open-File Report 03-29 (on-line only) (*http://pubs.usgs.gov/of/2003/of03-029/*).

Sohn, MF., Mahan, S.A., Knott, J.R., Bowman, D. D., 2007, Luminescence ages for alluvial-fans in southern Death Valley: Implications for climate-driven sedimentation along a tectonically active mountain front: Quaternary International, v. 166, p. 49-60.

Stine, S., 1994, Extreme and persistent drought in California and Patagonia during medieval time: Nature, v. 369, p. 546-549.

Stuiver, M., Grootes, P.M., and Vraziunas, T.F., 1999, Cooling cycles, Heinrich event 1, and the desiccation of Lake Victoria: Paleogeography, Paleoclimatology, Paleoecology, v. 183, no.1-2, p. 169-178.

Viles, H.A, and Goudie, A.S., 1990, Tufas, travertines and allied carbonate deposits: Progress in Physical Geography v. 14, p. 19-41.

Wallinga, J., 2002, Optically stimulated luminescence dating of fluvial deposits: a review: Boreas, v. 31, no. 4, p. 303-322.

Wang, Y., McDonald, E., Amundson, R.., McFadden, L., and Chadwick, O., 1996, An isotopic study of soils in chronological sequences of alluvial deposits, Providence Mountains, California: Geological Society of America Bulletin, v. 108, p. 379-391.

Wells, S.G., McFadden, L.D., and Harden, J., 1990, Preliminary results of age estimations and regional correlations of Quaternary alluvial fans within the Mojave Desert in southern California, *in* Reynolds, R.E., Wells, S.G., and Brady, R.H., compilers, At the end of the Mojave-Quaternary studies in the eastern Mojave Desert: Redlands, California, San Bernardino County Museum Association, p. 45-54.

Wells, S.G., Brown, W.J., Enzel, Y., Anderson, R.Y., and McFadden, L.D., 2003, Late Quaternary geology and paleohydrology of pluvial Lake Mojave, southern California, *in* Enzel, Y., Wells, S.G., and Lancaster, N., eds., Paleoenvironments and paleohydrology of the Mojave and Southern Great Basin Deserts: Geological Society of America Special Paper 368, p. 79-114.

Whitney, J.W., Taylor, E.M., and Wesling, J.R., 2004, Quaternary stratigraphy and mapping in the Yucca Mountain area, *in* Keefer, W.R., Whitney, J.W., and Taylor, E.M., eds., Quaternary paleoseismology and stratigraphy of the Yucca Mountain area: U.S. Geological Survey Professional Paper 1689, p. 11-21.

Wieser, A., Goksu, H.Y., Regulla, D.F., Fritz, P., Vogenauer, A., and Clark, I.D., 1993, ESR and TL dating of travertine from Jordan-complications in paleodose assessment: Applied Radiation and Isotopes, v. 44, p. 149-152.

Wintle, A.G., Lancaster, N., and Edwards, S.R., 1994, Infrared stimulated luminescence (IRSL) dating of Late Holocene aeolian sands in the Mojave Desert, California, USA: The Holocene v. 4, p. 74-78.

Chapter D

Debris-flow deposits and watershed erosion rates from the Kingston Range, CA

By Kevin M. Schmidt[1] and Christopher M. Menges

Abstract

Debris flows from the steep, granitic hillslopes of the Kingston Range, CA are commensurate in age with nearby fluvial deposits. Quaternary chronostratigraphic differentiation of debris-flow deposits is based upon time-dependent characteristics such as relative boulder strength, derived from Schmidt Hammer measurements, degree of surface desert varnish, pedogenesis, and vertical separation. Rock strength is highest for Holocene-aged boulders and decreases for Pleistocene-aged boulders weathering to grus. Volumes of age-stratified debris-flow deposits, constrained by deposit thickness above bedrock, GPS surveys, and geologic mapping, are greatest for Pleistocene deposits. Shallow landslide susceptibility, derived from a topographically based GIS model, in conjunction with deposit volumes produces watershed-scale erosion rates of ~2-47 mm ka^{-1}, with time-averaged Holocene rates exceeding Pleistocene rates.

Introduction

Considerable research has focused on deciphering depositional characteristics of alluvial fans in the arid Southwest of the United States (e.g., Hooke, 1987). Even under the presently arid conditions, alluvial fans in the Southwest stochastically flood and aggrade (e.g., Field & Pearthree, 1997). Although only locally dense populations of people exist, debris flows, hyperconcentrated flows, and flash floods occur episodically placing communities such as Las Vegas, NV at risk during intense and prolonged rainfall (Katzer et al., 1976), and are potentially more pronounced during El Niño climatic conditions. The magnitude and timing, however, of sediment transport and storage in the link between mass wasting processes on hillslopes and alluvial fan aggradation is commonly unconstrained. Interpreting watershed-scale erosion rates arising from mass wasting of hillslopes helps to define these relations as well as potential mass-wasting triggering mechanisms.

Through Quaternary time, magnitudes of erosion and sedimentation from debris flows respond to climatic forcing of precipitation/runoff characteristics, and related changes in weathering and vegetation assemblages. In addition, tectonics alters local base level or slope steepness thus influencing debris-flow activity. Debris-flow dominated alluvial fans, situated proximal to mountainous catchments, may serve as sediment storage zones by receiving coarse-grained material derived from hillslopes thereby buffering the downslope sediment supply. Determining the relative frequency of debris flows through Quaternary time provides insight into

[1]U.S. Geological Survey, 345 Middlefield Road, MS 973, Menlo Park, CA 94025

alluvial fan function, relative hazard, and time-scales of response between hillslopes and sediment deposition. Estimating frequency on a regional basis requires a means to discriminate debris-flow deposit age, thickness, and volume. Through a combination of geologic field mapping, surveying, and geographic information system (GIS) modeling, here we present evidence to distinguish debris-flow deposits and their relative ages, estimate volumes of age-stratified deposits, and infer watershed-scale erosion rates in the granitic Kingston Range of the Mojave Desert of California, United States.

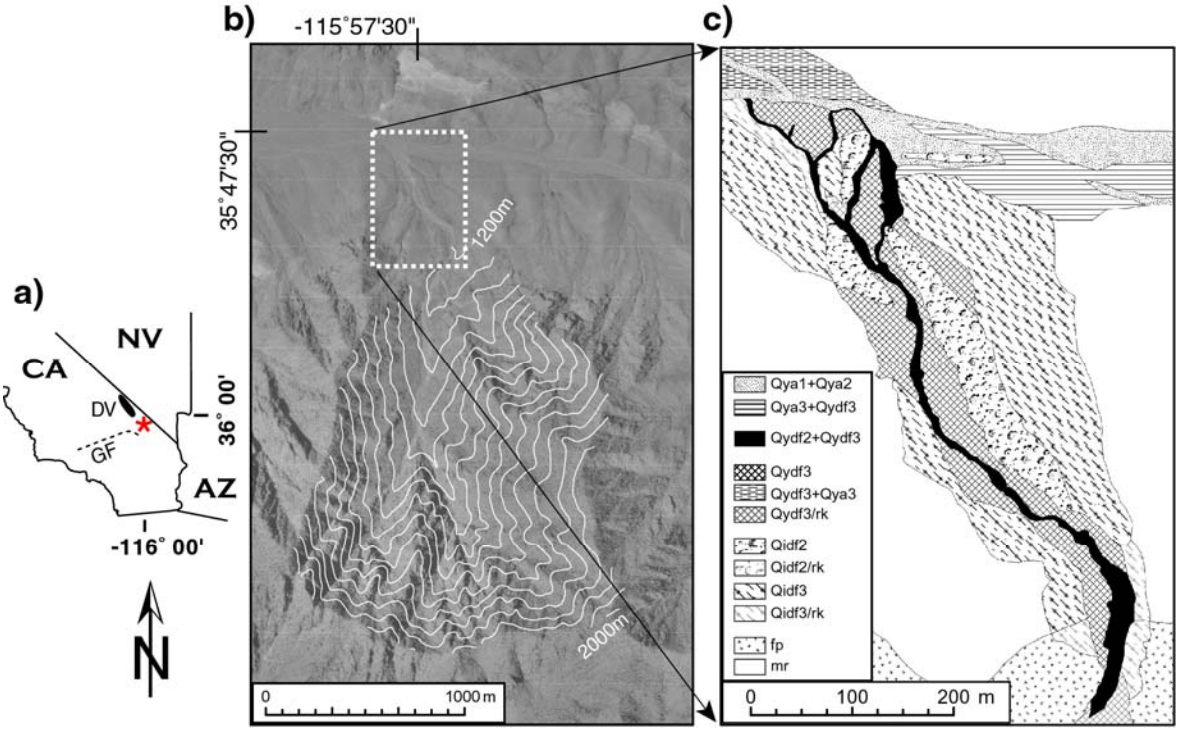

Figure 1. a) Location of Kingston Range denoted by star, DV is Death Valley, and GF is Garlock fault. b) Crystal Spring watershed denoted by digital orthophotoquadrangle with 50-m contours. Dashed box denotes limits of c) Crystal Spring debris-flow fan geologic map. Lower right-hand corner corresponds to downslope terminus of contributing watershed and upslope extent of fan. While the watershed source area is felsic plutonic rock (fp), metamorphic rock (mr) underlies the deposit. Mixed units are shown by (+) sign while Quaternary deposits thinner than 2 m are shown with (/rk) sign. Quaternary units are described in section 3.1.

Study Area

Located near the border between the Basin and Range and Mojave Desert Provinces, the Kingston Range is approximately 30 km northeast of the eastern terminus of the Garlock fault that generated the faulted front of the Avawatz Mountains (Fig. 1a). We studied debris-flow fans from the Kingston Range intensively because they have monolithologic sources and studied the tectonically active Avawatz Mountains on only a reconnaissance level because it has complex source rocks. Debris flows from the Kingston Range are composed of Tertiary granite so relative age inferences are not complicated by multiple source lithologies. Hillslopes and debris-flow deposits are solely composed of the Miocene Kingston Peak Formation; a medium-grained leucocratic, biotite granite porphyry containing quartz, sanidine, and plagioclase. The Kingston Peak Formation intruded into Proterozoic metamorphosed basement sedimentary rocks and is overlain by Quaternary sediments. Rising from a base elevation of about 1000 m to peaks over

2200 m, hillslopes in the uplands are generally steep (35-60˚) with large areas of exposed, relatively homogeneous granitic bedrock, or a thin (~1 m) cover of relatively unweathered colluvium. Angular colluvial deposits, likely derived from rocks falling off steep outcrops, are thickest in areas of topographic concavity. The thickest colluvium and shallow-landslide scars are located at higher elevations where vegetation is characterized by Singleleaf pinyon (*Pinus monophylla*) and White fir (*Abies concolor*). At the outlets of the steep tributary watersheds are gently to moderately sloping alluvial fans and nearly level basins. Within the valley floors, bedrock is overlain by prevalent Quaternary alluvium transported by combinations of streamflow, sheetflow, and mass wasting processes. At these lower elevations, vegetation is dominated by small shrubs such as creosote bush (*Larrea tridentata*), blackbush (*Coleogyne ramosissima*), and plants in the Agave Family such as yuccas. The present mean annual precipitation is typically <200 mm falling mostly as rain, with snow accumulating at higher elevations in the winter. Runoff is rapid from hillslopes and alluvial fans and channels are dry most of each year with surface flow only occurring after intense localized precipitation.

Debris-flow deposits within the Kingston Range, typically located just downslope of mountain fronts or tributary junctions, are commonly composed of a matrix of fine-grained material with granitic clasts up to meters in diameter. The randomly orientated clasts are rounded to angular with a wide range in grain size from clay to boulders with a typical matrix of sandy, fine gravel. These high-sediment-concentration debris-flow deposits are preserved in fans with rugged topography and relatively steep slopes (>5˚). Deposits are massive, matrix-supported to poorly sorted without internal sedimentary structures but locally imbricated at the snout. Surface morphology is characterized by lateral levees bounding the channels and coarse, steep-fronted, terminal lobes. The deposits also have isolated boulders as large as 7 m in diameter resembling glacial erratics and precariously balanced boulders. Younger, smaller volume fluvial units are generally confined to channel axes in the proximal fan. We named the tributary watershed studied here in detail the Crystal Spring watershed and fan (Fig. 1b).

Methods

We estimated watershed-scale, debris-flow erosion rates in the Kingston Range through a combintion of field studies and geographic information system (GIS) analyses. Relative ages of debris-flow deposits were determined in the field by their topographic and stratigraphic position, soil development, vegetation assemblages, and boulder characteristics. Absolute ages were obtained by identification of entrained historic material and by prior dating with infrared stimulated luminescence (IRSL). Deposit thickness was obtained by measuring with a tape the debris overlying bedrock exposures. Surface area of individual deposits was computed from GPS surveys and GIS analyses of geologic mapping from digital remotely sensed images. Deposit volumes were calculated from surface area and thickness estimates. Topographic attributes of the watershed and estimated relative shallow-landslide susceptibility were derived from GIS analyses of digital terrain. Reconnaissance-level studies of the Avawatz Mountains focused on Quaternary geologic mapping.

Classification of Quaternary chronostratigraphy

Classification of the Quaternary geology is based upon an ongoing regional mapping campaign of the Mojave Desert region by the U.S. Geological Survey (see Schmidt and McMackin, 2003 and *http://deserts.wr.usgs.gov*). Units are defined such that the first two characters in a label designate the relative age followed by a process label and a numeric age modifier. The relative ages of the units are sequentially numbered beginning with the youngest

deposit. For example, a Qy*x*2 surface is younger than a Qy*x*3 surface; where *x* is a placeholder for *df* (debris flow) or *a* (alluvium).

Active surfaces received deposition within the last few decades (Qy*x*1) or centuries (Qy*x*2). They are characterized by loose sediment, are prone to flooding and sediment transport, are typically unvegetated or moderately vegetated, and have rough surface microtopography such as strongly developed bar and swale or debris-flow morphology such as lobes and levees. Active surfaces are small in area and form discrete channels. Young surfaces are mid-Holocene (Qy*x*3) to early Holocene and latest Pleistocene (Qy*x*4) in age. They are abandoned or receive sediment infrequently and are characterized by loose to slightly compact sediments. Pedogenic soil is thin and weakly developed and typically expressed as an incipient to weak, sandy vesicular horizon (A_v), weak cambic horizon (B_w), and Stage I calcic horizon (B_k to K). Young surfaces are moderately vegetated, especially with shrubs, and have fairly smooth microtopography, with moderate to faint remnants of bar and swale topography. Although no desert pavement or incipient pavement is present, surface clasts have incipient varnish. Intermediate surfaces are late (Qi*x*2) and mid- (Qi*x*3) Pleistocene in age and have been abandoned for 10's to 100's of thousands of years. Sediments can be loose but are commonly compact. On intermediate surfaces, desert pavement is moderately to well developed with moderate to strong varnish on surface clasts. Microtopography of the surface is flat, lacking the original depositional morphology, but may exhibit weak to moderate incision locally. Pedogenic soil is well-developed with a silty A_v horizon, moderately to strongly developed B_t horizon and Stage I+ to III+ calcic horizon. Time-dependent processes such as pedogenesis, varnish development, and the vertical separation between units were judged from field relations.

Surface characteristics of debris-flow boulders

Rebound characteristics of boulders within debris-flow deposits were collected as a proxy for relative weathering. We selected granitic boulders at the surface of a given age deposit with varying states of weathering and oxidation. A minimum of 100 type-L, Schmidt Hammer measurements were distributed over 10 boulders of a debris-flow lobe with 10 measurements per boulder. The 10 Schmidt Hammer values (SHV) were distributed around the entire boulder to minimize any bias caused by direction-dependent weathering. Rebound characteristics of boulders were quantified at 34 locations within 8 fans at elevations ranging from 220 to 1350 m. Four watersheds were studied in detail where the chronostratigraphy was well expressed, including the Crystal Spring fan. Desert varnish maturity was gauged by the color of surface boulders determined with a Munsell® color chart for soils. Mean boulder diameter was measured on 20 clasts at the surface of each deposit.

Estimating alluvial fan volume, relative shallow-landslide susceptibility, and erosion rate

Volumes of the Crystal Spring debris-flow fan deposits were calculated based upon field estimation of deposit thickness from available bedrock outcrops, GPS surveys of unit boundaries, and GIS-based mapping and calculation of surface areas. Bedrock exposures, used to define 24 estimates of deposit thickness, were largely located within active channel banks. Mean heights above the active channel (Qya1) were determined from field measurements and topographic surveying. A detailed topographic map of part of the fan was surveyed using a targetless laser to quantify the vertical separation between the different-aged deposits and their respective surface areas. To conservatively account for material eroded over time from the fan axis, the present volumes of inset, younger deposits were added to calculations of older-deposit volumes because

fan morphology prior to post-depositional channel erosion was likely valley-spanning, with more material than presently preserved within the current active channel. Following Nanninga & Wasson (1985), we calculated watershed-average erosion rates, $\dot{\varepsilon}$, such that:

$$\dot{\varepsilon} = \frac{V\rho_s}{\rho_r PAI} \quad (1)$$

where V=volume of sediment contained within the debris-flow fan, ρ_s=sediment bulk density, ρ_r=rock bulk density, P=time-period of sediment accumulation, A=upslope contributing drainage area of the watershed, and I=proportion of A that is prone to shallow landslide initiation. Through field observations and image interpretation we concluded that shallow landsliding is the current primary source for debris flows. We assume post-depositional material densities of: ρ_s=2200 kg m^{-3} and ρ_r=2650 kg m^{-3}. For the Crystal Springs debris-flow fan, the estimated volume of material present is a minimum because sediment was likely transported by lower sediment-concentration flows downslope of the fan and material was likely eroded by channel incision.

Topographic analyses were carried out on digital elevation models (DEMs) with a 10-m grid node spacing in a GIS. Within the watershed boundaries shown by the area of contours in Figure 1b, we calculated topographic relief, slope, planform area (A), topographic surface area, and potential area of landslide initiation (I). We calculated both basin-averaged and landslide source-area erosion rates. Relative landslide susceptibility provides a means to infer debris-flow erosion rates in the portion of the landscape most prone to shallow landsliding (I). The GIS-based slope stability model used here (SHALSTAB) is a steady-state runoff approximation that incorporates the topographic influence on subsurface hydrologic response to calculate the ratio of precipitation to soil transmissivity. Landslide susceptibility, was modeled using the DEM of the present topography with generalized input variables assumed as follows: the colluvium has a friction angle of 45˚, a bulk density of 1700 kg m^{-3}, a uniform thickness of 1m, and cohesion arising from both root reinforcement and soil is neglected. We express susceptibility qualitatively to provide a relative rating because site-specific conditions surely varied over time and space. For more detailed discussions of the model and its assumptions see Dietrich et al. (1993) and Montgomery & Dietrich (1994).

Results

Debris-flow fans throughout the Kingston Range share the same number of depositional sequences and similar age-dependent surface characteristics as the more widespread streamflow-derived sediments. This regional consistency of chronostratigraphy indicates that roughly coeval aggradation existed in the mountain range and adjacent basins. Detailed mapping of the Crystal Spring fan (Fig. 1c), for instance, revealed four distinct debris-flow deposits (Qydf2, Qydf3, Qidf2, and Qidf3) that are correlative in number and areal extent with nearby streamflow-derived deposits. Although little to no fluvial deposits were interbedded within the stratigraphy of the steep, proximal debris-flow fans, they are common at distances > 1 km from the mountain front in the distal fans. No Qydf4-aged deposits were observed on the Crystal Spring fan but were identified elsewhere in the range. Debris-flow deposits older than Qidf3 were not recognized anywhere within the Kingston Range. In the following discussion we present results specific to

the Crystal Spring fan, general observations from throughout the Kingston Range, and attributes of four fans where the chronostatigraphy was well expressed.

Surface characteristics of debris-flow deposits on the Crystal Spring fan

Of the field-criteria used to distinguish the debris-flow chronostratigraphy, boulder characteristics, vegetation assemblages, pedogenesis, and relative height above the active channel were the most distinctive (Table 1). Ages of field-surveyed deposits (Fig. 1c) also correlate with tonal contrasts on digital orthophotographs that primarily reflect the degree of time-dependent development of desert varnish and vegetation colonization. Although the relationships described in Table 1 are consistent throughout the Crystal Spring fan, and similar trends were observed for fans throughout the range, these specific values cannot be extrapolated wholesale to the Kingston Range. Differences in elevation and aspect, for instance, regulate available moisture and thereby alter the vegetation assemblages, weathering rates, and to a lesser degree the varnish maturity.

As the surface morphology of the Crystal Spring fan becomes generally smoother over time, the boulders exhibit more mature varnish and progressively higher degrees of weathering (Table 1). In contrast, boulders within Qydf2 and Qydf3 deposits are unweathered and unvarnished, presumably the result of comminution of the exterior during transport. Even though desert varnish tends to form slowly on felsic-granitic rocks, boulders of Qydf2 surfaces that are initially light bluish gray in color varnish to a dark reddish gray or reddish black on older Pleistocene deposits. Similarly, clasts within Qydf2 and Qydf3 are strong (SHV>50), consistent with values for igneous rocks with no discoloration or mineralogic decomposition (Selby 1993), whereas weathered boulders in old deposits have values characteristic of weakly compacted sedimentary rocks (SHV<25). The most significant decrease in mean SHVs (~ 50%) occurs during the time frame of Qidf2 to Qidf3 and is associated with the longest time interval (middle to late Pleistocene).

Vegetation characteristics used to discriminate Holocene-aged deposits on the Crystal Spring fan are largely dependent on the density of shrubs such as cheesebush (*Hymenoclea salsola*), mormon tea (*Ephedra viridis*), and Mojave horsebrush (*Tetradymia stenolepis*). Qydf2 deposits are colonized by grasses with shrubs being absent or having a low density. Qydf3 deposits have a moderate density of shrubs but no Mojave yucca (*Yucca schidigera*), buckhorn cholla (*Opuntia acanthocarpa var. coloradensis*), or creosote bush that are common on Pleistocene-aged debris-flow deposits. Mojave yucca is typically absent from deposits younger than mid-Pleistocene.

Cryptobiotic soils, communities of soil cyanobacteria, lichen, and mosses, influence vascular plant germination and success, in addition to increasing physical soil stability. The presence and density of cryptobiotic soil crusts provide a rough measure of age given that lichen colonization requires long-term surface stability. Collema lichen, for instance, may require a surface to be stable for as long as 1000 years in order to successfully colonize (Belnap 1993). In the Crystal Spring fan, lichen was largely absent from Holocene deposits but common on Pleistocene ones (Table 1). Although soil development appears to be slightly impeded relative to the neighboring alluvial deposits, well-developed illuvial accumulations of silt, clay, and calcic material forming B_t, B_k, and K horizons are present ~1-1.5m below the surface within Qidf3 deposits throughout the range. Generally, Qidf2 deposits lack calcic horizons but have a weak to moderate reddish, B_w horizon. Qydf3 deposits exhibit only weak soil formation and Qydf2 deposits are generally devoid of pedogenic horizons. The slightly impeded pedogenesis on debris-flow deposits may be caused by extremes in grain size, presumed high bulk density, and relative impermeability of matrix material.

Table 1. Criteria used to infer relative ages of debris-flow deposits on Crystal Spring fan. SHV is Schmidt Hammer value. All deposits are composed of Kingston Peak Formation

Characteristic	Qydf2 (late Holocene)	Qydf3 (mid-Holocene)	Qidf2 (late Pleistocene)	Qidf3 (mid-Pleistocene)
Surface Morphology	Rough, no infilling of interstices w/	Rough, minor infilling of interstices w/ fines	Undulating, moderate infilling of interstices w/ fines	Undulating to smooth, moderate to high infilling of interstices w/ fines
Boulder weathering	Ũnweathered, no oxidation or varnish	Unweathered, minor oxidation & varnish	Low weathering, moderate oxidation & varnish w/ minor grus production	Low to high weathering, moderate to high oxidation & varnish w/ local high grus production
Mean boulder diameter (m)	0.25	1	1.2	1.5
Boulder Munsell® color	Gley 2 8/5PB light bluish gray	2.5YR 8/2 - 8/4 pinkish white to pink	2.5YR 3/1 dark reddish gray	2.5YR 2.5/1 reddish black
Boulder SHV mean ± standard deviation	56.0 ± 8.8	53.3 ± 9.4	48.4 ± 9.7	25.8 ± 12.2
Vegetation	Grasses & low density shrubs	Moderate density shrubs	High density shrubs; Mojave yucca, buckhorn cholla, & local creosote bush	High density shrubs; Mojave yucca, buckhorn cholla, & creosote bush
Cryptobiotic soil	Absent to low cyanobacteria & lichen	Low to moderate cyanobacteria, absent to low lichen	Moderate to high cyanobacteria & lichen	Moderate to high cyanobacteria & lichen
Pedogenesis	absent	Weak Av, absent to weak Bw	Slightly organic A, weak Av, weak Bw	Organic A, strong, red Bt, Stage I-IV Bk to K
Mean height above Qya1 (m)	0.5	1	3.5	4

Relative boulder weathering based upon Schmidt Hammer values

Schmidt Hammer values for 34 sites distributed through the Kingston Range (n=3084 measurements) reveal both a general decrease in the median value with age but also an increase in the range of values with deposit age. Each box in Figure 2 encloses 50% of the data with the median value displayed as a horizontal line and the upper quartile (UQ) and lower quartile (LQ) mark the interquartile distance (IQD) of the population. The vertical lines extending from the UQ and LQ mark the minimum and maximum values within the data set that fall within an acceptable range (>UQ+1.5*IQD or < LQ-1.5*IQD). Values outside this range plot as open circles. Although values from Qydf2 and Qydf3-aged deposits are similar, values of the LQ, median, and UQ consistently decrease with time. For all but the Qidf3 sites, the data are distributed with a negative skew.

With increasing time of boulder surface exposure, weathering by chemical alteration along small cracks or phenocryst boundaries is likely responsible for the decreased SHVs. The sharp decrease in values of the Qidf3 deposits coincides with the change in physical properties from coherent granitic boulders weathering to grus as feldspars weather to kaolin clay minerals. Maximum values for each deposit (SHV≈70) in Figure 2, however, do not decrease with time of

surface exposure such that some surface boulders in all deposits retain rebound characteristics of very strong rock. These high values may reflect compositional variations with some plutonic source rock being more resistant to weathering.

To examine boulder resistance with respect to chronostratigraphy, we examined four fans in detail. Figure 3 depicts SHVs for a subset of sites shown in Figure 2. As with the age progression depicted in Figure 2, the fans depicted in Figures 3a, b reveal similar values for boulders on Qydf2 and Qydf3 deposits and a sharp decrease in values for Qidf3 deposits. Deviations from the trend of decreasing SHVs over time are revealed in Figures 3c, d. In Figure 3c, for a lower altitude fan with an apex at 1040 m, the increase in SHVs for Qidf2-aged boulders is thought to correspond with the observed advanced stage of desert varnish, with low surface weathering on boulders. The advanced varnish on these boulders may provide an effective case hardening. Similar aged Qidf2 deposits on the fan in Figure 3d are also well-varnished but have more advanced weathering such that boulder surfaces are beginning to exfoliate with thin rinds of rock detaching from boulders. Although Qidf2-aged boulders in Figure 3d had an advanced state of weathering, they did not yet expose material weathered to grus, with lower SHVs, as was uniformly observed on Qidf3-aged boulders throughout the range.

To examine the rebound characteristics associated with the state of weathering, we selected two sets of boulders on the same Crystal Spring Qidf3-fan deposit, one with remnant varnish and the other with exposed grus. Figure 4 depicts the contrast in SHV for varnished boulders and for boulders weathering *in situ* to grus. The mean and standard deviation of SHVs on boulders with grus is 18.4±5.9 with a skew of -0.3, whereas varnished boulders express higher values of 39.3±10.4 with a skew of 0.1. The presence of varnish on boulders appears to provide an effective case hardening, increasing the rock strength and potentially retarding weathering.

Deposit characteristics outlined in Table 1, in conjunction with regional chronostratigraphy, provide the primary basis for dating relative deposit age. Although the relative dating control presented is largely qualitative, two sources of information are used to constrain absolute ages of Holocene fans. First, a Qydf3 deposit was dating using IRSL. Located ~ 25 km away from the Kingston Range front, the deposit was dated near the terminus of a large fan at 6.5 ± 0.5 ka (Miller et al. 2001a). Second, Qydf2 deposits from a watershed east of the Crystal Spring watershed contain asphalt and incorporate an automobile (roughly 1930's vintage) and hence must be historic. Figure 5 presents all the SHVs for a given age deposit to compare with the subset of sites with absolute dating control. In general, Qydf2- and Qydf3-aged deposits have boulders that are unweathered and express roughly the same distribution of SHVs. The deposit characteristics at both sites with absolute dating control also correlate with the relative attributes portrayed in Table 1. In the following analysis we assume that the sites with absolute dating control provide age constraints for those Holocene-aged fans with equivalent surface characteristics dated by relative means.

Watershed erosion rates from debris flows

Analyses within a GIS were used to determine morphometric attributes and relative susceptibility to shallow landsliding. Based on calculations from the 10-m grid DEM, the Crystal Spring watershed has a surface plan form area of 2.6 km^2, a topographic surface area of 3.3 km^2, and an alluvial fan area of 0.37 km^2 (Figs. 1b, c). Elevation in this northward-sloping watershed ranges from 1188 to 2010 m with a mean hillslope gradient of 36˚ and a maximum gradient of 63˚. Attributes of the three primary debris-flow sequences, representing the sum of all deposits within a given age range, are shown in Table 2. Sediment accumulation periods (P) were determined based upon dating control within the region and common geologic time scale boundaries and hence are generalized and subject to judgement of the exact temporal boundaries.

Late Holocene deposits are an order of magnitude smaller in volume than either early to mid-Holocene deposits or middle to late Pleistocene deposits. This volume contrast is a minimum as Pleistocene deposit volumes are likely under represented as older material has been removed via erosion.

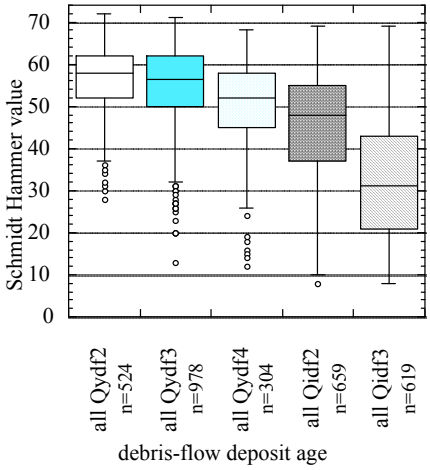

Figure 2. Type-L Schmidt Hammer values for surface boulders within active to mid-Pleistocene deposits.

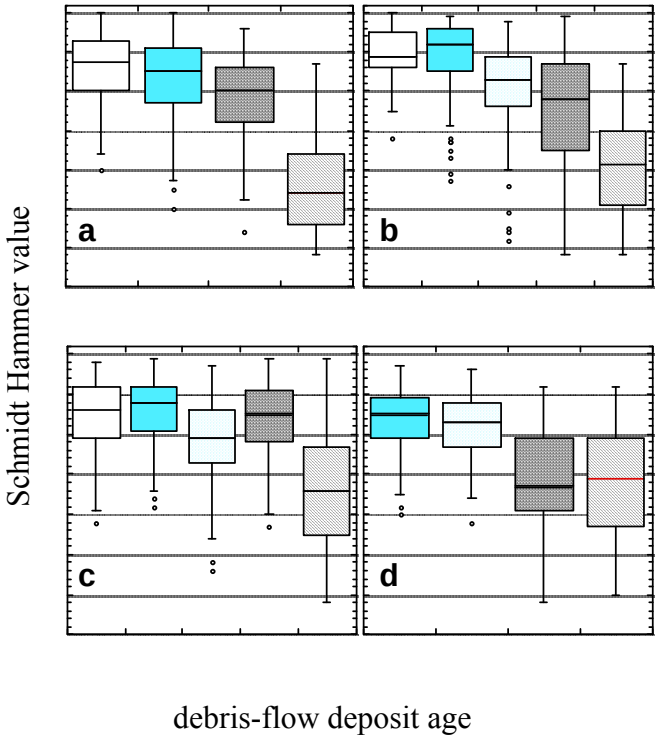

Figure 3. Schmidt Hammer values for surface boulders deposited within four fans increasing in age from active to mid-Pleistocene. Crystal Spring fan depicted in Figure 3a.

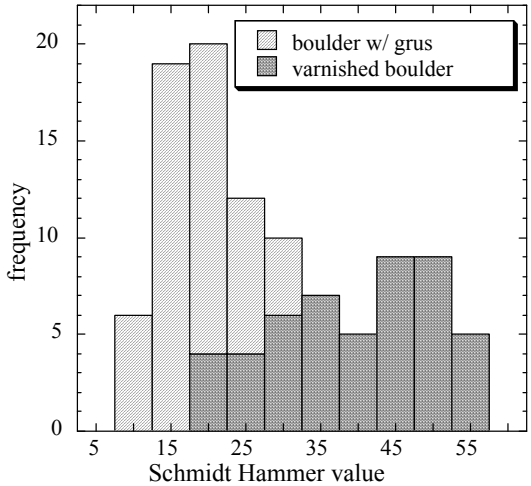

Figure 4. Comparison of SHVs for Qidf3-aged boulders retaining a varnished surface and those that are weathering to grus in Crystal Spring fan (n=102).

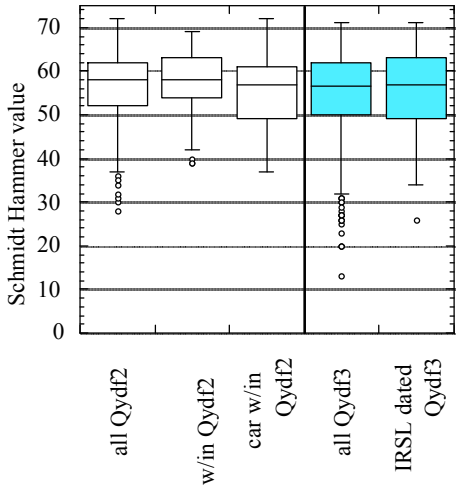

Figure 5. Comparison of all SHVs for active and young debris-flow deposits to sites with age control including entrained asphalt, a 1930's vintage car, and IRSL dating.

Table 2. Crystal Spring debris-flow fan characteristics used in equation 1 to calculate time-averaged erosion rates. Landslide source-area erosion rates are inferred from the SHALSTAB modeling results (Fig. 6).

Debris-flow deposit age	Sediment accumulation period, P (ka B.P.)	Area, A (km^2)	Volume, V (km^3)	Basin-average erosion rate I=1 (mm ka^{-1})	Landslide source-area erosion rate I=0.36 (mm ka^{-1})
Qydf2 (late Holocene)	present - 1	0.011	0.044	14	38
Qydf3 (early to middle Holocene)	1 - 12	0.254	0.650	17	47
Qidf2+Qidf3 (middle to late Pleistocene)	12 - 200	0.366	1.08	2	5

Assuming that the source of the debris-flow deposits is shallow landsliding, and that hillslopes are equally mantled with colluvial soil, the part of the landscape with the highest landslide susceptibility was inferred using the SHALSTAB model for heuristic purposes. The categories of stable, low-, medium-, and high-landslide susceptibility, and chronic instability, depicted in Figure 6, are based upon the predicted hydrologic conditions necessary to trigger landsliding (critical ratios of precipitation to soil transmissivity). As the categories are primarily topographically defined based upon gradient and upslope contributing drainage area, the regions of highest potential instability are located in the steep upland concavities. The proportion of the landscape represented by the chronic instability and high susceptibility categories represents 36% of the watershed (Fig. 6). This percentage was used to restrict the erosion estimates to the portion of the watershed predicted by the model to have the highest landslide susceptibility; hence I=0.36. We assume erosion focused in this portion of the landscape with the worst case topographic and hydrologic conditions regardless of the magnitude of hydrologic response associated with climatic variations over time. The basin-average erosion rates (I=1), independent of the assumptions involved in the SHALSTAB modeling, are approximately 2 to 3 times lower than the landslide source-area erosion rates (Table 2).

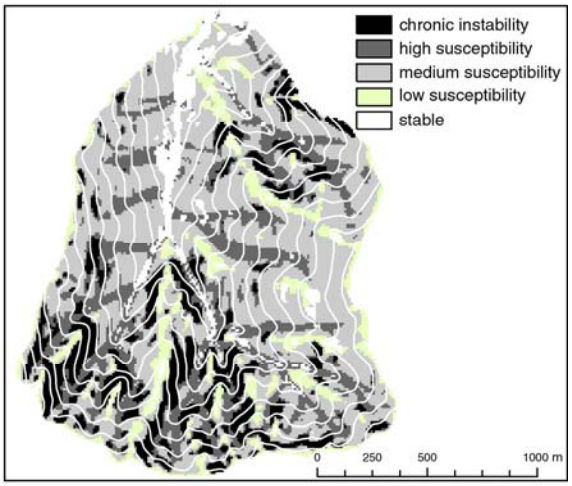

Figure 6. Estimate of relative shallow-landslide susceptibility for Crystal Spring watershed using SHALSTAB with generalized categories. Contour interval is 50 m.

Discussion

Regional patterns of erosion and deposition via debris flows provide insight into connectivity between hillslope sources and fan deposits as well as timing of triggering mechanisms. Up to five distinct sequences of debris-flow fan aggradation were observed with the oldest deposit directly overlying bedrock throughout the range. This erosional unconformity prior to mid-Pleistocene time represents a regional removal of older sediment before deposition of Qidf3 fans, possibly the result of tectonically driven base level changes or climatically driven high sediment transport rates that exceeded sediment production.

The relatively coarse timing resolution provided by the chronostratigraphic indicators, with progressively larger time steps with age does not allow for the direct evaluation of Pleistocene-aged debris-flow deposition and climatic cycles or tectonism. Hence, Pleistocene-aged deposits may have the lowest erosion rates because they are averaged over the longest time period and experienced the longest post-depositional modification by fluvial erosion within the valley axis.

During relatively wet intervals within the Pleistocene epoch, bedrock to regolith conversion was likely rapid, resulting in the production of abundant hillslope sediment. Deposition of Qydf4 sediment commenced during or immediately following the regional pluvial highstand at the end of the last glacial maximum (Quade et al., 1995). During the transition from a wetter to drier climate near the beginning of the Holocene, the landscape may have adjusted to changing vegetation, rainfall/runoff patterns, and colluvial cover by eroding hillslopes and aggrading fans (e.g., Bull & Schick, 1979). A shift to a drier climate, causing a decrease in the overall canopy cover, can increase both the intensity and amount of precipitation reaching the ground. In addition, decreased root densities arising from a likely shift from trees to shrubs diminishes cohesive reinforcement. Hence, colluvium that mantles hillslopes during wetter and/or cooler climatic regimes can be transported to fans during the transition to drier and/or warmer climates. Likewise, Miller et al. (2001b) concluded that hillslopes in central Nevada initially responded to drier climates by accelerating hillslope erosion and the concurrent aggradation of tributary and axial valley system fans.

Widespread Qydf3 deposits, representing the highest rates of inferred erosion, may be associated with mid-Holocene climatic fluctuations modifying tree-line elevations and species compositions, more intense precipitation, and/or fire regime. After cessation of widespread hillslope erosion, decreased sediment production, and subsequent fan stabilization during the mid-Holocene, the late Holocene is characterized by small volume Qydf2-aged flows deposited within channels eroded into older deposits. As active channels are presently incised into the older debris-flow deposits by many meters, the coarse-grained older deposits are disconnected from downstream fluvial reaches of the fan.

To evaluate how the Kingston Range relationships can be extrapolated regionally to similar steep topography, we examined the nearby Avawatz Mountains. The influence of different bedrock lithology and increased tectonic activity apparently results in markedly dissimilar debris-flow fans. In contrast to the general absence of active surface faulting in the Kingston Range, the front of the Avawatz Mountains is tectonically active. Long-term, reverse-slip along the easternmost Garlock fault system generated steep, dissected topography along the flanks of the Avawatz Mountains. This steep range front, underlain by altered and fractured plutonic rocks of variable composition, is especially susceptible to the generation of matrix-rich debris flows. The debris-flow fans issuing from this range exhibit complex geomorphic, sedimentologic, pedogenic, and stratigraphic relations that significantly differ from the relatively matrix-poor deposits derived from the unaltered bedrock of the Kingston Range. For example,

matrix material within the debris-flow deposits of the Avawatz Mountains appears to have very low infiltration capacities that enhance surface overland flow. Debris-flow fans have smoother surfaces, intra-fan channels are deeply incised, and soil development is impeded, compared to the nearby Kingston Range. Based on these observations, results from the Kingston Range should be extrapolated to the region with caution.

Conclusion

Debris flows have sculpted the Kingston Range over several hundred thousand years, during which numerous climatic cycles influenced variations in vegetation assemblages, rainfall/runoff characteristics, and shallow landslide susceptibility. Mass wasting via debris flows is also an active process during the present arid climate, as evidenced by the intermingling of asphalt and an automobile with debris-flow deposits. Based upon field-analyses of surface characteristics, we identified a total of five regionally extensive, Quaternary debris-flow deposits. Surface characteristics of the deposits provided regionally applicable age indicators such that the chronostratigraphy of streamflow sediments closely correlates to debris-flow deposits. Rebound characteristics of debris-flow boulders, as represented by Schmidt Hammer values, decrease with deposit age. Although mid-Holocene (Qydf3) deposits exhibit similar values to unweathered, recently transported (Qydf2) deposits, the Late Pleistocene to early Holocene (Qydf4) boulders exhibit decreased values indicative of weathering. The development of desert surface varnish on Late Pleistocene (Qidf2) boulders, acting as an effective case hardening, potentially increases boulder-rebound resistance. Boulders on mid-Pliestocene (Qidf3) deposits express substantially lower rebound strength as the varnished surfaces spall and the underlying granitic rock weathers to grus. Through field observations and GIS analyses we inferred basin-average and landslide source-area erosion rates based upon volumes of age-stratified debris-flow deposits. Although the inferred rates of ~2-47 mm ka^{-1} likely represent underestimates of the actual rates due to incomplete preservation of fans within narrow tributary valleys, they do provide a minimum estimate of the contribution from debris flows on the total sediment budget.

Acknowledgements

We are grateful for assistance from Stephanie Dudash in GIS modeling and Leila Gass for field surveying. We thank David Miller, Mark Reid, Lorenzo Marchi, and Markus Stoffel for providing insightful review comments.

References cited

Belnap, J. 1993. Recovery rates of cryptobiotic crusts: Inoculant use and assessment methods. *Great Basin Naturalist* 53: 89-95.

Bull, W.B. & Schick, A.P. 1979. Impact of climate change on an arid watershed, Nahal Yael, southern Israel. *Quaternary Research* 11: 153-171.

Dietrich, W.E., Wilson, C.J., Montgomery, D.R. & McKean, J. 1993. Analysis of erosion thresholds, channel networks, and landscape morphology using a digital terrain model. *Journal of Geology* 101: 259-278.

Field, J.J. & Pearthree, P.A. 1997. Geomorphic flood-hazard assessment of alluvial fans and piedmonts. *Journal of Geoscience Education* 45: 27-37.

Hooke, R.L. 1987. Mass movement in semi-arid environments and the morphology of alluvial fans. In M.G. Anderson & K.S. Richards (eds), *Slope Stability; geotechnical engineering and geomorphology*: 505-529. Chichester, United Kingdom: John Wiley & Sons, Ltd.

Katzer, T.L., Glancy, P.A. & Harmsen, L. 1976. A brief hydrologic appraisal of the July 3-4, 1975, flash flood in Las Vegas Valley, Nevada. *Open-File Report 76-100, U. S. Geological Survey*, Carson City, NV.

Miller, D.M., Yount, J.C. & Mahan, S.A. 2001a. Mid-Holocene debris-flow and lake stand events at Silurian Lake, Mojave Desert, California, *97th Annual Meeting Cordilleran Section. Geological Society of America, Universal City, CA*: A-70. Denver, Colorado: Geological Society of America.

Miller, J., Germanoski, D., Waltman, K., Tausch, R. & Chambers, J. 2001b. Influence of late Holocene hillslope processes and landforms on modern channel dynamics in upland watersheds of central Nevada. *Geomorphology* 38: 373-391.

Montgomery, D.R. & Dietrich, W.E. 1994. A physically based model for the topographic control on shallow landsliding. *Water Resources Research* 30: 1153-1171.

Nanninga, P.M. & Wasson, R.J. 1985. Calculation of the volume of an alluvial fan. *Mathematical Geology* 17 (1): 53-65.

Quade, J., Mifflin, M.D., Pratt, W.L. & McCoy, W. 1995. Fossil spring deposits in the southern Great Basin and their implications for changes in water-table levels near Yucca Mountain, Nevada, during Quaternary time. *Geological Society of America Bulletin* 107: 213-230.

Schmidt, K.M., and McMackin, M., 2003, Quaternary Geology of the Mesquite Lake 1:100,000-scale quadrangle, California and Nevada: Abstracts with Programs, 2003 Geological Society of America Annual Meeting, v. 34, no. 7, p. 73.

Selby, M.J. 1993. *Hillslope materials and processes*. Oxford: Oxford University Press.

Chapter E

Reconnaissance studies of soils-geomorphic correlations and late Quaternary deformation of alluvial fan deposits east of the Avawatz Mountains, Mojave Desert, California

By Heather L. Green[1], Joanna L. Redwine[2], and David M. Miller

Abstract

This surficial geologic mapping project investigated suspected warping of alluvial fans extending east from the Avawatz Mountains, California. We identified a sequence of alluvial fans and used their characteristics to estimate the timing of deformation. We defined a chronosequence of three fan units based on soil development and surficial characteristics with estimated ages ranging from early Holocene to late Pleistocene. The sequence shows an expected progression of soil profile development indices with increasing relative age as established by inset relations and surficial characteristics. The oldest of these fans appears to have weak soil development compared to fans elsewhere in the Mojave region that share similar surface characteristics. It is unknown whether this reflects relatively rapid development of surface characteristics, locally slow soil-forming processes (e.g., dust influx), or natural variations in soil development.

The tectonic investigation focused on a zone of apparently uplifted and stranded Pleistocene fan units located ~4-5 km west of Highway 127. These deposits contain numerous fractures and several faults. Several scarps are also formed on the fan surfaces. The scarps, most fractures, and three thrust faults are subparallel to one another and collectively can be explained by deformation associated with a blind west-dipping thrust fault. The faulted deposits are located in an apparent transition zone between the Mormon Spring thrust fault to the north and the Soda-Avawatz dextral-slip fault to the south. If oblique slip observed in the north is partitioned among multiple structures to the south, a blind thrust fault on the Avawatz fan complex may represent the thrust component and the Soda-Avawatz fault the dextral component.

Introduction

The Avawatz Mountains are located within the Eastern California Shear Zone, a zone of faults extending from the San Andreas fault, crossing the Mojave Desert, and continuing north of the Garlock fault zone (Dokka and Travis, 1990; Miller and others, 2001) and east of the Sierra Nevada. The Garlock fault zone is a zone of left-lateral reverse-oblique slip that curves southward

[1]U.S. Geological Survey, 345 Middlefield Road, MS 977, Menlo Park, CA 94025
[2]U.S. Geological Survey, 345 Middlefield Road, MS 973, Menlo Park, CA 94025

along the eastern front of the Avawatz Mountains (Brady, 1984). Here it is termed the Mule Spring fault, whose southeast continuation is the Mormon Spring fault (Troxel and Butler, 1979). The study area is located ~2 km east of the Mormon Spring fault, which is a north-striking thrust fault (Brady, 1984; Spencer, 1981). Southwest of the study area, the Mormon Spring fault is called the Soda-Avawatz fault and is a dextral-slip fault that strikes 335º (Grose, 1959). The Avawatz Mountains is an impressive, high mountain range with steep northern- and eastern-facing mountain fronts bordered by active thrust faults (Brady, 1984). Below these fronts, steep alluvial fan complexes flank the range. The study area, herein known as the Avawatz fan complex, forms the eastern piedmont of the Avawatz Mountains and is ~30 km north of Baker on the west side of California Highway 127 (Fig. 1). The fan complex extends from its source in the Avawatz Mountains ~7 km to Salt Creek, which forms the Silurian Valley axis. At its toe, the fan complex is ~7 km wide. Alluvial deposits of mixed source lithology (mainly Mesozoic granitoids) and age comprise the fan complex.

This paper is divided into two main sections: one focuses on the soil development and surficial characteristics of a part of the Avawatz fan complex; the other focuses on local deformation of the fan complex.

Soil Development and Surficial Characteristics of the Avawatz fan complex: Preliminary Results

The purpose of this section is to describe surface characteristics and associated soil development for three widespread alluvial fan units of the Avawatz fan complex (Fig. 1). Our surficial mapping strategy follows methods developed by many previous workers (e.g., Christenson and Purcell, 1985; McFadden and others, 1989) and relies on use of relative dating techniques for correlating surficial units in the Avawatz fan complex to those in areas where chronosequences have been completed and, especially, where numerical ages have been obtained. In this part of the Mojave Desert, fan correlations primarily rely on the work of Wells and others (1985, 1987, 1995), Taylor (1986), McFadden and others (1989), Reheis and others (1989), Bull (1991), McDonald (1994), McDonald and others (1995), Slate and others (1999), and Mahan and others (this volume). Our intent was to provide soil-pit exposures and a calibration location for those interested in observing soil profiles, in combination with surficial characteristics, for some of the fan units discussed at other FOP stops.

Methods

Fan unit surfaces were distinguished based upon aerial photo interpretation and field reconnaissance using the mapping scheme and nomenclature (Fig. 2) described by Menges and Miller (Introduction, Table 1, this volume) primarily based on work described in Yount and others (1994) and Bedford (2003). Brief descriptions were made of surface characteristics (including physiography, sedimentology, geomorphology, and flora) (Table 1) at each location. Four soil pits were excavated and described for surficial deposits of three different relative ages (Fig. 2): Qia2, the oldest unit, site HL05AM377 (Table 2); Qya4C, the next younger deposit, with sites HL05AM378s and HL05AM378b (Tables 3 and 4) on an individual swale and bar feature, respectively; and Qya4B, site HL05AM381 (Table 5). We did not excavate a soil pit in a younger Qya4A deposit adjacent to Qya4B. Soil profiles were described using nomenclature of the Soil Survey Staff (1975) as modified by Birkeland (1999). Carbonate stage morphology was described using nomenclature introduced by Gile and others (1966) as modified by Machette (1985). Profile Development Index (PDI) values were calculated using the method developed by Harden (1982)

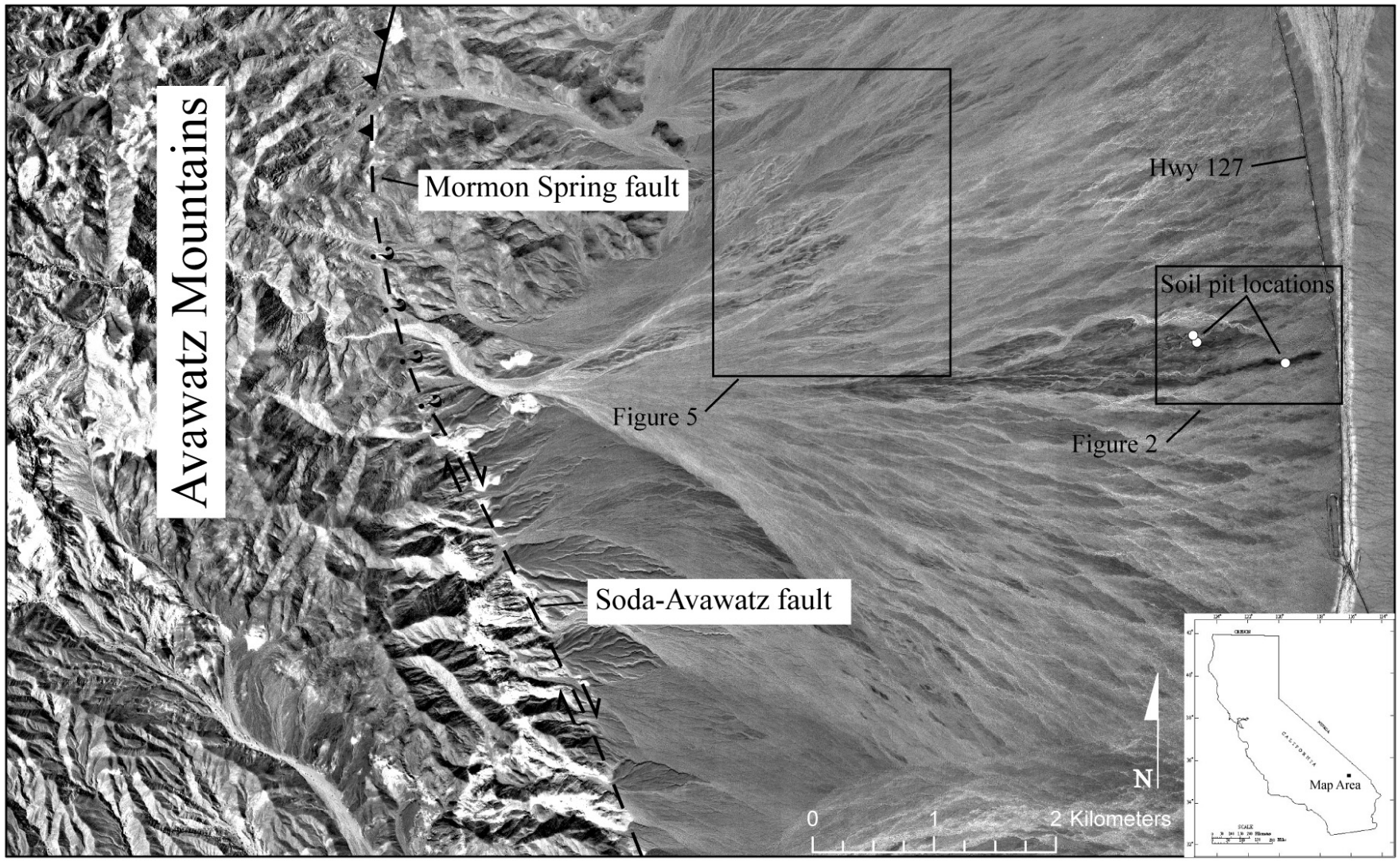

Figure 1. Image of digital orthophoto quadrangle of the Avawatz Fan Complex, located ~30 km north of Baker, California. Soil pit locations indicated by white circles within outline of Figure 2. Traces of Mormon Spring and Soda-Avawatz faults (Jennings, 1994) are approximate.

Table 1. Surface descriptions at soil pit locations on the Avawatz fan complex, Mojave Desert, California

Unit:	Qia	Qya4C	Qya4B
Station Information			
Station label	HL05AM377	HL05AM378(b&s)	HL05AM381
Altitude (m)	234	246	263
UTM-E, UTM-N	0575157, 3926121	0574547, 3926348	0574529, 3926370
Physiography			
General position	isolated deposit	along edge of Qia surface	inset in channel
Fan position	distal fan	medial-distal fan	medial-distal fan
Local drainage	yes	yes	yes
Surface drainage	no	low	low
Sedimentology			
Primary parent material lithologies	mafic plutonic, carbonate, felsic plutonic clasts	mafic plutonic, mafic volcanic, siliclastic rocks	mafic plutonic, mafic volcanic, siliclastic rocks
Clast size range (cm)	2-45	1-65	1-85
Sorting	poor	poor	poor
Rounding	sub-rounded to sub-angular	sub-rounded to sub-angular	sub-rounded to sub-angular
Geomorphology			
Pavement development	strong	incipient in swales	incipient in swales
Pavement compactness	strong	weak	weak
Pavement smoothness	strong	weak	weak
Interlocking clasts	strong	weak	weak
Microtopography development	no	yes	yes
Varnish development	moderate to strong	moderate	moderate
Eolian			
Activity	none	none	none
Coppice dunes	none	none	none
Flora			
% vegetation cover	<1	3	5
Pattern	none	in swales	none
Dominant species	creosote (*Larrea*)	creosote (*Larrea*)	creosote (*Larrea*)
Crown height (m)	0.5	0.75	1
Secondary species	none	bursage (*Ambrosia*)	bursage (*Ambrosia*)
Crown height (m)	n/a	0.3	0.25
Annuals	yes	yes	yes
% cover	20	15	10
Pattern	none	in swales, at plant drip line	in swales, at plant drip line

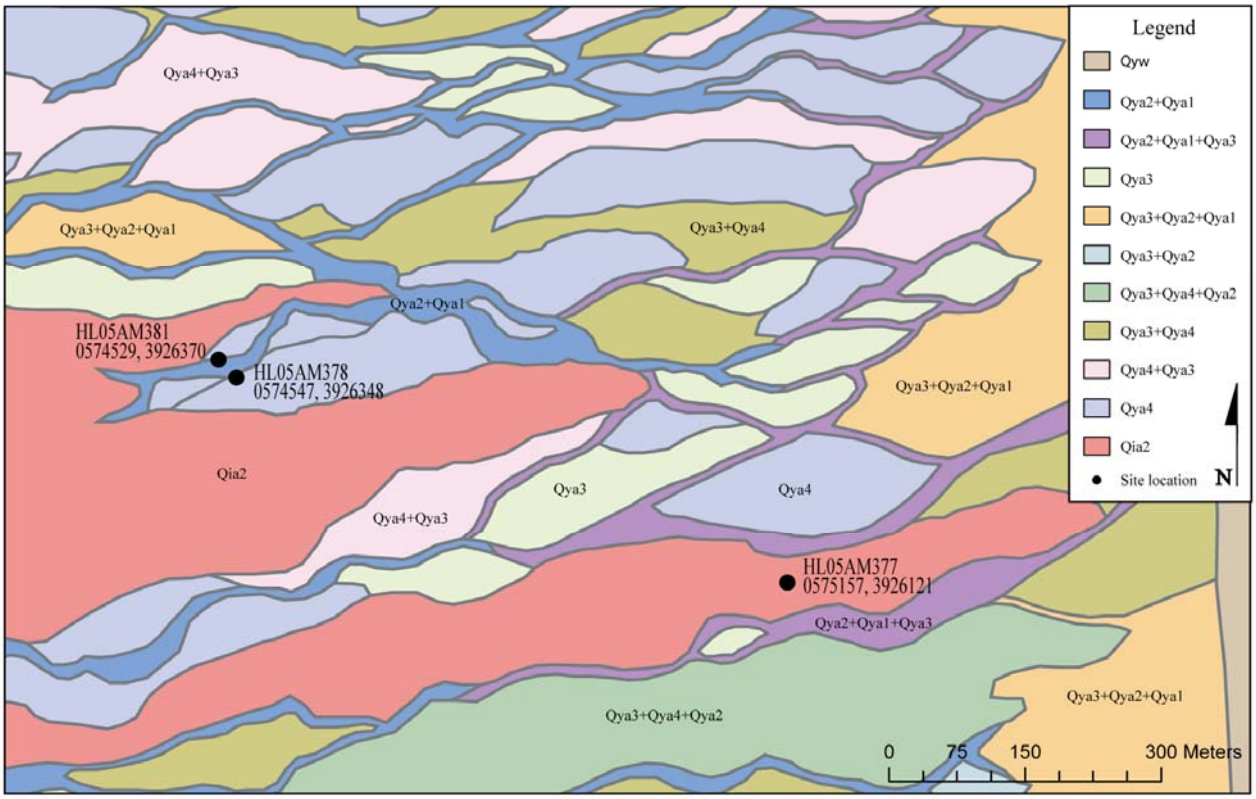

Figure 2. Surficial geologic map of a distal portion of the Avawatz fan complex (located in Fig. 1). Soil pit locations are marked in black with site number and GPS location (NAD 83). At least three levels of Qya4 surfaces are recognized in the field but are not differentiated on the map at this scale.

and Harden and Taylor (1983), as modified by Birkeland (1999) using nine properties: rubification, paling, lightening, texture, dry consistence, moist consistence, clay films, structure, and carbonate morphology (Table 6).

Results

The oldest unit studied is mapped as Qia2 and has well-developed desert pavement, strong varnish, a smooth surface with leveled pebble tops (Table 1; Fig. 3a), a dark-gray to black tone on black-and-white aerial photos, and local dissection ranging from 3-4 m near the fan head to 1-3 m in more distal fan areas. The soil developed into this unit at the reference site has an Av/Bwk/Bt soil profile with a maximum stage I+ carbonate morphology (Fig. 3b; Table 2). Although this deposit is mapped as a Qia2, it is herein referred to as Qia (undifferentiated) because relatively weak soil development suggests this deposit may be younger than most Qia2 surfaces. The normalized PDI value is 0.08 (Table 6).

The surfaces of the next younger fan unit (Qya4) have subdued bar-and-swale microtopography, incipient desert pavement development (mostly in swales), moderate desert varnish (Table 1; Fig. 4a), a medium- to dark-gray tone on black-and-white aerial photos, and local dissection ranging from 2-5 m near the fan heads to 0-1 m in distal fan areas. The Qya4 unit is undifferentiated on the map, but locally can be subdivided into younger and older sub units (Qya4B and Qya4C, respectively) based on relative inset geomorphic position and subtle differences in soil development. The soils developed into both Qya4B and Qya4C deposits have an Av/Bwk/C soil

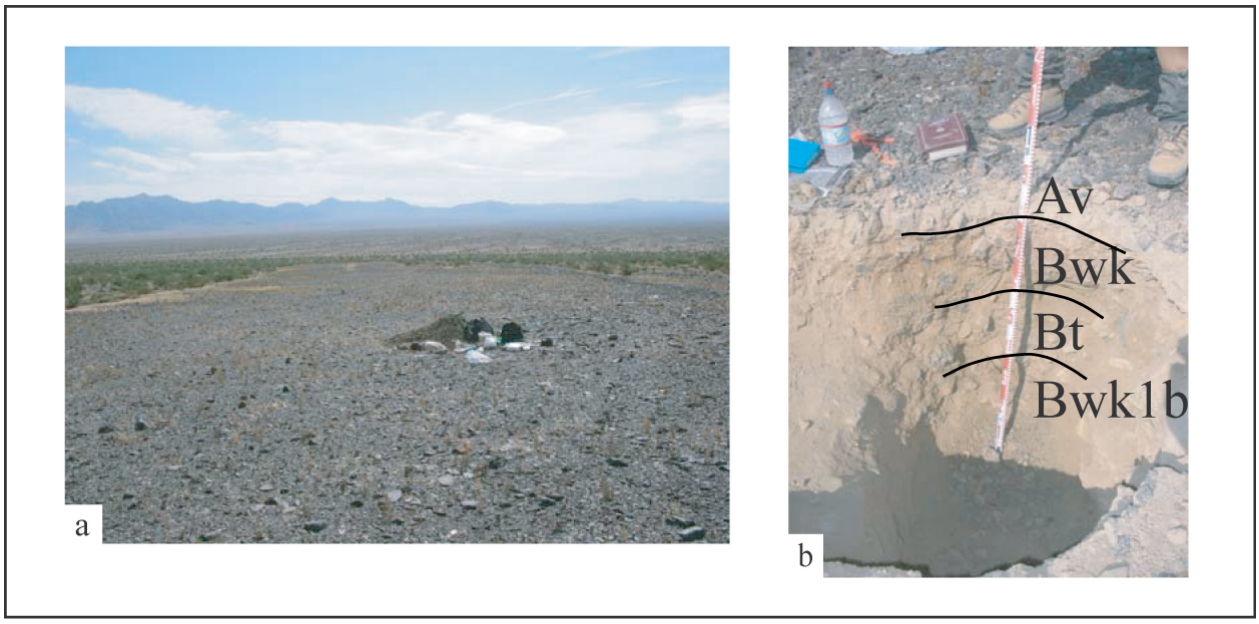

Figure 3. Photographs of (a) Qia surface and (b) associated soil. Note well-developed pavement and varnish.

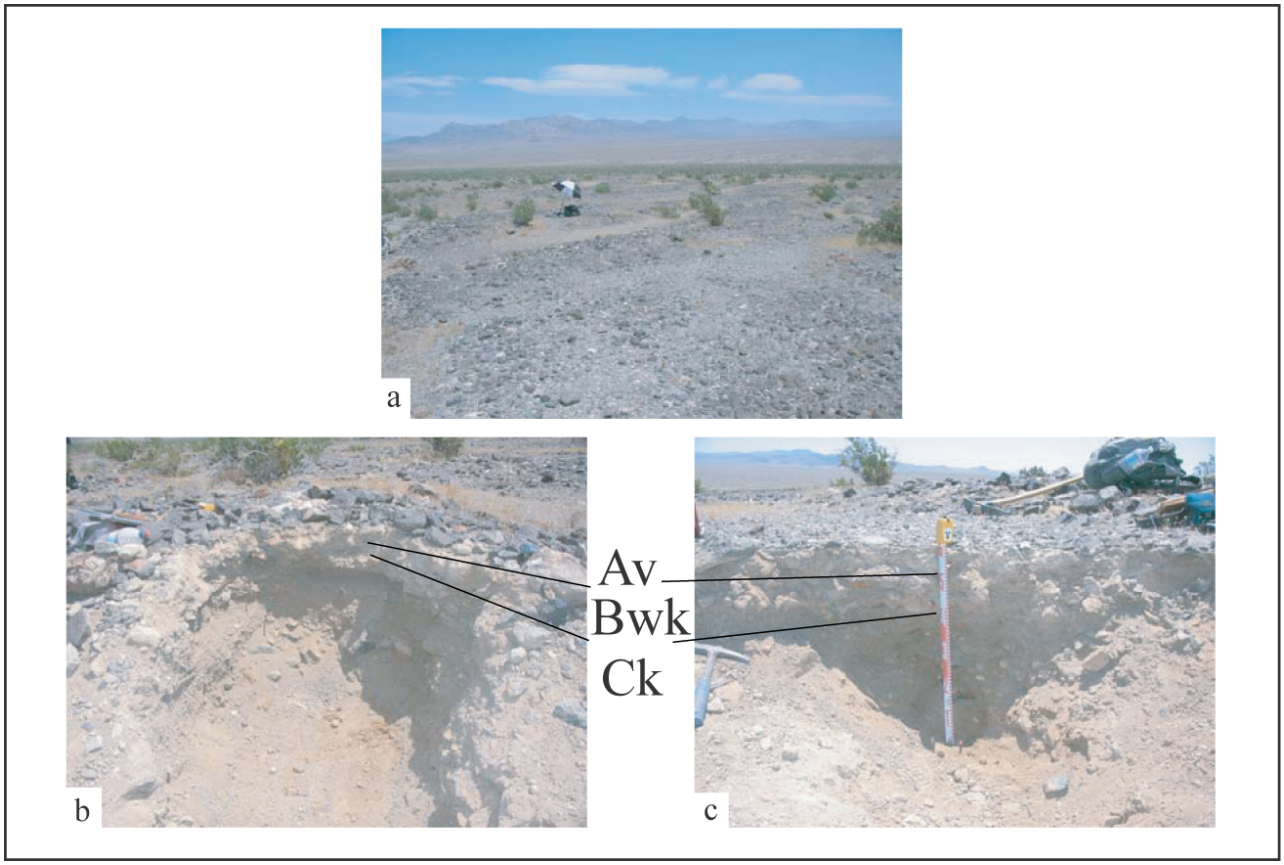

Figure 4. Photographs of (a) Qya4C surface and associated soils in (b) Qya4C bar and (c) Qya4C swale. Note remnant bar and swale topography, moderate varnish, and weak pavement development on surface.

profile and maximum stage I- carbonate morphology (Figs. 4b and c; Tables 3-5). These younger soils have reworked clasts from older deposits with stage I to I+ carbonate morphology. The normalized PDI values range from 0.06 to 0.05 (Table 6).

Discussion

Table 7 shows correlation of fan deposits examined in this study with deposits of nearby regions where detailed work has been completed. Comparison with the sites of Wells and others (1987), McFadden and others (1989) and Reheis and others (1989) from nearby Silver Lake proved the most useful because of their proximity to this study site. Correlations to other sites were based on the available published data that varied from full soil descriptions, to PDI values, to pedon descriptions with generalized genetic and diagnostic horizons. These are obvious limitations to these regional correlations related to local differences in key factors of soil formation (e.g., Jenny, 1941), such as parent material, dust influx, local climate, elevation, etc. In addition, the Avawatz chronosequence is a reconnaissance study that used only a few soil descriptions as a basis for correlations.

Despite the potential pitfalls in regional fan-deposit correlations, we find a consistent correlation between the Qya4 unit and other Holocene deposits, and most commonly with middle to late Holocene deposits (Table 7). These correlations are consistent with age estimates for Qya4 deposits in nearby areas based on several numerical ages for Qya4 deposits (Bedford, 2003; Mahan and others, this volume).

The Qia unit best correlates with late Pleistocene to early Holocene deposits in the region, although a few characteristics are more similar to deposits as old as middle to late Pleistocene. The weak carbonate development of the Avawatz Qia soil suggests a better correlation with the younger late Pleistocene to early Holocene surfaces. Bedford (2003) tentatively correlated his subdivided Qia unit, Qia1, to fans mapped by McDonald (1994) later dated at 22,000 to 90,000 years B.P. (McDonald and others, 2003), and his unit Qia2 to fans dated at 36,000 to 130,000 years B.P. (McDonald and others, 2003). Based partly on these correlations, work by Mahan and others (this volume) suggests that Qia units in the region include a range of deposits that span a fairly large age range of ~30,000 to 140,000 years old. The Qia unit studied on the Avawatz fan complex may represent a younger end member of these Qia deposits based on its apparently weak soil development, especially in terms of carbonate development.

There could be several reasons for the comparatively weak soil development associated with Qia deposits in the Avawatz area, relative to those elsewhere in the region:

1. There may be a slower rate of eolian $CaCO_3$ input at this site than is typical of soils in the region. This seems unlikely considering the nearby Silurian playa deposits, a likely dust source for these fans, has a $CaCO_3$ content of ~7.5-9% in the upper 1 m (Yount and Goldstein, 2005, written communication). However, this site is on the west side of Silurian playa, which is upwind during most winter storms and therefore may receive less dust from the playa than other locations.

2. Plutonic boulders and cobbles within the Qia surface have been weathered heavily by salts. The presence of salt could be responsible for retarding carbonate and clay accumulation within the profile as has been shown by Reheis (1984, 1987) and Harden and others (1991a). Analyses of some horizons within the soil profiles show there are significant concentrations of soluble salts and gypsum (Tables 2-5).

3. Another possibility is that it may be reasonable to consider one horizon (Bwk1b), originally interpreted in the field as part of a buried soil, to actually be part of the surficial deposit and soil. This is based on limited laboratory data (Table 2) which show a lessening of loi (loss on ignition, a proxy for organic matter content) and $CaCO_3$ percent down profile through the Bwk1b horizon and an increase of both materials in the underlying Bwk2b horizon, suggesting the possibility that the Bwk1b horizon is part of the surface soil. If the suggestion of the laboratory data is correct and the field interpretation was in error, the addition of this horizon increases the PDI value (Table 6). This larger PDI value is within the value of Qf1 fans of Wells and others (1987), McFadden and others (1989), and Reheis and others (1989) which may be as old as ~30,000 –50,000 years B.P., or at least older than the oldest shoreline of Lake Mojave which may be 16,000 years B.P. to 18,000 years B.P. (Wells and others, 2003). This additional B horizon thickness also more closely matches the soils correlations based on a qualitative comparison of soil properties, with the exception of carbonate stage morphology. However, the soil description and the remaining laboratory data seem to suggest the field interpretation was correct.

4. Another strong possibility demonstrated by many previous workers (e.g. Wood, 2000), is that this one soil pit is not representative of the soil development for this deposit, as there can be significant soil variation in a single aged surface. This is a likely scenario, especially because the logistical limitations of this FOP stop precluded the use of the best-suited sites to look at soil differences.

5. It is possible that because these are matrix-supported deposits (rather than coarser-grained deposits like those mapped as Qya4), the infiltration rates are lower and surface run-off rates are higher than Qya4 deposits. Miller and others (Chapter A, this volume) argue that fans on the northern side of the Avawatz Mountains (and sourced by rocks similar to the fan we studied) have retarded soils caused by this mechanism.

6. Alternatively, it is possible that this site could be showing us that the lumping of unit Qia based on surficial characteristics includes some units as young as latest Pleistocene to early Holocene.

Late Quaternary Deformation of the Avawatz fan complex

Methods

Surficial geologic mapping of the Avawatz fan complex revealed a zone of relatively high, isolated, and deeply-incised deposits. This zone is noticeable on aerial photos ~4-5 km west of California Highway 127 (Fig. 1). This zone is ~1.5 km wide and ~2 km long and trends ~330º. Exposures of the incised deposits in gully walls reveal numerous structures that suggest localized uplift across the zone. These structures were examined for information regarding timing, mechanism, and magnitude of deformation. Sites with potential tectonic significance were recorded with GPS, and individual features were measured, described, and photographed.

Results

The topographically high and deeply-incised deposits described above are remnants of Qoa, Qia3, and Qia2 fan deposits. Qoa deposits (Fig. 5) are preserved in balenas in an oval outcrop area,

and have well-rounded edges, have poorly preserved pavement, only a few strongly varnished clasts, and contain stage IV carbonate morphology. These deposits are deeply incised, up to ~6 m. Qia3 deposits, preserved in an elliptical area with long axis about 330, have slightly rounded edges, less preserved pavement than Qia2 deposits, and strong varnish. These deposits are moderately to deeply incised, ~5 m. Qia2 deposits are flat and smooth with well-developed pavement and strong varnish. These deposits are moderately incised, ~3-4 m decreasing to ~1-3 m in the distal end of the fan. The oldest preserved inset terraces are Qya4 in age.

Five faults and forty-two fractures were observed and measured in the study area (Fig. 5). A set of three thrust faults (site HL05AM367, Fig. 5) is depicted in Figure 6. All three faults are expressed in the gully wall but not at the surface. The deposit has soils characteristic of Qoa deposits. One fault, oriented 330º, 16º NE, offsets a fracture ~43 cm. The second fault, oriented 350º, 20º NE, offsets a fracture ~5 cm (Fig. 6, c). The third fault, oriented 315º, 12º NE, offsets a fracture ~12 cm. Two other planar discontinuities in this area are possibly faults. One fault, with an orientation of 330º, 42º SW (site HL05AM180, Fig. 5) appears to be a thrust fault, although definitive sense of offset could not be determined. The second (site HL05AM194, Fig. 5) is oriented 045º, 81º NW and has an apparent normal separation (northwest side down) of ~20 cm of a buried deposit beneath a Qia3 deposit. On a stereoplot of the poles to planes of faults, the set of thrust faults at site HL05AM367 cluster, illustrating their similar orientation and kinematic relations (Fig. 7a). The relation of the remaining faults to other structures in the area is not understood, which may be due to the few data points available for comparison. The normal fault at HL05AM194 has a northeast strike, almost perpendicular to the other faults. Several fracture orientations also show a northeast strike. The dip direction of the apparent thrust fault at HL05AM180 (Fig. 7) is opposite to the clustered northeast-dipping thrust faults but the strikes of all four faults are similar and similar to most fracture orientations discussed below.

Loose overlying material and rounded edges of gully walls made identification of many fractures difficult, and at most sites, they were only located on one side of gully. At site HL05AM186 (Fig. 5), calcium-carbonate-filled fractures, oriented 305º, 66º NE, were traceable from one wall through the gully floor and into the opposite wall. This was the sole instance of an indisputable relation between fractures in adjacent gully walls. The fractures in Figure 6 (site HL05AM367) exemplify fracture appearances in the study area. This site also contains the set of faults (discussed above) that are not present at other sites. Fracture spacing ranges from tens of centimeters to 100 or more meters; four meters is the average spacing. Most of the fractures are calcium-carbonate filled, with zones of calcium-carbonate up to 15 cm thick. Detectable offset along fractures could be determined in only one location (HL05AM149, Fig. 5). This fracture, oriented 310º, 72º NE, contained a pebble in the fracture plane that was used as a piercing point to establish ~4 mm reverse and ~6 mm right-lateral offset. A stereoplot of poles to fracture planes (at all sites) shows clustering of poles, which indicates a preferred orientation with a northwest strike and steep northeast dip (Fig. 7b). The average orientation, as determined by a conical best-fit plane, is 330º, 74º NE

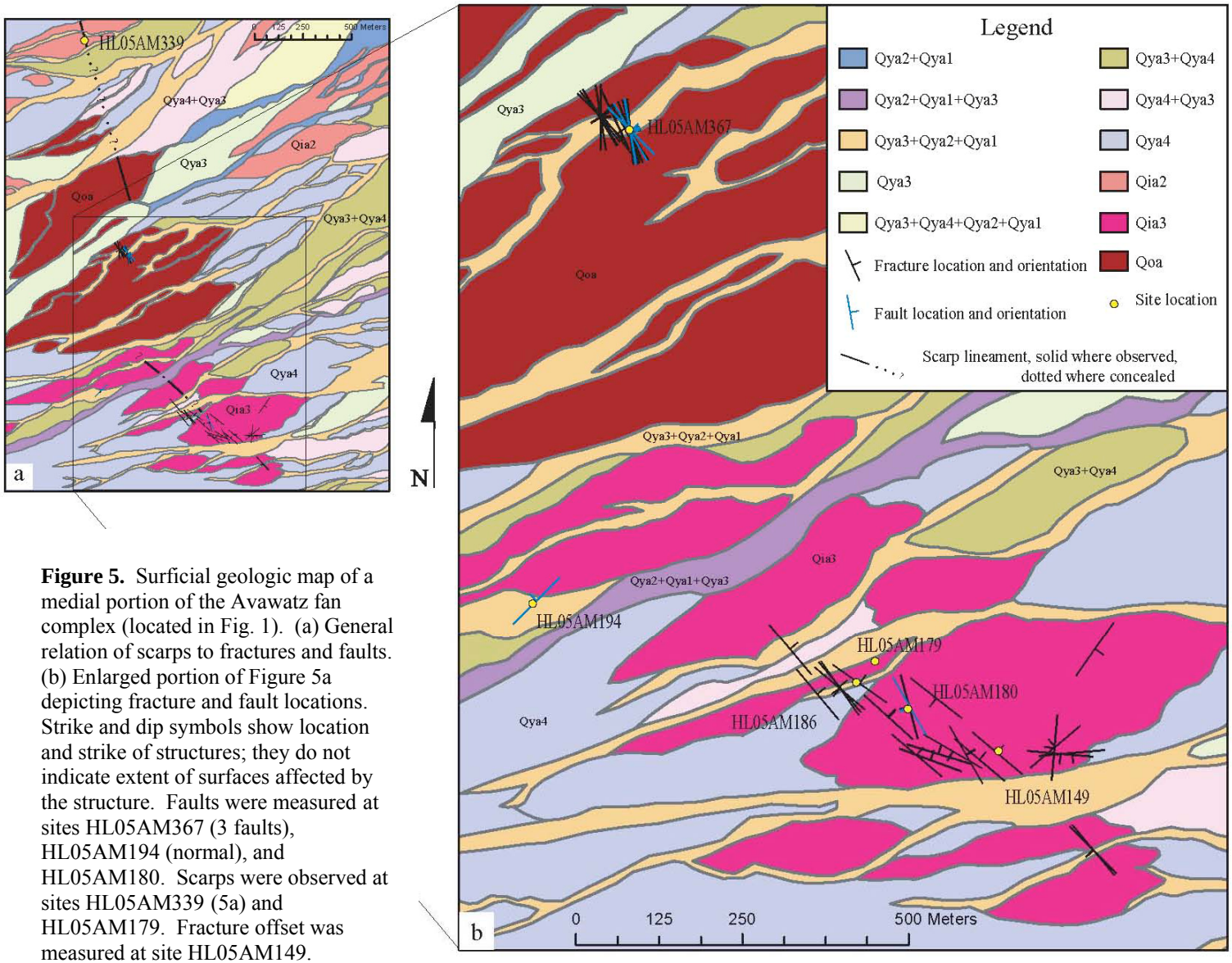

Figure 5. Surficial geologic map of a medial portion of the Avawatz fan complex (located in Fig. 1). (a) General relation of scarps to fractures and faults. (b) Enlarged portion of Figure 5a depicting fracture and fault locations. Strike and dip symbols show location and strike of structures; they do not indicate extent of surfaces affected by the structure. Faults were measured at sites HL05AM367 (3 faults), HL05AM194 (normal), and HL05AM180. Scarps were observed at sites HL05AM339 (5a) and HL05AM179. Fracture offset was measured at site HL05AM149. Fractures were observed in gully walls and floor at site HL05AM186.

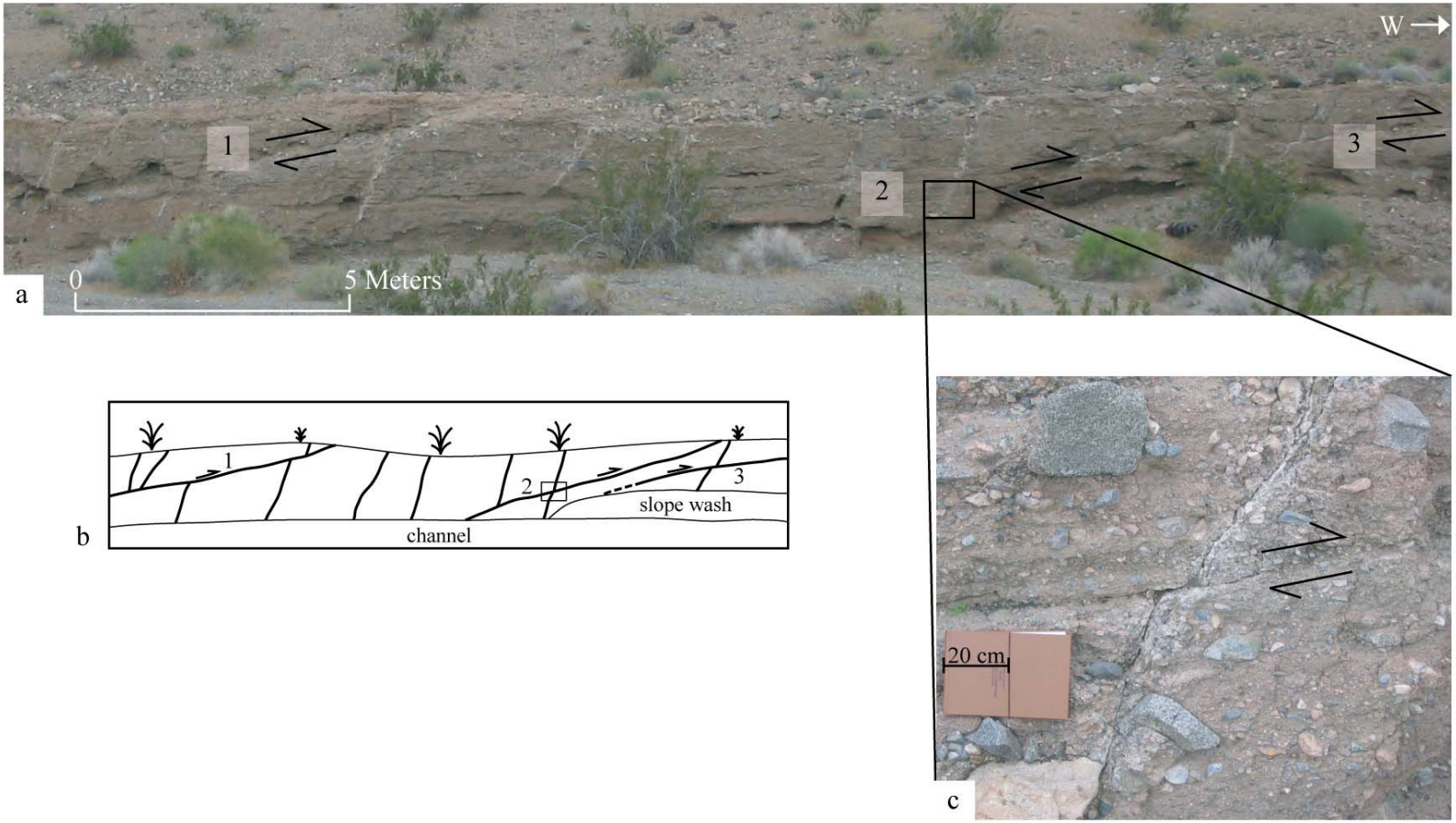

Figure 6. (a) Photographs of a segment of a gully wall with exposed fractures and parts of faults at HL05AM367 looking south (Fig. 2). One fault enters photo from left (1). The second fault is in right-center of photo, shown in its entirety (2). The third fault exits photo at right (3). Fractures are filled with calcium carbonate, whereas faults exhibit minor pits and caverns. (b) Line drawing of photo illustrating fractures and faults. (c) Middle of three faults displays 5 cm of reverse separation of a fracture. Field notebook for scale.

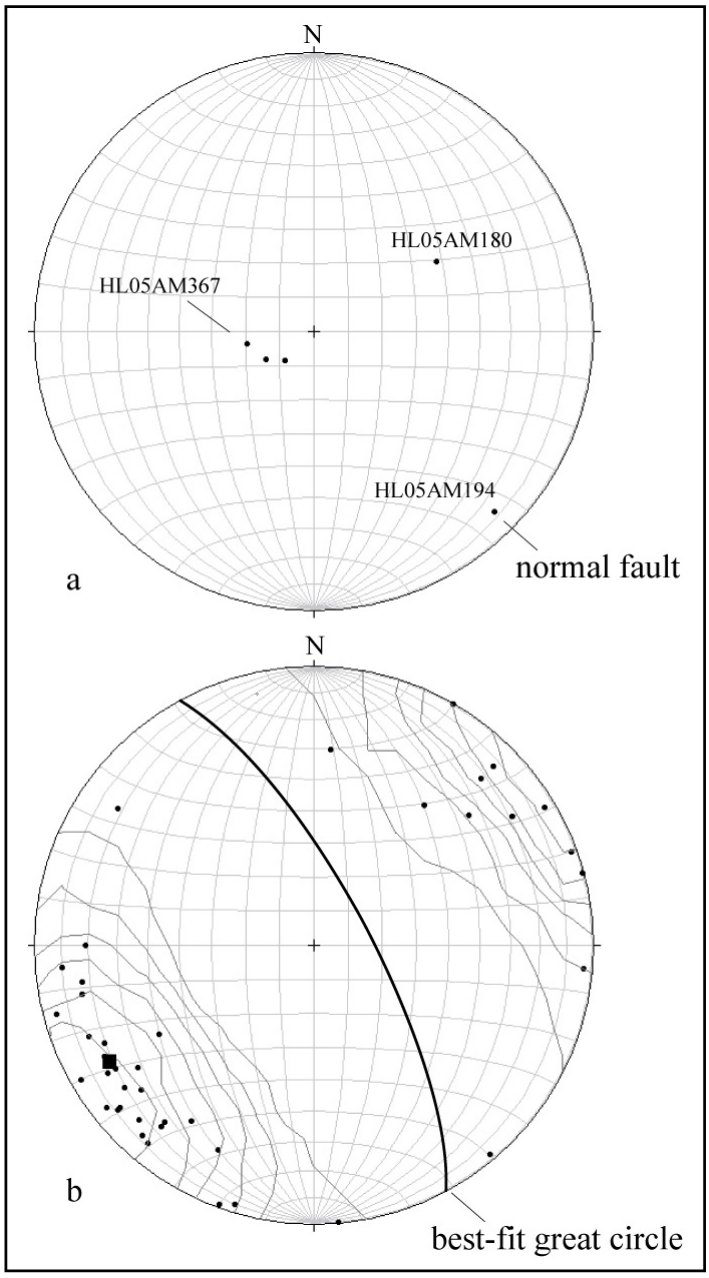

Figure 7. Equal-area, lower hemisphere stereonet plots of poles to fault and fracture planes in the Avawatz fan complex. (a) Poles to fault planes (n=5). Cluster of three poles near center represents those at site HL05AM367 (Fig. 5). Note that HL05AM194 is a normal fault, and others are thrust faults. (b) Kamb contour (interval=2) of poles to fracture planes (n=42). Conical best-fit great circle and pole to great circle (square) indicate an average fracture orientation of 330º, 74º NE for all fracture sites.

Lineaments consisting of aligned saddles and scarps further suggest deformation of the Avawatz fan complex (Fig. 5). A ~345°-trending, northeast-facing scarp is expressed on the Qia2 surface at site HL05AM339. The scarp is ~2 m high, perpendicular to the fan slope, and projects to a scarp on an adjacent Qia2 surface to the north and to a subtle saddle in a Qoa surface to the south (Fig. 5a). A second ~310º-trending lineament is defined by a subtle saddle in a Qia3 deposit (site HL05AM179) that projects to subtle saddles in two adjacent Qia3 deposits immediately to the north (Fig. 5a). Although there is no unequivocal evidence that these two lineaments are tectonic in origin, the similarity of their orientations with smaller-scale faults nearby (Figs. 5b and 7), and the lack of plausible alternative hypotheses for the origin of the scarps support this structural interpretation.

Discussion

One possible model to explain the geomorphic and structural relations of the deformed fan deposits is a west-dipping blind thrust fault (Fig. 8). This model is consistent with surface deformation/uplift that appears to be distributed broadly in the form of a northwest-oriented tectonic bulge. The numerous subparallel fractures may have formed in response to bending-moment tension in the bulge. The east-dipping thrust fault may represent faults that are antithetic to the main, concealed thrust fault. The fractures may have occurred in response to initial warping above the blind thrust fault and the antithetic thrust faults may have occurred with continued slip along the blind thrust fault as it propagated toward the surface. The normal fault, which is nearly perpendicular to all other structures, is not easily accommodated within the blind thrust model, but it could represent local extension in response to differential hanging wall deformation (i.e., local uplift).

Timing of deformation can be inferred based on cross-cutting relations. In one area (at HL05AM367), the uppermost beds exposed in unit Qoa (early to middle Pleistocene age), are not obviously cut by faults lower in the deposit. Thus, some fault offsets occurred prior to latest Qoa deposition. Elsewhere, Qoa deposits exhibit scarps and lineaments that extend into middle to late Pleistocene Qia3 and Qia2 deposits. However, Qya4 deposits, the oldest preserved units inset within channels incised into Qia3 and Qia2 surfaces, are not deformed in any exposures we studied. Thus, much or most of the incision into older surfaces appears to be latest Pleistocene. The youngest deformation is constrained to post Qia2 deposition and prior to Qya4 deposition. Lack of deformation of Qya4 or younger deposits suggests deformation has not been active in the Holocene, but it is also possible that deformation has occurred in the Holocene and the evidence is not preserved in the younger deposits we inspected.

The faults that bound the northern and eastern escarpments of the Avawatz Mountains are complex. West of its intersection with the Death Valley fault zone, the Mule Spring fault forms the northern branch of the Garlock fault and is characterized by left-lateral reverse-oblique slip (Brady, 1984) (Fig. 9). To the east, the Mule Spring fault curves southward along the Avawatz Mountains range-front and is dominantly a reverse-slip fault (Brady, 1984; Mendonca, Chapter G, this volume). The southeast continuation of the Mule Spring fault, which is considered by Troxel and Butler (1979) to be the Mormon Spring fault, is located ~2 km west of the deformed fan units examined in this study (Spencer, 1981). The Mormon Spring fault is mapped as a thrust fault that strikes ~N-S and dips 39º W (Spencer, 1981)(Fig.1). Southward from the Avawatz Mountains, the Mormon Spring fault is termed the Soda-Avawatz fault and is considered to be a dextral-slip fault that strikes 335º (Grose, 1959). It is possible that the deformation in the Avawatz fan complex examined by this study plays a role in the transition from thrust to dextral fault style (Fig. 10).

Two proposed models for the thrust to dextral transition are: 1) eastward translation of the Avawatz block in the north adds a component of east-west shortening not present in the south; and, 2) complex oblique slip in the north is partitioned into separate thrust and dextral faults in the south. In the case of model 1, a bend in the fault and distinct change in geomorphology would be expected, neither of which is clearly present. In the case of model 2, the deformation of the Avawatz fan complex examined in this study could represent the thrust component and the Soda-Avawatz fault the dextral component. Further work at this site is needed to understand the relation of the smaller features examined by this study to the larger scale structures in the region.

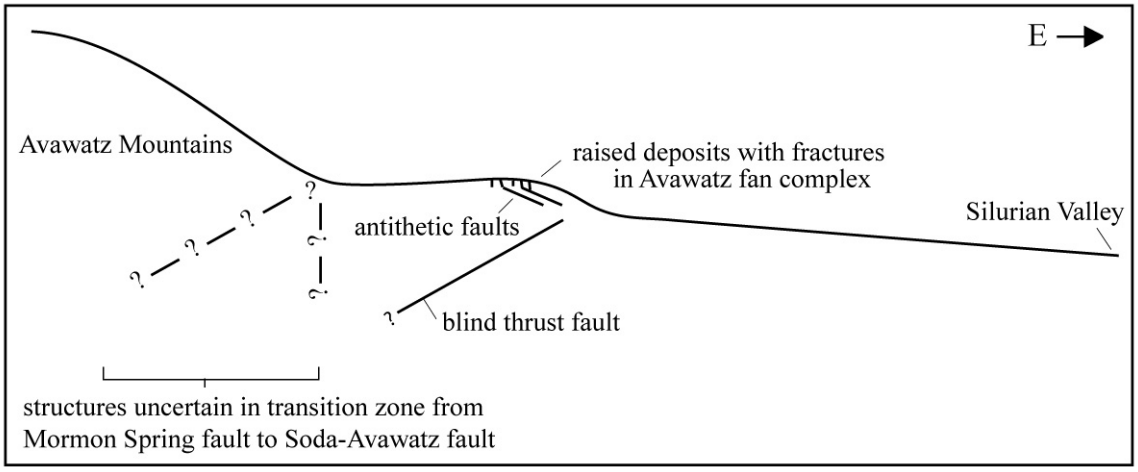

Figure 8. Schematic cross-section of one possible model of the relation of the structures at the east front of the Avawatz Mountains to those in the Avawatz fan complex, where movement along a blind thrust fault is causing the surface to deform. Extension in the hanging wall is producing fractures. The thrust faults observed at site HL05AM367 are interpreted as antithetic faults in the model.

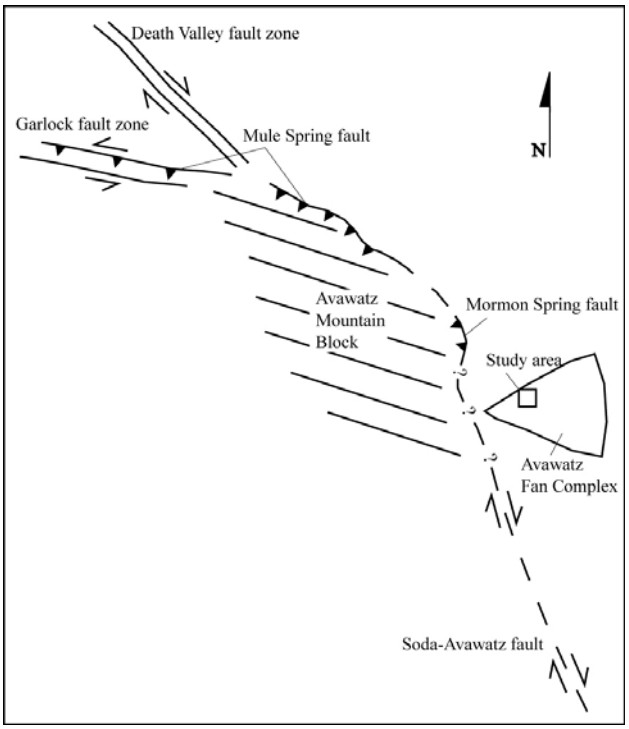

Figure 9. Relation of regional structures to the Avawatz fan complex. Note the Avawatz fan complex is located in an area where the relation of regional structures is uncertain. Thrust faulting dominates northwest of the fan complex, and dextral faulting dominates to the southwest. Modified from Jennings, 1994.

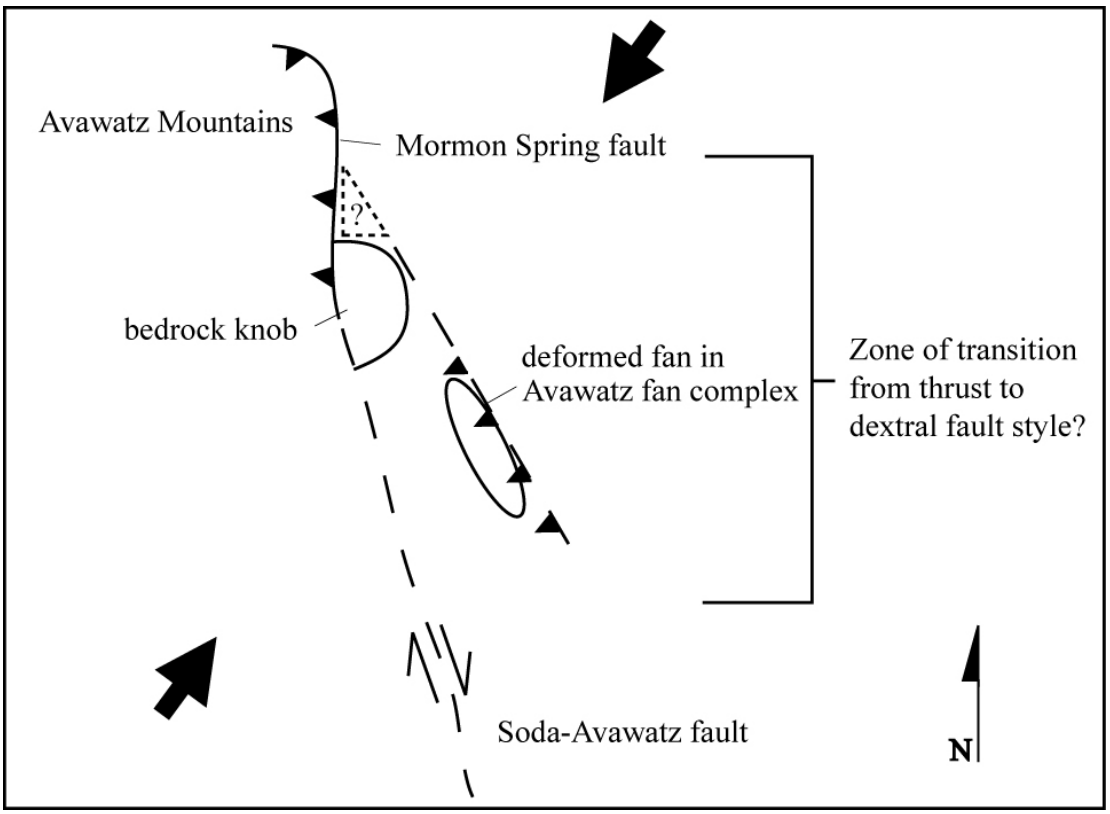

Figure 10. Map view of a model showing the Avawatz fan complex in a zone of transition from thrust to dextral fault style. Principle stress directions shown as large, solid arrows.

Table 2. Soil Description of Unit Qia

General Information:

Location	Avawatz fan complex	parent materials	eolian/alluvial fan/alluvial fan
site no.	HL05AM377	geomorphic surface	alluvial fan- Qia
date	5/29/05	described by	Redwine
time	6:30 AM	notes by	Green

[a]Field Description

[b]HSL#	Depth (cm)	Horizon	color		structure	gravel visual %	consistence			texture	B	CF	pores	roots	notes
			moist	dry			wet	moist	dry						
05-158	0-7	Av	2.5Y 5/3 silt coats 2.5Y 7/3 matrix	10YR 4/4 silt coats 10YR 6/3 matrix	3vcsbk	<10	svp	fi	vh	L	cw	nil	1 vf, f, m 1 c	1vf	silt skins, contains windblown sand within cracks of structure
05-159	7-17	Bwk	10YR 4/4	10YR 6/4	2csbk	25	sps	vfr	h	SL	cw	v1vfpfpo	2 vf, f, 1 m	1 vf	silt skins, contains windblown sand within cracks of structure
05-160	17-26	Bty	10YR 4/4 7.5YR 5/6 oxidation	10YR 5/4 10YR 6/4 oxidation	2msbk-25% sg-75%	65	sspo	vfr	h	SCL	cw	nil	nil	nil	salt present? patches of red and green colors
05-161	26-55	Bwk1b	2.5Y 3/3	2.5Y 5/4	1fsbk	75	sspo	vfr	h	SL	gw	nil	2 vf	nil	
05-162	55-65	Bwk2b	2.5Y 3/3	2.5Y 6/4	2fsbk	75	sps	vfr	so	SL	cw	nil	1 vf, f, m 1 c	nil	abundant shot mafics
05-163	65-85	Ckyb	2.5Y 3/3	2.5Y 5/4	sg	50-75	sopo	lo	lo	SL	as	nil	nil	nil	
05-164	85-90+	Btkb'	7.5Y 4/4	7.5Y 5.5/4	2fsbk	10	ssps	fr	h	SL	na	3vfpf	2 vf, m 1 f	nil	

Table 2. Soil Description of Unit Qia—Continued

						[h]Laboratory Data									
HSL#	Depth (cm)	Horizon	[c]Eff.	$CaCO_3$ stage	silica stage	gravel weight %	[d]loi	[e]sol. salts %	[f]gypsum %	clay %	silt %	sand %	MF	$CaCO_3$ %	weight loss %
05-158	0-7	Av	EV	nil	nil	24	2.0	[g]ND	ND	24	47	28	0.98	11.5	2.3
05-159	7-17	Bwk	EV	nil	nil	32	1.2	ND	ND	19	28	53	0.98	8.3	1.1
05-160	17-26	Bty	ES 45% EV 55% spotty	I+, filaments in places	nil	36	1.2	0.69	0.64	24	22	54	0.99	2.6	0.3
05-161	26-55	Bwk1b	EV	I-	nil	49	0.8	ND	ND	11	27	62	0.99	1.7	1.9
05-162	55-65	Bwk2b	EV	I	nil	49	1.4	ND	ND	9	27	65	0.99	6.1	0.8
05-163	65-85	Ckyb	EV	I, not on all stones	nil	42	1.1	0.96	0.01	8	28	64	0.99	4.4	2.1
05-164	85-90+	Btkb'	EV	I-, few filaments	nil	27	2.1	ND	ND	11	22	68	0.99	8.9	1.2

[a]USDA Soil Survey nomenclature (1993) as modfied by Birkeland (1999) and stages after Machette (1985) and (Reheis, 1987). [b] Humboldt State University Soils Laboratory #. [c] Degree of effervescence, EV-violently, ES-slightly. [d] loss on ignition. [e] % Soluble salts. [f] % gypsum. [e and f] Work done at the USGS, sediment laboratory in Golden CO. [g] No Data. [h] Bulk density.

Table 3. Soil Description of Unit Qya4C-swale

General Information:

Location	Avawatz fan complex	parent materials	eolian/alluvial fan
site no.	HL05AM378s-swale	geomorphic surface	alluvial fan- Qya4 / Qia (?)
date	5/30/05	described by	Redwine
time	12:30 PM	notes by	Green

[a]Field Description

[b]HSL#	Depth (cm)	Horizon	color		structure	gravel	consistence			texture	B	CF	pores	roots	notes
			moist	dry		visual %	wet	moist	dry						
05-174	0-7	Av	10YR 5/3	10YR 7/2	3vcpl to 2csbkk	<10	sp	fr	h	L	cw	nil	2vf, f, m	v1vf	
05-175	7-16	Bwk	10YR 4/4	10YR 6/4	2msbk	25	sps	vfr	h	SL	gw	nil	2vf, f	v1vf	
05-176	16-42	Ck(z?)	10YR 4/4	10YR 5/4	sg	50-75	sopo	lo	lo	S	cs	nil	nil	nil	salt I--
05-177	42-58	Ckz	10YR 4/4	10YR 5/4	sg	75	sopo	lo	lo	S	aw	nil	nil	nil	salt I-
[e]ND	58+	Btb	10YR 4/4	10YR 5/4	ND	ND	ND	ND	ND	ND	ND	2ppf	ND	ND	

[h]Laboratory Data

HSL#	Depth (cm)	Horizon	[c]Eff.	$CaCO_3$ stage	silica stage	gravel weight %	[d]loi	[e]sol. salts %	[f]gypsum %	clay %	silt %	sand %	MF	$CaCO_3$ %	weight loss %
05-174	0-7	Av	EV	nil	nil	18	1.7	[g]ND	ND	23	41	35	0.99	11.4	3.7
05-175	7-16	Bwk	EV	nil	nil	38	1.7	ND	ND	15	29	57	0.99	4.9	1.6
05-176	16-42	Ck(z?)	EV	nil	nil	62	0.7	ND	ND	5	6	89	1.00	4.9	0.5
05-177	42-58	Ckz	ES	I-	I-	63	0.7	0.61	0.68	6	6	88	0.99	4.9	0.3
05-169	58+	Btb	ND	ND	ND	80	1.5	ND	ND	15	20	64	0.99	7.0	1.68

[a]USDA Soil Survey nomenclature (1993) as modfied by Birkeland (1999) and stages after Machette (1985) and (Reheis, 1987). [b] Humboldt State University Soils Laboratory #. [c] Degree of effervescence. [d] loss on ignition. [e] % Soluble salts. [f] % gypsum. [e and f] Work done at the USGS, sediment laboratory in Golden CO. [g] No Data.

Table 4. Soil Description of Unit Qya4C-bar

General Information:			
Location	Avawatz fan complex	parent materials	eolian/alluvial fan
site no.	HL05AM378b-bar	geomorphic surface	alluvial fan- Qya4C / Qia (?)
date	5/29/05	described by	Redwine
time	1:45 PM	notes by	Green

[a]Field Description

[b]HSL#	Depth (cm)	Horizon	color		structure	gravel visual %	consistence			texture	B	CF	pores	roots	notes
			moist	dry			wet	moist	dry						
05-165	0-5	Av	10YR 5/4	10YR 7/4	2msbk	<10	sp	fr	h	L	aw	nil	2vf, f, 1 m	1 vf	
05-166	5-9	Bwk	10YR 5/4	10YR 7/4	sg	50	sopo	lo	lo	LS	cb	nil	nil	1 vf	Structure is sometimes v1sbk, it is discontinuous, but traceable to Qya4-swale. Different than the C horizon based on color.
05-167	9-35	Ck	10YR 5/4	10YR 6/4	sg	65	sopo	lo	lo	S	cs	nil	nil	nil	ES in certain stratigraphy. Eolian silt infiltration. Reworked $CaCO_3$ coatings.
05-168	35-76	Ckz	10YR 4/3	10YR 6/4	sg	75	sopo	lo	lo	S	aw	nil	nil	nil	Gypsum? Clast supported deposit.
05-169	76+	Btb	10YR 4/4	10YR 5/4	ND	ND	ND	ND	ND	SL	ND	2ppf	ND	ND	

[h]Laboratory Data

HSL#	Depth (cm)	Horizon	[c]Eff.	$CaCO_3$ stage	silica stage	gravel weight %	[d]loi	[e]sol. salts %	[f]gypsum %	clay %	silt %	sand %	MF	$CaCO_3$ %	weight loss %
05-165	0-5	Av	EV	nil	nil	45	1.8	[g]ND	ND	20	28	51	0.99	5.3	1.77
05-166	5-9	Bwk	EV	nil	nil	51	0.6	ND	ND	6	13	81	1.00	7.8	1.39
05-167	9-35	Ck	nil, spotty ES	I+	nil	40	0.4	ND	ND	4	4	93	1.00	4.0	0.16
05-168	35-76	Ckz	nil	I-	I-	43	0.3	0.03	0.00	3	4	93	1.00	5.5	-0.63
05-169	76+	Btb	ND	ND	ND	80	1.5	ND	ND	15	20	64	0.99	7.0	1.68

[a]USDA Soil Survey nomenclature (1993) as modfied by Birkeland (1999) and stages after Machette (1985) and (Reheis, 1987). [b] Humboldt State University Soils Laboratory #. [c] Degree of effervescence. [d] loss on ignition. [e] % Soluble salts. [f] % gypsum. [e and f] Work done at the USGS, sediment laboratory in Golden CO. [g] No Data.

Table 5. Soil Description of Unit Qya4B-inset surface

General Information:

Location	Avawatz fan complex		parent materials	eolian/alluvial fan	
site no.	HL05AM381		geomorphic surface	alluvial fan- Qya4B	fan inset into channel
date	5/30/05		described by	Redwine	
time	11:30 AM		notes by	Green	

[a]Field Description

[b]HSL#	Depth (cm)	Horizon	color moist	color dry	structure	gravel visual %	consistence wet	consistence moist	consistence dry	texture	B	CF	pores	roots	notes
05-170	0-2	Av	10YR 5/4	2.5YR-10YR 7/3	2mpl to 2msbk	<10	sps	fr	h	LS	ai	nil	2vf, f, 1 m	1vf	
05-171	2-8	Bwk	10YR 4/4	10YR 6/4	v1vfsbk	<10	sopo	vfr	so	SL	cb	nil	v1 vf, f	2 vf	oxidized, reddish
05-172	8-36	Ck	10YR 4/3	10YR 6/3	sg	>85	sopo	lo	lo	LS	cs	nil	nil	2 vf	more silt than underlying horizon
05-173	36-65	Ckzy	10YR 4/4	10YR 6/4	sg	>85	sopo	lo	lo	S	cs	nil	nil	v1 f	salt?
	65+	Bb	ND	ND	ND	ND	ND	ND	ND	ND	ND	ND	ND	ND	

[h]Laboratory Data

HSL#	Depth (cm)	Horizon	[c]Eff.	$CaCO_3$ stage	silica stage	gravel weight %	[d]loi	[e]sol. salts %	[f]gypsum %	clay %	silt %	sand %	MF	$CaCO_3$ %	weight loss %
05-170	0-2	Av	EV	nil	nil	16	1.6	[g]ND	ND	17	41	42	0.986	7.3	0.08
05-171	2-8	Bwk	EV	nil	nil	12	1.2	ND	ND	12	20	68	0.994	4.4	0.76
05-172	8-36	Ck	EV	I--	I--	77	0.6	ND	ND	4	10	86	0.997	5.7	-0.10
05-173	36-65	Ckzy	ES, EV in pockets	I-	I-	71	0.5	0.02	0.01	4	6	91	0.998	4.3	0.55
	65+	Bb	ND	ND	ND	ND	ND	ND	ND	ND	ND	ND	ND	ND	ND

[a]USDA Soil Survey nomenclature (1993) as modfied by Birkeland (1999) and stages after Machette (1985) and (Reheis, 1987). [b] Humboldt State University Soils Laboratory #. [c] Degree of effervescence. [d] loss on ignition. [e] % Soluble salts. [f] % gypsum. [e and f] Work done at the USGS, sediment laboratory in Golden CO. [g] No Data.

Table 6. Profile Development Index values for soils on the Avawatz fan complex

Unit	Site	[a]PDI		
		Sum	Normalized by profile thickness	Normalized by thickest profile in the chronosequence
Qia	HL05AM377	6.11	0.24	0.08
Qia, with extra B horizon	HL05AM377	11.83	0.22	0.16
Qya4-swale	HL05AM378s	4.59	0.08	0.06
Qya4-bar	HL05AM378b	4.38	0.06	0.06
Qya4-inset	HL05AM381	3.62	0.06	0.05

[a] Profile Development Index (PDI) values were calculated using the method developed by Harden, (1982), Harden and Taylor (1983), as modified by Birkeland (1999).

Table 7. Correlation of Avawatz fan soils and surface characteristics with other soil and alluvial fan studies in the region

Our Unit	Qia-HL05AM377		Qya4-bar-HL05AM378b		Qya4-swale-HL05AM378s		Qya4-inset-HL05AM381		Correlated age based on soils	Correlated age based on surficial characteristics	Correlated age based on soils	Correlated age based on surficial characteristics	NOTES:
correlation using: Reference:	soils	surf. char.	soils	surf. char.	soils	surf. char.	soils	surf. char.	Qia	Qia	Qya4	Qya4	
Yount and others (1994)	[a]Qia1	Qia1	Qya2	Qya3	Qya2 to Qya3	Qya3	Qya2 to Qya3	Qya3	20ky - 180ky (Qia1)	20ky - 180ky (Qia1)	<1kyr (Qya2) to mid to late Holocene (Qya3)	mid to late Holocene (Qya3)	Avawatz Qia fit the weakest descriptions of soils of Yount and others Qia, barely, but better than the Qya3 descriptions.
Bedford (2003)	Qya4-Qia1	Qya4-Qia1	Qya3	Qya4	Qya4	Qya4	Qya4	Qya4	~9kyr to 14kyr (Qya4) - ~20kyr to 35kyr (Qia1)	~9kyr to 14kyr (Qya4) - ~20kyr to 35kyr (Qia1)	~9kyr to 14kyr (Qya4)	~9kyr to 14kyr (Qya4)	Soils are on the weakest side of the decriptions.
Wells and others (1987)	[b]*Qf2 to Qf1	Qf3 to *Qf2	*Qf4 to Qf3	Qf4	*Qf3 to Qf2	Qf4	*Qf3 to Qf2	Qf4	*early Holocene to late Pleistocene (Qf2) - late Pleistocene (Qf1)	early to mid Holocene (Qf3) to *early Holocene to late Pleistocene (Qf2)	*early to mid Holocene (Qf3) to mid to late Holocene (Qf4)	mid to late Holocene (Qf4)	Avawatz soils have less carbonate development than Silver lake soils.
Reheis and others (1989)	*Qf2 to Qf1	NA	*Qf4 to Qf3	NA	*Qf3 to Qf2	NA	*Qf4 to Qf3	NA	*early Holocene to late Pleistocene (Qf2) - late Pleistocene (Qf1)	NA	*early to mid Holocene (Qf3) to mid to late Holocene (Qf4)	NA	Silver lake soils are more red than Avawatz soils.

Table 7. Correlation of Avawatz fan soils and surface characteristics with other soil and alluvial fan studies in the region—Continued

McFadden and others (1989) - Silver Lake	*Qf2 to Qf1	Qf3 to *Qf2	Qf4 to *Qf3	Qf4	Qf4 to *Qf3	Qf4	Qf4 to *Qf3	Qf4	*early Holocene to late Pleistocene (Qf2) - late Pleistocene (Qf1)	early to mid Holocene (Qf3) to *early Holocene to late Pleistocene (Qf2)	*early to mid Holocene (Qf3) to mid to late Holocene (Qf4)	mid to late Holocene (Qf4)	
McFadden and others (1989) - Silver Lake- from PDI only	[c]**Qf4 to Qf2** *Qf6 to Qf5*	NA	**Qf4** *Qf6*	NA	**Qf4** *Qf6*	NA	**Qf4** *Qf6*	NA	late Holocene (Qf4) to latest Pleistocene to early Holocene (Qf2)	NA	late Holocene (Qf4)	NA	
McFadden and others (1989) - Salt Spring Hills	Not a confident correlation.	NA	Not a confident correlation.	NA	Not a confident correlation.	NA	Not a confident correlation.	NA	*early Holocene to late Pleistocene (Qf2) - late Pleistocene (Qf1)	NA	*early to mid Holocene (Qf3) to mid to late Holocene (Qf4)	NA	
McFadden and others (1989) - Salt Spring Hills - from PDI only	**Qf3 to Qf2** *Qe2 to Qf2*	NA	**Qf4 - Qf3** *Qf6 - Qe2*	NA	**Qf4 - Qf3** *Qf6 - Qe2*	NA	**Qf4** *Qf6*	NA	latest Pleistocene to Early Holocene (Qf2) to mid Holocene (Qf3)	NA	mid Holocene (Qf3) to Late Holocene (Qf4)	NA	
Harvey and Wells (2003)	Qf2 to *Qf1	Qf2	Qf3	Qf3	Qf3	Qf3	Qf3	Qf3	*early Holocene to late Pleistocene (Qf2) - late Pleistocene (Qf1)	*early Holocene to late Pleistocene (Qf2)	early Holocene (Qf3)	early Holocene (Qf3)	Avawatz soils have less carbonate than the Zzyzx Qf3.

[a]Using nomenclature of cited references. [b]* Denotes favored correlation. [c]Bold is McFadden and others (2003) nomenclature.
Italics is nomenclaturecorrelated from McDonald and others (2003).

Table 7. Correlation of Avawatz fan soils and surface characteristics with other soil and alluvial fan studies in the region—Continued

Our Unit	Qia-HL05AM377		Qya4-bar-HL05AM378b		Qya4-swale-HL05AM378s		Qya4-inset-HL05AM381		Correlated age based on soils	Correlated age based on surficial characteristics	Correlated age based on soils	Correlated age based on surficial characteristics	NOTES:
correlation using: Reference:	soils	surf. char.	soils	surf. char.	soils	surf. char.	soils	surf. char.	Qia	Qia	Qya4	Qya4	
McDonald (1994) and McDonald and others (2003)	*Qf5 to Qf4, very unlikely Qf3 or Qf2	*Qf5 to Qf4	Qf6	Qf6	Qf6	Qf6	Qf6	Qf6	22-130 ka	*early Holocene to latest Pleistocene (Qf5) to late Pleistocene (Qf4)	late Holocene (Qf6)	late Holocene (Qf6)	Avawatz soils seem to be finer grained than those at Providence Mts. Soils may match the QM or PM parent material groups. Any moderate to strong pavement is associated with carbonate stage morphology more advanced than that in the Avawatz fans. Avawatz Qia fits pavement, texture, pavement and pedon of McDonald PM Qf4, but the Avawatz has a stage I vs the McDonald stage III carbonate.

Table 7. Correlation of Avawatz fan soils and surface characteristics with other soil and alluvial fan studies in the region—Continued

McDonald and others (2003)-using PDI	*Qf5 to Qf6	NA	Qf6	NA	Qf6	NA	Qf6	NA	*early Holocene to latest Pleistocene (Qf5) to late Holocene (Qf6)	NA	late Holocene (Qf6)	NA	
Harden and others (1991b) in McDonald and others (2003)-using PDI	Qf4 to Qf2	NA	*Qf5 to Qf4	NA	*Qf5 to Qf4	NA	*Qf5 to Qf4	NA	late Holocene (Qf4) to early Holocene to latest Pleistocene (Qf2)	NA	late Holocene (Qf5) to late Holocene (Qf4)	NA	
Klinger (1998)	<Q2, > Q3	Q2	Q4 - Q3	Q4 & Q3	Q4 - Q3	Q4 & Q3	Q4 - Q3	Q4 & Q3	between latest Pleistocene (Q3) and mid to late Pleistocene, ~145-160 kyr (Q2)	mid to late Pleistocene, ~145-160 kyr (Q2)	early Holocene (Q4) to latest Pleistocene (Q3)	early Holocene (Q4) to latest Pleistocene (Q3)	Klinger fans have more carbonate than Avawatz fans.
Menges and others (2001)	Qfi to Qfo	Qfo	Qfi	Qfi	Qfi	Qfi	Qfi	Qfi	middle to early Holocene (Qfi) to Pleistocene (Qfo)	Pleistocene (Qfo)	middle to early Holocene (Qfi)	middle to early Holocene (Qfi)	
Slate and others (1999)	Qai	Qai	Qay	Qay	Qay	Qay	Qay	Qay	early Holocene and Pleistocene	early Holocene and Pleistocene	Holocene	Holocene	

Acknowledgments

We thank Tricia Collins for field assistance. We also thank John Caskey for comments and suggestions, and Emily Taylor and Christopher Menges for reviews, all of which led to improvement and clarity in many parts of this paper.

References Cited

Bedford, D.R., 2003, Surficial and Bedrock Geologic map database of the Kelso 7.5 Minute Quadrangle, San Bernardino County, California, U.S. Geological Survey, Open-File Report 03-501, p.33.

Birkeland, P.W., 1999, Soils and Geomorphology: New York, Oxford University Press, 448 p.

Brady, R.H., 1984, Cenozoic geology of the northern Avawatz Mountains in relation to the intersection of the Garlock and Death Valley fault zones, San Bernardino County, California: Davis, University of California, Ph.D. Thesis, 292 p., 2 pls., 19 figs.

Bull, W.B., 1991, Geomorphic response to climate change: New York, Oxford University Press, 326 p.

Christenson, G.E., Purcell, C., 1985, Correlation and age of Quaternary alluvial-fan sequences, Basin and Range province, southwestern United States *in* Weide, D.L., ed., Soils and Quaternary Geomorphology of the southwestern United States: Geological Society of America Special Paper 203, p. 115-122.

Dokka, R.K., and Travis, C.J., 1990, Late Cenozoic strike-slip faulting in the Mojave Desert, California: Tectonics, v. 9, no. 2, p. 311-340.

Gile, L.H., Peterson, F.F., and Grossman, R.B., 1966, Morphological and genetic sequences of carbonate accumulations in desert soils: Soil Science, v. 101, no. 5, p. 347-360.

Grose, L.T., 1959, Structure and Petrology of the Northeast Part of the Soda Mountains, San Bernardino County, California: Bulletin of the Geological Society of America, v. 70, p. 1509-1548.

Harden, J.W., 1982, A quantitative index of soil development from field descriptions-Examples from a chronosequence in central California: Geoderma, v. 28, p. 1-28.

Harden, J.W., Taylor, E.M., 1983, A quantitative comparison of soil development in four climatic regions: Quaternary Research, v. 10, p. 342-359.

Harden, J.W., Taylor, E.M., Reheis, M.C., and McFadden, L.D., 1991a, Calcic, gypsic, and siliceous soil chronosequences in arid and semiarid environments, *in* Nettleton, W.D., ed., Occurrence, Characteristics, and Genesis of Carbonate, Gypsum, and Silica Accumulations in Soils: Soil Science of America Special Publication No. 26, p. 1-16.

Harden, J.W., Taylor, E.M., Hill, C., Mark, R.L., McFadden, L.D., Reheis, M.C., Sowers, J.M., and Wells, S.G., 1991b, Rates of Soil Development from four soil chronosequences in the southern Great Basin, Quaternary Research, v. 35, p. 383-399.

Harvey, A.M., and Wells, S.G., 2003, Late Quaternary variations in alluvial fan sedimentologic and geomorphic processes, Soda Lake basin, eastern Mojave Desert, *in* Yehouda Enzel, Stephen G. Wells, and Nicholas Lancaster, eds., Paleoenvironments and Paleohydrology of the Mojave and Southern Great Basin Deserts, GSA Special Paper 368, p. 207-230.

Jennings, C.W., 1994, Fault activity map of California and adjacent areas with location and ages of volcanic eruptions: California Geologic Data Map Series No. 6, California Division of Mines and Geology, scale 1:750,000.

Jenny, H., 1941, Factors of Soil Formation, McGraw-Hill, New York, 281 p.

Klinger, R.E., 1998, Scarp morphology, alluvial stratigraphy, and late Quaternary activity on the Bare Mountain Fault, *in* Interconnectivity and Relationships Between Soil Science, Geomorphology, Geology, and Paleoclimatology, PSSAC Annual Meeting, p. 65-79.

Machette, M.N., 1985, Calcic Soils of the southwestern United States, *in* Weide, D.L., ed., Soils and Quaternary Geomorphology of the southwestern United States: Geological Society of America Special Paper 203, p. 1-21.

Mahan, S., Miller, D.M., Menges, C.M., Yount, J.C., 2005, Late Quaternary Stratigraphy and Luminescence Geochronology of the Northeastern Mojave Desert, with Emphasis on the Valjean Valley Area, this volume.

McDonald, E.V., 1994, The relative influences of climatic change, desert dust, and lithologic control on soil-geomorphic processes and soil hydrology of calcic soils formed on Quaternary alluvial-fan deposits in the Mojave Desert, California, University of New Mexico, Ph.D. Dissertation, 382 p.

McDonald, E.V., McFadden, L.D., and Wells, S.G., 1995, The relative influences of climate change, desert dust, and lithologic control on soil-geomorphic processes on alluvial fans, Mojave Desert, California; summary of results: Quarterly of San Bernardino County Museum Association, v. 42, no. 3, p. 35-42.

McDonald, E.V., McFadden, L.D., and Wells, S.G., 2003, Regional response of alluvial fans to the Pleistocene-Holocene climatic transition, Mojave Desert, California, *in* Yehouda Enzel, Stephen G. Wells, and Nicholas

Lancaster, eds., Paleoenvironments and Paleohydrology of the Mojave and Southern Great Basin Deserts, GSA Special Paper 368, p. 189-206.
McFadden, L.D., Ritter, J.B., and Wells, S.G., 1989, Use of Multiparameter Relative-Age Methods for Age Estimation and Correlation of Alluvial Fan Surfaces on a Desert Piedmont, Eastern Mojave Desert, California, Quaternary Research, v. 32, p. 276-290.
Menges, C.M., Taylor, E.M., Workman, J.B., and Jayko, A.S., 2001, Regional surficial-deposit mapping in the Death Valley area of California and Nevada in support of ground-water modeling *in* Michael N. Machette, Margo L. Johnson, and Janet L. Slate eds., Quaternary and Late Pliocene Geology of the Death Valley Region: Recent Observations on Tectonics, Stratigraphy, and Lake Cycles (Guidebook for the 2001 Pacific Cell-Friends of the Pleistocene Fieldtrip), Open-File Report 01-51, pgs. H151-H166.
Miller, D.M., Menges, C.M., and McMackin, M.R., Introduction, this volume.
Miller, M.M., Johnson, D.J., Dixon, T.H., and Dokka, R.K., 2001, Refined Kinematics of the Eastern California Shear Zone from GPS Observations, 1993-1998, Journal of Geophysical Research, v. 106, p. 2245-2264.
Reheis, M.C., 1984, Chronologic and climatic control on soil development, northern Bighorn Basin, Wyoming and Montana: University of Colorado, Boulder, Ph.D. thesis, 346 p.
Reheis, M.C., 1987, Gypsic Soils on the Kane Alluvial Fans, Big Horn County, Wyoming, U.S. Geological Survey Bulletin 1590-C, 39 p.
Reheis, M.C., Harden, J.W., McFadden, L.D., and Shroba, R.R., 1989, Development Rates of Late Quaternary Soils, Silver Lake Playa, California, Journal of Soil Science Society of America, v. 53, p. 1127-1140.
Slate, J.L., Berry, M.E., Rowley, P.D., Fridrich, C.J., Morgan, K.S., Workman, J.B., Young, O.D., Dixon, G.L., Williams, V.S., McKee, E.H., Ponce, D.A., Hildenbrand, T.G., Swadley, W.C., Lundstrom, S.C., Ekren, E.B., Warren, R.G., Cole, J.C., Fleck, R.J., Lanphere, M.A., Sawyer, D.A., Minor, S.A., Grunwald, D.J., Laczniak, R.J., Menges, C.M., Yount, J.C., and Jayko, A.S., 1999, Digital geologic map of the Nevada Test Site and vicinity, Nye, Lincoln, and Clark Counties, Nevada, and Inyo County, California: U.S. Geological Survey Open-File Report 99-554-A, p. 53, scale 1:120,000.
Soil Survey Staff, 1975, Soil taxonomy-A basic system of soil classification for making and interpreting soil surveys: U.S. Department of Agriculture, Soil Conservation Service Agricultural Handbook no. 436, 754 p.
Spencer, J.E., 1981, Geology and Geochronology of the Avawatz Mountains, San Bernardino County, California: Massachusetts, Massachusetts Institute of Technology, Ph.D. Thesis, 183 p.
Taylor, E.T., 1986, Impact of time and climate on Quaternary soils in the Yucca Mountain area of the Nevada Test Site: unpublished Masters thesis, University of Colorado, Boulder, 217 p.
Troxel, B.W., and Butler, P.R., 1979, Tertiary and Quaternary fault history of the intersection of the Garlock and Death Valley fault zones, southern Death Valley, California: unpublished report submitted to U. S. Geological Survey, Menlo Park, California, 29 p.
Wells, S.G., Dohrenwend, J.C., McFadden, L.D., Turrin, B.D., and Mahrer, K.D., 1985, Late Cenozoic landscape evolution on lava flow surfaces of the Cima volcanic field, Mojave Desert, California: Geological Society of America Bulletin, v. 96, no. 12, p. 1518-1529.
Wells, S.G., McFadden, L.D., and Dohrenwend, J.C., 1987, Influence of Late Quaternary Climatic Changes on Geomorphic and Pedogenic Processes on a Desert Piedmont, Eastern Mojave Desert, California, Quaternary Research, 27, 130-146.
Wells, S.G., McFadden, L.D., Poths, J., and Olinger, C.T., 1995, Cosmogenic (super 3) He surface-exposure dating of stone pavements; implications for landscape evolution in deserts: Geology, v. 23, no. 7, p, 613-616.
Wells, S.G., Brown, W.J., Enzel, Y., Anderson, R.Y., and McFadden, L.D., 2003, Late Quaternary geology and paleohydrology of pluvial Lake Mojave, southern California, *in* Yehouda Enzel, Stephen G. Wells, and Nicholas Lancaster, eds., Paleoenvironments and Paleohydrology of the Mojave and Southern Great Basin Deserts, GSA Special Paper 368, p. 79-114.
Wood, Y.A., 2000, Mesoscale Patterns of Plant Cover, Soils, and Surface Mosaics of a Pleistocene Desert Pavement Landscape, Cima Volcanic Field Mojave Desert, California, unpublished Ph.D. Dissertation, University of California Riverside, p. 176.
Yount, J.C., and Goldstein, H., 2005, written communication.
Yount, J.C., Schermer, E.R., Felger, T.J., Miller, D.M., and Stephens, K.A., 1994, Preliminary Geologic Map of Fort Irwin Basin, north-central Mojave Desert, California, U.S. Geological Survey, Open-File Report 94-173, p. 25.

Chapter F

Preliminary Results on Neotectonic and Geomorphic Evolution of the Northeastern Avawatz Mountains, Southern Death Valley, California

By Jennifer Mendonça[1]

Abstract

Field mapping of alluvial fan deposits and structures currently in progress within the northeastern Avawatz piedmont show an eastward propagation of reverse faults within the area. These faults have southwest-dipping fault planes and involve both bedrock and fan deposits. They suggest the presence of the southern Death Valley fault zone southeast of its intersection with the Garlock fault zone and its involvement in Quaternary deformation within the piedmont.

Introduction

The Avawatz Mountains, located in southern Death Valley approximately 30 miles north of Baker, California, are unique in their structural complexity. The sinistral Garlock fault zone and the dextral southern Death Valley fault zone form the northern and eastern boundaries of the range, respectively (Figure 1). Their intersection in the northern portion of the range, resulting in extensive local contraction, transpression, uplift and thrusting in the formation of north- and northeast-vergent thrust faults and folds within Quaternary fan sediments (Brady, 1986a).

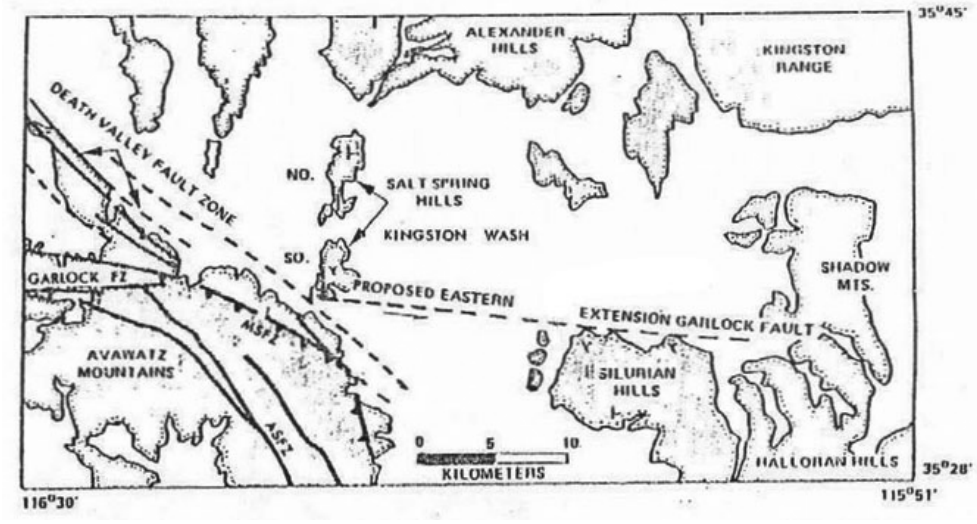

Figure 1. Generalized map of the intersection between the Garlock Fault Zone and the southern Death Valley fault zone. MSFZ = Mule Springs fault zone; ASFZ = Arrastre Spring fault zone (modified from Brady, 1986b).

[1]San José State University, San José, CA 95192

The kinematics of and relation between the Garlock and southern Death Valley fault zones to the south and east of this intersection are controversial. Geologic mapping by Troxel and Butler (1998) and Brady (1986b) suggested that the older branches of the southern Death Valley fault zone (SDVFZ) are truncated by the Mule Springs fault while the younger branches continue past the intersection as a series of reverse faults that are responsible for Quaternary deformation in the piedmont. Spencer (1981) suggested that all branches of the SDVFZ die out in the Mule Springs fault and that all Quaternary deformation is associated with branches and splays of the Mule Springs fault.

Field mapping of the northeastern portion of the Avawatz piedmont is currently in progress to describe the Quaternary stratigraphy and assess the kinematics, style, and timing of deformation within the piedmont and its possible association with the SDVFZ. The area of investigation covers a 25 square mile area bound to the north by the southern Salt Spring Hills, to the south by the Old Mormon Spring road, to the east by Highway 127 and to the west by the Mule Springs fault. This area is covered by USGS 7.5 minute Sheep Creek Spring and Silurian Lake topographic map quadrangles. This paper will present evidence for eastward-propagating faults within the piedmont, suggesting the presence of the SDVFZ south of the intersection and generally supporting the conclusions of Troxel, Butler, and Brady.

Lithologic Units

Precambrian and Paleozoic Rocks

Rocks of these ages are not widely exposed as outcrop within the area of investigation. They mostly occur as clasts within fan deposits. The few outcrops that exist are located within fault zones near the range front (Plate 1). The largest of these outcrops is a medium-grained felsic gneiss that contains abundant hornblende and biotite, concentrated in closely spaced wavy foliation planes. The gneiss is part of the crystalline basement that is believed to underlie the Avawatz Mountains. Crystal Springs Formation may also occur as outcrop, however further field investigation is needed for accurate identification. Clasts within fan deposits are derived from these two units as well as the Wood Canyon Formation, and fans locally may include Carrara Formation, Zabriski Quartzite, and Stirling Quartzite.

Mesozoic Avawatz quartz monzodiorite complex

The Avawatz quartz monzodiorite complex makes up the bedrock core of the Avawatz Mountains and comprises the majority of clasts within the fan deposits. Rocks of the unit are dark- to medium-green, medium- to coarse-grained, and contain biotite and hornblende in varying proportions (Brady, 1986b). They are also lithologically diverse, ranging from granite to diorite (Brady, 1986b). The complex was dated by Spencer (1981) using K-Ar and cross-cutting relationships. An age of 200±20 million years was obtained, proposing an early Jurassic age.

Tertiary Sedimentary Rocks and Volcanics

Sandstones, breccias, and conglomerates exposed as fault slices extend along the western margin of the area of investigation adjacent to the range front. The rocks consist of moderately consolidated, moderately- to poorly-sorted debris-flow and fluvial fan deposits that range in color from maroon, pink, tan, and gray. Clast provenance is locally derived, consisting primarily of Avawatz quartz monzodiorite with carbonates and minor volcanics. A small body of brecciated andesite was mapped in the southern half of the area, however no association with any local

volcanics has been made. These sediments and volcanics are in fault contact with the Avawatz quartz monzodiorite complex to the west and Quaternary fan deposits to the east. Structural and cross-cutting relationships suggest these sediments and volcanics to be Tertiary in age, but their association with other mapped Tertiary units in the area is uncertain.

Quaternary Alluvial Fan Units

Three relative age classes and nine generations of fan deposits have been recognized within the area of investigation. They are mostly debris flow in origin, composed of poorly sorted clasts of various sizes in a silt- to fine-sand matrix with a few interbedded fluvial deposits observed within some of the more deeply incised channels. They unconformably overly the Precambrian and Mesozoic bedrock and deformed Tertiary sediments and have variable thicknesses throughout the piedmont.

These classes were delineated using criteria outlined by Menges (2003, personal communication) and described in Miller and Menges (this volume). These criteria include general physiography, stratigraphy/sedimentology, geomorphic surface characteristics (pavement, bar and swale topography, varnish), clast surface weathering, soils, eolian deposits, flora, and deformation.

Fan deposits included in the "young" class possess the geomorphic characteristics of an actively-forming surface. Bar and swale topography is the diagnostic feature of fan deposits within this class. The younger deposits possess high-relief bar and swale topography while the older deposits display eroded remnants of such topography. Desert pavement is poorly developed, clasts are not heavily varnished, and soils display stages I to II carbonate development. Surfaces of this class are also heavily incised and possess large drainage densities. Fan deposits of this class are interpreted to be Holocene in age (Menges, personal communication).

Fan deposits included in the "intermediate" class possess the geomorphic characteristics of a mature surface. Desert pavement is the diagnostic feature of fan deposits within this class. Pavement is smooth and interlocking, with no evidence of bar and swale topography. Clasts are heavily varnished and display reddening of the undersides. Soils of this class display stages II to III carbonate development, with the oldest deposits displaying up to stage IV. Fan deposits of this class are interpreted to be Pleistocene in age (Menges, personal communication).

Fan deposits included in the "old" class possess the geomorphic characteristics of an actively eroding surface. Carbonate stage is the diagnostic feature of fan deposits within this class. Soils of this class display stages IV and V carbonate development and surfaces contain abundant carbonate chips. Fan deposits of this class are heavily eroded and dissected, forming knife-edge interfluves. Desert pavement is also weaker than in the intermediate class and clasts are not heavily varnished. Fan deposits of this class are interpreted to be earliest Pleistocene or older in age (Menges, personal communication).

Geographic distribution of each of the three fan classes displays a general younging away from the range front towards the east. Old class fan deposits are located at the range front and are the topographically highest surfaces on the piedmont. Intermediate class fan deposits are primarily located in the medial part of the piedmont and young class fan deposits are located primarily in the distal portions of the piedmont. Some of the intermediate and young fan deposits also display evidence of a reworked origin, containing anomalously highly varnished clasts and carbonate stage development. These deposits are isolated, small in scale, and mostly found in the distal portions of the piedmont.

Structures

One of the most striking features within the area is a 6 km^2 section of dissected bedrock and fan deposits that forms an apron-like structure in the proximal region of the piedmont. The apron structure is deeply incised, with relatively flat interfluves. It extends from the range front eastward 2 km into the piedmont, where it terminates at an abrupt change to a steep eastward slope or scarp that is 15 to 30 meters in height. Beds of Qidf4 and Qoa deposits exposed within incised channels in this structure dip shallowly to the east near the scarp and rotate to west dips farther east in the apron, suggesting that the change in dip represents surficial expressions of fault propagation folds formed by blind thrust faults (Plate 1).

In addition to fault propagation folds, several faults were mapped within the apron structure and along the range front. They are all east-vergent, west- to southwest-dipping reverse faults that show an eastward propagation of faulting within the piedmont. Thrust slices of deformed Precambrian basement and breccia within the apron structure and along the range front have also been mapped, however their kinematics are currently not well understood (Figure 2).

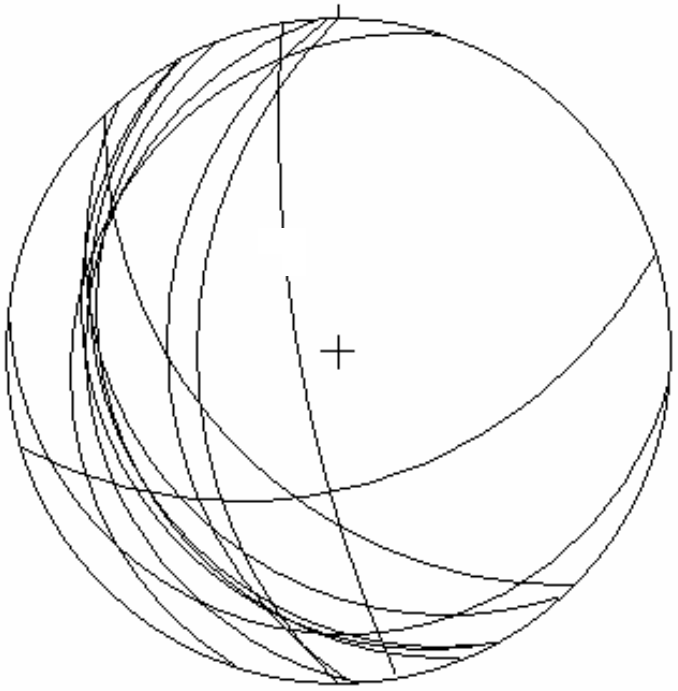

Figure 2. Lower hemisphere stereonet plot of measured faults within the area of investigation. Almost all faults dip west-southwest and are mostly shallow dip.

The westernmost faults in the piedmont are strands of the Mule Springs branch of the Garlock fault. It is a northwest-striking thrust fault that emplaces Avawatz quartz monzodiorite over Tertiary sedimentary strata. A well-exposed section of the fault approximately 3 miles southwest of the Salt Spring Hills displays dips between 30-35^o to the southwest. A possible younger strand or southern continuation of this fault system, called the Mormon Spring fault, emplaces Avawatz quartz monzodiorite over Quaternary fan deposits (Spencer, 1981) (Figure 3). Fan deposits mapped along these fault contacts range in age from Qoa to Qidf3, suggesting that activity along this fault system occurred within the early to middle Pleistocene. Along both fault systems, no evidence for lateral offset has been observed.

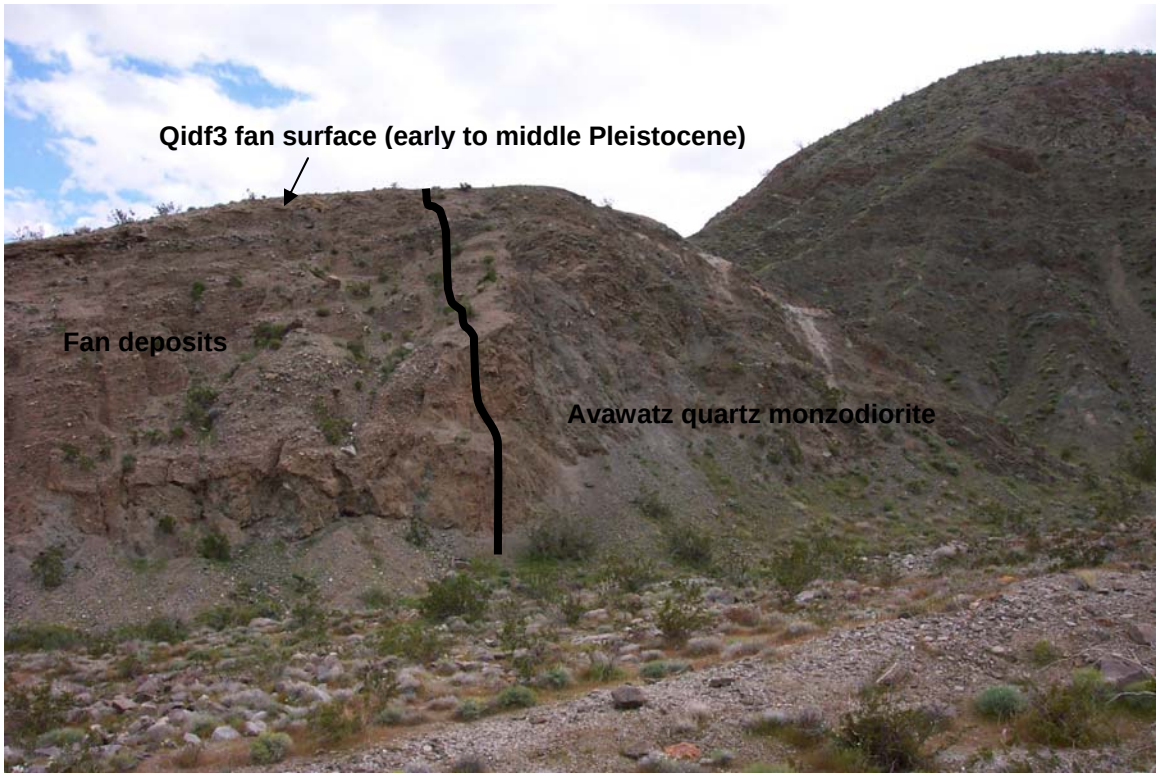

Figure 3. Exposure of the Mormon Springs fault in a large channel approximately 1 km north of Mormon Springs. The fault at this location strikes almost due north and possesses a near vertical dip.

Slightly eastward of the Mule Spring fault zone are thrust faults that place Tertiary sediments and volcanics over Quaternary fan deposits. These faults are found within the apron structure and possess northwest strikes and shallow westward dips. Large, open folds occur within some of the Tertiary sediments, with axial planes parallel to fault strike. Qidf4 deposits cap the Tertiary deposits along these faults and evidence for surface rupture has been observed, suggesting that activity along this fault system occurred during the early Pleistocene.

The easternmost faults in the piedmont place Quaternary fan deposits over Quaternary fan deposits. These faults exist within the apron structure as well as within the medial portions of the piedmont. The faults within the apron structure occur within Qidf4 deposits, with visible surface rupture. The steep slopes or scarps that form the eastern margin of the apron structure bring Qidf4 deposits in contact with Qidf3 and Qydf4 deposits. The nature of these contacts suggests a potential fault contact with Qidf3 deposits and a depositional contact with Qydf4 deposits, constraining an uplift interval between early Pleistocene and early Holocene. Further east, in the medial portions of the piedmont, the faults occur within Qidf3 deposits, however their kinematics are currently not well understood.

Topographic profiles

Topographic and longitudinal profiles constructed in ArcView 3.2 using 10 meter DEM's support an eastward propagation of faulting within the piedmont. Profile A-A' is a longitudinal profile of a channel and associated interfluve in the northern section of the apron structure (Figure 4a; refer to Plate 1 for geographic location). Perturbations from the typical concavity of alluvial fan profiles at the eastern margin suggest the presence of a growing fold possibly formed by a blind thrust fault and support field observations of fault propagation folds shaping this margin.

These perturbations are recorded both in the interfluve and channel profiles, suggesting that this is an actively growing structure.

Profile B-B' is a topographic cross-section of the apron structure, parallel to the strike of the range front (Figure 4b; refer to Plate 1 for geographic location). The profile clearly displays a non-uniform surface, with southern surface elevations, on average, 20 meters higher than surfaces in the north. These variations in the southern surfaces correspond with the mapped thrust fault slice of Tertiary sediments and volcanics bound by Avawatz quartz monzodiorite to the west and Qidf4 deposits to the east.

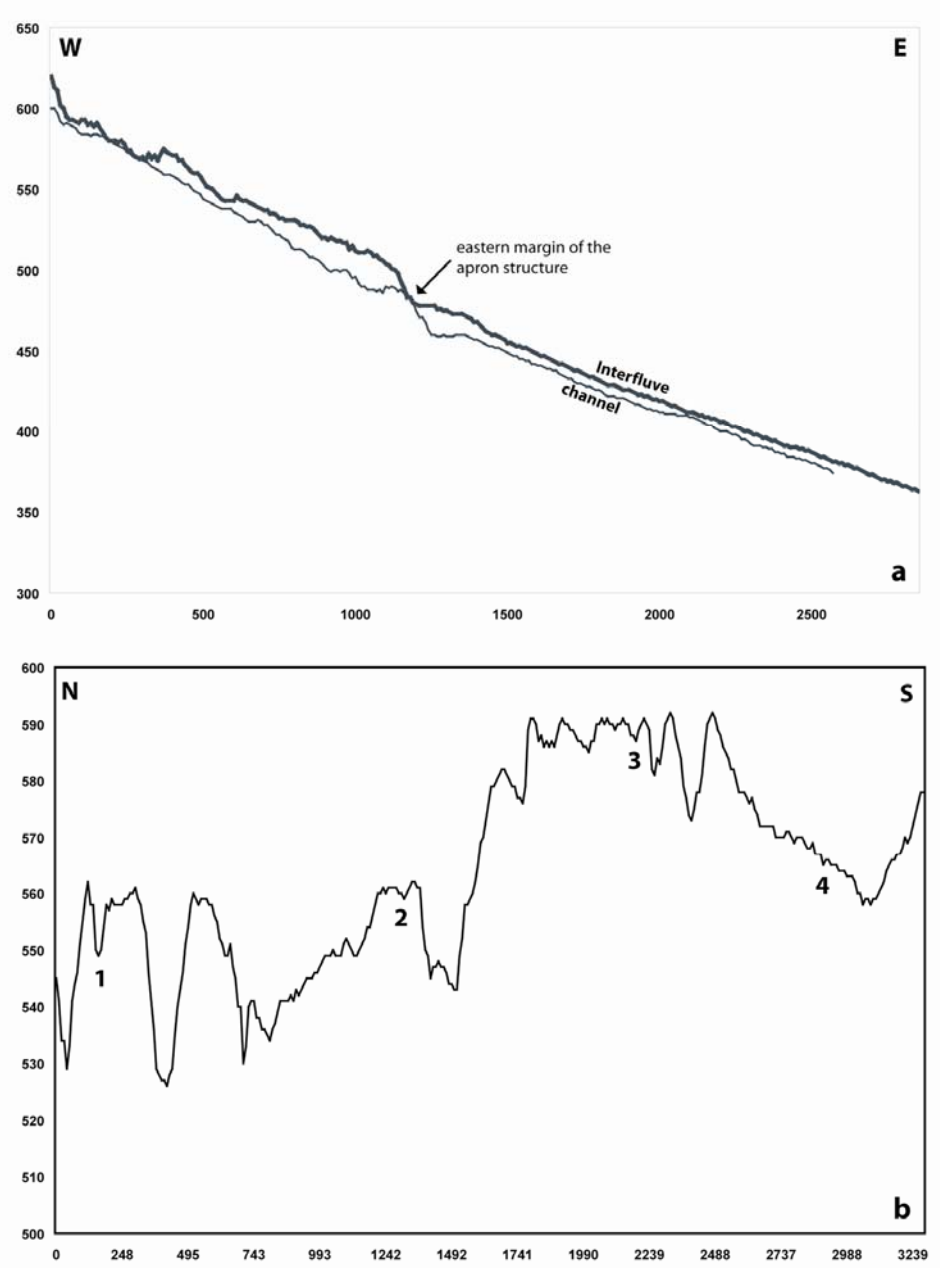

Figure 4. Longitudinal and topographic profiles of the apron structure. Horizontal and vertical units are in meters, and vertical exaggeration is 6 for A-A' and 23 for B-B'.

Preliminary Geologic Map of the Northeastern Avawatz Piedmont

by Jennifer A. Mendonça

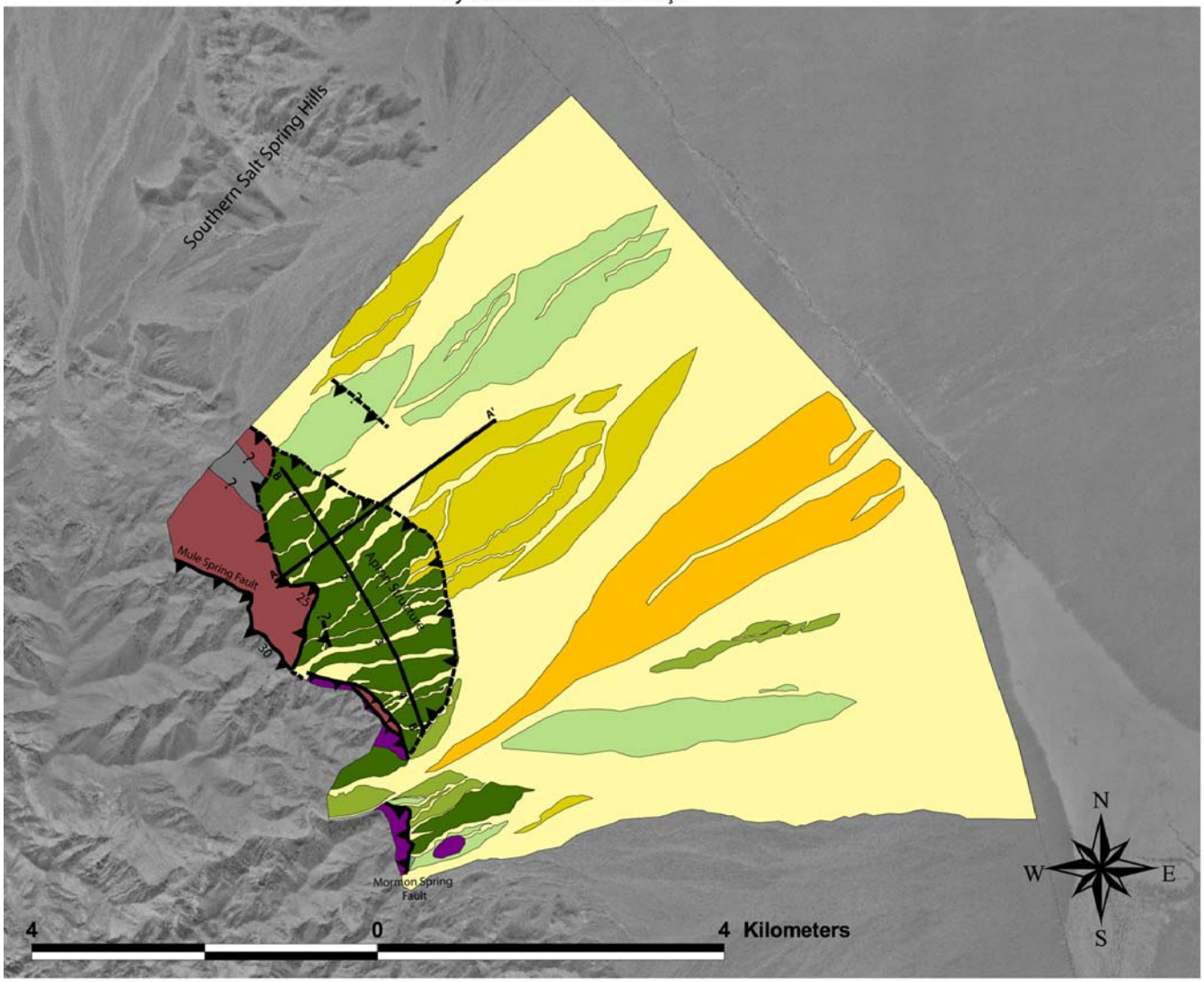

Legend

- Precambrian basement
- Qydf1, Qydf2, and Qydf3
- Qydf4
- Qydf4 and Qidf1
- Qidf2
- Qidf3
- Qidf4
- Qoa
- Tertiary sediments and volcanics
- Jurassic Avawatz quartz monzodiorite
- Thrust Fault (dashed where inferred)

Base Map: US Geological Survey Sheep Creek Spring and Silurian Lake DOQQ

Plate 1: Preliminary geologic and structural map of the area of investigation.

Conclusions

The northeastern Avawatz Mountains, south of the intersection between the Garlock and southern Death Valley fault zones, represents a tectonically complex and active area. Preliminary mapping of the area suggest an eastward propagation of thrust faulting within the piedmont, supporting the conclusions made by Troxel and Butler, and Brady of the presence of the SDVFZ south of the intersection between the Garlock and southern Death Valley fault zones. Future field work and mapping will hopefully provide more information on the kinematics and rates of faulting.

References Cited

Brady, R.H., 1986a. Stratigraphy and tectonics of the northern Avawatz Mountains at the intersection of the Garlock and Death Valley fault zones, San Bernadino County, California – a field guide. in Quaternary tectonics of southern Death Valley, California; field trip guide. Troxel, B.W. (ed), Friends of the Pleistocene, Pacific Cell; 1986 Annual meeting and field trip. Oct. 31-Nov. 2, 1986.

Brady, R. H., 1986b. Cenozoic geology of the northern Avawatz Mountains in relation to the intersection of the Garlock and Death Valley fault zones, San Bernardino County, California. PhD dissertation, University of California, Davis. 292 p.

Menges, C.M., 2003. Surficial Deposits Mapping field data sheet, version 9.1. unpublished.

Spencer, J. E., 1981. Geology and geochronology of the Avawatz Mountains, San Bernardino County, California. PhD dissertation, Massachusetts Institute of Technology. 183 p.

Troxel, B.W., and Butler, P.R., 1998. Tertiary and Quaternary fault history of the intersection of the Garlock and Death Valley fault zones, southern Death Valley, California. in Finding Faults in the Mojave: the 1998 Desert Research Symposium Field Trip Guide and Volume, San Bernardino County Museum Association, Calzia, J.E., and Reynolds, R.E. (eds), p. 91-98.

Chapter G

Dumont Dunes

By Roger S.U. Smith[1]

Abstract

Balanced and opposed seasonal winds characterize the wind regime of the Dumont Dunes, California. Northerly, winter winds give way during the spring to southerly, summer winds. Postulated west winds cannot be documented from the sparse instrumental record of wind.

Orthophotographs document seasonal transitions of dune form between peaked, star-like winter dunes and north-facing summer barchanoid dunes. These small dunes moved northward during the 16 months of the orthophoto record. Arms of large star dunes have changed only slightly during this interval.

Introduction

The Dumont Dunes are a small field of large dunes (fig. 1). These dunes cover about 13 square kilometers. They are about 20 kilometers south of Tecopa and 50 kilometers north of Baker. They extend approximately five kilometers northeastward from the Salt Spring Hills. They diminish in height eastward and their northeastern margin encroaches on the abandoned roadbed of the Tonopah and Tidewater Railroad (fig. 2). They lie on an old, southwest-sloping alluvial-fan surface that heads in the Dumont Hills. The entrenched course of the Amargosa River is several kilometers northwest of the dunes (fig. 1).

Star dunes are the predominant dune type in the Dumont Dunes. These dunes are pyramidal in form with sinuous arms radiating from a central peak. The tallest dunes (80 meters and 120 meters) lie in the central part of the dune field. Smaller star dunes (10-40 meters tall) and barchanoid dunes occupy the eastern part of the dune field. Sinuous dune ridges occupy the southwest and northwest parts of the dune field. These dune ridges extend about one kilometer north-northeastward and typically head at bedrock knobs. A few barchan dunes occur in the southwestern part of the dune field.

MacDonald (1966, 1970) was one of the first to study the Dumont Dunes. Specifically, he noted that dune slip faces reversed seasonally from north-facing during the summer to south-facing during fall through spring. From observations, he inferred that dune morphology indicated northward net sand transport.

Smith (1984) studied the Dumont dunes using sequential air photos dating from 1945. The barchan dunes in the eastern part of the dune field had moved north at five meters per year and

[1]107 N. 4th, Suite 22, Ponca City, OK 74601

those in the southwestern part had moved NNE at 3.5 meters per year. Seasonal sand streaks suggested that sand-blowing events from south-to-southeast winds were more frequent than those from north and west-to-southwest winds. Many other dune features also suggested opposing winds.

Nielson and Kocurek (1987) studied star dunes in the Dumont Dunes. They mapped ripples to determine wind flow around a dune 50 meters tall (probably hill 314). They noted that wind from any given direction will cross some dune arms obliquely, some transversely and some longitudinally. They inferred that the minimum height needed for a star dune to persist was 20 meters. Growth of star dunes was favored by balanced, opposed winds that reversed frequently. They suggested that star dunes could develop from modification or merging of crescentic dunes or from modification of linear dunes. They documented the development of a peaked star-like dune from a barchan dune 6 meters tall during June 1982 to January 1983. However, this effect was seasonal and these small peaked dunes reverted to barchans with seasonal wind shift.

Figure 1. Oblique aerial view northeastward across the Dumont Dunes toward the Amargosa River valley. Photo by R.S.U Smith, 10 May 1982.

Seasonal change and dune movement from orthophotos

Distinct changes in dune shape occur seasonally in the Dumont Dunes. Southerly winds during spring and summer drive barchanoid dunes northward. Northerly fall and winter winds distort barchanoid dunes into transverse ridges and into peaked dunes with stubby multiple arms (star dunes). These revert back to barchanoid form during summer. Large star dunes persist

through the seasonal changes in wind pattern with little change in form except for the position of slip faces along their arms.

These conclusions are based on the study of orthophotos of the Dumont Dunes. Orthophotos have digital format, uniform scale, georeferencing and freedom from the radial and oblique geometric distortions that characterize air photos. Orthophotos do not allow stereo viewing. Sequential orthophotos allow the user to locate features precisely and thus document their movement and changes in shape. This study uses the overlap between orthophotos made from air photos taken 1.4 years apart to document seasonal changes in the Dumont Dunes fig. 3).

Figure 2. Oblique aerial view westward across the Dumont Dunes toward the Salt Spring Hills. Note small barchans, larger star dunes and transitional forms. The abandoned roadbed of the Tonopah and Tidewater Railroad is near the east edge (bottom right) of the image. Barchans northeast of the railroad grade in 1982 had vanished by 1994. Photo by R.S.U. Smith, 10 May 1982.

There is an overlap of about one kilometer between adjacent DOQQs (digital orthophoto quarter quads). Each DOQQ is based on an air photo centered on the quarter quad. Adjacent photos are commonly taken within a few days of each other. However, sometimes photos are taken a year or more after their adjacent neighbors were taken. In these cases, fast-changing features (like dunes) look different on the overlap strip between adjacent DOQQs.

Sixteen months elapsed between the date of the first DOQQ photos of the Dumont Dunes and the date of the last (22 May 1994 to 29 September 1995) used in this study. The 1994 photos are of the eastern and western parts of the dune field and the 1995 photos are of the central part of the dune field. In addition, the 22 May 1994 and 29 September 1995 photos were taken near the beginning and end, respectively, of the summer wind season. Thus, 1995 changes from 1994

shapes of features in the overlap area are changes that occurred mostly during the summer wind season.

Dune shape on the May,1994, photos may be a proxy for dune shape during spring in other years and dune shape on the September, 1995, photos may be a proxy for dune shape during fall in other years. If so, changes in dune shape during the fall-to-winter wind season can be inferred as well, and the dune shapes seen in the fall should revert to the dune shapes seen in the spring. Inspection of air photos dating back to 1945 indicates that this is the case. During 1994-1995, distinct changes in dune shape are seen, despite little net movement of individual dunes.

Smaller peaked dunes on the 1994 image became distinct barchanoid dunes by 1995. Their peaks had disappeared. Twelve small barchanoid dunes had moved an average of nine meters northward (range two meters to 20 meters). Their stubby left (west) arms in 1994 became distinct and longer by 1995, but not as long as their right (east) arms. 1994 dune ridges appeared generally symmetrical, except for slip faces along the north side of east-west dune ridges. 1995 dune ridges had slip faces along their north or northwest sides. Six arms on star dunes shifted an average of four degrees in azimuth (range 0-9 degrees). Summits of four star dunes may have shifted a few meters east and south during 1994-5, but the 1995 summit position was hard to determine.

The distinct difference between the appearance of these dunes in 1994 and 1995 is attributable to three factors: 1) Prominence and facing of slip faces; 2) Peaking of sand on barchan crests as their left arms are destroyed during fall and winter; and 3) Absence of slip faces on many lower dune forms after the winter wind season. Lighting and shading also affect dune appearance. No substantial changes in dune trend or position were seen except for northward movement of barchanoid dunes and the seasonal destruction and redevelopment of their left arms.

Orthophotos can be overlaid with registered digital topographic maps to determine dune migration. The Dumont Dunes 7.5 minute quadrangle was made from 1978 air photos in the area that covers the dunes. These photos were taken on 15 June for the western part of the dunes and 16 August for the eastern part. This date is 16 to 17 years earlier than the date of photos used for the orthophotos. Preliminary results indicate that dunes within the orthophoto overlap area moved N. 15 E. at about 1.5 meters per year. These dunes are less than 20 meters tall. Migration can only be determined for dunes that can be resolved by 10-meter contours.

Orthophotos can also be used to approximately register sequential sets of air photos to determine dune migration over longer time periods. Although many barchanoid dunes survive seasonal conversion into peaked, star-like dunes, many barchans have vanished from the eastern part of the dune field. Their seasonal conversion may diminish and eventually destroy them.

Wind Regime

The wind regime of the Dumont Dunes is complex and imperfectly known. MacDonald (1966, 1970) and Smith (1984) inferred that the wind regime was one of balanced winds from seasonally-opposed directions. MacDonald (1966, p31-2) presented maps that showed how inferred west, north and south winds should move across the dunes and around the adjoining hills. Nielson and Kocurek (1987) inferred three seasonal wind regimes: north winds during winter, west winds during spring and early summer and south winds during summer.

The nearest long-term hourly wind record is the 1939-50 record from Silver Lake airport, 40 kilometers south of the dunes. This weather station is now inactive. Smith (1984)analyzed this record to determine potential sand transport based on the cube of speed above threshold. With north and south winds balanced, west wind dominated the ESE resultant of potential sand

transport. MacDonald's (1966) earlier analysis of part of this record inferred an oscillating wind regime for the Dumont Dunes.

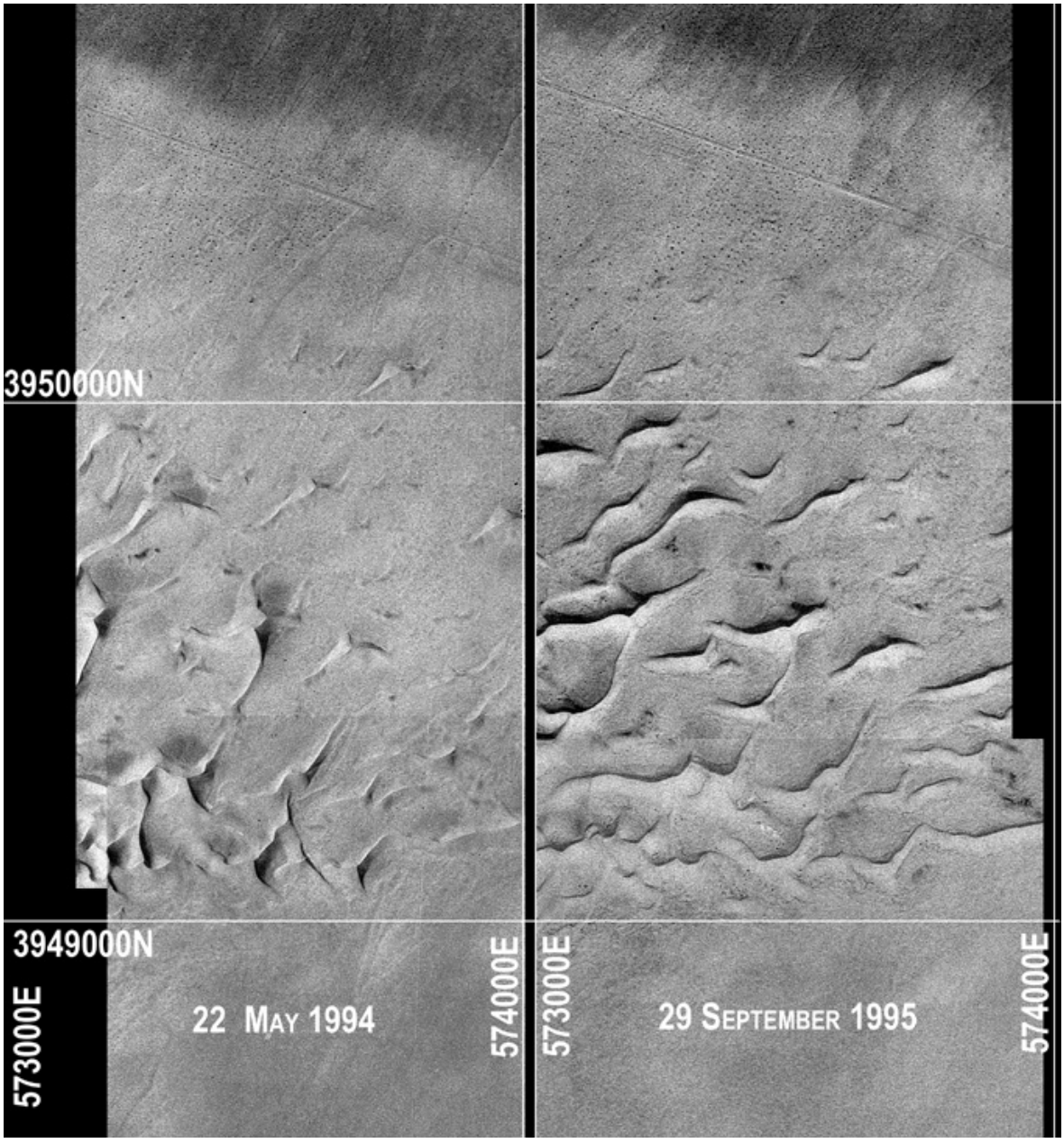

Figure 3. Digital orthophotos of the overlap area between the DOQQs for the east and west halves of the Dumont Dunes 7.5 minute quadrangle. Left side: 22 May 1994; right side: 29 September 1995. The NAD 1927 UTM grid lines are one kilometer apart.

At Riggs, another wind station 20 kilometers south of the dunes, south winds balance and oppose north winds. This inference is based on the record of only one year of hourly wind data (Table 1). North-to-northwest winter winds give way to south-southeast, south and south-southwest summer winds during spring, the windiest season. Summer winds give way to winter winds during the fall, the least windy season. The resultant for potential sand transport is modest and eastward, despite the absence of west wind. These results are based on winds that exceed six meters per second, weighted by velocity cubed.

Table 1. Annual 1987-8 Wind Data from Riggs, CA

Speed meters/sec	0.5-2	2-4	4-6	6-9	9-12	12-15	15-18
N	0.9	2.7	2.7	2.2	0.7	0.1	0.0
NNE	0.9	1.1	0.2	0.2	0.0	0.0	0.0
NE	1.2	0.7	0.1	0.0	0.0	0.0	0.0
ENE	1.2	1.2	0.2	0.1	0.0	0.0	0.0
E	1.3	3.0	1.2	0.2	0.0	0.0	0.0
ESE	1.1	4.0	2.1	0.4	0.1	0.0	0.0
SE	0.8	2.5	3.3	0.6	0.3	0.0	0.0
SSE	0.7	2.8	4.2	3.4	0.3	0.0	0.0
S	0.8	2.8	5.9	4.5	0.5	0.0	0.0
SSW	0.6	1.8	2.5	1.5	0.1	0.0	0.0
SW	0.2	0.8	0.8	0.6	0.0	0.1	0.0
WSW	0.3	0.4	0.2	0.2	0.0	0.0	0.0
W	0.6	0.3	0.0	0.0	0.0	0.0	0.0
WNW	0.7	0.9	0.0	0.0	0.0	0.0	0.0
NW	1.3	2.5	1.6	0.8	0.4	0.1	0.0
NNW	0.9	4.0	4.2	2.7	1.3	0.3	0.0
SUM	13.5	31.5	29.2	17.4	3.7	0.6	0.0

Compiled from Anonymous (1988a,b,c,d). Values are percent. Calm winds total 4.1%. Instrument height is 10 meters.

The instrumental record of wind south of the dunes confirms seasonal shift between northerly winter winds and southerly summer winds. It confirms that wind is roughly balanced between the two seasons. It fails to confirm a strong component of westerly wind. West wind is nearly absent in the one-year record of wind at Riggs, 20 kilometers south of the dunes. However, west wind is significant in the Silver Lake record, twice as far from the dunes. It is not known whether this difference is real or represents differences in record periods or topographic setting between Riggs and Silver Lake. The topographic setting of the Dumont Dunes differs from that of either weather station. Despite long wind fetch to the west, the Dumont Dunes lie in the lee of the Salt Spring Hills.

Discussion and Conclusions

New wind data from the Riggs station support the premise that balanced, seasonally-opposed winds operate in the Dumont Dunes. These winds are northerly during winter and southerly during summer. The conspicuous absence of west winds from this wind record does not answer the question of whether westerly winds operate in the Dumont Dunes, 20 kilometers north of Riggs. New wind data becoming available from the Fort Irwin National Training center will likely not help with this problem, inasmuch as none of the stations are sited on low ground along the north side of Fort Irwin west of the Dumont Dunes. The nearest station is high in the Avawatz Mountains, 20 kilometers southwest of the dunes. The nearest RAWS station is 30 kilometers east-northeast of the dunes in a topographically-sheltered site at Horse Thief Springs. The new Tecopa-Shoshone CEMP station, 30 kilometers north of the dunes, became active during February, 2006. See Appendix 1 for explanation of the RAWS and CEMP acronyms, as well as URL links to data from Fort Irwin and many other desert sites.

Orthophotographs can be used to document short-term changes in dune shape and position. In the Dumont Dunes, they document changes from winter peaked, starlike dunes summer barchanoid dunes. They document that smaller dunes moved about nine meters (range two to 20

meters) northward during 1.4 years in 1994-1995. The arms of large star dunes changed slightly during these 1.4 years. Due to their lack of stereo viewing, orthophotographs have limited use in documenting changes in the upper parts of large dunes. In addition, their image quality is commonly worse than that of the air photos originally used to construct them. They can be no better than the digital elevation models used to construct them so it may be folly to rely on them to determine small changes.

Orthophotographs can be registered with older topographic maps to measure dune migration. Dunes 10 to 20 meters tall appear to have moved northward at about 1.5 meters per year during 1978 to 1994-1995. However, these dunes are larger than many of the small dunes whose migration cannot be measured because they do not show up on contours spaced 10 meters apart. Migration of these small dunes can be measured best from air photos registered approximately to the orthophotographs.

Appendix—Climatic Data

Riggs

The Riggs station operated from 9 September, 1987 until 31 August, 1988 (Anonymous, 1988a,b,c,d). It was established to provide data for a low-level radioactive waste facility. U.S. Ecology proposed building this facility south of Riggs station on the abandoned Tonopah and Tidewater Railroad. Anemometers at 10 meters and two meters above ground surface were sited about two kilometers SW of the foot of the Silurian Hills (center, NW 1/4 sec. 10, T16N, R8E, UTM ~3928000N, ~580050E (NAD27).

Other Sources of Online Data (many are hourly)

Arizona Meteorological Network (AZMET): http://ag.arizona.edu/azmet/azdata.htm

California Air Resources Board: http://www.arb.ca.gov/qaweb/

California Climate Data Archive (includes airport stations): http://www.calclim.dri.edu/ccda/scaall.html

California Irrigation Information System (CIMIS): http://wwwcimis.water.ca.gov/cimis/data.jsp

China Lake Navy Ranges: http://www.nawcwpns.navy.mil/~weather/chinalake/wxstn2.html

Clark County [Nevada] Regional Flood Control District: http://www.ccrfcd.org/SensorMaps.htm

Community Environmental Monitoring Program (CEMP) (27 stations, mostly in southern Nevada): http://www.cemp.dri.edu/index.html

Fort Irwin National Training Center (15 stations, current month only): http://www.irwin.army.mil/weather/weather/weather.html Click on "Current Sensor Weather," then on "NTC Map Display"

Remote Automated Weather Stations (RAWS): http://www.fs.fed.us/raws/ Click on "searched online"

RAWS data from the California Data Exchange Center (CDEC): http://cdec.water.ca.gov/queryStation.html

RAWS stations (Interactive map): http://www.raws.dri.edu/index.html

U.S.G.S. Clim-Met data (3 stations each in the Devils Playground & Utah):
http://esp.cr.usgs.gov/info/sw/clim-met/

Western Region Climate Center (includes Nevada Test Site and Yucca Mountain):
http://www.WRCC.dri.edu/PROJECTS.html

Mesowest: http://www.met.utah.edu/mesowest/

References Cited

Anonymous, 1988a, Air monitoring component, U.S. Ecology Site Characterization Study, low level radioactive waste disposal Data Summary Report, Fall Quarter 1987, Silurian monitoring station, Oct. 1988: San Francisco-Los Angeles: Environmental Science Associates.

Anonymous, 1988b, Air monitoring component, U.S. Ecology Site Characterization Study, low level radioactive waste disposal Data Summary Report, Winter Quarter 1988, Silurian monitoring station, Oct. 1988: San Francisco-Los Angeles: Environmental Science Associates.

Anonymous, 1988c, Air monitoring component, U.S. Ecology Site Characterization Study, low level radioactive waste disposal Data Summary Report, Spring Quarter 1988, Silurian monitoring station, Oct. 1988: San Francisco-Los Angeles: Environmental Science Associates.

Anonymous, 1988d, Air monitoring component, U.S. Ecology Site Characterization Study, low level radioactive waste disposal Data Summary Report, Summer Quarter 1988, Silurian monitoring station, Oct. 1988: San Francisco-Los Angeles: Environmental Science Associates.

MacDonald, A.A., 1966, The Dumont dune system of the northern Mojave Desert: San Fernando State College (now California State University, Northridge), unpublished Master's thesis, 106p.

MacDonald, A.A., 1970, The northern Mojave Desert's little Sahara: California Division of Mines and Geology, Mineral Information Service, v. 23, no. 1, v. p. 3-6.

Nielson, Jamie, and Kocurek, Gary, 1987, Surface processes, deposits and development of star dunes: Dumont dune field, California: Geological Society of America Bulletin, v. 99, no. 2, p. 177-186.

Smith, R.S.U., 1984, Eolian geomorphology of the Devils Playground, Kelso Dunes and Silurian Valley, California: p. 239-251 in: Lintz, Joseph, Jr., ed, 1984, Western geological excursions, v. 1: Reno, NV: Department of Geological Sciences of the Mackay School of Mines, 281p.

Chapter H

A new Quaternary view of northern Mojave Desert tectonics suggests changing fault patterns during the late Pleistocene

By David M. Miller, Stephanie L. Dudash[1], Heather L. Green, David J. Lidke[2], Lee Amoroso[3], Geoff A. Phelps[1], and Kevin M. Schmidt

Abstract

New surficial geologic mapping studies across the northern Mojave Desert have located faults and folds that cut and deform Quaternary materials, providing a systematically developed new data set for evaluating several tectonic problems. Several previously unrecognized faults we identify by tectonic geomorphic features in deformed Quaternary materials. These faults do not show large magnitudes of offset in bedrock and may represent relatively youthful fault systems. Faults cutting early and middle Quaternary materials form a wide structural network of faults spanning much the northern Mojave Desert. In contrast, faults that cut late Pleistocene deposits (approximately 30-90 ka) are more restricted geographically, in particular being much less common in the area south of the Cady fault. The relatively few faults that cut latest Pleistocene to earliest Holocene deposits (approximately 9 to 15 ka) are restricted to the Lenwood-Lockhart faults, Gravel Hills-Harper Lake faults, northern part of the newly identified Paradise fault system and nearby East Goldstone fault, and the east-striking Manix system of faults including the newly identified Mesquite Springs fault. This apparent focusing of Holocene strain onto relatively few fault zones may represent a change in strain partitioning from a pattern similar to that of the southern Mojave Desert, where numerous faults are active, to one similar to the Basin and Range, where only three principal faults are active. If so, patterns of regional deformation apparently can change appreciably within periods of 100 ka or less, and such changes identified through surficial geologic mapping can help pinpoint critical areas requiring focused seismic hazard studies and kinematic analyses.

Introduction

Our understanding of late Cenozoic fault distribution and kinematics in the Mojave Desert has evolved considerably since the syntheses from geologic mapping first defined young faults (e.g., Hewett, 1954; Dibblee, 1961). These and other early geologic mapping studies identified several northwest-striking faults that stretch discontinuously from the San Andreas fault to the

[1]U.S. Geological Survey, 345 Middlefield Road, MS 973, Menlo Park, CA 94025
[2]U.S. Geological Survey, Box 25046, Denver Federal Center, MS 980, Denver, CO 80225
[3]U.S. Geological Survey, Flagstaff Field Center, 2255 North Gemini Dr., Flagstaff, AZ 86001

Garlock fault, as well as several east-striking faults that cut parts of the Transverse Ranges and the northeast Mojave Block (as defined by Hewett, 1954). Garfunkel (1974) presented a kinematic model for dextral shear on most faults of the Mojave Desert, rigid-block boundary conditions north and south of the Mojave Desert, and predicted that tectonic blocks underwent vertical-axis rotation. The hypothesized 30° counterclockwise rotation of blocks is amenable to paleomagnetic analysis. The kinematic model has been refined with more realistic boundary conditions after paleomagnetic studies indicated that blocks bounded by northwest-striking faults have undergone little or no rotation, whereas blocks bounded by east-striking sinistral faults have undergone as much as 60° clockwise rotation (e.g., Carter et al., 1987; Luyendyk, 1991; Schermer et. al., 1996). Ground ruptures associated with the recent Landers (1992) and Hector Mine (1999) earthquakes in the southern Mojave Desert unexpectedly sliced northward across major fault blocks, thus demonstrating that neighboring northwest-striking dextral faults are kinematically linked (e.g., Hauksson et al., 1993). These patterns of rupture led Nur et al. (1993) to hypothesize that recent changes in the regional stress field are causing a new set of north-striking faults to form in the Mojave Block.

Previous kinematic models relied on geologic mapping from the 1930's to 1960's, which proved inadequate for anticipating the complex rupture patterns of the Landers and Hector Mine earthquakes (e.g., Nur et al., 1993). Since this early geologic mapping was completed much has been learned about the net displacement of individual faults, vertical-axis block rotations, ages of key offset rock units along faults, and geodetically determined rates of crustal deformation. However, there have been relatively few advances in the understanding of Quaternary fault networks and associated regional deformation, owing to limited trenching and paleoseismology studies, limited detailed geologic mapping, and only rare comprehensive studies employing modern concepts of Quaternary pedology and sedimentology, and tectonic geomorphology.

North-striking oblique ruptures of the Landers and Hector Mine earthquakes show that some major fault blocks are internally dissected and that a single ground-rupturing event can link major dextral faults that were formerly thought to be mechanistically independent. These revelations arguably imply that new faults are forming in the Mojave Desert (Nur et al., 1993). Alternatively, oblique linkages between the major faults may have begun forming during the Quaternary but evidence was overlooked by geologic mapping that focused on rocks in mountain blocks. We sought to evaluate these alternate hypotheses with surficial geologic mapping.

Our ongoing survey spans most of the northern Mojave Desert, and focuses primarily on faults cutting Quaternary and Pliocene deposits. Results to date indicate that the fault patterns shown on previous maps are essentially correct, but that many more faults dissect blocks previously thought to be unbroken, and that some previously unrecognized fault systems appear to have originated during the Quaternary. In addition, stratigraphic evidence for the age of latest fault rupture reveals that the spatial distribution of active faults in the northern Mojave Desert changed dramatically during the past 200 ka. Most of the mapped faults were active at the start of this period, then a restricted set was active 30-90 ka, and finally only a few widely spaced zones apparently were active during the Holocene. These findings, if borne out by detailed studies and assuming that fault rupture recurrence intervals are on the order of thousands of years, have profound implications for understanding the neotectonic evolution of the Mojave Desert and for anticipating areas of heightened seismic hazards.

Mojave Desert neotectonic setting

The northern Mojave Desert, stretching from Barstow on the south to the Garlock Fault on the north (Fig. 1), lies within a zone of active dextral shear associated with oblique plate

convergence. This zone presently accommodates 15 to 25% of net shear between the Pacific and North American plates as indicated by geodetic data (8 to 10 mm/yr of dextral shear; Sauber et al., 1986, 1994). Schelle and Grunthal (1996) summarized geophysical data demonstrating that brittle behavior of the upper crust extends to about 10 km depth, and that maximum principal stress in the brittle crust is oriented about 010º. However, recent analysis of earthquake focal mechanisms indicates that maximum principal stress is oriented about 020º (Hardebeck and Hauksson, 1999).

The eastern, more active part of this zone of shearing (Fig. 1) was termed the eastern California shear zone by Dokka and Travis (1990). We follow Miller and Yount (2002) in applying a more general term, Mojave strike-slip province, to address the broader region of late Cenozoic faulting that includes all of the western Mojave Desert. The Mojave strike-slip province apparently is related kinematically to deformation of the adjoining "Big Bend" segment of the San Andreas fault (Garfunkel, 1974) that is shown in Figure 1 and, as originally proposed by Dokka and Travis (1990), shearing likely continues northward through the western part of the northern Basin and Range province. Near the Mojave Desert, the strike-slip province consists of four domains (Fig. 1) corresponding to the Transverse Ranges, southern and northern Mojave Desert, and western Basin and Range. South of the Mojave Desert, a zone of east-striking faults with sinistral slip is associated with the eastern Transverse Ranges domain, which lie directly north of the San Andreas fault. We divide the Mojave Desert itself into south and north domains separated by a physiographic low extending west-northwest from Bristol Lake to beyond Barstow (Bristol-Barstow trough). Some faults are not mappable across this regional trough and others exhibit breaks that have led to separate names on either side of the trough. The Garlock fault defines the boundary between northern Mojave Desert and Basin-and-Range domains. Few faults can be mapped to the Garlock fault zone, and the three principal faults of the Basin and Range domain also terminate north of the Garlock fault (Garfunkel, 1974).

Quaternary faults within the Mojave domains have been depicted as occurring over a broad area 150 to 200 km wide, within which dextral faults are spaced fairly evenly, roughly 10 to 20 km apart (Fig. 1). By contrast, strike-slip faults in the adjoining the Basin and Range domain are limited to three principal systems, from west to east the Sierra Nevada frontal fault, Panamint fault, and Death Valley fault zone (Fig 1); these faults are more widely spaced, about 40 to 60 km apart. Faults of the northern Mojave Desert domain do not align with those of the adjacent Basin and Range domain in most cases, but they do align moderately well with faults of the southern Mojave Desert domain.

The northern Mojave domain exhibits several perplexing tectonic relations. The southern Mojave domain experienced two large earthquakes in the recent past, the 1992 M_W=7.3 Landers and 1999 M_W=7.1 Hector Mine events. Each earthquake ruptured northward nearly to the Bristol-Barstow trough, and some aftershocks clustered within and directly north of the trough. However, most parts of the northern Mojave domain have remained relatively aseismic during and following these earthquakes and also for the several preceding decades, and the few clusters of microseismicity do not lie along previously mapped faults. Youthful faults in the western part of the northern Mojave Desert domain generally strike northwest and are dextral, whereas most faults in the eastern part strike east and are sinistral (Schermer et al., 1996; Miller and Yount, 2002). The boundary between these eastern and western parts consists in part of little-studied north-striking faults (Miller and Yount, 2002) whose kinematic role is not understood. Although geodetically-determined high rates of strain occur in some areas (McClusky et al., 2001; Miller et al., 2001; Peltzer et al., 2001) the strain coincides with previously mapped faults that have not ruptured during the late Quaternary (Oskin and Iriondo, 2004).

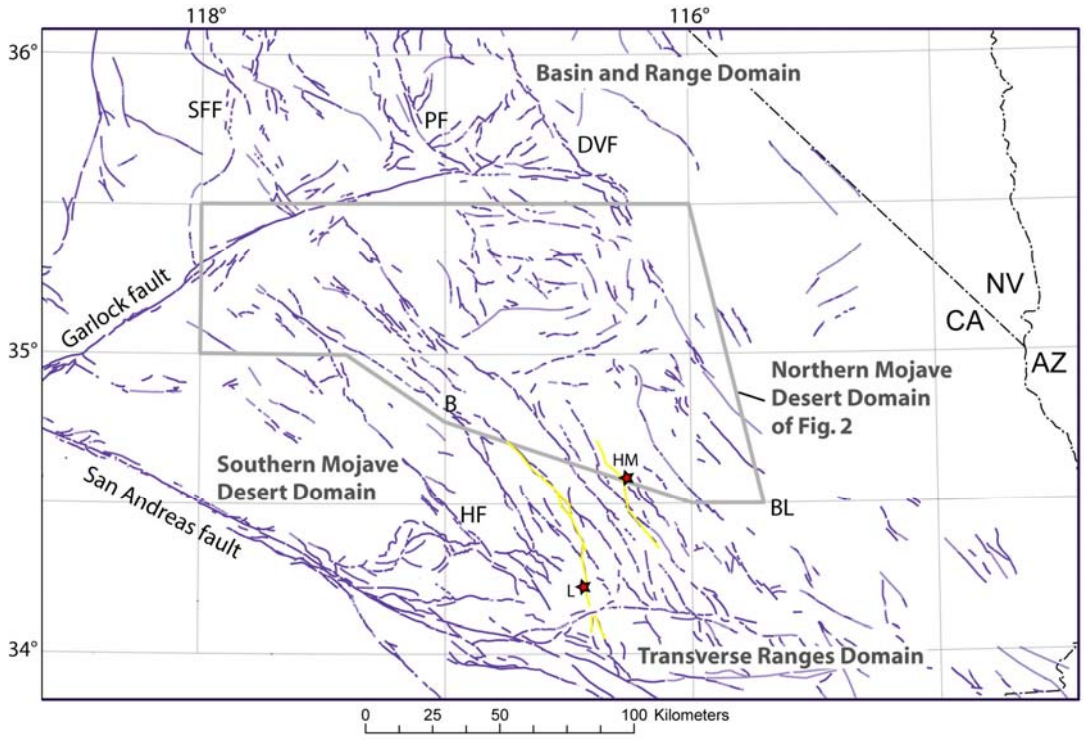

Figure 1. Location map showing previously mapped young faults in domains north of the San Andreas fault system. Simplified from Jennings (1994). B, Barstow; BL, Bristol Lake; SFF, Sierran frontal fault; PF, Panamint fault; DVF, Death Valley fault zone; HF, Helendale fault. Rupture zones associated with the Landers (L) and Hector Mine (HM) earthquakes highlighted in yellow.

Methods

Surficial geology of the northern Mojave Desert was mapped at a scale of 1:100,000 (Amoroso and Miller, 2006; Bedford et al., 2006; U.S. Geological Survey, maps in preparation) and locally in more detail (e.g., Yount et.al., 1994) using standard field methods including description of landforms, deposit characteristics, and pedogenesis. Tectonic features were described from natural exposures, and included data such as fault plane orientations, striae orientation and characteristics, folds, ages of deposits involved, height and steepness of scarps, and offset of channels and similar features. Criteria for field identification of Quaternary faults included: tectonic scarps, shutter ridges, linear valleys and troughs, offset channels and other features, unembayed mountain fronts, faceted spurs on ridges, and folded Quaternary deposits. Mapping was conducted by stereoscopic analysis of aerial photographs, field study, evaluation of Landsat 7 satellite imagery, and reference to published geologic maps. In most cases, published geologic maps emphasize bedrock relations, and have identified the faults that cut bedrock map units, but they generally reveal few details about Quaternary deposits and associated deformation. Studies by Richter (1947), Clark (1973), Brady (1984), McGill and Sieh (1991, 1993), Cox and Wilshire (1993, 1994), Schermer et al. (1996), Miller and Yount (2002), and Dudash (2006) provided information on Quaternary faulting.

The main age criterion used to constrain timing of fault activity is the age of mappable deposits, as determined from a combination of surface characteristics and soil development (the soils-geomorphic approach of Birkeland, 1990). Our age estimates are calibrated through reference to Mojave Desert soil chronosequence studies by Reheis et al. (1989) and McFadden and Weldon (1987), supplemented by ages provided by Mahan et al. (this volume). We identified four widely distributed sets of soil-geomorphic alluvial fan deposits all of which predate modern

alluvial stream channels. From young to old, these deposits are mid-Holocene (unit Qya3, about 3 to 6 ka), earliest Holocene to latest Pleistocene (Qya4, about 9 to 15 ka), late Pleistocene (Qia2, about 30 to 90 ka), and middle Pleistocene (Qia3, poorly dated at about 150 to 220? ka). A summary of surface characteristics and soils for these units is presented by Menges and Miller (Introduction, this volume). Older Quaternary deposits exist in the region but are generally not areally extensive enough to be systematically applied to fault age evaluations.

Limitations of data

We conducted intermediate-scale mapping, commonly focusing on suspected Quaternary faults identified from geomorphic features evident in aerial photographs, but we have conducted only two systematic detailed mapping studies of faults (Dudash, 2006; Green and others, this volume). Only rarely did we consult detailed air photos (>1:30,000) and detailed LiDAR elevation data. Faults on the China Lake Naval Weapons Center between the northern Blackwater fault and Goldstone Lake were mapped exclusively from air photos and none of them were field checked. Very limited scarp profiling was employed and no fault trenching was done. As a result of the foregoing limitations, we probably have overlooked some small faults and may have falsely identified some linear features as faults.

Small scarps in granular low-cohesion Holocene deposits may be under-represented owing to poor preservation. For instance, sinistral slip of about 5 cm was measured shortly after the 1947 M_W=6.5 Manix earthquake (Richter, 1947), but Holocene deposits along this rupture zone no longer show evidence for this event, probably due largely to the rupture coinciding with surface deposits of grus-rich Mojave River sand and fine gravel. In several places we followed clearly identifiable scarps developed in Pleistocene to early Holocene materials, yet found the scarp with great difficulty in younger deposits. This is true even for historic ruptures, and suggests that cohesion of the deposit is a principal factor in identifying scarps. The cohesion that permits early Holocene and older deposits to preserve tectonic geomorphic features is principally their soil development. Since soil development of the magnitude seen in a Qya4 deposit, which is roughly 15 ka or younger, requires several thousand years to develop, any scarp preserved in deposits of this age we consider to represent Holocene rupture.

Some basins lack exposure of deposits older than middle Holocene, limiting our analysis to only very young scarps. Although we experimented with geophysical methods to identify buried faults in these basins, we did no systematic geophysical study to detect buried traces of faults. Because only limited field checking was done, we may have incorrectly connected aligned faults that are in fact discontinuous.

Results

Our fault map (Fig. 2) resembles the compilation by Jennings (1994) but there are a few striking differences. Because our mapping focused on surficial deposits and tectonic geomorphology rather than offset of bedrock, we were able to identify several new principal faults and hundreds of new minor faults and fault splays. These refinements reveal some intriguing neotectonic patterns. In addition, we catalogued ages of units cut by faults as well as deposits overlapping faults, allowing approximate assignments for ages of last fault rupture. These age assignments reveal temporal progressions of fault activity.

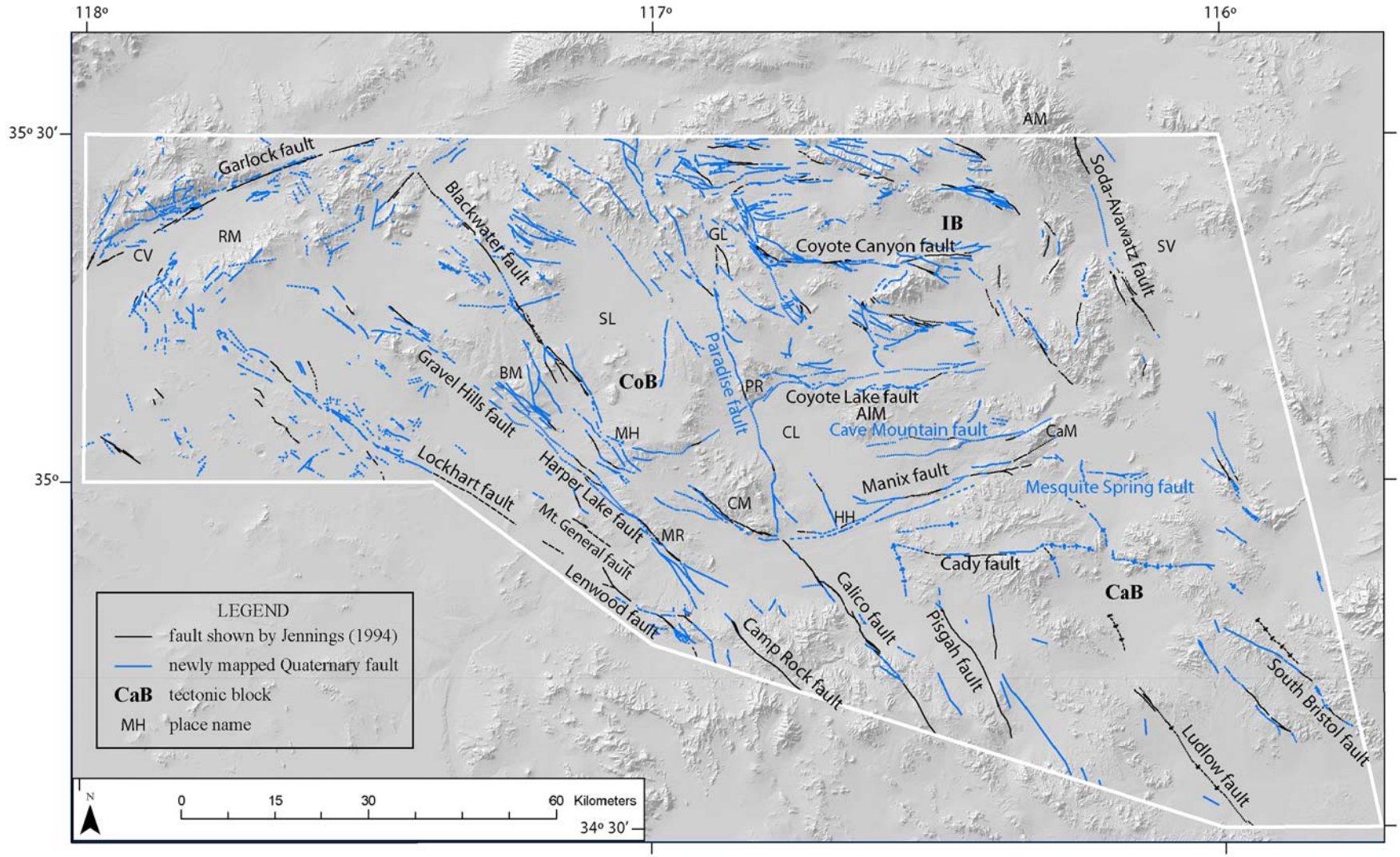

Figure 2. Quaternary faults of the northern Mojave Desert mapped by U.S. Geological Survey. While the overall pattern is similar to the fault compilation by Jennings (1994), note that some newly identified faults (named in blue) occur within areas formerly depicted as broad unbroken blocks. The newly recognized Paradise fault system and other north-striking faults depart from better known northwest- and east-striking faults. AM, Avawatz Mountains; AlM, Alvord Mountain; BM, Black Mountain; CaM, Cave Mountain; Cab, Cady Block; CoB, Coolgardie Block; CL, Coyote Lake; CM, Calico Mountains; CV, Cantil Valley; GL East Goldstone Lake, HH, Harvard Hill; IB, Irwin Block; MR, Mitchell Range; MH, Mud Hills; PR, Paradise Range; RM, Rand Mountains; SL, Superior lakes, SV, Silurian Valley.

Newly identified fault systems

In order to illustrate major new structural patterns, we have highlighted three newly identified fault systems with bold labels on Figure 2; several others were identified but are not emphasized for this analysis. The north-striking Paradise fault zone consists of several faults, including the Tin Can Alley fault in the south (Dudash, 2004, 2006), a fault in the western Paradise Range, and previously unmapped faults in pediments northwest of the Paradise Range. The segment within the pediment northwest of the Paradise Range displays Holocene scarps. The fault system apparently extends north to the Goldstone Lake area, where eolian sand cover makes fault identification difficult. Goldstone Lake itself exhibits straight playa edges that are co-linear with Quaternary faults mapped southeast of the playa, and probably represents an active sag in a fault-stepover or similar fault interactions. Stretching from southeast of Goldstone Lake to north of Goldstone Lake, the East Goldstone Lake fault has numerous scarps in mid-Holocene (Qya3) deposits. The northern part of the East Goldstone Lake fault interacts with the Paradise fault zone in a poorly exposed area of several recent playas and scattered Holocene scarps. Scarps extend discontinuously northward from Goldstone Lake about 5 km, beyond which youthful geomorphology is difficult to detect in a boulder-strewn landscape underlain by basaltic lava flows. The Paradise fault zone strikes nearly north, an unusual orientation in the Mojave block and one previously noted by Miller and Yount (2002) for faults separating structural regions characterized by east-striking and northwest-striking faults.

The east-striking faults in the eastern part of the northern Mojave Desert domain define east-elongate tectonic blocks that are about 10 km by 40 km (Fig. 2), except for one unusually large block between the Coyote Lake and Manix faults, which is about 20 km by 40 km. Our mapping identified a new fault zone north of the Manix fault, which we name the Cave Mountain fault. The Cave Mountain fault fronts the steep north face of Cave Mountain, where a short segment of a scarp in Pleistocene fan deposits is present. Westward, the fault consists of several strands, some of which cut Pleistocene fan deposits and Lake Manix deposits as young as ~22 ka (Reheis et al., 2007). Two of these fault strands appear to extend westward along the south side of Alvord Mountain, where aligned folds in faulted Pliocene gravels suggest adjacent buried faults and where steep undissected mountain fronts trend east. We have not recovered evidence for total offset along the Cave Mountain fault. The Cave Mountain fault apparently breaks the unusually large block, described previously, into two parts that have dimensions more typical of tectonic blocks in this part of the northern Mojave Desert domain.

Directly east of the Manix fault system, another east-striking fault, the Mesquite Spring fault, cuts lower Holocene to upper Pleistocene deposits, producing north-facing scarps. The fault locally is decorated by a linear spring mound known as Mesquite Spring. Together, this fault and the nearly aligned Manix Fault, form a 65-km-long east-striking sinistral fault system. This sinistral fault system extends east across an area formerly modeled as having through-going northwest-striking faults (Dokka and Travis, 1990), requiring more complex models of the easternmost part of the Mojave strike-slip province.

Connections among the principal faults

Although the principal faults that outline tectonic blocks of the northern Mojave Desert have been long recognized, Schermer et al. (1996) and Miller and Yount (2002) showed that detailed mapping can illuminate complex splays and faults that cross the tectonic blocks and that accommodate a significant part of the total strain. Our mapping has revealed several more cases where splays and cross-block faults are evident in scarps and folds in Quaternary deposits. For example, along the southwest fronts of the Calico Mountains and the Mitchell Range, the Calico

and Harper Lake faults (respectively) were mapped based on bedrock offsets. Outboard (southwest) of these principal faults we have mapped several splays that exhibit evidence for more youthful rupture than do the principal faults. Here, middle Pleistocene fan deposits are cut by the principal Harper Lake fault but late Pleistocene deposits are not cut. Splays to the southwest cut late Pleistocene fan deposits. Farther southeast, the Harper Lake fault diverges into three or more widely spaced splays (Cox and Wilshire, 1993, 1994). Similar younging of faults southwest from the principal fault holds for the Calico fault, but the younger splays diverge from the principal fault along the northwestern part of the mountain front, where the youngest faults (cutting Qia2 deposits) strike west-northwest and align with faults southwest of the Mud Hills that cut similar age deposits. The youngest splays may have transferred slip to the northern part of the Harper Lake fault. These relations suggest that some mountain-front faults are being abandoned and that the northern Mojave Desert may have a potential for future intra-block earthquakes, similar to the Landers and Hector Mine events.

Faults that were previously overlooked or mapped as single strands are shown to consist of several subparallel strands, such as the Manix and Coyote Lake faults and the newly identified Cave Mountain fault. The Manix fault has three or more splays along most of its length, and all splays appear to step left in scallop-shaped steps that segment the fault into five or more distinct parts. Some of the steps occur at intersections with nearly north-striking faults, such as near Harvard Hill (Reheis et al. 2007). Anastamosing faults that are exceptionally well exposed in some Quaternary basins, such as northwest of the Coyote Canyon fault, may exemplify the degree of internal structural complexity that is typical of many tectonic blocks. Miller and Yount (2002) pointed out similar complexity in less completely exposed areas south of the Coyote Canyon fault, and hints of comparable complexity exist in well exposed areas across the northern Mojave Desert domain, such as Black Mountain and the pediments along the Lockhart fault.

Topography and faults

The Coolgardie block (Fig. 2), a large region of higher altitude than much of the northern Mojave Desert, has a central sag occupied by the Superior Lakes. The block is framed by the Blackwater fault and the newly recognized Paradise fault zone. Northwest-striking faults mapped in the northern part of this block cut middle Pleistocene deposits in places we field checked; if field studies within China Lake Naval Weapons Center bear out our mapping, this northern area of the block has several older faults but none as young as parts of the framing faults. Southward convergence of the framing faults in part may be responsible for the uplift of this block. The Mud Hills exhibit evidence of Quaternary shortening, including folding, faulting, and uplift of pediment surfaces mantled by middle Pleistocene deposits. The shortening may be associated with stepover of the Calico fault to the Harper Lake fault, discussed above, which caused uplift of the southern part of the Coolgardie block.

The Paradise fault zone also appears to bound the Coyote Lake low region, which may also be bounded by the Coyote Lake and Cave Mountain faults. However, the kinematic origin of this sag remains elusive because interactions among the north- and east-striking faults remain obscure.

The Avawatz Mountains form one of the highest areas in the Mojave Desert and have the greatest relief, descending precipitously to the north and east into Death and Silurian Valleys (Miller and Yount, 2002; Miller et al., this volume). The Irwin block southwest of the Avawatz Mountains shows little evidence for Holocene faulting but is elevated relative to the Silurian Valley to the east and the area south of Alvord Mountain. Quaternary fault-propagation folds and thrust faults deforming the alluvial fans north of the Avawatz Mountains (Miller et al., this

volume; Mendonca, this volume), and the asymmetry of the adjacent valleys, reinforce that the mountain mass has recently been thrust over the down-folded valleys. Similarly, newly identified folds and faults in alluvial fan deposits east of the Avawatz Mountains (Green et al., this volume) reinforce the conclusion that Silurian Valley is a tectonic feature and that it may play an important role in accommodating regional strain.

The geomorphology and structure of the Rand Mountains south of Cantil Valley suggests its development is due to interactions between the Garlock fault zone and northwest-striking dextral faults to the south. This range has an asymmetric north-south profile with a steep, eroded north flank and a gentle granitic pediment on the south flank. The drainage basins along the north flank are generally well-integrated toward the southwest and less well integrated to the northeast. Conversely, topographic relief increases to the northeast, presumably in response to differential uplift induced by tilting or normal faulting. The inferred tilting and faulting may be the result of interaction of the Cantil Valley pull-apart basin (Westaway, 1995) that was caused by a left step in the Garlock fault zone, and counter-clockwise rotation of a tectonic block bounded by the Lockhart and Gravel Hills-Harper Lake faults. Transtension along the northern edge of the rotating block may have opened a triangular void and associated deep basin that is indicated by a pronounced gravity low (Mabey, 1960) southwest of the Cantil Basin pull-apart basin.

Inactive principal faults

Several principal faults, such as the Calico fault adjacent to the Calico Mountains, Harper Lake fault adjacent to the Mitchell Range, and most of the Blackwater fault (Oskin and Iriondo, 2004), cut middle Pleistocene (Qia3) and older deposits but do not cut late Pleistocene deposits. Thus, these faults have not ruptured since middle Pleistocene time. Younger fault splays nearby, or in the case of the Blackwater fault, the adjacent Gravel Hills-Harper Lake fault, were active during the late Pleistocene or Holocene and appear to accommodate strain formerly associated with the presently inactive principal faults. As a result, the faults appear to migrate systematically with time. Our analysis agrees with that of previous workers in showing that principal faults south of the Cady fault and in the Irwin block show no evidence for rupture since late Pleistocene (30-90 ka) deposits formed, suggesting that these faults lie within large areas that presently deform by mechanisms that do not produce noticeable fault scarps.

Reassessment of fault patterns in space and time

One of the most provocative results of our study is the discovery of several previously unrecognized approximately north-striking faults, many of them in or alongside the Irwin and Cady blocks (Fig. 2). Although this group includes faults striking NNW, due north, and NNE, the great majority of them strike NNW. Most of the faults are best displayed by their deformation of Quaternary materials and less so by offsets of bedrock. On the basis of linear arrays of earthquake epicenters from the last half century combined with the unanticipated north-striking ruptures of the 1992 Landers earthquake, Nur et al. (1993) speculated that a new set of north-striking faults only recently began forming in the Mojave Desert. However, our recognition of north-striking faults in the northern Mojave Desert domain, particularly those of the Paradise fault zone, demonstrates that faults with northerly strikes are more common than previously recognized, and that they form integrated fault zones that probably have been active during much of the Quaternary. Although these faults appear to be relatively newly developed in that bedrock offsets are small compared to many of the block bounding faults previously mapped, we have not established ages of initiation for the faults. The southern Tin Can Alley fault (southern part of the Paradise fault system) shows small (a few 100 m) dextral displacement of Middle Miocene strata

(R.E. Reynolds, written commun., 2005), suggesting that it has (1) oblique slip, (2) low rates of dextral slip, or (3) higher rates of slip but over a short time interval. The central part of the Paradise fault northwest of the Paradise Range offsets early Pleistocene deposits more than late Pleistocene deposits, suggesting a long Quaternary history of fault activity, but we cannot determine when the fault was formed. At present it appears that many north-striking faults have been active during the middle Quaternary, and that they may have formed during the early Quaternary.

Fault migration in space and time may have affected the Blackwater fault. Miller et al. (2001) and Peltzer et al. (2001) proposed, on the basis of geodetic inversions and INSAR analysis, that the Blackwater fault had accumulated significant strain since the 1992 Landers earthquake and was possibly poised for failure. Oskin and Iriondo (2004) described contrary evidence, however, noting that average slip rates on the Blackwater fault are low and that it has not ruptured recently. If recurrence intervals are typical of other Mojave Desert faults (~1,00-3,000 yr), the geologic evidence indicates that the Blackwater fault is not active. Our field and air photo studies bear out Oskin and Iriondo's conclusions; we observed no evidence for Holocene rupture or strain south of China Lake Naval Weapons Center, and evidence for rupture since the middle Pleistocene only in two sites south of Black Mountain. As described in a previous section, slip on the northern part of the Calico fault apparently has been transferred by WNW-striking splays to the Harper Lake fault during late Pleistocene time. The northern part of the Harper Lake fault exhibits late Pleistocene and Holocene deformation. We cannot explain the results of geodetic studies given the geologic constraints.

One striking finding of our work is that many faults with Quaternary expression deform the middle Pleistocene deposits (Qia3), shown in Figure 3a, and fewer deform younger Quaternary deposits (Fig. 3b, c). For this analysis, we evaluated fault history as recorded by multiple ages of deformed deposits, including Pleistocene to Pliocene gravels, to establish that most Holocene faults exhibit evidence for multiple ruptures and have been active throughout the time period evaluated. Typical observations that indicate long fault activity are progressively higher scarps in older deposits, multiple slopes on scarps indicating several ruptures, and adjacent highly deformed Pleistocene to Pliocene deposits. It was previously suggested that strike-slip faulting started in easterly parts of the Mojave Desert and migrated westward (Dokka and Travis, 1990; Howard and Miller, 1992). However, the spatial-temporal patterns of faulting determined by our studies suggest that westward younging of faults best applies south of the Mequite Spring fault and east of the Calico fault. Elsewhere, the pattern is unexpected. The reduced area of faults deforming Qia2 and Qya4 deposits (Fig. 3) does not display a simple younging westward pattern but rather a restriction of faults into three relatively widely spaced belts.

The Holocene fault belts north of the Bristol-Barstow trough include: (1) the Lockhart and Harper Lake faults in the west, (2) the Paradise and East Goldstone faults farther east, and (3) the Manix and Mesquite Spring faults in the east. Fault belt 1 includes numerous Holocene scarps and local ponding along the Lockhart fault, but Holocene deformation is difficult to trace along the southeast part of the fault as it approaches the Lenwood fault. The northern part of the Lenwood fault likewise shows no definitive evidence for Holocene deformation but farther south has prominent Holocene scarps (Oskin et al., 2007). Fault belt 1 includes Holocene scarps and folds along the Gravel Hills fault and northern Harper Lake fault. It also includes Holocene scarps on the Mt. General fault, which lies west of a segment of the Harper Lake fault that shows no evidence for Holocene rupture. Father southeast, faults on line with the Harper Lake fault show evidence for Holocene rupture in trenches dug in the Mojave River (Cox and Wilshire, 1994); some of these faults tilt Pliocene(?) gravels to form linear ridges. Farther southeast, the

Camp Rock fault is on line with the Harper Lake and experienced some rupture during the 1992 Landers earthquake.

Fault belt 2 is newly mapped and has several uncertainties due to the reconnaissance nature of our work. The Calico fault has prominent Holocene scarps in the area east of Barstow but displays no evidence for Holocene deformation northwest of the area where the Manix fault projects west to it. Rather, the newly mapped faults of the Paradise fault zone lie north of this intersection, where they show evidence for Holocene scarps in a few segments. Northward, the Paradise fault apparently dies out along Goldstone Lake, where Holocene deformation appears to step over to the East Goldstone Lake fault. Holocene playas and a few isolated scarps north of Goldstone Lake suggest that Holocene deformation continues north of Goldstone Lake.

Fault belt 3 consists of the Manix fault system, which is composed of two to three splays in many places, and the Mesquite Springs fault. The Manix faults are not through-going, but rather step left in scallop shaped segments. The faults cannot be traced east of Afton Canyon, but shortly to the southeast the Mesquite Spring fault begins and it extends eastward at least 20 km before it is buried by eolian sand. The Manix-Mesquite Spring fault belt exhibits numerous Holocene scarps as well as large offsets of older Pleistocene deposits and Pliocene deposits (Reheis et al., 2007).

If the three belts of Holocene faulting are correctly identified, active faults in the northern Mojave Desert have been reduced in number with time. Broad areas consist of inactive faults, especially in the Cady, Irwin, and Coolgardie blocks. These areas apparently now have lower rates of deformation or increased off-fault deformation by folding and tilting than they did in the middle Pleistocene.

Discussion

Holocene fault activity in the northern Mojave Desert domain appears to be concentrated into three belts of faults separated by broad relatively stable blocks. Fault belts 1 and 2 include dextral faults that extend nearly to the Garlock fault, but have noticeably different strikes: NW for belt 1 and NNW to N for belt 2. Fault belt 3 is sinistral and strikes east to the Soda Lake area, where it may link with the Soda-Avawatz fault. Although we found no evidence for Holocene activity on the Soda-Avawatz fault zone, more detailed work is needed to establish if it or the adjacent tectonically controlled Silurian Valley (Green et al., this volume) may tectonically connect the active Death Valley fault system with the Soda Lake area. That all three zones end in areas of diffuse deformation along the boundaries of the Mojave tectonic block suggests that those boundaries may be zones of complex, distributed deformation whose tectonic elements do not readily retain evidence for Holocene faulting.

The locations of Holocene fault belts offer clues to current regional strain partitioning. Widely spaced belts of active faults in the northern Mojave Desert domain may accommodate most intra-plate strain, in which case intervening blocks are changing shape by folding and warping. The belts of Holocene faults terminate northward near the Garlock fault near where fault zones of the Basin and Range province intersect it, suggesting through-going deformation. The Soda-Avawatz fault does not show evidence for Holocene scarps, yet it intersects the Holocene Mesquite Springs and the probable Holocene southern Death Valley fault system. We hypothesize that more detailed study of the Soda-Avawatz will uncover evidence for Holocene fault or off-fault deformation. Strain in the middle crust may be partitioned along threes paths related to the three belts of faults. If so, the broad zone of shear in the southern Mojave may

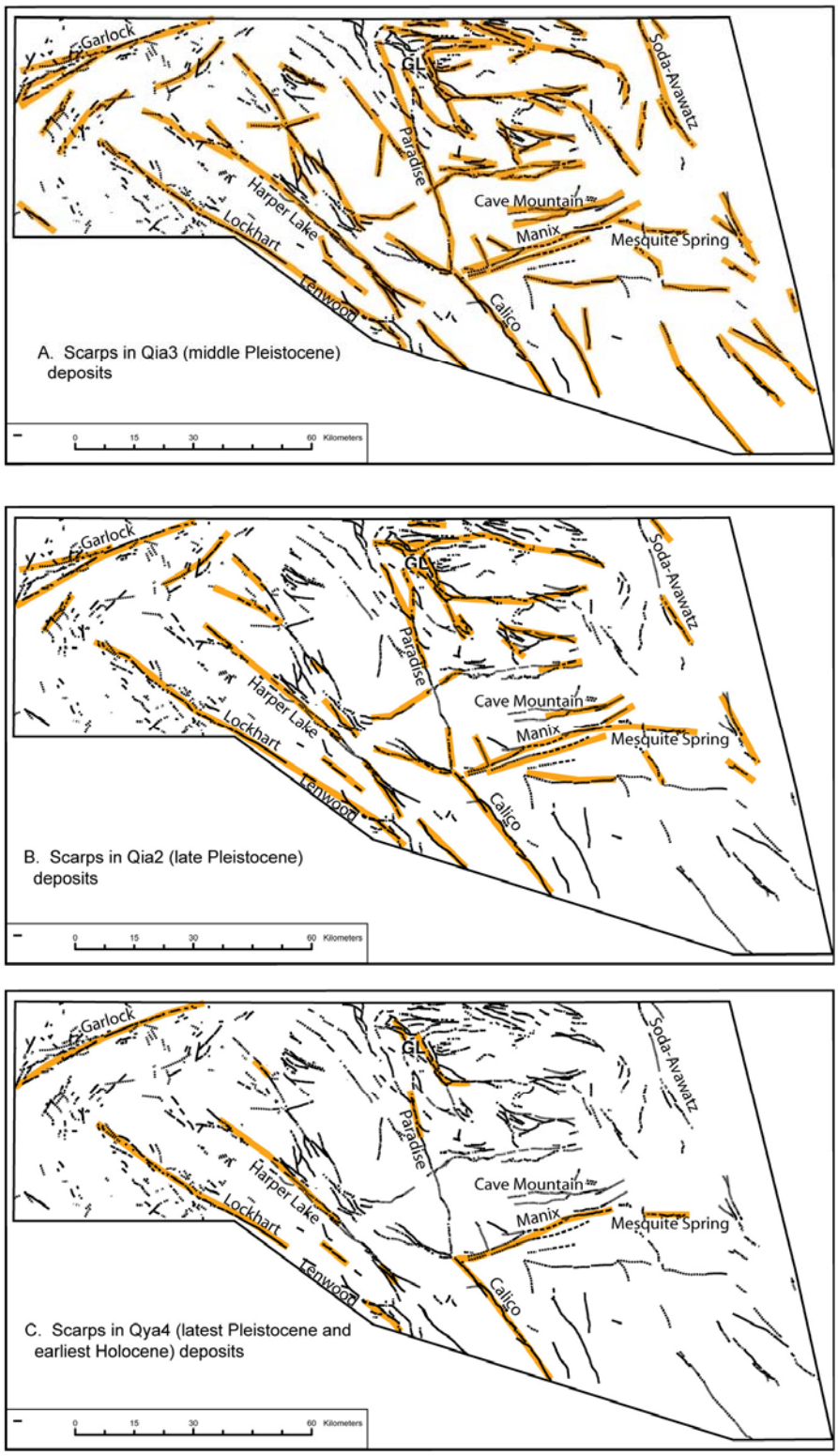

Figure 3. Quaternary deposits cut by faults or related deformation (shaded) during slices of late Quaternary time. A. Middle Quaternary deposits. B. Middle late Quaternary deposits, about 90 to 30 ka in age. C. Pleistocene-Holocene boundary deposits, about 15 to 9 ka. Note the reduced numbers of active faults with time, and increasingly large areas with little or no faulting. Area same as that for Fig. 2. GL, Goldstone Lake area.

change to three belts of focused shear in the northern Mojave that connect with three principal shear zones in the Basin and Range.

Is deformation in the southern Mojave Desert block likewise being restricted into a few widely spaced belts? Our work supports the observation by Howard and Miller (1992) that several northwest-striking fault zones in the Cady block and to the southeast have been inactive since the middle Pleistocene (post Qia3), but our mapping is not sufficiently detailed to evaluate whether the dextral faults within the broad zone of active shear between the Pisgah and Helendale faults are evolving like their counterparts in the northern Mojave Desert domain. The pattern of ruptures displayed by the Landers and Hector Mine events may signal a consolidation of faulting into fewer and more northerly striking belts (Nur et al., 1993).

If Holocene faulting in the northern Mojave Desert has consolidated into a few principal belts, the kinematics of this domain are fairly straightforward and can be tested with mapping and geodetic methods. The kinematic genesis of the patterns depicted in Figure 3 could be explored using geodetic observations to examine whether: (1) compared to stable North America, step-function decreases in northwest-oriented slip vectors occur across the Lockhart, Harper Lake, and Paradise fault systems; (2) the Irwin block shows clockwise rotation, as should most of its bordering faults; and (3) strain internal to the Irwin block includes faulting and folding. The latter may account for origin of synclinal basins such as Coyote Lake, Soda Lake, and Silurian Valley, anticlinal uplifts such as the Avawatz Mountains, and generally elevated terrain in the northern part of the Irwin block.

Conclusions

In the northern Mojave Desert, some mountain-front faults are presently inactive and nearby parallel and oblique faults accommodate late Pleistocene and possibly Holocene strain. Along the Calico Mountains, these late Quaternary features transfer strain between older faults in much the same manner observed for ruptures of the recent Landers and Hector Mine earthquakes in the southern Mojave Desert. The Paradise fault zone strikes north-northwest across much of the northern Mojave Desert, and it apparently accommodates significant dextral shearing along the western side of the Irwin block. It separates contrasting regions of mainly sinistral and dextral faulting, and its history may shed light on key neotectonic questions, such as how strain is transferred northward from the Mojave Desert to the Basin and Range province, and how the Garlock fault acquired its concave-south planform trace.

Areas undergoing active faulting in the northern Mojave Desert have consolidated progressively through late Pleistocene and Holocene time. The focusing of strain to three narrow belts from a former east-west extent of greater than 200 km occurred over about 200 ka, and represents a pronounced change in upper crustal response to plate-boundary deformation. The late Pleistocene and Holocene fault patterns show that an integrated system of north-striking faults, the Paradise fault system, spans the northern Mojave Desert, linking the Calico fault with the Garlock fault. The Paradise-Garlock connection lies near the southern terminus of the Panamint fault system. The Manix fault system extends eastward via the Mesquite Springs fault to the southern Soda Lake area, crossing an area previously considered to be represented by northwest-striking dextral faults, and possibly imparting strain to the Soda-Avawatz fault zone. The apparent focusing of strain into three fault belts during the late Pleistocene can be tested with detailed field studies of faults and geomorphology and geodetic methods.

Acknowledgements

We thank Brett Cox, Chris Menges, Mike Oskin, Bob Reynolds, and Dave Bedford for valuable discussions that clarified ideas presented in this paper, although erroneous conclusions are strictly the responsibility of the authors. Brett Cox and Dave Bedford reviewed earlier versions of this paper, substantially improving it.

References cited

Amoroso, L., and Miller D.M., 2006, Surficial geologic map and geodatabase of the Cuddeback Lake 30' x 60' Quadrangle, San Bernardino and Kern Counties, California: U.S. Geological Survey Open-file Report 2006-1276, scale 1:100,000, 30 p.

Bedford, David R., Miller, David M., and Phelps, Geoffrey A., 2006, Preliminary surficial geologic map database of the Amboy 30x60 minute quadrangle, California: U.S. Geological Survey Open-File Report 2006-1165 [available on the World Wide Web at URL http://pubs.usgs.gov/of/2006/1165/].

Brady, R.H., III, 1984, Neogene stratigraphy of the Avawatz Mountains between the Garlock and Death Valley fault zones, southern Death Valley, California: Implications as to late Cenozoic tectonism: Sedimentary Geology, v. 38, p. 127-157.

Birkeland, P.W., 1990, Soil geomorphic research—A selective overview: Geomorphology, v. 3, p. 207-224.

Carter, J.N., Luyendyk, B.P., and Terres, R.R., 1987, Neogene clockwise rotation of the eastern Transverse Ranges, California, suggested by paleomagnetic vectors: Geological Society of America Bulletin, v. 98, p. 199-206.

Clark, M.M., 1973, Map showing recently active breaks along the Garlock and associated faults, California: U.S. Geological Survey Miscellaneous Geologic Investigations Map I-741, scale 1:24000.

Cox, B.F. and Wilshire, H.G., 1993, Geologic map of the area around the Nebo Annex, Marine Corps Logistics Base, Barstow, California: U.S. Geological Survey Open-File Report OF-93-568, scale 1:12000.

Cox, B.F. and Wilshire, H.G., 1994, Geologic map of the Yermo Annex and vicinity, Marine Corps Logistics Base, Barstow, California: U.S. Geological Survey Open-File Report OF-94-681, scale 1:12000.

Dibblee, T.W., Jr., 1961, Evidence of strike-slip movement on northwest-trending faults in the western Mojave Desert, California: U.S. Geological Survey Professional Paper 424-B, p. B197-199.

Dokka, R.K., and Travis, C.J., 1990, Role of the eastern California shear zone in accommodating Pacific-North American plate motion: Geophysical Research Letters, v. 17, p. 1323-1326.

Dudash, S.L., 2004, Quaternary geology of the Calico Mountains piedmont and Coyote Lake, Mojave Desert, California. Geological Society of America Abstracts with Programs, v. 36, no.5, p. 582.

Dudash, S.L., 2006, Preliminary surficial geologic map of a Calico Mountains piedmont and part of Coyote Lake, Mojave Desert, San Bernardino County, California: U.S. Geological Survey Open-File Report 06-1090, 48 p. pamphlet, scale 1:24,000.

Garfunkel, Z., 1974, Model for the late Cenozoic tectonic history of the Mojave Desert, California, and its relation to adjacent areas: Geological Society of America Bulletin, v. 85, p. 1931-1944.

Hardebeck, J.L., and Hauksson, E., 1999, Roles of fluids in faulting inferred from stress field signatures: Science, v. 285, p. 236-239.

Hauksson, E., Jones, L.M., Hutton, K., and Eberhart-Phillips, D., 1993, The 1992 Landers earthquake sequence: Seismological observations: Journal of Geophysical Research, v. 98, p. 19835-19858.

Hewett, D.F., 1954, General geology of the Mojave Desert region, California: *in* Jahns, R.H., ed., Geology of southern California: Californian Division of Mines and Geology, Bulletin 170, v. II, p. 5-20.

Howard, K.A., and Miller, D.M., 1992, Late Cenozoic faulting at the boundary between the Mojave and Sonoran blocks: Bristol Lake area, California, *in* Richard, S.M., ed., Deformation associated with the Neogene eastern California shear zone, southwestern Arizona and southeastern California: Redlands, CA, San Bernardino County Museum Special Publication 92-1, p. 37-47.

Jennings, C.W., 1994, Fault activity map of California and adjacent areas with location and ages of volcanic eruptions: California Geologic Data Map Series, Map No. 6, California Division of Mines and Geology, scale 1:750,000.

Luyendyk, B.P., 1991, A model for Neogene rotations, transtension and transpression in southern California: Geological Society of America Bulletin, v. 103, p. 1528-1536.

Mabey, D.R., 1960, Gravity survey of the western Mojave Desert, California: U.S. Geological Survey Professional Paper 316-D, p. 51-73.

McClusky, S.C., Bjornstad, S.C., Hager, B.H., King, R.W., Meade, B.J., Miller, M.M., Monastero, F.C., and Souter, B.J., 2001, Present day kinematics of the Eastern California shear zone from a geodetically constrained block model: Geophysical Research Letters, v. 28, p. 3369-3372.

McGill, S.F., and Sieh, K., 1991, Surficial offsets on the central and eastern Garlock fault associated with prehistoric earthquakes: Journal of Geophysical Research, v. 96, p.21,597-21,621.
McGill, S.F., and Sieh, K., 1993, Holocene slip rate of the central Garlock fault in southeastern Searles Valley, California: Journal of Geophysical Research, v. 98, p.14,217-14,231.
McFadden, L.D., and Weldon, R.J., II, 1987, Rates and processes of soil development on Quaternary terraces in Cajon Pass, California: Geological Society of America Bulletin, v. 98, p. 280-293.
Miller, D.M., and Yount, J.L., 2002, Late Cenozoic tectonic evolution of the north-central Mojave Desert inferred from fault history and physiographic evolution of the Fort Irwin area, California: Geological Society of America Memoir, 195, p. 173-197.
Miller, M.M., Johnson, D.J., Dixon, T.H., and Dokka, R.K., 2001, Refined kinematics of the eastern California shear zone from GPS observations: Journal of Geophysical Research, v. 106, p.2245-2264.
Nur, A., Hagai, R., and Beroza, G.C., 1993, The nature of the Landers-Mojave earthquake line: Science, v. 261, p. 201-203.
Oskin, M. and Iriondo, A., 2004, Large magnitude transient strain accumulation on the Blackwater fault, Eastern California shear zone: Geology, v. 32, no. 4, p. 313-316.
Oskin, M., Perg, L., Blumentritt, D., Mukhopadhyay, S., and Iriondo, A., 2007, Slip rate of the Calico fault: Implications for geologic versus geodetic rate discrepancy in the eastern California shear zone: J. Geophys. Res., 112, B03402, doi:10.1029/2006JB004451.
Peltzer, G., Crampe, F., Hensley, S., and Rosen, P., 2001, Transient strain accumulation and fault interaction in the Eastern California shear zone: Geology, v. 29, p. 975-978.
Reheis, M.C., Harden, J.W., McFadden, L.D., and Shroba, R.R., 1989, Development rates of late Quaternary soils, Silver Lake Playa, California: Soil Science Society of America Journal, v. 53, p. 1127-1140.
Reheis, M.C., Miller, D.M., and Redwine, J.L., 2007, Quaternary stratigraphy, drainage-basin development, and geomorphology of the Lake Manix basin, Mojave Desert: U.S. Geological Survey Open-File Report 2007–1281, 31 p.
Richter, C. F., 1947, The Manix (California) earthquake of April 10, 1947: Bulletin of the Seismological Society of America, v. 37(8), p. 171-179.
Sauber, J., Thatcher, W., and Solomon, S., 1986, Geodetic measurement of deformation in the central Mojave Desert, California: Journal of Geophysical Research, v. 91, p. 12683-12694.
Sauber, J., Thatcher, W., Solomon, S., and Lisowski, M., 1994, Geodetic slip rate for the eastern California shear zone and the recurrence time of Mojave Desert earthquakes: Nature, v. 367, p. 264-266.
Schelle, H., and Grunthal, G., 1996, Modeling of Neogene crustal block rotation: Case study of southeastern California: Tectonics, v. 15, p. 700-710.
Schermer, E.R., Luyendyk, B.P., and Cisowski, S., 1996, Late Cenozoic structure and tectonics of the northern Mojave Desert: Tectonics, v. 15, p. 905-932.
Westaway, R., 1995, Deformation around stepovers in strike-slip fault zones: Journal of Structural Geology, v. 17, p. 831-846.
Yount, J.C., Schermer, E.R., Felger, T.J., Miller, D.M., and Stephens, K.A., 1994, Preliminary geologic map of Fort Irwin Basin, north-central Mojave Desert, California: U.S. Geological Survey Open File Report 94-173, 27 p., scale 1:24,000.